

NASA Contractor Report 4145

LEWIS  
SR-41  
111-34  
145713  
2273

# Two-Equation Low-Reynolds-Number Turbulence Modeling of Transitional Boundary Layer Flows Characteristic of Gas Turbine Blades

Rodney C. Schmidt and Suhas V. Patankar

GRANT NAG3-579  
MAY 1988



NASA Contractor Report 4145

# Two-Equation Low-Reynolds-Number Turbulence Modeling of Transitional Boundary Layer Flows Characteristic of Gas Turbine Blades

Rodney C. Schmidt and Suhas V. Patankar  
*University of Minnesota*  
*Minneapolis, Minnesota*

Prepared for  
Lewis Research Center  
under Grant NAG3-579



National Aeronautics  
and Space Administration

Scientific and Technical  
Information Division

1988

**TABLE OF CONTENTS**

<b>1.0 INTRODUCTION</b>	<b>1</b>
1.1 The Scope and Objectives of This Thesis	1
1.2 Overview of Turbine Blade Heat Transfer	3
1.2.1 General description	3
1.2.2 Transition	7
1.2.3 Free-Stream Turbulence	9
1.2.4 Pressure Gradients	12
1.2.5 Curvature	14
1.3 Literature Survey	16
1.3.1 Overview of Turbulence Modeling	16
1.3.2 Predicting Transition with Two-Equation Turbulence Models	23
1.3.3 Relevant Transition Experiments	27
1.4 Outline of the Thesis	29
<b>2.0 THE MATHEMATICAL REPRESENTATION OF THE PROBLEM AND THE NUMERICAL SOLUTION PROCEDURE</b>	<b>35</b>
2.1 The Boundary Layer Equations	35
2.2 The Turbulence Models Employed	38
2.2.1 k- $\epsilon$ Low-Reynolds-Number Turbulence Models	38
2.2.2 The Jones-Launder and Lam-Bremhorst Models	41
2.3 The Numerical Solution Procedure	44

2.3.1 The Patankar-Spalding Parabolic Solution Method	45
2.3.2 Near Wall Grid Refinement	47
2.3.3 Specification of Initial Starting Profiles and Boundary Conditions	50
2.3.4 Numerically Representing $f_{\mu}$ and $f_1$	57
3.0 EVALUATING THE TRANSITION PREDICTION CHARACTERISTICS OF TWO LRN k- $\epsilon$ MODELS	62
3.1 Objectives of the Evaluation	62
3.2 Sensitivity to the Starting Profiles of k and $\epsilon$	64
3.3 Sensitivity to the Starting Location	67
3.4 Sensitivity to Free-Stream Turbulence	69
3.5 Summary	71
4.0 DEVELOPMENT OF AN IMPROVED APPROACH TO SIMULATE TRANSITION WITHIN THE FRAMEWORK OF THE k- $\epsilon$ LRN TURBULENCE MODELS	77
4.1 Preliminary Comments	78
4.1.1 Method of Rodi and Scheuerer	79
4.1.2 Desired Characteristics	80
4.2 A Simple Improvement to The Lam-Bremhorst Model	81
4.2.1 The Problem and it's Cause	81
4.2.2 A Solution	83
4.3 The Mechanism by which the Model Simulates Transition	84

4.4	Stability Considerations	86
4.5	A Modification to the Production Term	88
4.5.1	Applying a Stability Criteria	89
4.5.2	Limiting the Growth Rate of the Production Term	90
4.5.3	Numerical Implementation	92
4.5.4	Determining the Transition Parameters $A$ and $B$	94
4.5.6	The Effects of High Free-stream Dissipation Rate	98
4.6	Transition Calculations with the PTM version of the Lam-Bremhorst Model	99
4.7	Application of the Modification to the Jones-Launder Model	101
4.8	Starting Conditions and the PTM models	105
5.0	COMPARISON OF THE PROPOSED MODEL WITH EXPERIMENTAL DATA	132
5.1	Simple Flat Plate Flow with Free-Stream Turbulence	134
5.1.1	Data of Wang	134
5.1.2	The Use of the Streamwise vrs. Total Turbulence Intensity	136
5.1.3	Data of Rued	137
5.1.4	Data of Blair and Werle	139
5.1.5	Discussion and Summary	142
5.2	Transitional Flows with Acceleration	143
5.2.1	Some Limitations Inherent in the 2-Equation Approach	144
5.2.2	Data of Blair and Werle	146
5.2.3	Data of Rued	148

5.2.4 Summary of the Prediction Capabilities for Flows with Acceleration	153
5.3 Turbine Blade Cascade Data	154
5.3.1 Preliminary Comments about the Calculations	155
5.3.2 Comparison with the Data of Daniels	157
5.3.3 Comparison with the C3X blade of Hylton et al.	158
5.3.4 Brief Summary of the Turbine Blade Data Predictions	160
6.0 CONCLUDING REMARKS	190
6.1 Contributions of this Work	190
6.2 Limitations of the Approach Developed	192
6.3 Thoughts about Further Research	193
REFERENCES	195
APPENDIX A1; The Computer Code	205
A Brief Description of the Code	205
Definitions of FORTRAN variables and arrays	208
A Listing of the Subroutines and Functions	217
The UM1 functions used	230
A Listing of program MAIN	235
Sample Input Files	240
APPENDIX A2; Variable property equations	246
APPENDIX A3; Tabulated experimental data	249
APPENDIX A4; Code used to calculate starting location velocity profile parameters	261

## NOMENCLATURE

arc	The total surface arc length on either the suction or the pressure side of the turbine blade of interest
$A, B$	Empirical parameters in the proposed modification. See eq. (4.6). Correlated as functions of $Tu_e$
$C_f$	Skin friction coefficient
$C_p$	Specific heat at constant pressure
$C_\mu, C_1, C_2$	Constants in the k- $\epsilon$ turbulence models. See Table 2.1
$dx$	Computational step size in the streamwise direction
$D$	Empirical function introduced in some low-Reynolds-number models to modify the dissipation rate variable near the wall. See eq. (2.11) and Table 2.2
$E$	Empirical function introduced in some low-Reynolds-number models. See eq. (2.13) and Table 2.2
$f_1$	A low-Reynolds-number function used to modify the near wall behavior of the production term in the $\epsilon$ equation.
$f_2$	A low-Reynolds-number function used to modify the near wall behavior of the destruction term in the $\epsilon$ equation.
$f_\mu$	A low-Reynolds-number function used to modify the near wall behavior of the turbulent viscosity. See eq. (2.10)
$h$	Mean static enthalpy
$h'$	Fluctuating static enthalpy
$h$	local heat transfer coefficient

$\overline{h'v'}$	Apparent turbulent heat flux
H	Total or stagnation enthalpy. See eq. (2.4)
k	Turbulent kinetic energy
K	Acceleration parameter. See eq. (1.4)
l	A mixing or a turbulence length scale. See eqs. (1.5) and (1.9)
$L_e^u$	A free-stream turbulence length scale. See eq. (1.3)
M1	The number of computational nodes in the cross-stream direction
M2	M1-1
M3	M1-2
Nu	Nusselt Number
P	Static pressure
$P_k$	Modelled production term in the k equation
Pr	Molecular Prandtl number
$Pr_t$	Turbulent Prandtl number
$q_w$	Heat flux at the wall
R	Gas constant in the ideal gas law (eq. (2.6)) or radius of a cylinder (eqs. (2.41)-(2.49))
$Re_x$	Reynolds number based on x
$Re_\theta$	Reynolds number based on momentum thickness
$Re_{\theta,C}$	Momentum thickness Reynolds number below which $P_k$ is set to zero in the implementation of the "PTM" model
$Re_{\theta,S}$	Momentum thickness Reynolds number at the start of transition
$Re_{\theta,E}$	Momentum thickness Reynolds number at the end of transition
$R_x, R_y$	Turbulent Reynolds numbers defined in eqs. (2.14) and (2.15)
s	A very small number. $s \approx 10^{-10}$ See section 2.3.4

<b>S</b>	Streamwise distance from the stagnation point around either surface of a turbine blade
<b><math>S(\lambda)</math></b>	Shear correlation. $S(\lambda) \approx \frac{\tau_w \theta}{\mu U}$
<b>St</b>	Stanton number. See eqs. (5.1) and (5.4)
<b>Tu</b>	Turbulence intensity
<b>U</b>	Mean velocity in the x direction
<b><math>u_\tau</math></b>	friction velocity. $u_\tau = \sqrt{\tau_w / \rho}$
<b><math>u', v', w'</math></b>	Fluctuating velocities in the x, y, z directions
<b><math>\overline{u'v'}</math></b>	Apparent turbulent stress
<b>W</b>	Pseudo-vorticity density. See eq. (1.8)
<b>x</b>	Streamwise distance from the leading edge
<b>y</b>	Cross-stream distance from the wall
<b><math>y^+</math></b>	Non-dimensional distance from the wall defined in eq. (2.16)
<b><math>\rho</math></b>	Fluid density
<b><math>\delta</math></b>	Boundary layer thickness
<b><math>\delta_T</math></b>	Thermal boundary layer thickness
<b><math>\theta</math></b>	Momentum thickness of the boundary layer
<b><math>\varepsilon</math></b>	Dissipation rate
<b><math>\hat{\varepsilon}</math></b>	Modified dissipation rate variable. See eq. (2.11)
<b><math>\tau_w</math></b>	Shear stress at the wall
<b><math>\mu</math></b>	Molecular viscosity
<b><math>\mu_t</math></b>	Eddy or turbulent viscosity
<b><math>\nu</math></b>	Kinematic viscosity, $\nu = \mu / \rho$
<b><math>\nu_t</math></b>	Turbulent kinematic viscosity, $\nu_t = \mu_t / \rho$

$\sigma_k, \sigma_\epsilon$	Empirical constants in the turbulence models. See Table 2.1 and eqs. (2.12)-(2.13)
$\omega$	Nondimensional stream function. See eq. (2.21)
$\psi$	Stream function. See eq. (2.22)
$\chi$	Grid coordinate used in grid generation method. See eq. (2.23)
$\lambda$	Local acceleration parameter based on the momentum thickness See eq. (2.31)
$\Lambda$	Local acceleration parameter based on the boundary layer thickness $\delta$ . See eq. (2.32)

### Subscripts

e	Denoting free-stream value
i	Denoting value at the initial starting location of the calculation
w	Denoting value at the wall, ie. $y=0$
0	Denoting value at $x=0$

### Special

$\min(a,b)$	Denoting the minimum of the two values $a, b$
$[a]_{\max}$	Denoting the maximum allowable value of $a$
$\log_e(a)$	Denoting the logarithm to the base $e$ of $a$
$\bar{a}'$	Denoting the time average of the fluctuating quantity $a'$
LRN	Short for Low-Reynolds-Number
PTM	Acronym for Production Term Modified. Used to denote the $k$ - $\epsilon$ LRN model modifications developed in this thesis.

## **CHAPTER ONE**

### **INTRODUCTION**

#### **1.1 THE SCOPE AND OBJECTIVES OF THIS THESIS**

As desired operating temperatures and efficiency levels of advanced turbine engines continue to increase, the accurate prediction of gas side heat transfer on the turbine blades becomes increasingly critical in the development and design process. Although methods to accurately solve a variety of fluid flow and heat transfer problems have been developed, efforts to apply and extend these methods to the calculation of heat transfer on turbine blades have so far proved somewhat unsatisfactory. This is due to the complex nature of the transitional and turbulent flow inherent in the problem and the failure of our mathematical models to consistently simulate these phenomena correctly.

The main goal of this thesis is to describe the development of an improved method of predicting transition in boundary-layer flows developing under conditions characteristic of gas turbine blades. Knowing somewhat the complexities of this problem from the start, certain limitations were of necessity made on the scope this work. The first of these was to consider only the time averaged two-dimensional aspects of the problem. On a turbine blade, where endwall effects can be significant, this translates to considering only the nearly two-dimensional midspan region. Furthermore, since there are a large number of potential approaches to solving this problem, a restriction was made on the framework within which an

improved solution method was sought. The work presented here will focus on exploring and developing the potential of low-Reynolds-number  $k$ - $\epsilon$  turbulence models for solving this problem.

A variety of different low-Reynolds-number ( hereafter referred to as "LRN") modifications to the standard  $k$ - $\epsilon$  model have been proposed in the literature. These modifications are designed to extend the validity of two equation turbulence models through the viscous sublayer to the wall. One attractive characteristic of this type of model is the seemingly natural process by which boundary layer transition is simulated when the free-stream flow is turbulent. However, since these methods are relatively new, there is a lack of adequate documentation showing how well the starting location and length of transition is predicted by these methods for simple flows. Thus, one objective of this thesis is to test and clearly document the predictive capabilities of two of these models. Both an empirical correlation and specific experimental data sets will be used to provide a broad background within which to evaluate and contrast these models.

The next objective is to use knowledge gained by exploring these methods on less complex flows, to propose modifications designed to improve the transition predictions in more general situations typical of a turbine blade. These modifications will then be thoroughly tested against a wide range of experimental data. Factors known to influence transition and which will be included in these tests include the effects of free-stream turbulence, strong favorable pressure gradients, and variable properties. In concluding these tests, the predictions of the method will be compared with the results from a number of actual turbine blade cascade experiments.

## **1.2 OVERVIEW OF TURBINE BLADE HEAT-TRANSFER**

Although the focus of this thesis is on only one aspect of the total external heat transfer problem (transition), a somewhat broader overview of the problem will be given here as a means of setting a proper perspective.

### **1.2.1 General description**

The problem of external heat transfer on turbine blades has become especially important in recent years as the desired operating combustion temperatures have now significantly surpassed the melting temperatures of the materials available for constructing the turbine components. In the past, most design decisions have been made from the results of very expensive experimental work. As numerical models have become more sophisticated, and computers have increased in speed, the potential to reduce the number of required experiments by using appropriate computer simulation in the design loop has been recognized. And indeed, this has been realized in many areas of the design process. However, although much progress has been made, agreement between experiment and the numerical predictions for the heat transfer on the surface of the turbine blades themselves has still not been consistently satisfactory, especially for the region of the blade over which transition occurs.

In a typical turbine engine, large numbers of blades extend radially outward from a central shaft, the tips leaving only a very small clearance between the blade and the outer endwall. Hot gas from the combustion

chamber, at a temperature on the order of 2500 F (1370 C) and at a pressure of 20-25 atm. enters the turbine region in a highly agitated, turbulent condition. The gas then proceeds through alternating rows of blades (moving ) and vanes (fixed) where lateral kinetic energy from the combustion gases is converted into rotational kinetic energy.

A cross-section at midspan of a typical turbine blade is shown in Figure 1.1. The underside of the blade is commonly called either the "pressure" or "concave" side. The top side of the blade is commonly called either the "suction" or the "convex" side. On each blade there exists a stagnation point, the place on the blade where a line drawn normal to the surface is exactly parallel to the approaching upstream flow. It is from this point, and extending around each side of the blade, that a thin viscous region, the boundary layer, develops and grows. Outside of this region, although the flow may still be complicated, the flow field is essentially inviscid. Because of the distinctly different nature of these two regions, most attempts to model or simulate the flow field are made by analyzing the two regions separately. The larger inviscid region is calculated using methods which solve the inviscid Navier Stokes equations, ie. Euler's equations. The thin region close to the surface is solved using equations which include the important viscous terms, but neglect other terms due to the parabolic nature of flow.

In a real turbine, both the inviscid outer region and the thin boundary layer region are three dimensional in character. However, in the midspan region, three dimensional effects appear to be of secondary importance. It is generally believed that in this region an analysis neglecting these effects

should not be seriously in error. Furthermore, it is in this region that the gas temperatures are usually highest and thus of greatest concern. This is not to say that three dimensional effects are unimportant. For example, the endwall region heat transfer problem, strongly three dimensional in nature, is also of great importance. That problem, however, can hardly be expected to be fully solved unless the flow is first well understood in the neighboring nearly two dimensional midspan region.

The most serious challenge to the validity of the two dimensional assumption has been the theory that the observed increase in heat transfer on the concave side was caused by three-dimensional streamwise vortices similar to the Taylor-Gortler vortices seen in laminar flow. However, Kays and Moffat [40] have argued very convincingly that this is not the case and conclude that "a two dimensional code should work as well in the concave region as in the convex". Thus from here on we will concentrate on those factors which can be modeled within the framework of a two dimensional boundary layer approach.

The boundary layer development on a typical gas turbine blade is influenced by a great number of complicating factors, many of which are not yet fully understood. A list of topics which are important would include the following:

- \* free-stream turbulence effects,
- \* effects of adverse and favorable pressure gradients,
- \* laminar-turbulent transition,
- \* relaminarization,

- \* near-wall, "low-Reynolds-number" effects,
- \* stagnation flow with free-stream turbulence,
- \* curvature effects,
- \* body force effects (due to spinning),
- \* variable property effects,
- \* effects of surface roughness.

This is a formidable list, and most of these continue to be in and of themselves topics of continuing extensive research. Nevertheless, in order to accurately solve the turbine blade heat transfer problem, we must in some way account for all of these effects which prove significant. Furthermore, any major synergistic effects, if they occur, must also be appropriately modeled.

It is not possible within the scope of this introduction to give a thorough discussion and literature review for each of these topics individually. However, a brief introduction and review of some of the more recent literature with respect to four of the most important of these topics will be given next. The topics and factors that are generally believed to be of greatest importance include transition, free-stream turbulence effects, pressure gradient effects, and curvature effects. The reader may also wish to consider the excellent overview of many of these factors as they relate to turbine blade heat transfer presented by Graham [28]. Other references which provide a good source of general information relating to this problem include Martin and Brown [49] and the introductory material in Hylton et al [34].

### 1.2.2 Transition

The process by which a laminar boundary layer changes to a turbulent boundary layer is termed transition. Since the flow and heat transfer characteristics of these two regimes are so dramatically different, the accurate prediction of this process is very important. Unfortunately, in most fluid flow problems of interest, transition is also a very difficult process to model. It is one of the major stumbling blocks in the prediction of the external heat transfer on gas turbine blades [28].

Transition is a complex phenomenon and is influenced by a variety of factors. Reynolds number, free-stream turbulence, pressure gradient, surface roughness, and curvature are just a few of the parameters found to be important. The details of the mechanisms by which transition occurs are not completely understood despite a vast amount of research. We do know that the onset of transition is essentially a stability problem. For example, from the mathematics of stability theory, we are able to learn the conditions under which small perturbations are amplified instead of damped, a necessary first step in the transition process.

Early research focused primarily on the simple case of transition occurring on a flat plate under a relatively quiescent free-stream flow. Theory has predicted and experiments now verified that for this case the process begins with the formation of two-dimensional Tollmien-Schlichting waves moving in the direction of the flow. The process becomes three-dimensional and non-linear as the waves develop spanwise variations and are amplified. From then on there is a cascade of vortex breakdowns which end

in fully three dimensional fluctuations of an almost random nature. Experimentally one finds that the breakdown of the laminar boundary layer does not occur everywhere across the flow at the same streamwise location. The breakdown occurs instead at apparently random spots, with bursts so to speak of turbulence. These turbulent spots spread laterally downstream until the entire boundary layer is engulfed. The final stages of the transition process manifest themselves by a relatively sharp increase in the skin friction coefficient. In the case of heat transfer, this will also correspond to a sharp increase in the Stanton number. Tani [84] is one source of a fairly detailed review of this process as it is currently understood.

Probably the most dominant factor modifying the process of transition is the magnitude of the free-stream turbulence intensity. The major effect of this influence is to displace the location of transition upstream, and to shorten the length over which it occurs. It also tends to increase the spanwise homogeneity of the transition process. This will be discussed in more detail next in section 1.2.2.

Adverse pressure gradients and convex curvature also tend to promote the transition process, as both of these factors are destabilizing to the boundary layer. Conversely, favorable pressure gradients and concave curvature are stabilizing, and thus tend to inhibit the start of transition. Unfortunately, research has not yet clearly distinguished the separate effects of these parameters in a well quantifiable manner.

### 1.2.3 Free-Stream Turbulence

Free-stream turbulence has been found to influence every stage in the development of the boundary layer. Its importance to the work in this thesis is made clear in the following quotation.

"The major uncertainty in predicting gas side heat transfer rates anywhere on the blade is the interaction of the free-stream unsteadiness and turbulence with the boundary layers on the blade. Such interaction will determine the nature of the boundary layer, control the mechanism of transition and in the last analysis, establish the levels of heat transfer."

R. W. Graham, 1979 [28]

The definition of free-stream turbulence intensity is not always consistent within the literature. This variation is caused by the inclusion of the turbulent fluctuations in each direction for some cases, but only the streamwise direction in others. When a distinction is needed within this thesis, the following nomenclature and definitions will be used.

$$Tu_e = \frac{\sqrt{\overline{u'^2}}}{U_e} \quad (1.1)$$

$$Tu_{e,T} = \frac{\sqrt{\frac{1}{3}(\overline{u'^2} + \overline{v'^2} + \overline{w'^2})}}{U_e} \quad (1.2)$$

The primary effects of free-stream turbulence are the enhancement of skin friction and heat transfer, and the displacement upstream of the transition region. However, the degree to which this occurs varies depending upon both the local nature of the boundary layer over which it occurs, and according to other free-stream conditions such as the pressure gradient.

The effect of free-stream turbulence on stagnation flow heat transfer has been studied over the years by Kestin and co-workers [41,43]. They have both documented the observed increase in heat transfer for various levels of  $Tu_e$ , and presented evidence suggesting a particular mechanism as responsible for this increase.

The effect of free-stream turbulence on a developing laminar boundary layer is somewhat more difficult to determine. This is because as the free-stream turbulence is increased, the region over which the boundary layer remains laminar becomes increasingly short, and measurements correspondingly more difficult. It was initially reported by researchers such as Junkhan and Serovy [38], and Kestin et al [42], that laminar heat transfer rates were not perceptibly increased for zero pressure gradient conditions. However, other work presented by Dypan and Epik [24], has reported significant increases in heat transfer for the laminar case.

In the case of fully turbulent flows, the research has been more unified and consistent in showing an increase in heat transfer and skin friction. Some of the more recent published papers which deal with this include the work of Hancock and Bradshaw [31], Meier and Kreplin [53], and Blair [11,12]. The results of Blair are representative of the basic characteristics described in all of these papers. He reports that higher free-stream turbulence leads to

slightly fuller velocity profiles, resulting in higher momentum thicknesses and smaller form parameters. This also leads to an increase in skin friction and heat transfer. For example, Blair found that for a 6% turbulence intensity level, the heat transfer and skin friction are increased by 18% and 14% respectively. He also reports that the effects of free-stream turbulence can be correlated reasonably well with two parameters,  $Tu_e$  (eq. 1.1) and  $L_e^u$ , a free-stream turbulence length scale defined as;

$$L_e^u = \frac{-(\bar{u}^{\prime 2})_e^{3/2}}{U_e \frac{d(\bar{u}^{\prime 2})_e}{dx}} \quad (1.3)$$

The effect of  $Tu_e$  on transition has also been extensively studied, and it is the results of this research that are of primary concern to the work of this thesis. Representative of the many experiments dealing with this topic for zero pressure gradient conditions are those of Blair and Werle [8], Rued [72,73], Wang et al [90,91], Abu-Ghannam and Shaw [2], and Junkhan and Serovy [38]. In each of these studies the previously mentioned upstream displacement of transition is clearly exhibited. Furthermore, although there is significant scatter in the data, it has been found that these experiments can be reasonably correlated to the local momentum and displacement thickness Reynolds numbers. Correlations of this type have been presented by Hall and Gibbings [30], Van Driest and Blumer [89], and more recently by Abu-Ghannam and Shaw [2].

Other experiments have attempted to show the combined influence of free-stream turbulence and pressure gradients on transition. This is discussed in the next section.

#### 1.2.4 Pressure Gradients

The other dominant factor influencing boundary layer development, transition, and the heat transfer on a turbine blade is the pressure gradient influence. The pressure side of a turbine blade is commonly characterized by a strong acceleration ("favorable" pressure gradient) along the entire length of the blade. In contrast, the suction side is often characterized by an initial region of extremely strong acceleration, followed by at least a short region of mild deceleration ("adverse" pressure gradient). The effects of pressure gradients on laminar and turbulent boundary layers has been a long standing topic of research. Much of the past research has been dedicated to the study of pressure gradients on either fully turbulent, or fully laminar boundary layers, without other complications. An excellent review of the literature dealing with this topic can be found in Kays and Moffat [40].

Recently, studies have focused more strongly on the combined influence of free-stream turbulence and pressure gradient on both fully turbulent boundary layers, and on transition. These studies are of even greater relevance to the turbine blade heat transfer since they would include any synergistic interactions that might occur. Recent studies of particular importance to the work in this thesis include those of Blair and Werle[9,10], Rued and Wittig [72,73], Abu-Ghannam and Shaw [2], Junkhan and Serovy

[38], and Van Driest and Blumer [89]. The following outline summarizes some of the important qualitative aspects of acceleration which are important to the work in this thesis.

Acceleration of the free-stream flow;

- 1) causes stretching of the turbulent eddies which results in reduced turbulent intensities.
- 2) is stabilizing, ie. it tends to prevent or hold off transition, and when it does occur the transition length is longer.
- 3) can cause relaminarization, a process whereby an originally turbulent boundary layer reverts to a quasi-laminar state.
- 4) tends to diminish heat transfer rates
- 5) is often measured with reference to an acceleration parameter  $K$  defined as

$$K = \frac{v}{U_e^2} \frac{\partial U_e}{\partial x} \quad (1.4)$$

Deceleration of the free-stream flow;

- 1) enhances turbulent intensities
- 2) increases heat transfer and skin friction
- 3) is destabilizing, ie. promotes transition
- 4) may lead to separation

### 1.2.5. Curvature

It has been known for many years that surface curvature can significantly affect both laminar and turbulent boundary layers. These effects have been found to occur even for very small radii of curvature ( $\delta/R=100$ ). Qualitatively one finds that concave curvature tends to increase the skin friction and the heat transfer, whereas convex curvature tends to decrease the skin friction and heat transfer.

The effects of curvature on a boundary layer are different in magnitude for turbulent flow as compared to laminar flow, although still qualitatively similar. The fractional change in shear stress due to curvature in laminar flow is of the same order of magnitude as the ratio of the shear layer thickness to the radius of curvature ( $\delta/R$ ). In contrast, turbulent flow experiments show changes in shear stress an order of magnitude greater than for laminar flows of the same curvature [14]. This would indicate that streamline curvature increases the Reynolds stresses in turbulent flow roughly ten times as much as it changes the viscous stresses.

Experiments have shown that convex curvature affects the turbulence in the boundary layer such that large scale eddies are destroyed and the turbulent length scales reduced. These effects are stronger in the outer regions of the boundary layer than in the inner, and tend to be two dimensional in nature. These changes result in reduced heat transfer and skin friction coefficients [26,27,81]. In contrast, concave curvature tends to increase the turbulence intensity and Reynolds shear stress across the middle and outer parts of the boundary layer, causing an increase in the heat transfer

and skin friction. Furthermore, these effects can be three dimensional in nature. In laminar flow these three-dimensional effects manifest themselves as the so-called Taylor-Gortler longitudinal vortices. Unfortunately, the effects on turbulent boundary layers are still not completely defined and the topic somewhat controversial. Barlow and Johnston [6] have reported one of the most recent major studies in this area.

A peculiar characteristic of turbulent boundary layers subjected to a curved region and then returned to flat plate conditions, is a surprisingly slow recovery to flat plate conditions. Experimental results show that when curvature is suddenly removed after a region of convex curvature, that there is a quick partial recovery followed by a slow exponential-decay-like return to flat plate conditions [3,27].

The relative importance of curvature effects on transition have yet to be extensively studied. We do know that convex curvature is qualitatively stabilizing (ie. suppresses transition) and concave curvature destabilizing (ie. promotes transition). The study of Wang and Simon [93,(91)] is a recently reported effort to gain a better understanding of these effects. This study was done at two different levels of free-stream turbulence and with convex curvature. Their results seem to indicate that except for very low free-stream turbulence levels, the effect of convex curvature on transition is minor. This conclusion has important implications to the turbine blade heat transfer problem because in general, the free-stream turbulence levels are moderate to high over most of the blade. Thus, based on these results curvature effects would not be expected to strongly influence the transition process on turbine blades

### **1.3 LITERATURE SURVEY**

This literature review will focus on published work directly related to the low-Reynolds-number modeling technique developed in this thesis. Also, the experimental data with which to test the model will be reviewed. For perspective, a brief overview of turbulence modeling in general, and the place that two-equation "k- $\epsilon$ " models have among the spectrum of techniques available will also be given.

#### **1.3.1 Overview of Turbulence Modeling**

The calculation of transition by necessity requires the capability to model fully turbulent flow after the transition process is complete. Thus, all transition models must in some manner be coupled to a turbulence model. Since a large variety of methods to model turbulent flow have been developed over the years, a brief overview will be given here so as to place the k- $\epsilon$  turbulence model in perspective.

There are tremendous differences in complexity and range of applicability among turbulence models. Usually the cost of increased generality is a corresponding increase in complexity and computational effort. Furthermore, there are many more models that have been proposed, than there are that have been adequately tested against experimental data.

Turbulence models may generally be classified according to their complexity in the following manner;

- a) mixing-length models (zero order models)
- b) "N" equation models,  $N=1, 2, \dots$
- c) Large eddy simulation models (full Navier Stokes equations)

The oldest, simplest, most well known, and even today, most commonly used type of models are variations of Prandtl's original approach introduced back in 1925 [63]. This method relates knowledge of a so called mixing length " $l$ ", to the magnitude of the Reynolds shear stress through the concept of a turbulent or eddy viscosity " $u_t$ " proposed by Bousinesq [16] in 1877. This relationship is shown below.

$$-\rho \overline{u'v'} \approx u_t \left( \frac{\partial U}{\partial y} \right) = l^2 \left( \frac{\partial U}{\partial y} \right)^2 \quad (1.5)$$

One implication of models of this type is the presumed equivalence between the "generation" and "destruction" of the turbulence quantities affecting the Reynolds shear stress. This is the so called "near-equilibrium" assumption.

Application of the Prandtl mixing length method requires empirically determined knowledge of the mixing length. Fortunately a vast amount of experimental data has been gathered for this purpose. This has provided the engineer with a very valuable tool for analyzing many commonly encountered flows. Furthermore, with today's computer capabilities most calculations are quick and inexpensive. However, outside the domain for

which an appropriate mixing length has been empirically determined the method cannot be applied with confidence.

To calculate transition within the framework of a mixing-length model, additional empirically based sub-models must be introduced in order to determine the start, the length, and the path of transition. The basic idea is to algebraically vary the magnitude of  $u_t$  from zero to an appropriate fully turbulent value during the simulated transition process. An excellent review and evaluation of the these types of transition models as applied to convex-curved transitional boundary layers has been given by Park and Simon [60]. In a similar manner, Hylton et al [34] have evaluated, developed and applied this type of modeling to a variety of turbine blade data sets. Another study of this kind is that of Forest [25]. These studies have helped to establish the limits of applicability for models of this type, and also provided motivation to continue to explore higher order turbulence models so that the dependence on near-equilibrium empiricism can be relaxed.

The "N" equation model category implies that N additional transport equations are solved to determine local values of N statistical properties of the turbulence. These turbulence quantities are then related to appropriate effective transport properties in the time-averaged momentum and energy equations. The general form of these additional equations can usually be written as follows;

$$\rho \frac{D\phi}{Dt} - \text{div} (\Gamma_\phi \text{grad } \phi) - S_\phi = 0 \quad (1.6)$$

where  $\phi$  is the turbulence quantity,  $D/Dt$  is the substantial derivative,  $\Gamma_\phi$  is a diffusion coefficient, and  $S_\phi$  is a source term(s). This concept in turbulence modeling was first introduced by Kolmogorov [44] and Prandtl [64], but it was not until computers became available that these approaches could effectively be developed.

Most one equation models choose the turbulent kinetic energy "k", as the turbulence property of interest (some work has been done with an equation for the shear stress  $\overline{u'v'}$ ). Examples of models of this type include those of Bradshaw et al [15], Nee and Kovaszney [56], Hassid and Poreh [33], and Grundmann and Nehring [29]. To account for the near wall damping of turbulence, these models can be modified such that the turbulence viscosity includes a functional dependence on a local turbulence Reynolds number. Since in this method an appropriate length scale must still be prescribed algebraically according to previously determined empirical information, the method also suffers from a significant dependence on flow dependent empirical information.

A variation on the one equation approach that is simpler in some respects, is the solution of an integrated form of eq. (1.6) for the turbulent kinetic energy. This introduces additional information into the turbulence modeling without the need to solve an additional partial differential equation. However, other empirical and theoretical relationships must be used in addition to the prescription of the length scale profile in order to compute the flow. A model of this type has been developed by McDonald and Camarata [51] and was extended to incorporate a transition modeling capability by McDonald and Fish [52]. They also provide a way to include the effect of

free-stream turbulence and of surface roughness. This method was tested against a number of flows and shown to give reasonable results. However, when applied by Daniels and Browne [20] to the turbine blade data of Daniels [19], the method did not appear to show improvement over simpler mixing length models.

Two-equation turbulence models, like most one equation models, solve an equation for  $k$ , the turbulent kinetic energy. In addition, they also solve an equation for a parameter related to the local turbulence length scale. Choices for this parameter have varied, and three of the most common are " $\varepsilon$ ", the dissipation rate; " $W$ ", a pseudo-vorticity density; and " $k \cdot l$ ", where  $l$  is a turbulence length scale. These quantities are related to each other through the following definitions;

$$\varepsilon = \nu \overline{\frac{\partial u_i}{\partial x_k} \frac{\partial u_i}{\partial x_k}} \quad (1.7)$$

$$W = \left( \frac{\varepsilon}{C_D k} \right)^2 \quad (1.8)$$

$$l = \frac{C_D k^{3/2}}{\varepsilon} \quad (1.9)$$

where  $C_D$  is a constant.

Thus, it is possible to transform a set of  $k$ - $W$  equations, into say an equivalent set of  $k$ - $\varepsilon$  equations. This can be instructive for it clarifies that the real differences between the various models lie in the representation of the transport and source terms, and in the constants employed. Since "exact"

equations governing both  $k$  and  $\epsilon$  can be derived, the differences between the various models are introduced in the process of reducing these exact forms into a tractable approximate form suitable for computation. Modelers must choose which terms can be considered insignificant and dropped, and how best to approximate the higher order correlations that remain. These choices, and then the determination of the constants that are introduced, are the essence of turbulence modeling in the "N-equation" category.

Examples of the  $k$ - $\epsilon$  model that have been proposed are Harlow and Nakayama [32], and Jones and Launder [36]. Spalding [83], Ilegbusi and Spalding [35], and Saffman [75] have used the  $k$ - $W$  formulation, while Rotta [71] and Ng and Spalding [57-59] have developed  $k$ - $kl$  models. The reader is referred to an excellent monograph by Rodi [70], and a paper by Launder and Spaulding [48] for more detailed information.

It is important now to introduce and explain what a low-Reynolds-number form of a two-equation turbulence model is. In regions adjacent to solid walls, the character of turbulent motions is significantly altered. To properly account for this region, additional modifications must be made to the turbulent transport equations. This is usually done through the introduction of so called low-Reynolds-number functions. Thus any of the "high-Reynolds-number" two-equation models mentioned earlier, if further modified to account for this effect, can be referred to as a LRN form of that particular model.

This "LRN" type of formulation is central to the work contained in this thesis because of an additional characteristic possessed by these models. This characteristic is that the model becomes computationally valid in laminar,

transitional, and turbulent flow regimes without additional modifications. Furthermore, the influence of free-stream turbulence is naturally accounted for.

Since the focus of this thesis is on the use of two-equation models to predict transition, a more specific literature review and discussion relative to this topic will be given next. Also, in chapter two, a more detailed description of this approach from a mathematical and computational point of view will be given. Before doing this, a brief comment about even higher order turbulence models is in order.

"Reynolds stress or "stress equation" type models add additional partial differential equations which may compute all of the components of the turbulent stress tensor. One difficulty in applying this type of model to transitional boundary layers is the lack of appropriate low-Reynolds-number functions to simulate the near wall conditions. Another problem is the lack of information about the turbulence quantities which must be specified at the free-stream boundary. For each quantity calculated as part of the method, appropriate boundary conditions and starting profiles must be specified. Adequate information about these properties within the turbulent gas flow exiting the combustion chamber of a gas turbine engine is not currently available.

Finally, methods have been developed which actually compute the three-dimensional time dependent large eddy structure of the turbulent flow, but use simpler empirical models for the smaller scale turbulence. These methods are currently not sufficiently developed, and too computationally expensive and time consuming to be used for the problems considered here.

### **1.3.2 Predicting Transition with Two-Equation Turbulence Models**

It appears that Pridden [65] was the first to explore the use of a two-equation turbulence model in predicting transition on external boundary layer flows. Although Pridden's published work was basically limited to showing the potential of the procedure, the results of exploratory calculations for the pressure surface side of Turners experimental turbine blade data [87] were later published by Launder and Spaulding [48]. These results showed fairly good reproduction of the data. Unfortunately, no details of the procedure relative to initial conditions, boundary conditions, and or the application to simpler flows is given.

Wilcox [95,96] appears to be the next to use a two equation model to predict transition. He used the Saffman-Wilcox two-equation turbulence model [76] (a k-W formulation) and developed a method to modify two constants in the model with an empirical function of turbulence Reynolds number. His comparison with limited experimental data showed good agreement for the start of transition, but the predicted length of transition was not shown. Daniels and Browne [20] independently applied this method to the calculation of the turbine blade data of Daniels [19]. This was part of an evaluation of five different computational techniques. Unfortunately, one conclusion of this comparison and evaluation was that no significant advantages were gained from the use of this (or other) more complex

turbulence model over the mixing length type models tested. The major difficulty for all of the methods considered was the accurate prediction of the transition region. A further refinement [97] uses linear stability analysis to derive the empirical model function and the initial turbulence profiles, but has not yet been extensively tested to this author's knowledge.

Dutoya and Mitchard [23] develop a low-Reynolds-number  $k$ - $\epsilon$  model specifically for use in predicting gas-turbine blade heat transfer. In formulating the LRN functions, they provided for one constant to be calibrated with the onset of transition. For flat plate adiabatic flow they report good agreement between their model and the displacement thickness Reynolds number data at the onset of transition as predicted by McDonald and Fish [52]. They also compare the qualitative predictions of the model against the data from a cooled turbine inducer blade, showing correct trends on the suction side, but a problem with relaminarization on the pressure side. Flat plate calculations were not compared to specific data nor was the question of a correct transition length considered. Initial turbulence profiles were all specified relative to a Blasius velocity profile and calculations were started at  $Re_x=10^3$  for the flat plate cases. They reported (but do not document) that the transition predictions were insensitive to starting profiles for starting locations of  $Re_x<10^4$ . This does not agree with the results that will be described later in chapter 3. This model was later considered in an evaluation of of Low-Reynolds number models presented by Patel et al. [62]. They report that compared to the other models tested, this particular formulation was not as successful as many other models.

Arad et al. [4] applied the k- $\kappa$  turbulence model of Ng [57] modified by the LRN functions proposed by Wolfshtein [98], to predict transitional flow in axisymmetric boundary layers. No additional modifications were made to influence transition. Some limited comparisons between calculated Reynolds Numbers at the start of transition showed good agreement with data for zero pressure gradient flow. No discussion of transition length is made nor is there an indication as to whether or not the calculations are sensitive to the starting profiles used or to the starting location.

Hylton et al.[34], as part of their analytical methods evaluation process, attempted to use an implementation of the Jones-Launder two-equation LRN model [37] to predict flows over a variety of turbine blade cascade data sets. However, they found that their implementation failed to predict transition when applied to the turbine blade cascade data conditions. Although they indicate the method succeeded for simpler flows with free-stream turbulence, that work was not documented. Thus an evaluation of transition predictions was not possible.

Wang, Jen, and Hartel [90] have applied the LRN model of Jones and Launder [37] to the calculation of boundary layers on flat plates and to the turbine blade cascade data of Hilton et al. [34]. Although results from flat plate transition calculations are shown, no attempt to compare either the start or the length of transition with experimental data or with a correlation is given. Furthermore, the sensitivity of the calculations to the initial starting location and profiles is not discussed. For the airfoil predictions, a two-zone method near the stagnation region is developed for prescribing the turbulence boundary conditions. The key parameter is a critical velocity.,

which was correlated with turbulence level and a leading edge Reynolds number such that the data is reasonably reproduced. Also, the pressure side and suction side require different correlations.

Some of the most extensive previous work in this area is that of Rodi and Scheuerer [66,67,77]. They use the Low Reynolds Number model of Lam and Bremhorst [45], together with an empirically correlated method of prescribing the initial profiles for  $k$  and  $\epsilon$ . They are the first to begin to focus on the sensitivity of the calculations to the prescribed initial conditions and boundary conditions, pointing out the lack of adequate documentation of these areas in previously published work. The model was tested and an empirical coefficient " $a_1$ " calibrated against the data of Blair and Werle [8]. Also, the turbine blade data of Daniels [19] was calculated. More recently, the model was independently applied by Zerkle and Lounsbury [99], once again to the data of Blair and Werle [8], and then to vane cascade tests. This model was also tested as part of the evaluation section of the work presented in this thesis. This evaluation of the method resulted in two criticisms. The first, also recognized by Rodi and Scheuerer themselves, is that the length of transition is consistently under predicted. The second is that when tested against a range of flat plate zero pressure gradient flows with different free-stream turbulent intensities, the method did not consistently predict the start or end of transition in accordance with the correlation of Abu-Ghannam and Shaw [2]. The details of this evaluation and some of the computations are given in chapter 3.

In summary, a review of the literature reveals that the potential of LRN two-equation turbulence models to predict the qualitative aspects of

transition for boundary-layer flows with free-stream turbulence has clearly been shown by previously published work. However, in assessing this work it appears that further research may benefit from a closer evaluation and documentation of the prediction of simple flows before the models are applied to more complex situations. In particular, the capability to predict not only the start of transition, but also the path and the end of transition needs to be further clarified. Also, how best to specify, and where to specify the initial turbulence profiles needs to be better explored, and the sensitivity of the transition predictions to these choices determined.

### **1.3.3 Relevant Transition Experiments**

An important relationship in transition modeling is the experimentally observed correlation between the momentum thickness Reynolds number and turbulence intensity in the free-stream flow. Of those who have proposed a functional approximation for this relationship (see 1.1), Abu-Ghannam and Shaw [2] appear to have gathered the most comprehensive collection of experiments to base this on. It is also the most recent. This correlation is shown for zero-pressure gradient flow in Figure 1.2 and will be used both as a development tool, and as one method to check the accuracy of our transition calculations.

Although a large number of experiments have been conducted over the years investigating transition and free-stream turbulence, only a few of them can be used as specific test cases for a two-equation turbulence model. This is

because most have not documented a sufficient amount of the free-stream turbulence information. Typically, experiments have reported only a mean value, or an upstream value of the turbulence intensity. Since  $Tu_e$  can be related to  $k_e$ , this is sufficient for the  $k$  equation boundary condition. However, since the model requires boundary conditions for both  $k$  and  $\epsilon$ , this information alone is inadequate. Since calculations have shown that the value of  $\epsilon_e$  does have a perceptible influence on the location of the computed transition region, this cannot be neglected. At a minimum, one must know the value of  $Tu_e$  at at least two locations. This is then sufficient to estimate  $\epsilon$ . To the authors knowledge, the only work meeting these requirements are the experiments of Blair and Werle [8-9,(10-12)], Rued [72,(73-74)], Wang [91,(92-93)], and Abu-Ghannam [1].

Blair and Werle have investigated flow over a heated test section where the total wall to free-stream temperature differences were about 10 K. The effect of different levels of free-stream turbulence was found by installing four different turbulence generating grids resulting in free-stream turbulence intensities ranging from about .5-8%. All three components of the normal Reynolds stress were documented over the length of the test section. Tests included both zero pressure gradient flow, and flows with constant acceleration.

Rued has conducted an extensive number of tests for both constant and accelerating free-stream velocity conditions. Turbulence generating grids provided initial turbulence intensity levels from about 0.8 to 11%, but only  $\bar{u}'^2$  and  $\bar{v}'^2$  components were measured ( $\bar{w}'^2$  was assumed equal to  $\bar{v}'^2$ ). These were reported at various locations along the test section. The free-

stream air was heated and the test section cooled such that wall to gas temperature ratios of from 0.55 to 0.84 could be investigated.

Wang conducted an experimental study of transitional boundary layer flow with free-stream turbulence levels of 0.7 % and 2.0% and for a heated test section of nearly uniform heat flux. Local heat transfer coefficients, skin friction coefficients, profiles of velocity, temperature are reported. The streamwise direction turbulence intensity was measured at several locations, providing adequate data with which to determine the free-stream dissipation. The data of Wang was also used in a recent study of mixing length transition models, made by Park and Simon [60] which will provide an opportunity for comparison later in this thesis.

Abu-Ghannam's [1] experiments were somewhat different than the others with respect to the measurement technique and the experimental results. The experiments were conducted over a smooth aluminum flat plate in a wind tunnel of variable speed. The transition data was taken by continuously monitoring the velocity at a single fixed point near the wall while the tunnel speed was gradually changed. Free-stream turbulence intensities ranged from .5 to 5%. Heat transfer measurements were not taken.

## **1.4 OUTLINE OF THE THESIS**

This chapter has provided the basic aims and objectives of this thesis and tried to place them in their proper perspective relative to the problem of predicting external heat transfer on gas turbine blades. The importance of

transition has been described, and the predominant factors influencing this phenomenon introduced. An overview of techniques available to model this kind of problem has been provided, and a specific literature survey was made of previous attempts to use two-equation turbulence models in predicting transition. Finally, the data currently available which is sufficiently complete to provide an adequate basis for testing these models has been presented. A brief description of the remaining chapters in this thesis will now be given as a guide to the reader.

Chapter 2 will describe the mathematical representation of the problem and the numerical procedure used to solve the equations. This will begin by introducing the time averaged boundary-layer equations and the unknown turbulence quantities that must be determined. Next a more detailed description of  $k$ - $\epsilon$  LRN turbulence models will be given with a special focus on the Lam-Bremhorst [45] and Jones-Launder [36,37] models. Finally, the numerical solution procedure will be described. This will include an introduction to the Patankar-Spalding [61] solution procedure, the near wall grid refinement strategy used, and the method used to specify the initial starting profiles and boundary conditions.

In chapter 3, the prediction characteristics and capabilities of the Lam-Bremhorst and Jones-Launder models will be carefully evaluated with respect to transition on flat plates under the influence of free-stream turbulence. This work will show the importance of both the initial profiles specified, and the streamwise location where the calculations are started. Also, the effect of different free-stream turbulence conditions will be documented and compared with the recently developed correlation of Abu-

Ghannam and Shaw [2]. Finally, the results of the evaluation will be summarized to form the basis of improving the models in later work.

In chapter 4, the major objective of this thesis is addressed, ie. the development of an improved approach to simulating transition within the framework of  $k$ - $\epsilon$  LRN turbulence models. As a basis for this, four topics are initially considered. First, the method of Rodi and Scheuerer [66,67] is evaluated in more detail. This method addresses some of the difficulties described in chapter 3 and the results of this section provide motivation to continue seeking for better methods. Next, a defect in the Lam-Bremhorst model which adversely effects transition predictions for low free-stream turbulence conditions will be described and a solution to the problem explained. Third, the mechanism by which  $k$ - $\epsilon$  models simulate transition is explored in more detail and the results of chapter 3 clarified in this light. Finally, the importance of stability considerations is briefly discussed and the current limitations of  $k$ - $\epsilon$  LRN models with respect to this explained.

The next section in chapter 4 is dedicated to describing the modification which is proposed to improve the transition predictions. This starts with an explanation of the basic characteristics desired, and then provides a description of the actual modification chosen. The numerical implementation is explained and a method for calibrating the additional parameters introduced. The results of calibrating these parameters for the Lam-Bremhorst model are then presented.

In section 4.6, calculations of simple flat plate flows are presented as given by the modified LRN model of Lam-Bremhorst. These are compared to the results previously presented in chapter 3 and a significant improve-

ment demonstrated. In section 4.7, the application of the model to the Jones-Launder LRN model is explained, the calibration of the new parameters given, and the calculations also compared.

In order to clearly document the prediction capabilities of the new method, chapter 5 presents a comparison between the new method and the results of a large number of different experiments. The first section considers experiments in flat plate, zero pressure gradient conditions, but with turbulence intensities ranging from 1% to 9%. Data from three completely independent sources is used. Next, experiments that have the additional complication of acceleration are used. These experiments cover turbulence intensities of from 1-11%, and provide cases with both constant and strongly varying acceleration. Finally, the calculations are compared to the experimentally determined heat transfer data from two different turbine blades.

Chapter 6 provides closing remarks relative to the contributions made by this thesis. Also, some comments about the direction future work might best proceed are given.

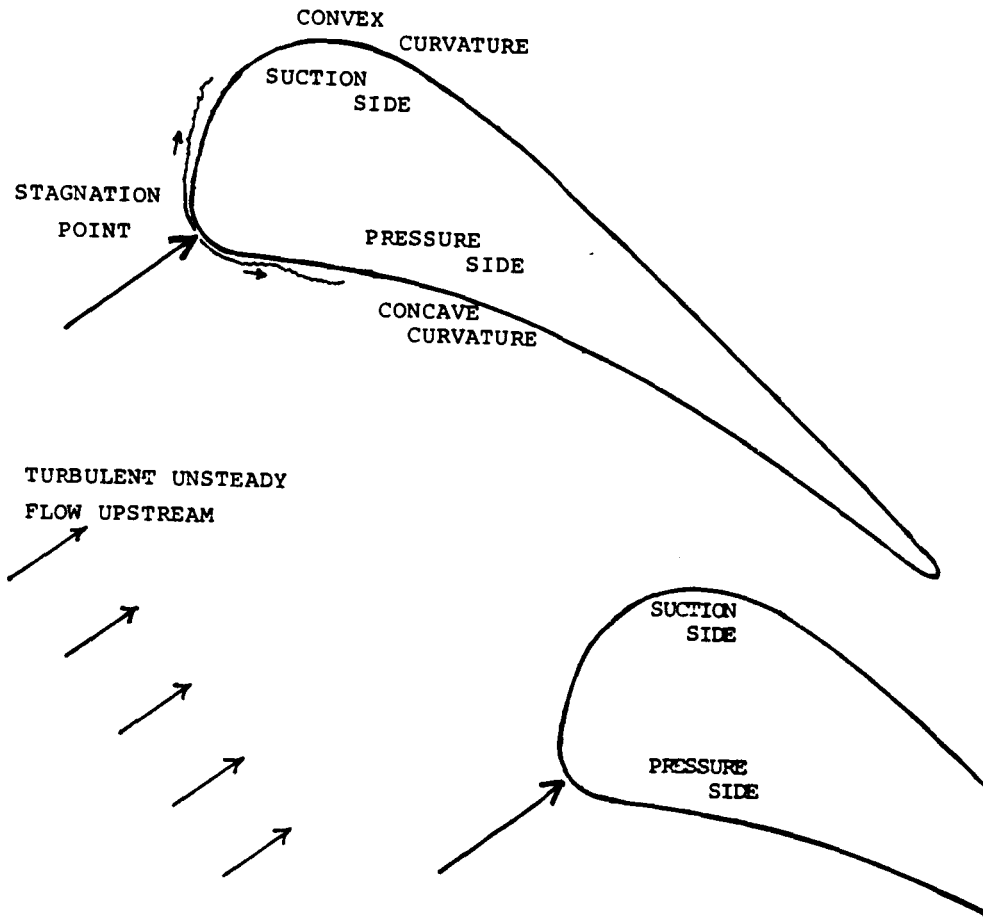


Figure 1.1 Cross-section of the flow around a turbine blade

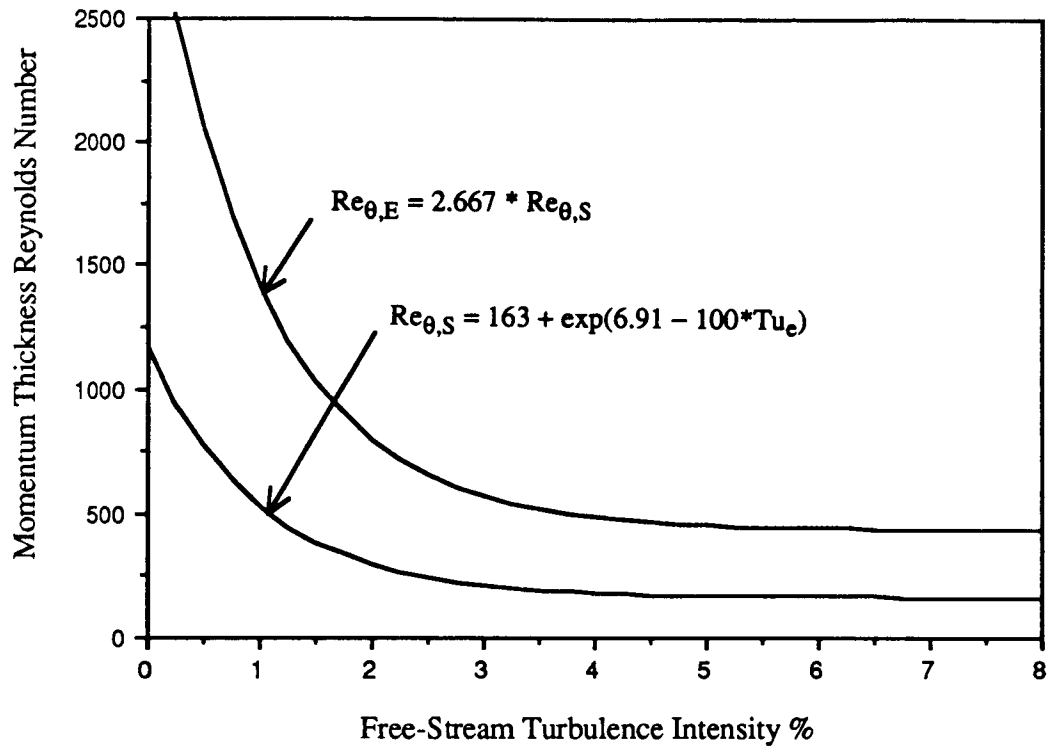


Figure 1.2 The relationship between  $Re_{\theta}$  and  $Tu_e$  for the start and end of transition as correlated by Abu-Ghannam and Shaw

## CHAPTER TWO

### THE MATHEMATICAL REPRESENTATION OF THE PROBLEM AND THE NUMERICAL SOLUTION PROCEDURE

#### 2.1 THE BOUNDARY LAYER EQUATIONS

Since the focus of this thesis is on the thin viscous region near a solid wall, the equations used in the analysis can be the simpler "boundary-layer" equations. These equations are approximations which describe the conservation of mass, momentum, and energy. To describe the turbulence effects these equations will be solved in their time-averaged, but steady state form. We also will neglect variations in the span-wise direction of the blade or test section, and reduce the equations to their two-dimensional form. Since velocities at certain locations around a turbine blade often approach and sometimes exceed mach 1, and temperature variations can also be large, in general we will not be able to invoke incompressible, constant property simplifications. Furthermore, the conversion of mechanical energy to thermal energy through viscous effects cannot be neglected in the energy equation. However, we will assume that  $C_p$  is constant in deriving the energy equation. This assumption, while having only a very small effect on our computed results, allows important simplifications.

Since the derivation of the boundary layer equations can be found in many standard reference books, it will not be repeated here. A more important need is to show them as they are properly expressed in the nomenclature and symbols that will be used throughout the remainder of this thesis. In Fig. 2.1, a simple sketch of the geometry, x-y coordinate system, and basic nomenclature is given. For a two-dimensional rectangular coordinate system such as this, the conservation of mass and momentum can be written in the following form.

$$\frac{\partial}{\partial x}(\rho U) + \frac{\partial}{\partial x}(\rho \tilde{V}) = 0 \quad (2.1)$$

$$\rho U \frac{\partial U}{\partial x} + \rho \tilde{V} \frac{\partial U}{\partial y} = -\frac{dP}{dx} + \frac{\partial}{\partial y}(\mu \frac{\partial U}{\partial y} + \rho u'v') \quad (2.2)$$

where  $U$  and  $V$  are the time averaged mean velocities, and  $u'$  and  $v'$  are the instantaneous velocity fluctuations. The overbar " $\bar{\quad}$ " implies a time averaged quantity, the prime a fluctuating quantity, and the expression  $\tilde{V}$  indicates a mass weighted averaging (see Cebeci and Smith [17]) where

$$\rho \tilde{V} = \rho V + \rho \bar{v'} \quad (2.3)$$

It is convenient for high speed flow to solve the energy equation in terms of the "total" or "stagnation" enthalpy  $H$ , defined as follows;

$$H = h + \frac{U^2}{2} \quad (2.4)$$

Assuming that the specific heat is constant and the gas is ideal, the static temperature to static enthalpy relationship, and the state equation are simply;

$$h = C_p T \quad (2.5)$$

$$\rho = \frac{P}{RT} \quad (2.6)$$

Using these definitions, the total enthalpy equation can be written as;

$$\rho U \frac{\partial H}{\partial x} + \rho \tilde{V} \frac{\partial H}{\partial y} = \frac{\partial}{\partial y} \left\{ \frac{\mu}{Pr} \frac{\partial H}{\partial y} - \rho h'v' + U \left[ \left(1 - \frac{1}{Pr}\right) \mu \left(\frac{\partial U}{\partial y}\right) - \rho u'v' \right] \right\} \quad (2.7)$$

To solve these equations, we must specify the turbulent shear stress and heat flux. To do this we define a "turbulent" or "eddy" viscosity, and a turbulent Prandtl number such that;

$$-\rho u'v' = u_t \left(\frac{\partial U}{\partial y}\right) \quad (2.8)$$

$$-\rho h'v' = \frac{u_t}{Pr_t} \left(\frac{\partial h}{\partial y}\right) \quad (2.9)$$

For the purposes of this thesis, the turbulent Prandtl number will be assumed constant and equal to 0.9. Although this is not in general true, it has been found to be a reasonably good approximation for most situations and should not detract from our major focus, which is the transition predictions. The role of the turbulence model now becomes that of determining the correct value of  $u_t$ .

## 2.2 THE TURBULENCE MODELS EMPLOYED

The purpose of this section is to clearly describe the mathematical representation and implementation of the LRN k- $\epsilon$  type turbulence models used in this thesis. After providing a generalized description and outline of all of the models currently proposed, the details of two relatively popular models will be given and differences explained.

### 2.2.1 k- $\epsilon$ Low-Reynolds-Number Turbulence Models

Although many different proposals have been suggested for introducing LRN functions into the k- $\epsilon$  turbulence model, Patel et al. [62] have shown that it is possible to generalize these variations by writing the basic equations in a manner to be described here. The basic relation defining the turbulent viscosity is

$$u_t = \rho C_\mu f_\mu \frac{k^2}{\hat{\epsilon}} \quad (2.10)$$

where  $C_\mu$  is a constant,  $f_\mu$  is one of the LRN functions to be described, and  $k$  and  $\hat{\epsilon}$  are the turbulent kinetic energy and dissipation rate function respectively. The top hat symbol has been placed over  $\epsilon$  so that differences between the meaning of  $\epsilon$  used by the various models can be clarified. The relationship between  $\epsilon$  as defined in eq. (1.7), and  $\hat{\epsilon}$ , can be written as

$$\varepsilon = \hat{\varepsilon} + D, \quad (2.11)$$

where in some models the quantity  $D$  is assigned to be a function of  $k$ . The reason for the addition of the function  $D$  by these developers, is to provide a means whereby the boundary condition in the  $\varepsilon$  equation can be specified as zero. More will be explained about this later.

The transport equations for  $k$  and  $\varepsilon$  follow the pattern of equation (1.6) and can be written as;

$$\rho U \frac{\partial k}{\partial x} + \rho \tilde{V} \frac{\partial k}{\partial y} = \frac{\partial}{\partial y} \left\{ \left( \mu + \frac{\mu_t}{\sigma_k} \right) \frac{\partial k}{\partial y} \right\} + \mu_t \left( \frac{\partial U}{\partial y} \right)^2 - \rho (\hat{\varepsilon} + D) \quad (2.12)$$

$$\rho U \frac{\partial \hat{\varepsilon}}{\partial x} + \rho \tilde{V} \frac{\partial \hat{\varepsilon}}{\partial y} = \frac{\partial}{\partial y} \left\{ \left( \mu + \frac{\mu_t}{\sigma_\varepsilon} \right) \frac{\partial \hat{\varepsilon}}{\partial y} \right\} + \frac{\hat{\varepsilon}}{k} \left\{ C_1 f_1 \mu_t \left( \frac{\partial U}{\partial y} \right)^2 - \rho C_2 f_2 \hat{\varepsilon} \right\} + E \quad (2.13)$$

Looking closely, one can see that contained within equations (2.10) to (2.13) there are five empirical constants;  $C_\mu$ ,  $C_1$ ,  $C_2$ ,  $\sigma_k$ ,  $\sigma_\varepsilon$ , and five empirical functions;  $f_\mu$ ,  $f_1$ ,  $f_2$ ,  $D$ , and  $E$ . The five constants all pertain to conditions far from the wall, and only small differences exist between different models. They all have been introduced during the process of simplifying more exact forms of these equations (which are derived from the Navier-Stokes relations). The values for these constants are found by recourse to certain limiting flow conditions where experimental data is known, and to numerical optimization ( See for example Rodi [70]). The values used in this thesis are those suggested as "standard" by Launder and Spaulding [48]. They are given in Table 2.1.

TABLE 2.1 The k- $\epsilon$  Turbulence Model Constants

$C_\mu$	$C_1$	$C_2$	$\sigma_k$	$\sigma_\epsilon$
.09	1.44	1.92	1.0	1.3

Turbulent motions immediately adjacent to solid walls are significantly influenced by the presence of the wall. Here the magnitude of the effective turbulent viscosity becomes small, and the effects of the molecular viscosity become important. Experimental work has shown that in some turbulent flow situations there exists a common structure or behavior near the wall. Under these conditions both the mean velocities and the measurable turbulence quantities exhibit nearly universal behavior. The knowledge of this structure has allowed the formulation and use of the so-called wall functions. These functions algebraically bridge the near wall region and eliminate the need for more expensive and time consuming calculations with a fine grid near the wall.

Unfortunately, there are also many flow situations of interest where this near wall similarity breaks down. Large pressure gradients and mass transfer at the wall, for example, both result in significant alterations of the near wall flow, thus wall functions cannot always be used. To incorporate these effects into turbulence models, a variety of different suggestions have been made. A well known example of one such modification for mixing length type turbulence models is the Van Driest damping function [88]. The purpose for the functions  $f_\mu$ ,  $f_1$ , and  $f_2$  is to provide a somewhat similar kind

of modifying influence on the k- $\epsilon$  model, thus extending the validity of the equations clear through the viscous sub-layer to the wall. To do so, they are made functions of one or more "turbulent Reynolds numbers", or the inner wall coordinate  $y^+$ . These are defined as follows;

$$R_t = \frac{k^2}{\nu \epsilon} \quad (2.14)$$

$$R_y = \frac{\sqrt{k} y}{\nu} \quad (2.15)$$

$$y^+ = \frac{y u_\tau}{\nu} \quad (2.16)$$

A good discussion of these functions is given by Patel et al [62] and the reader is referred there for a discussion of each of these functions individually. Here we will press on and consider the specific low-Reynolds-number functions incorporated into two of the more popular models.

### 2.2.2 The Jones-Launder and Lam-Bremhorst Models

The specific LRN functions of the Jones-Launder model and of the Lam-Bremhorst model as used in this thesis are given in Table 2.2. These two models were chosen for closer evaluation in this thesis for a number of reasons. First, they both have seen application to a variety of different flows by a number of independent researchers. Furthermore, both have been applied by previous researchers to predicting transitional flows on turbine blades [66,67,90]. Second, when compared with other LRN k- $\epsilon$  models, tests

have shown both of these to be among the best at predicting the characteristics of fully turbulent flow[62]. Third, they represent two somewhat different approaches to introducing LRN modifications.

TABLE 2.2 The Low Reynolds-Number Functions used in the Jones-Launder and Lam-Bremhorst models

	Jones-Launder Model	Lam-Bremhorst Model
$f_{\mu}$	$\exp\left(\frac{3.4}{[1 + .02R_t]^2}\right)$	$(1 - \exp(-.0163R_y))^2 \left(1 + \frac{20}{R_t}\right)$
$f_1$	1.0	$1. + \left(\frac{.055}{f_{\mu}}\right)^3$
$f_2$	$1. - 0.3\exp(-R_t^2)$	$1. - \exp(-R_t^2)$
E	$2\nu\mu_t \left(\frac{\partial U}{\partial y}\right)^2$	0
D	$2\nu \left(\frac{\partial \sqrt{k}}{\partial y}\right)^2$	0
$\hat{\epsilon}_w$ -boundary condition	0	* $\frac{\partial \hat{\epsilon}}{\partial y} = 0$

\* See Patel, Rodi, and Scheuerer [62]

The differences between the models stem from two basic choices; what dissipation rate variable to use, and how to functionalize  $f_\mu$ . Exactly at the wall, the value of  $k$  must go to zero. However, it can be shown that the dissipation rate defined in equation (1.7) does not. The correct boundary condition for  $\varepsilon$  is

$$\varepsilon \Big|_{y=0} = \nu \frac{\partial^2 k}{\partial y^2} \Big|_{y=0} \quad (2.17)$$

For computational reasons, many models have avoided this boundary condition by introducing a simple change of variables. By choosing a function  $D$  (see equation 2.11) such that  $D \Big|_{y=0} = \varepsilon \Big|_{y=0}$ , the boundary condition for the variable  $\hat{\varepsilon}$  becomes zero.

The function  $D$  shown for the Jones-Launder model in Table 2.2 is one possible choice which allows  $\hat{\varepsilon}$  to be specified as zero at the wall. The Lam-Bremhorst model on the other hand introduces no such change of variables. The original approach of Lam and Bremhorst was simply to apply the boundary condition (2.17) directly. However, others have found that due to the influence of the other LRN functions chosen, the computations are relatively insensitive to this boundary condition, and the simpler condition shown in Table 2.2 can be applied without any change in predictions [62].

Another significant difference relates to the turbulent Reynolds numbers chosen to correlate  $f_\mu$  with. In the case of Jones-Launder, a single parameter correlation with  $R_t$  is introduced. This implies only an indirect effect of the wall through the variables  $k$  and  $\varepsilon$ . In contrast, the Lam-

Bremhorst formulation makes  $f_{\mu}$  a function of both  $R_t$  and  $R_y$ , which introduces a very direct dependence on the relative proximity of the wall.

The details of how each of the other functions were chosen can be found in the original papers by Lam and Bremhorst [45], and by Jones and Launder [37]. It is important to know that although some of the functional dependence can be justified directly through empirical or physical arguments, other choices were made add-hoc. This freedom to explore different approaches coupled with the initial success that came from models such as the Jones-Launder model, is one of the main reasons that so many different models have been introduced in recent years.

Although others have explored the effect these differences have on fully turbulent predictions, the work in this thesis is the first such attempt known by the author to explore the effect these choices have on the transition prediction capabilities.

### **2.3 THE NUMERICAL SOLUTION PROCEDURE**

A number of excellent computational methods have been developed in recent years to efficiently solve sets of two-dimensional parabolic partial-differential equations. Because the purpose of this thesis is not related to developing an improved solution algorithm, any of these methods could have been used. However, the correct and consistent application of any method is essential for the numerically computed results to be reliable. Thus the purpose of this section is to discuss the numerical solution techniques and procedures used in this development work.

Based on the author's familiarity with the Patankar-Spalding solution procedure [61] and its common use in engineering applications, this method was used throughout this thesis work. Since details of this algorithm can be found elsewhere, only a summary will be given here by way of introduction. Next, the method of near-wall grid refinement and the specification of the streamwise direction step size will be discussed. This is important since sufficient resolution of all spatial gradients is essential to any numerical method in assuring that the solution is truly accurate. In 2.3.3, the approach to specifying the boundary conditions and the initial starting profiles will be described. And in 2.3.4, a few comments about some practical aspects of representing the different LRN functions will be given.

### **2.3.1 The Patankar-Spalding Parabolic Solution Method**

The solution method of Patankar and Spalding is based on solving the governing equations in the " $x, \omega$ " coordinate system, instead of the more traditional " $x, y$ " system. Here  $\omega$  is a non-dimensionalized form of the stream-function coordinate  $\Psi$  which von-Mises first suggested (see Schlichting [78]). The utility of this transformation is two-fold. First, the normal velocity  $V$  is eliminated from the equations and continuity is identically satisfied. Second, the formulation allows the computational grid to vary smoothly and naturally with the growth of the boundary layer. This variation is regulated during the computations by appropriate control of the entrainment of free-stream fluid into the computational region.

As an example, the time averaged streamwise momentum equation can be written in this coordinate system as;

$$\frac{\partial U}{\partial x} + b\omega \frac{\partial U}{\partial \omega} = \frac{\partial}{\partial \omega} \left( c \frac{\partial U}{\partial \omega} \right) - \frac{1}{\rho U} \frac{dP}{dx} \quad (2.18)$$

where

$$b = \frac{\dot{m}_E''}{\psi_E} \quad (2.19)$$

$$c = \frac{\rho (\mu + u_t)}{2 \psi_E} \quad (2.20)$$

and  $\omega$  and  $\psi$  are defined as;

$$\omega = \frac{\psi}{\psi_E} \quad (2.21)$$

$$\psi = \left[ \int_0^y \rho U dy \right]_{x=\text{constant}} \quad (2.22)$$

The subscript "E" refers to the free-stream edge of the computational domain, and  $\dot{m}_E''$  is the entrained mass flow rate at the edge, which is controlled as part of the computational procedure.

The finite differencing equations are developed by integrating the appropriate transport equations over a small but finite control volume. To do this, one assumes that over the extent of the control volume, the profiles of the dependent variables behave in a certain linear fashion. The streamwise derivatives are "up-winded", thus yielding an implicit set of coupled algebraic relations. Since the resulting matrix has coefficients in the center

three diagonals only, a very efficient tri-diagonal-matrix algorithm can be used to solve these equations.

Over each forward step, the equations are decoupled from each other. For example, when  $k$  is required in a source term in the  $\epsilon$  equation, the old "upstream" value at that location is used. This choice requires that the step-size in the stream-wise direction be kept small, and the sensitivity of the results carefully checked to insure the accuracy of the solution. For most of the calculations presented here, setting  $dx=.5*\theta$  was found to be completely adequate in satisfying this requirement.

A more detailed description of this entire method can be found in [61].

### **2.3.2 Near Wall Grid Refinement**

In turbulent flow, the important viscous sublayer region is very thin relative to the total boundary-layer thickness. It is also a region of large velocity gradients. Thus to accurately approximate the solution of equations (2.1)-(2.13), a refined computational grid must be used in this very near wall region in order to properly resolve the important physical effects. Conversely, in the outer regions of the boundary layer, gradients are generally small because the velocity, enthalpy, and turbulence quantities asymptotically approach their free-stream values. In this region, a relatively coarse computational grid is sufficient.

In situations such as this, it is advantageous to use a variable grid. How this was specified in this thesis will be explained here.

In figure 2.2 a sketch of y direction control volumes and node locations is shown. Note that for any grid of M1 nodes, there exist M1-2 finite control volumes within the computational domain. For the purpose of generating a variable grid, it is useful to define a grid coordinate " $\chi$ ", in terms of these node locations. At any node location  $J > 1$ ,  $\chi$  can be defined as;

$$\chi = \frac{J-1.5}{M3} \quad (2.23)$$

A common way to specify the actual grid location in terms of the grid coordinate is to set

$$\frac{Y(J)}{Y(M1)} = \chi^b \quad (2.24)$$

where the exponent b must be greater than 1 to refine the grid near the wall.

One disadvantage of the simple relationship (2.24), is that when M1 is fairly large (say on the order of 100), and b is set greater than 1 (say 3), the variation in the widths of neighboring control volumes very near the wall becomes quite large. This is detrimental to computational accuracy and should be avoided.

To avoid the difficulty mentioned, and still refine the grid adequately in the near-wall region, the following two-region relationship between  $\chi$  and  $Y(J)$  was adopted.

$$\frac{Y(J)}{Y(M1)} = \begin{cases} m \chi & ; \chi < \chi_1 \\ a\chi^b + c & ; \chi > \chi_1 \end{cases} \quad (2.25)$$

where at  $\chi = \chi_1$ , the function is continuous through the first derivative, i.e.;

$$m\chi_1 = a(\chi_1)^b + c \quad (2.26)$$

$$\frac{1}{Y(M1)} \frac{\partial Y(J)}{\partial \chi} = m = a b (\chi_1)^{b-1} \quad (2.27)$$

This procedure has  $Y(J)$  varying linearly with  $\chi$  in the very near wall region  $\chi < \chi_1$ , but proportional to  $\chi^b$  for  $\chi > \chi_1$ . Figure 2.3 is useful in depicting this relationship and also in explaining the practical implementation of this procedure.

To implement this procedure, three quantities must be specified; the total computational boundary layer width  $Y(M1)$ , the matching point in terms of the grid coordinate  $\chi_1$ , and the exponent  $b$ . With this information, equations (2.26)-(2.27) can be applied to yield;

$$\frac{Y(J)}{Y(M1)} = \begin{cases} \eta [b (\chi_1)^{b-1}] \chi & ; \chi < \chi_1 \\ \eta [\chi^{b+(b-1)(\chi_1)^b}] & ; \chi > \chi_1 \end{cases} \quad (2.28)$$

where

$$\eta = \frac{1}{1 + (b-1)(\chi_1)^b} \quad (2.29)$$

Equations (2.25)-(2.29) have all been represented in terms of the normal rectangular coordinate  $y$ . However, as mentioned in section 2.3.1, the Patankar-Spalding solution method uses the  $\omega$  coordinate defined in equations (2.21) and (2.22). Thus, to implement these relationships using the Patankar-Spalding solution method, equation (2.22) must be integrated in terms of the initial starting velocity profile to yield the appropriate grid distribution in terms of  $\omega$ .

For most of the computations presented here,  $M_1$  was set equal to 88,  $\chi_1 = .1$ , and  $b \approx 2.5$ . These settings gave approximately 15 control volumes within the viscous region  $y^+ < 10$  of a fully turbulent boundary layer. Tests showed that the grid thus specified was sufficiently refined to yield essentially grid independent results.

### **2.3.3 Specification of Initial Starting Profiles and Boundary Conditions**

Since equations (2.1)-(2.13) are not valid at  $x=0$ , before they can be solved, profiles for  $U$ ,  $k$ , and  $\hat{\epsilon}$  at some appropriate initial starting location " $x_i$ " must be given. In addition, correct boundary conditions must be continuously specified as the computations march forward in the streamwise direction. Except for the specification of  $x_i$ , the procedures adopted for accomplishing this task will be explained here. Further discussion of this aspect of the problem will also be given in succeeding chapters.

**Velocity:**

For the velocity, we specify  $U=0$  at  $y=0$ , and  $U=U_e$  at  $y=Y(M1)$ . The free stream velocity  $U_e$  can in general vary with  $x$ , and so must be specified in terms of the experimental data.

To approximate the variation of  $U$  with  $y$  at  $x=x_i$ , a Pohlhausen polynomial representation of the velocity profile was used, such that;

$$\frac{U}{U_e} = 2\left(\frac{y}{\delta}\right) - 2\left(\frac{y}{\delta}\right)^3 + 4\left(\frac{y}{\delta}\right)^4 + \frac{\Lambda}{6}\left(\frac{y}{\delta}\right)\left(1 - \frac{y}{\delta}\right)^3 \quad (2.30)$$

This requires an approximation for the local boundary layer thickness  $\delta$ , and an acceleration parameter  $\Lambda = \delta^2(\partial U/\partial x)/\nu$ . The following steps illustrate how this was accomplished;

- i) Apply the method of Thwaites to determine  $\theta$  at  $x=x_i$ . This requires integration of the following approximate relationship;

$$\theta^2 \approx \frac{0.45\nu}{U^6} \int_0^x U^5 dx \quad (2.31)$$

- ii) Calculate the local acceleration parameter  $\lambda$  defined as

$$\lambda = \frac{\theta^2}{\nu} \frac{\partial U}{\partial x} \quad (2.32)$$

and find the shear correlation  $S(\lambda)$  from the tabulated correlation of Thwaites [85] (also found in White [94] pg 316, Table 4-8).

iii) Iteratively solve the following two equations for  $\Lambda$  and  $\delta$ . Note that eq. (2.33) is the functional relation for  $S$  derived directly from the Pohlhausen Polynomial.

$$S(\lambda) = (2 + \Lambda) \sqrt{\frac{\lambda}{\Lambda}} \quad (2.33)$$

$$\Lambda = \lambda \left(\frac{\delta}{\theta}\right)^2 \quad (2.34)$$

A simple fortran program to accomplish this task is included in the appendix of this thesis.

### k and $\epsilon$

The wall boundary conditions for  $k$  and  $\epsilon$  have been explained previously in Section 2.2.2. In the free-stream, equations (2.12) and (2.13) reduce to a set of coupled ordinary differential equations as all cross-stream derivatives vanish. They are;

$$U_e \frac{dk_e}{dx} = -\epsilon_e \quad (2.35)$$

$$U_e \frac{d\epsilon_e}{dx} = -C_2 \frac{\epsilon_e^2}{k_e} \quad (2.36)$$

The specification of  $k_e$  and  $\epsilon_e$  at any location  $x_1$  is sufficient to determine what the boundary values are at any other location  $x$  by integrating equations (2.35) and (2.36). Alternatively, the specification of  $k_e$  at two locations is

also sufficient to allow one to determine the correct value of  $\epsilon_e$  at any other location. This is may be the situation when comparing with experimental data. However, since experiments generally only report turbulence intensities,  $k$  must be determined from the following relationship;

$$k_e = 1.5(Tu_{e,T}U_e)^2 \quad (2.37)$$

When  $\overline{u'^2}$  is the only component measured, we must assume the turbulence is isotropic, and the total turbulence intensity  $Tu_{e,T}$  appearing in equation (2.37) (see eq. (1.2)) is replaced by the streamwise turbulence intensity  $Tu_e$  defined in equation (1.1).

In any case, once  $k_e$  and  $\epsilon_e$  are determined at our initial starting location, equations (2.35) and (2.36) are simply integrated each step to determine the correct free-stream value at the next streamwise location.

The specification of the initial profiles for  $k$  and  $\epsilon$  when starting in the laminar region is a problem. Very little experimental data exists in the literature to guide us in this choice. The only applicable work the author has found is that of Dyban, Epik, and Suprun [24]. They report measured  $\overline{u'^2}$  values through a "pseudo-laminar" boundary layer at  $Re_x = 6.2 \times 10^3$ , and for several different levels of free-stream turbulence. However, the limited nature of the data presented makes it difficult to justify basing ones calculations upon it. Previous workers have had to rely on add-hoc methods with little more than the known boundary conditions and intuition to guide them. One such practice is that proposed by Rodi and Scheuerer [66,67]. They propose to set

$$k = k_e \left( \frac{U}{U_e} \right)^n, \quad n=2 \quad (2.38)$$

$$\varepsilon = a_1 k \frac{\partial U}{\partial y}, \quad \varepsilon > \varepsilon_e \quad (2.39)$$

where  $x_i$  is located such that  $Re_\theta=100$ , and  $a_1$  is an empirical function correlated to the free-stream turbulence intensity.

The importance of knowing the correct initial profiles of  $k$  and  $\varepsilon$  depends entirely upon how sensitive the results are to these values. This is one of the items not clearly documented in previous work and which will be investigated in this thesis. Leaving the justification for the next chapter, the practice adopted here is to apply equations (2.38) and (2.39), but set  $a_1=1$ , and choose  $x_i$  such that  $Re_\theta < 25$ .

### Total enthalpy:

The total enthalpy in the free-stream was assumed to remain constant for all cases considered. At the wall, either the experimental wall temperature, or experimental wall heat flux was related to the appropriate enthalpy or enthalpy flux through equations (2.4)-(2.5)

For flat plate flows the starting enthalpy profile was derived from the approximate temperature-velocity profile relationship given below.

$$T = T_w + (T_e - T_w) \frac{U}{U_e} \quad (2.40)$$

Since each of the experimental data sets with which calculations were compared had a small unheated starting length where the wall was assumed adiabatic,  $T_w$  was set equal to  $T_e$  for these cases. The total enthalpy profile was then simply backed out using equations (2.4) and (2.5). This procedure is identical to that of Rodi and Scheuerer [66,67].

For the turbine blade calculations, which are started near a stagnation point, this procedure was modified to allow the thermal boundary layer  $\delta_T$ , to be different than the velocity boundary layer. The essence of this is to use a simple estimate of the the stagnation point heat transfer coefficient as a means of varying the starting value of  $\delta_T$ .

Crawford and Kays [18] suggest that stagnation point heat transfer on a two-dimensional cylinder of radius  $R$  can be estimated by;

$$Nu_R = \frac{hR}{k} \approx 0.81 Re_R^{.5} Pr^{.4} \quad (2.41)$$

where

$$Re_R = \frac{\rho U_\infty R}{\mu} \quad (2.42)$$

and

$$q_w = -k \frac{\partial T}{\partial y} \Big|_{y=0} \approx h (T_\infty - T_w). \quad (2.43)$$

If we assume that the temperature profile remains similar to equation (2.40), but that it is stretched by the ratio  $\delta_T/\delta$ , we can rewrite eq. (2.40) as

$$T = T_w + (T_e - T_w) \frac{U}{U_e} [y/\delta_T] \quad (2.44)$$

where the term  $\frac{U}{U_e}[y/\delta_T]$  implies that  $\delta_T$  has replaced  $\delta$  in eq. (2.30).

At the wall we can now write that

$$\frac{\partial T}{\partial y}\bigg|_{y=0} = \frac{(T_w - T_e)}{U_e} \frac{\delta}{\delta_T} \frac{\partial U}{\partial y}\bigg|_{y=0} \quad (2.45)$$

and

$$\mathbf{h} = \frac{k}{U_e} \frac{\delta}{\delta_T} \frac{\partial U}{\partial y}\bigg|_{y=0} \quad (2.46)$$

For a Pohlhausen polynomial given by eq (2.30),

$$\frac{\partial U}{\partial y}\bigg|_{y=0} = \frac{U_e}{\delta} \left[ 2 + \frac{\Lambda}{6} \right] \quad (2.47)$$

thus

$$\mathbf{h} = \frac{k}{\delta_T} \left[ 2 + \frac{\Lambda}{6} \right] \quad (2.48)$$

Applying the definition of  $Nu_R$  given in eq. (2.41) and solving for  $\delta_T$  we finally arrive at;

$$\delta_T = \frac{R}{Nu_R} \left[ 2 + \frac{\Lambda}{6} \right] \quad (2.49)$$

Equation (2.44) can now be directly applied by letting  $R$  be the local radius of curvature on the turbine blade at the stagnation point. Since the starting location  $x_1$  is very near the stagnation point, we neglect any change due to this initial offset and determine a corresponding total enthalpy profile by use of eqs. (2.4) and (2.5). It should be noticed that since the velocities are all

relatively low in this near stagnation region and also since this is only an approximation, differences between total and static temperature have been neglected.

Equations (2.44) and (2.49) are only simple approximations that were developed for convenience of use in this thesis. Because of this they can not be recommended as very accurate. However, since the stagnation point heat transfer problem is not the focus of this thesis, it was deemed sufficiently accurate for the work considered herein. Others have developed more accurate, albeit more complicated procedures which can incorporate the effects of free-stream turbulence and compressibility on the estimation of the stagnation Nusselt number. One such method that is recommended is the procedure developed by Hylton et al. [34], which is a modified form of the Miyazaki and Sparrow approach [54].

#### **2.3.4 Numerically Representing $f_{\mu}$ and $f_1$**

Near the wall, the LRN functions  $f_{\mu}$  and  $f_1$  adopted by Lam and Bremhorst become very small and very large respectively. In fact, the function  $f_1$  is actually singular at  $y=0$ . As a result, computational difficulties can arise if these functions are not properly represented. A typical result is that the calculation will "crash" when numbers either larger or smaller than the limits of the computer are encountered in computation.

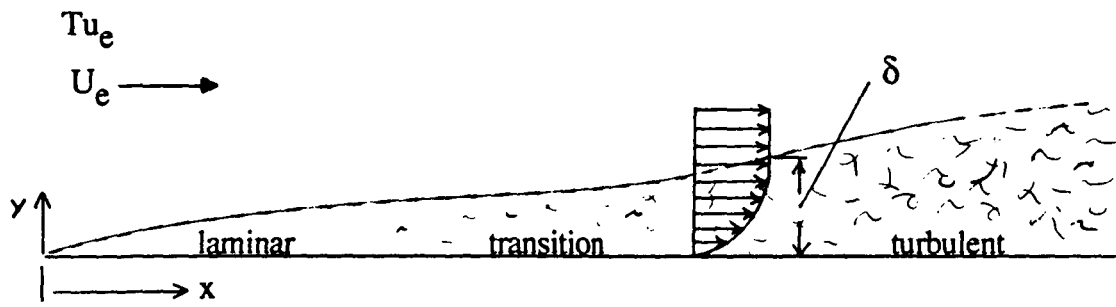
To avoid these problems a very small number was introduced at appropriate places in the numerical representation of the functions. This practice was also followed in the source terms in the  $k$  and  $\epsilon$  equations which

have a  $k$  in the denominator. For the computations presented in this thesis,  $f_\mu$  and  $f_1$  were represented as follows;

$$f_\mu = (1 - \exp(-.0163R_t - s))^2 \left(1 + \frac{20}{R_t + s}\right) \quad (2.50)$$

$$f_1 = 1 + \left(\frac{.055}{f_\mu + s}\right)^3 \quad (2.51)$$

where  $s = 10^{-10}$ .



$$Tu_{e,T} = \frac{\sqrt{\frac{1}{3}(\overline{u'^2} + \overline{v'^2} + \overline{w'^2})}}{U_e}$$

$$k_e = \frac{(\overline{u'^2} + \overline{v'^2} + \overline{w'^2})}{2}$$

Figure 2.1 Transitional flow developing on a flat plate with free-stream turbulence

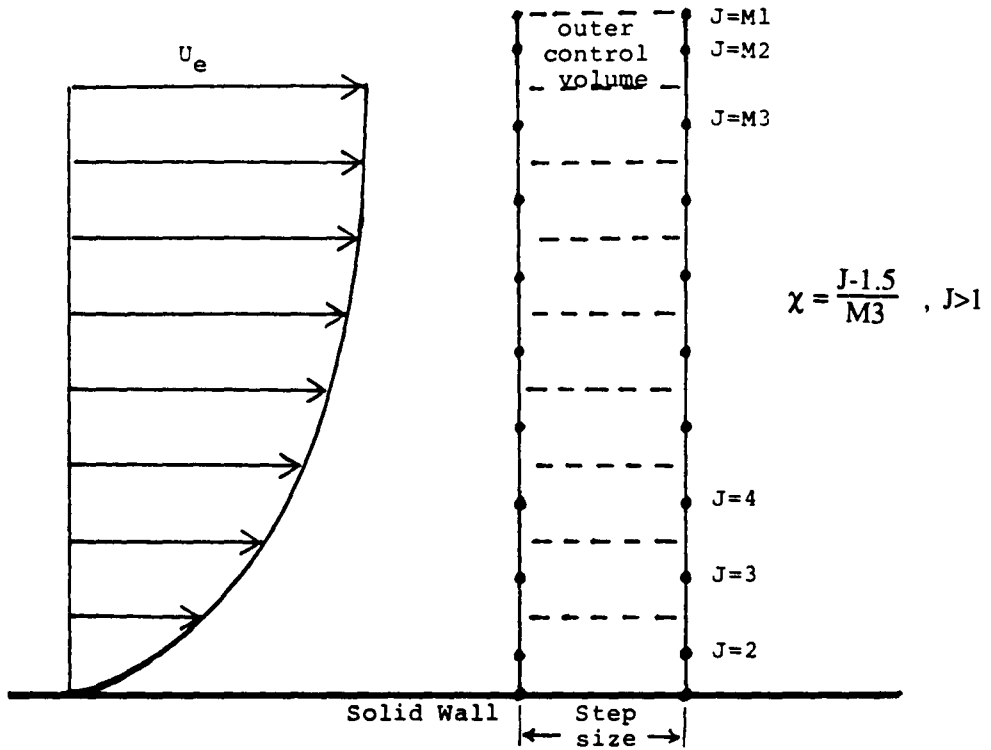


Figure 2.2 The computational control volumes, node locations and the grid coordinate "x"

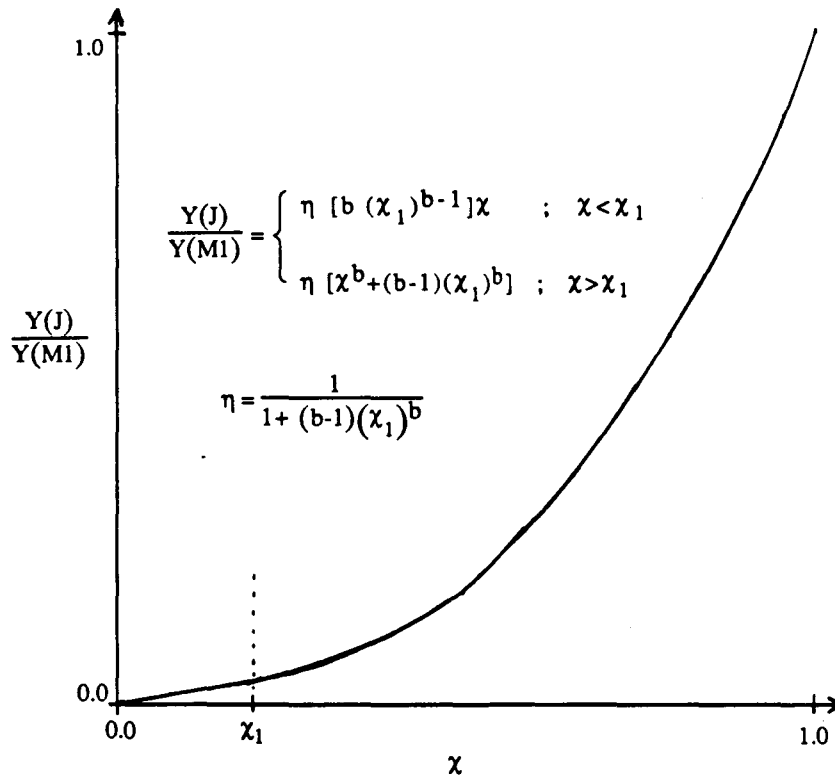


Figure 2.3 The near-wall grid refinement scheme

## CHAPTER THREE

### EVALUATING THE TRANSITION PREDICTION CHARACTERISTICS OF TWO LRN $k$ - $\epsilon$ MODELS

#### 3.1 OBJECTIVES OF THE EVALUATION

In this section the results of a sequence of computational tests will be presented. The purpose of these tests are to help answer some specific questions about the transition prediction characteristics of  $k$ - $\epsilon$  LRN turbulence models. Those questions and an explanation of each is given here by way of introduction.

1. How important to the transition predictions is the specification of the initial profiles of  $k$  and  $\epsilon$  ?

Since little is known about the actual behavior of the  $k$  and  $\epsilon$  profiles in the pre-transition "pseudo-laminar" boundary layer developing with free-stream turbulence, previous developers have had to rely on what are essentially "ad-hoc" methods to specify these profiles. The relative importance of this aspect of the problem needs to be determined if consistent and accurate predictions are to be made.

2. How important to the transition predictions is the exact location at which the calculations are started?

In some ways this question is an extension of question 1 with an additional factor, the velocity profile, being tossed in. Prior to transition, we know the velocity profile behaves at least approximately like the profile in a simple laminar boundary layer. It is somewhere in this region that a starting point for the computations must be chosen and initial profiles specified. Since there has been no consistency among previously published work relative to where in this "pseudo-laminar" boundary layer the computations are started, the relative importance of this question also needs to be determined if consistent and accurate predictions are to be made.

3. What are the quantitative differences in the transition predictions when the free-stream turbulence varies and how do these predictions compare with a well known correlation?

Previous work has clearly established that  $k-\epsilon$  LRN turbulence models simulate the correct qualitative trends, ie. a continuous transition from laminar to turbulent flow, the onset of which moves upstream with increasing free-stream  $Tu$ . However, a systematic documentation over a broad range of  $Tu$ , and a quantified comparison of these predictions with known correlations has not previously been performed. Furthermore, a specific comparison of two different LRN models with respect to these predictions has not been available. This information is essential in

determining the reliability of the models as they now stand, and in guiding future modeling efforts aimed at improving the calculations.

In each of the following sections a description of, and the results from a number of computational tests designed to help answer these questions are given. In each case, both the Jones-Launder model and the Lam-Bremhorst model are considered.

### 3.2 SENSITIVITY TO STARTING PROFILES OF $k$ AND $\epsilon$

Equations (2.38) and (2.39) describe the initial profile specification of  $k$  and  $\epsilon$  as suggested by Rodi and Scheuerer. The nature of these equations is such that they also provide a convenient way to vary the initial profiles of  $k$  and  $\epsilon$ . For example, choosing  $n$  large, reduces the  $k$  profile, while setting  $a_1$  large, increases the magnitude of the  $\epsilon$  profile. Since increasing  $\epsilon$  tends to decrease  $k$ , the combination of specifying both  $n$  and  $a_1$  as large yields a starting profile with essentially no turbulent kinetic energy except at the free-stream edge.

To evaluate the sensitivity of the calculations to the specification of these profiles, calculations were performed for the following conditions but with two distinctly different starting profiles and at two different starting locations.

\*  $Tu_e = \text{constant} = 3.00\%$  ( $\epsilon_e$  was set very small)

\*  $dP/dx = 0$  (Constant Velocity)

\* Flat Plate (No Curvature)

The two profiles considered correspond to  $n=2$ ,  $a_1=.375$  (the recommended values of Rodi and Scheuerer at this  $Tu_\epsilon$ ), and  $n=8$ ,  $a_1=2.0$ . The two starting locations were  $Re_x = 2.27 \times 10^4$  and  $Re_x = 1.0 \times 10^3$ . The value of  $Re_x = 2.27 \times 10^4$  was chosen because it corresponds to  $Re_\theta = 100$ , which is the starting location recommended by Rodi and Scheuerer. When using the Jones-Lauder model, which uses the modified dissipation variable  $\hat{\epsilon}$ , eq. (2.39) was slightly modified by removing the restriction  $\epsilon > \epsilon_c$ . This allowed  $\hat{\epsilon}$  to decrease to zero at the wall.

To represent the calculated transition process, the coefficient of friction ( $C_f$ ) is plotted vs. Reynolds number based on  $x$ . This was done because excellent correlations of  $C_f$  are available for both the laminar and the fully turbulent regimes, which when compared to, offer a clear reference with which to appraise the transition predictions.

Figures 3.1-a and 3.1-b are plots of the calculated variation in  $C_f$  vs.  $Re_x$  for the four test cases described and using both LRN models. Examination of these figures leads to the following general conclusions valid for both models;

- \* At any given starting location, minimizing the starting kinetic energy profiles results in the onset of transition beginning at the farthest downstream location.
- \* The sensitivity of the transition predictions to the initial profiles of  $k$  and  $\epsilon$  decreases as the starting location moves upstream, eventually becoming independent of these profiles.

Taken together, these observations yield another important conclusion about these tests.

- \* Appropriate specification of initial profiles at  $Re_x = 2.27 \times 10^4$  (where A and B were started) would yield transition predictions identical to either of those which were started at  $Re_x = 1.0 \times 10^3$  (C and D). However, *it is not possible* to specify any profiles which, when starting the calculations at  $Re_x = 1.0 \times 10^3$ , would yield transition predictions identical to either of those which were started at  $Re_x = 2.27 \times 10^4$ .

This last conclusion is quite significant in light of comparisons with experimental data that will be presented later. It stems from the transition process (as simulated in these models) being strongly controlled by the transport of  $k$  into the boundary layer. By moving the starting location upstream, you effectively increase the area over which  $k$  will have been diffused and convected into the boundary layer before reaching any particular downstream location. The next set of tests will further clarify this point.

Although the above mentioned conclusions can be applied to both models, obvious differences between the transition predictions also exist. Because the differences between  $\epsilon$  and  $\hat{\epsilon}$  mean that the starting profiles as applied to the two models are not exactly the same, some care must be used in comparing the two results directly. However, it is quite clear that the Jones-Launder model tends to predict transition further downstream than the Lam-

Bremhorst model. Tests to be presented in the succeeding sections will be beneficial in clarifying these differences also.

### 3.3 SENSITIVITY TO THE STARTING LOCATION

To further explore the sensitivity of the predictions to the initial starting location, a set of calculations were made with identical initial profiles (scaled on  $\delta$ ) but at different starting locations. The basic conditions were the same as the calculations presented previously in section 3.2, ie.  $Tu_e=3\%$ ,  $dp/dx=0$ , flat plate. The initial profiles for  $k$  and  $\epsilon$  were specified using equations (2.38) and (2.39) but with  $n=8$ ,  $a_1=2$ . These are the same specifications used in runs "B" and "D" in Figure 3.1. Recall that this will yield transition at the farthest downstream location possible.

Figures 3.2-a and 3.2-b show the results of these calculations. The results shown further illustrate how strongly the transition predictions are dependent on the initial starting location. For the Lam-Bremhorst model at this free-stream turbulence level, the location of transition is strongly dependent on starting location for  $Re_{x,i} > 10^3$ , but basically independent for  $Re_{x,i} < 10^3$ . In contrast, the Jones-Launder model calculations show differences until the starting location is reduced to about  $Re_{x,i} = 10^2$ , and even then a close inspection reveals a very slight down-stream shift when compared to  $Re_{x,i} = 10^1$ . Since the figures are plotted using a logarithmic scale, the actual distance between these starting locations is of the same magnitude as this small shift.

The difference between the models in this respect is apparently due to the direct influence of the wall introduced in the Lam-Bremhorst model by

using  $R_y$  as well as  $R_t$  in the  $f_\mu$  function. To justify this assertion, consider the following.

A well known exact solution to the laminar boundary layer equations with constant free-stream flow is the Blassius solution. This solution is expressed in terms of a similarity variable  $\eta$  defined as;

$$\eta = \frac{y}{\sqrt{ux/U_e}} \quad (3.1)$$

The inner wall coordinate  $y^+$  defined in eq. (2.16) can be expressed in terms of  $\eta$  by substitution of eq. (3.1) to eliminate  $y$ . Further rearrangement allows  $y^+$  to now be expressed as

$$y^+ = .576 \eta (Re_x)^{1/4} \quad (3.2)$$

Alternately, if we remember that for a Blassius profile,  $\theta = .664 \sqrt{ux/U_e}$ , we can write;

$$y^+ = \eta \sqrt{.5 Re_\theta} \quad (3.3)$$

The turbulent Reynolds number  $Re_y$  defined in eq. (2.15), can be written in terms of  $y^+$  as

$$Re_y = y^+ \sqrt{k^+} \quad (3.4)$$

where

$$k^+ = \frac{k}{u_\tau^2} \quad (3.5)$$

It is now possible to see how for a Blassius boundary layer, the Lam-Bremhorst formulation for  $f_\mu$  can be written in the following ways;

$$f_{\mu} \approx \left( 1 - \exp[-.0163 k^+ \eta \sqrt{.5 Re_{\theta}} ] \right)^2 \left( 1 + \frac{20.0}{Re_t} \right) \quad (3.6)$$

$$f_{\mu} \approx \left( 1 - \exp[-.0095 k^+ \eta (Re_x)^{1/4} ] \right)^2 \left( 1 + \frac{20.0}{Re_t} \right) \quad (3.7)$$

Thus in the laminar region when a Blassius profile is a reasonable approximation, the magnitude of  $f_{\mu}$  at any similar location is a function of the Reynolds number. For low Reynolds numbers  $f_{\mu}$  is reduced, limiting both the production and diffusion of  $k$  in the boundary layer. This is why the transition predictions of the Lam-Bremhorst model become insensitive to the starting location as  $Re_{x,i}$  becomes small. In contrast, the Jones-Launder formulation introduces no such direct dependence.

### 3.4 SENSITIVITY TO FREE-STREAM TURBULENCE

The next set of computational tests consider the effect that different levels of  $Tu_e$  have on the transition predictions. The conditions considered are once again flat plat, zero pressure gradient flow, and the computations are all started at  $Re_{x,i}=10^3$ . The initial profiles are specified as per equations (2.38) and (2.39) with  $n=8$ , and  $a_1 = 2.0$ . Calculations were done for free-stream turbulence intensity levels ranging from 1.0 % to 6.0%. Free-stream dissipation rates were specified low enough for the decay in  $Tu_e$  to be negligible. Figures 3.3-a and 3.3-b show the results of these calculations.

The first thing to be noted is that a calculation with  $Tu_e=1\%$  is not shown for the Lam-Bremhorst model. This is because transition to a turbulent state was not predicted by this model for  $Tu_e=1\%$ . This failure was also mentioned by Rodi and Scheuerer [67], although they imply that the result seems physically plausible. It is clear from these tests that the reason is related to the LRN formulation chosen by Lam and Bremhorst since the Jones-Launder model does predict transition under these conditions.

In general terms the qualitative characteristics of the variation of  $C_f$  during transition seem reasonable for both models with the onset of transition moving progressively upstream with increasing  $Tu_e$  as it should. However, significant differences between the predictions of the two models occur at higher  $Tu_e$  where the Lam-Bremhorst model shows a much smoother and more gradual transition region than the Jones-Launder model. The previously noted tendency of the Lam-Bremhorst model to predict transition earlier than the Jones-Launder model is also quite apparent.

In figures 3.4-a and 3.4-b the momentum-thickness Reynolds number at the start ( $Re_{\theta,S}$ ) and the end ( $Re_{\theta,E}$ ) of transition are plotted and compared with the correlation of Abu-Ghannam and Shaw [2]. Here, the beginning and end are defined as the point of minimum and maximum  $C_f$  respectively. From figure 3.4-a, we can once again see that both models predict the correct qualitative trends, but the onset of transition is predicted too early for both models. At  $Tu_e=5\%$ , both models are predicting transition occurring at  $Re_{\theta,S} < 150$ . However, the Jones-Launder model clearly does better than the Lam-Bremhorst model.

The results shown in figure 3.4-b begin to quantify an important deficiency apparent in all of the tests. The region over which transition is predicted to occur is always very short. As a result, both models consistently predict a  $Re_{\theta,E}$  of less than 50% of the correlation.

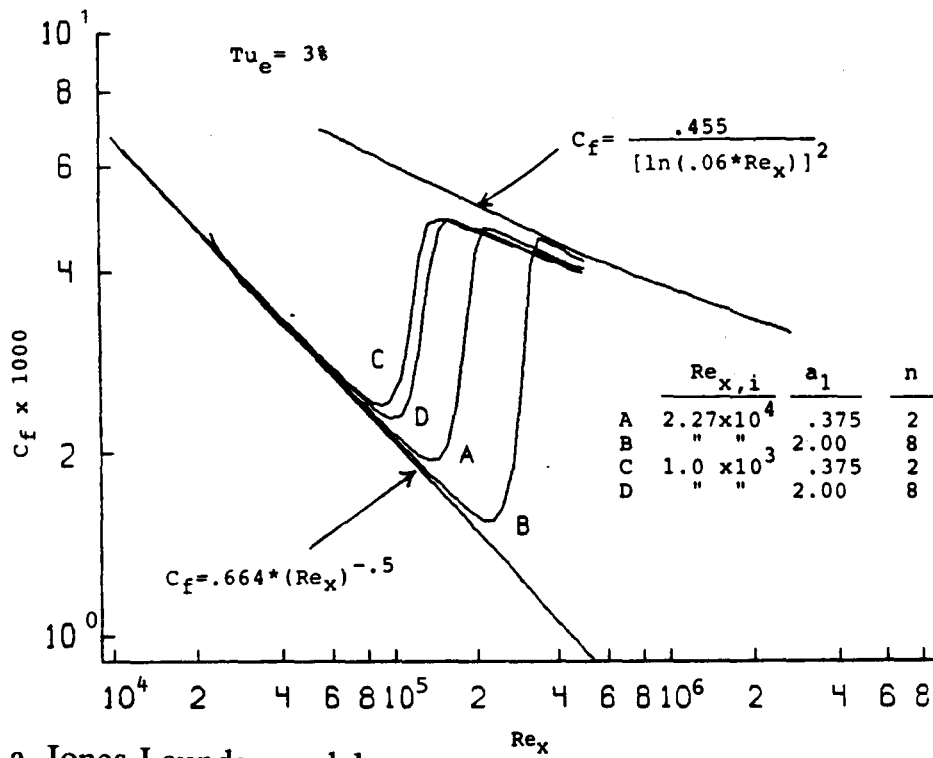
### 3.5 SUMMARY

A series of numerical experiments have been performed to evaluate the transition prediction characteristics of the Lam-Bremhorst and the Jones-Launder LRN k- $\epsilon$  turbulence models. Both models showed, as expected, the ability to correctly model the basic qualitative aspects of transition, ie. the continuous transition from laminar to turbulent flow, the onset of which moves upstream with increasing  $Tu_e$ . The answers to three specific questions have also been sought through the completion of these tests. The results indicate the following conclusions as answers to these questions.

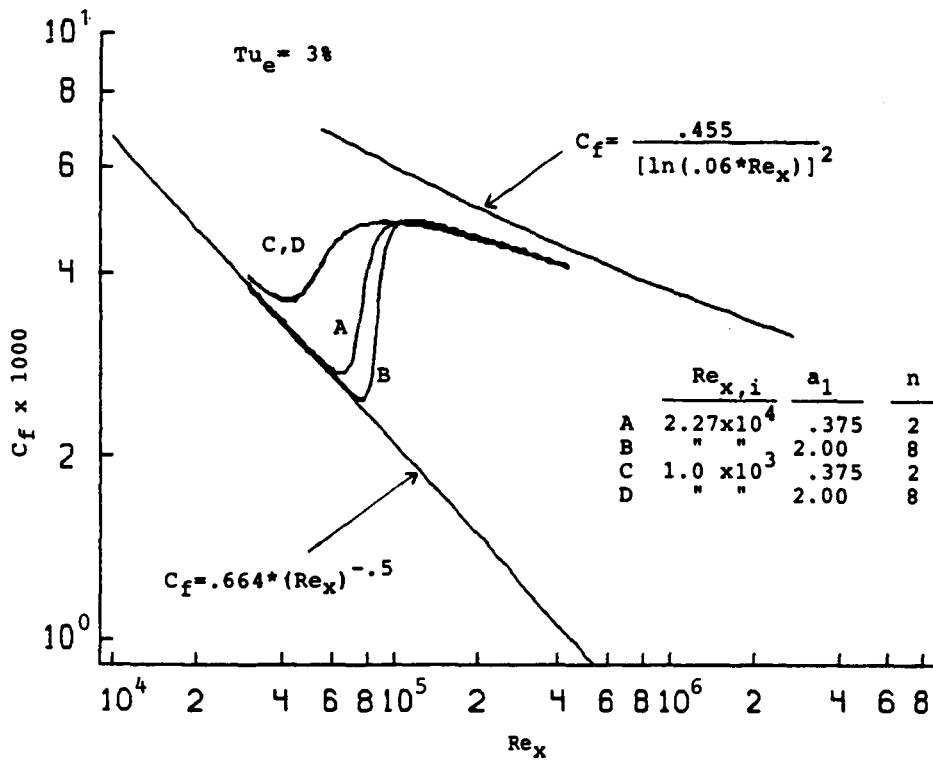
1. The predicted location of transition is moderately sensitive to the initial profiles specified for k and  $\epsilon$ . Lower k and higher  $\epsilon$  profiles yield transition occurring somewhat farther downstream. This sensitivity decreases with decreasing  $Re_{x,i}$ , especially for the Lam-Bremhorst model.
2. The prediction of transition is very sensitive to the location at which the calculations are started. The reason for this is attributed to the basic process which must occur for the models to simulate transition, ie the transport of k into the boundary layer. The extent to which this can occur is largely a function of the distance over which the

calculations have proceeded. However, this sensitivity does appear to decrease with decreasing  $Re_{x,i}$ , especially for the Lam-Bremhorst model. The differences in this aspect are clearly related to the LRN functions employed.

3. For calculations started at low  $Re_{x,i}$  (where the sensitivity to the initial profiles for  $k$  and  $\epsilon$  is small), transition is predicted at unrealistically early locations. Also, both models predict transition lengths significantly shorter than experiment.

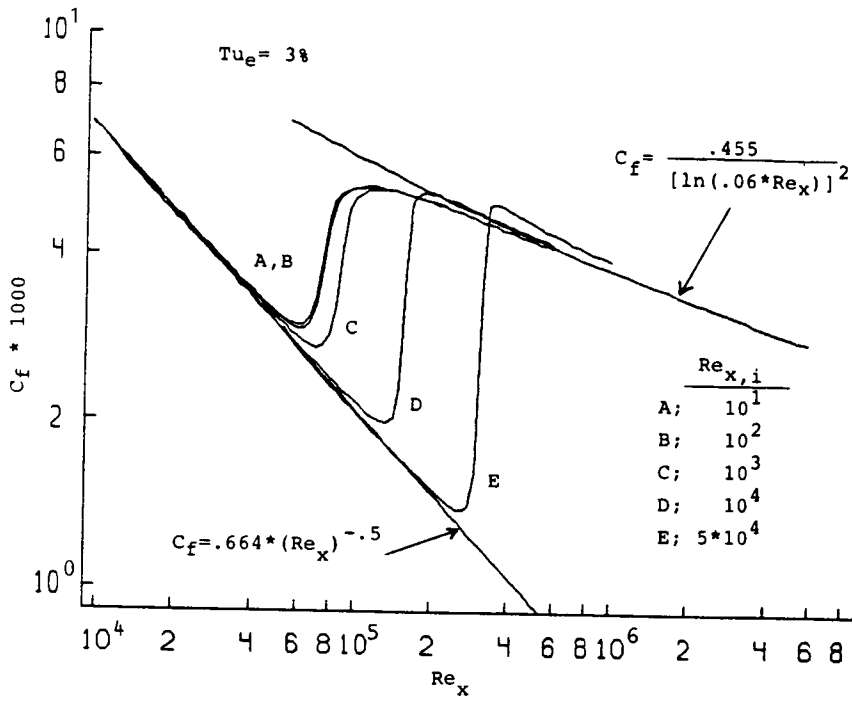


a. Jones-Launder model

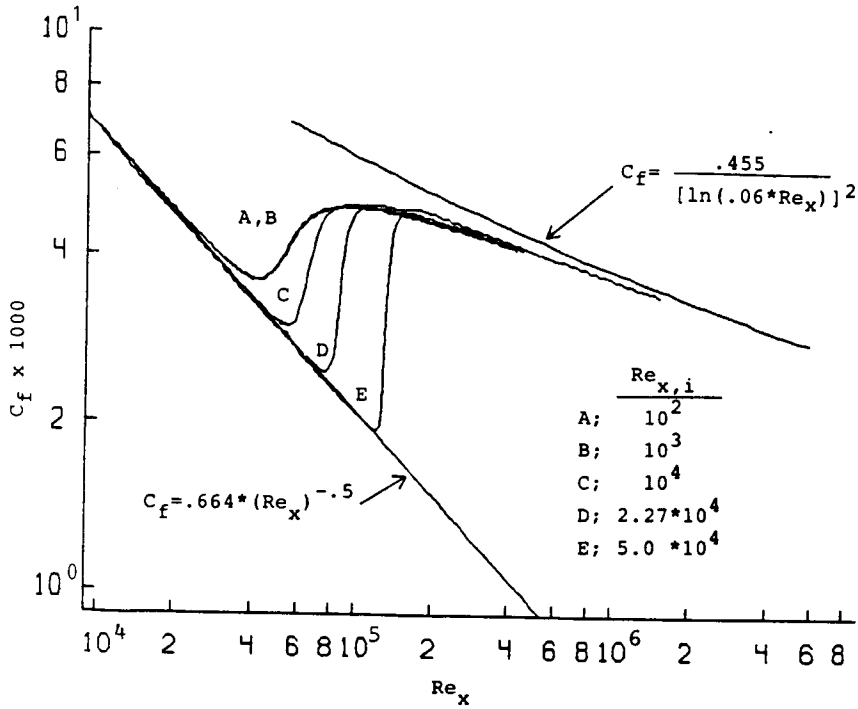


b. Lam-Bremhorst model

Figure 3.1 Plot of  $C_f$  vs  $Re_x$  for different initial profiles of  $k$  and  $\epsilon$

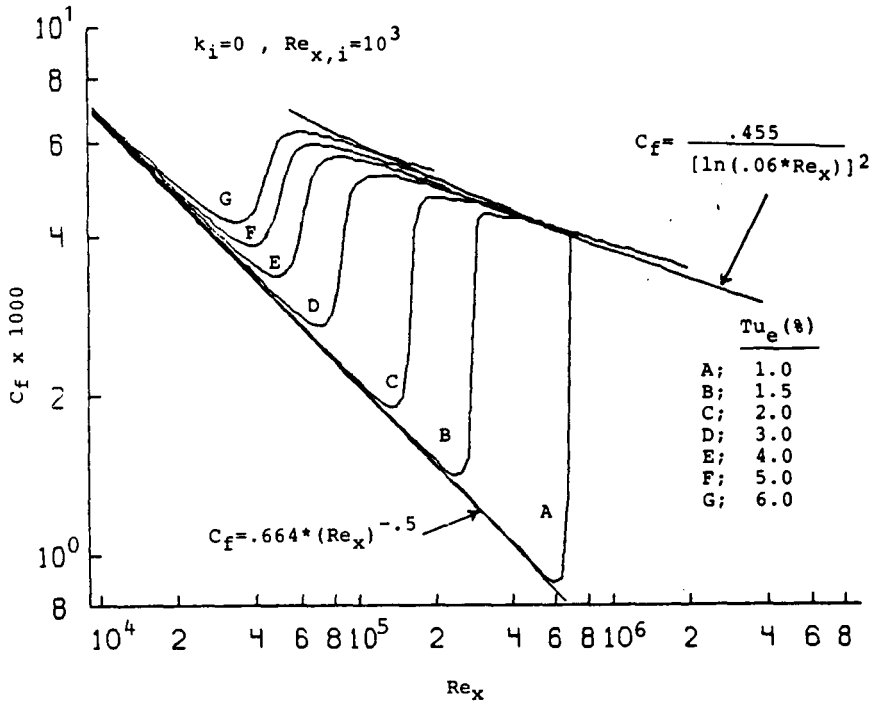


a. Jones-Lauder model

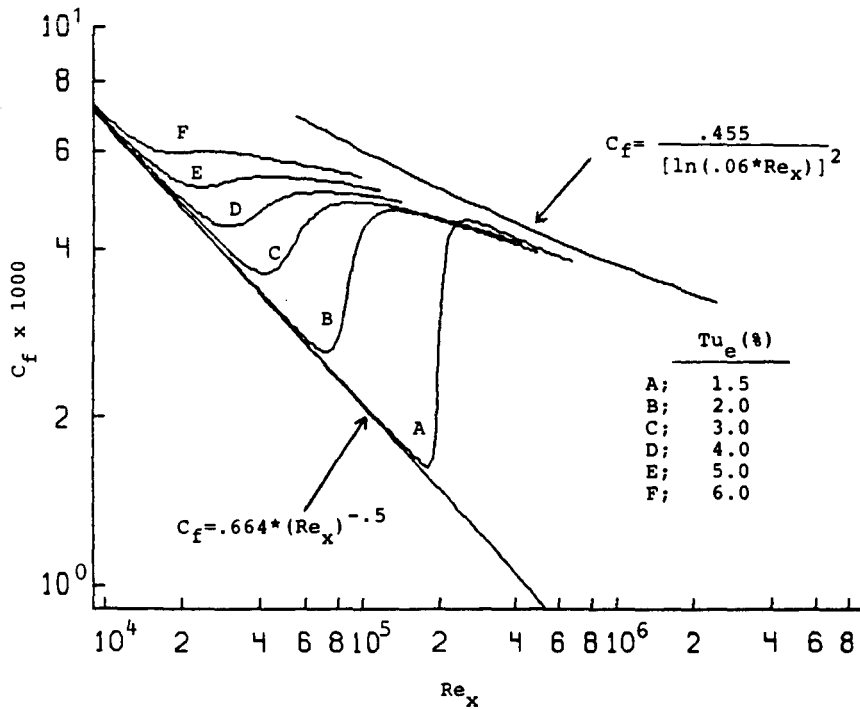


b. Lam-Bremhorst model

Figure 3.2 Plot of  $C_f$  vrs  $Re_x$  for different starting locations

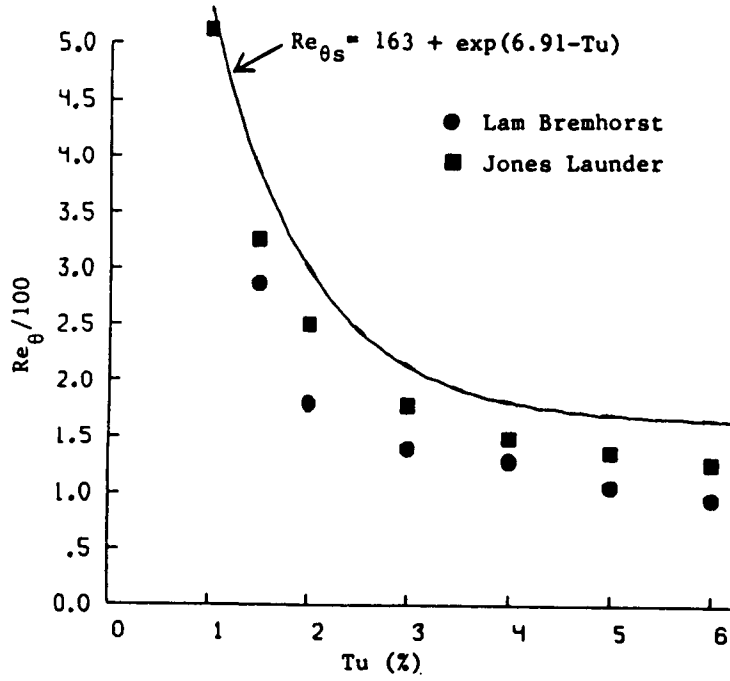


a. Jones-Lauder model

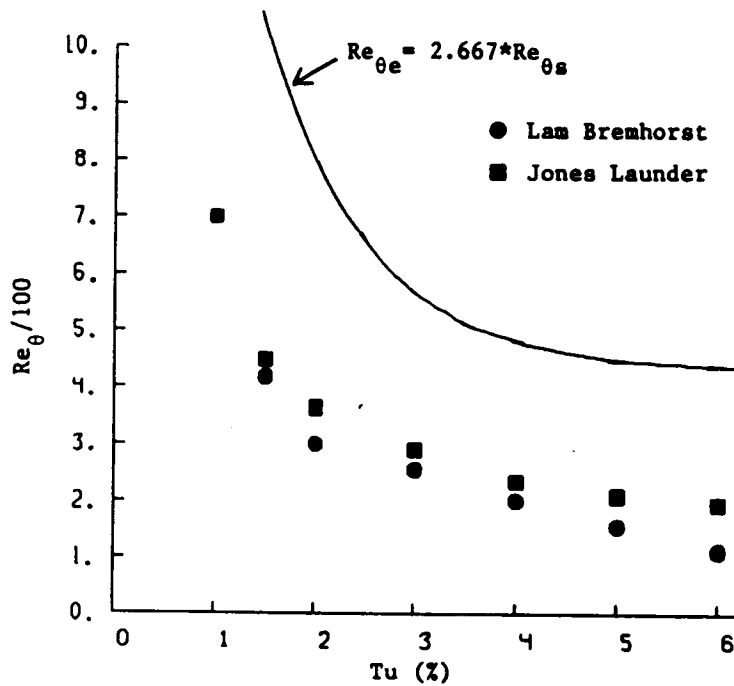


b. Lam-Bremhorst model

Figure 3.3 Plot of  $C_f$  vrs  $Re_x$  for different levels of free-stream turbulence intensity



a) Start of transition



b) End of transition

Figure 3.4 Calculated momentum thickness Reynolds numbers at the start and end of transition compared to the correlation of Abu-Ghannam and Shaw

## CHAPTER FOUR

### DEVELOPMENT OF AN IMPROVED APPROACH TO SIMULATE TRANSITION WITHIN THE FRAMEWORK OF THE $k$ - $\epsilon$ LRN TURBULENCE MODELS

The results presented in chapter 3 reveal significant problems in directly applying  $k$ - $\epsilon$  LRN models to predict transitional boundary layer flows. However, the potential of this approach is also apparent, and it clearly seems wise to pursue ways to eliminate these problems without abandoning the basic technique. One way of seeking improvement is to examine the LRN functions themselves, looking for alternative ways to specify these functions which will yield both the desired fully-turbulent near-wall behavior and also improved transition predictions. Another way is to seek simple modifications or empirical constraints that would provide a means of eliminating the deficiencies, without changing the basic LRN models themselves. This is the way that improvements are sought in the work to be presented in this chapter. Although less elegant or general than a new formulation of LRN functions might be, it is nonetheless quite practical, and excellent improvement will be shown by the modifications developed.

In working to improve the transition predictions, we are somewhat hampered by ignorance about certain aspects of the problem's physics. This difficulty, mentioned earlier, centers around the lack of experimental data for  $k$  and  $\epsilon$  profiles at locations upstream of transition. Although our  $k$ - $\epsilon$

models require this as input, insufficient knowledge is currently known about the values of these turbulent quantities within the quasi-laminar region prior to the start of transition. Thus, in searching for ways to improve on the current models, it seems we must be content (for the present) with "reasonable" profiles in this region, and try to minimize the sensitivity of the predictions to small variations in them.

We will initially work with the Lam Bremhorst model. This model was chosen for basically three reasons; first, the favorable results of the study by Patel et al. [62], second, the previous use of this model by Rodi and Scheuerer [66,67] in working on this same problem, and third, the simpler form of the source terms present in the  $k$  and  $\epsilon$  equations (a result of the dissipation rate variable used in this model). Once an approach has been developed, the application to the Jones-Launder model will be described and tested.

#### **4.1 PRELIMINARY COMMENTS**

Before proceeding it is valuable to review in more detail the method for predicting transitional flows developed by Rodi and Scheuerer [66,67]. This work has been mentioned numerous times in this thesis, and has been a rich source of valuable information on this problem. With that method as additional background, we will then outline the desired characteristics to be sought in a new approach to improving the predictions.

#### 4.1.1 Method of Rodi and Scheuerer

Rodi and Scheuerer [66,67,77]. have proposed a procedure to predict transition using the Lam-Bremhorst LRN model. They apparently recognized some of the problems which have been discussed in Chapter 3 and in essence, recommend a particular procedure to deal with them. In developing their method they chose to begin all calculations at a starting location corresponding to  $Re_\theta=100$ . To determine where this location is in the streamwise direction, they use the method of Thwaites ( see eq. (2.31)). They also proposed particular forms for the  $k$  and  $\epsilon$  profiles - eqs. (2.38) and (2.39) - which seemed reasonable, and which gave them a simple empirical parameter " $a_1$ " with which to tune their results. The coefficient  $a_1$  was correlated with free-stream turbulence intensity and it's value varies from about 0.1 to 2.0 [77].

This method effectively addresses two of the problems which were discussed in chapter 3, ie. the sensitivity to starting profiles and to starting location. However, the importance of the starting location remaining consistent was apparently not recognized because some of their later computations against experimental data were not started at  $Re_\theta=100$ . Also, the problem of transition length is not addressed in this procedure.

Figure 4.1 shows results obtained by this author when following this procedure for a range of  $Tu_e$  of 1.5 to 6%. The conditions are identical to those considered in section 3.4, ie. constant velocity flat plat flow. Since the Lam-Bremhorst LRN model is employed, we can compare these calculations to Fig. 3.3-b. The major benefit is the downstream shift in the predicted start

of transition for the higher turbulence intensities. This yields values of  $Re_{\theta,S}$  which are in better agreement with the correlation of Abu-Ghannam and Shaw. Unfortunately, the transition length is actually somewhat shortened, causing that aspect of the prediction to deteriorate. Note that by examining Fig. 3.2-a, this characteristic appears to be related to the starting location being relatively far down-stream. This downstream starting location is also the reason why varying the initial profiles yields improved predictions.

For turbine blade calculations, where the transition length can sometimes extend over most of the blade surface, the failure to predict the transition length is very significant. In addition, it may not always be possible to accurately specify the exact location where say, the momentum thickness is equal to 100. Thus, the result of the evaluation illustrated here, was to conclude that improved methods should still be sought.

#### **4.1.2 Desired Characteristics**

The results presented earlier provide evidence that the models tested need considerable improvement before quantitatively correct predictions of transition can be made using LRN  $k-\epsilon$  models. In seeking to improve the prediction capabilities, we should consider the specific characteristics that we desire in our model. Based on our previous evaluation, we will seek the following two characteristics as a minimum standard to be achieved for flat-plate zero pressure gradient flow.

- 1) Transition starting and ending in good agreement with the correlation of Abu-Ghannam and Shaw.

- 2) The freedom to start the calculations at any location within some reasonable area without affecting the transition predictions.

## 4.2 A SIMPLE IMPROVEMENT TO THE LAM-BREMHORST $f_\mu$ FUNCTION

### 4.2.1 The Problem and it's Cause:

In section 3.4 it was pointed out that the Lam-Bremhorst model did not predict transition when  $Tu_e$  was reduced to 1%, although the Jones-Launder model did. Since experimental evidence clearly shows that the location of transition is sensitive to free-stream turbulence levels significantly lower than 1%, a correction for this is needed.

To determine the cause, a series of computations were made at progressively lower turbulence intensities. During each of these runs, the calculated profiles for  $k$ ,  $\epsilon$  and other related turbulence quantities were printed out at regular intervals. Analysis of these profiles revealed a simple explanation for the deficiency; the value for  $f_\mu$  was being unrealistically over predicted ( $\gg 1$ ) under certain conditions that could develop as the computed boundary layer moved toward transition. Furthermore, these conditions only occurred when  $Tu_e$  was low. To explain, we need to consider more closely the two parameter Lam-Bremhorst formulation for  $f_\mu$ .

The function  $f_\mu$  is introduced in  $k$ - $\epsilon$  LRN models as a means of directly reducing the turbulent viscosity in the near-wall region (see eq. (2.10)). Outside of this region, it's value should be unity as near-wall effects are not

present. Thus in no situation is it intended to have a value outside of the range 0 to 1. Under fully turbulent conditions, this is always the case for the Lam-Bremhorst model, as well as all other proposed formulations. However, in the Lam-Bremhorst formulation, if the behavior of  $k$  and  $\epsilon$  does not follow the near-wall pattern, as may be the case during transition, it is possible for  $f_\mu$  to become very large. To illustrate this, we re-consider the equation for  $f_\mu$  given below.

$$f_\mu = (1 - \exp(-.0163R_y))^2 \left(1 + \frac{20}{R_t}\right) \quad (4.1)$$

Under normal conditions near a wall,  $Re_t$  and  $Re_y$  have the following approximate relationship for  $y^+ > 30$  [62],

$$Re_t \approx 2.5 Re_y \quad (4.2)$$

If  $Re_t$  is say 150, then  $Re_y \approx 60$  and the value for  $f_\mu$  would be approximately 0.44. However, if a situation develops such that say  $Re_t=1$ , and  $Re_y = 60$ , then  $f_\mu$  would be equal to 8.2. In analyzing the results of the tests mentioned, values for  $f_\mu$  as high as 300-400 were found!

To arrive at this situation, a local imbalance between  $k$  and  $\epsilon$  must occur where  $\epsilon$  is higher relative to  $k$  than normal. The high  $f_\mu$  then adds to the problem by unrealistically changing the various source terms in the  $k$  and  $\epsilon$  equations. Numerically, this leads to an extreme imbalance in the  $\epsilon$  equation source terms where the production of  $\epsilon$  is much greater than the

destruction. This effectively destroys any turbulent kinetic energy that would otherwise have been transported further into the boundary layer.

In summary, although the problem appears to have both numerical and mathematical aspects, the root cause is the unrealistic  $f_\mu$  predictions, and this can be handled in a simple way to be explained next.

#### 4.2.2 A Solution

To eliminate the problem, all one must do is prevent  $f_\mu$  from becoming too large. The simplest solution is to set

$$f_\mu = \min ( f_{\mu,LB} , 1.0 ) \quad (4.3)$$

where  $f_{\mu,LB}$  refers to eq. (4.1). However, when testing this at  $Tu_e = .5\%$ , although transition was predicted, the predictions were still being affected, preventing the proper correlation of a transition modification which will be introduced later. A stronger limitation was therefore introduced in the following manner;

$$f_\mu = \min(f_{\mu,LB} , 1.0, .5 + .0025*R_t) \quad (4.4)$$

A plot of  $f_\mu$  vrs.  $Re_t$  for a fully turbulent flow, as shown in fig. 4.2, shows that this simply places a more stringent limitation on how large  $f_\mu$  can get extremely close to the wall. Since any restriction which remains above the fully turbulent behavior will not affect the fully turbulent calculations, the

particular form chosen is somewhat arbitrary. Equation (4.4) was chosen because it was simple, and because it was sufficient to allow proper correlation of the transition model to be introduced. It must be remembered however, that this choice does not affect the fully turbulent predictions, and thus lies entirely within the realm of a modification to improve transition. Furthermore, it turns out that this change has no effect at all on the transition predictions for  $Tu_e > 2\%$ , and is only really significant for  $Tu_e < 1.5\%$ .

The modified  $f_\mu$  function of eq. (4.4) is used for all subsequent Lam-Bremhorst calculations in this thesis unless otherwise specified.

### 4.3 THE MECHANISM BY WHICH THE MODEL SIMULATES TRANSITION

Before starting to consider ways to improve the transition prediction characteristics of the model, it is important to consider carefully how the process occurs in the model as it stands.

Figure 4.3 shows the typical development of the turbulent kinetic energy profiles as the simulated flow proceeds from a laminar to a turbulent state using the Lam-Bremhorst model. Initially, the kinetic energy profile is monotonic, increasing slowly from zero at the wall, to  $k_e$  at the boundary. As the calculations march downstream, turbulent kinetic energy from the free-stream is convected and diffused into the boundary layer. As this continues, the production term in the model,  $P_k = \mu_t (\partial U / \partial y)^2$ , starts to become significant. This in turn increases the local value of  $k$ , and thus  $\mu_t$ . This process feeds on itself, causing the rapid increase in  $k$  shown. Note that a large overshoot initially occurs, which then slowly decays until the

parameters achieve a relatively stable state due to the low-Reynolds-number functions and the wall boundary conditions.

This process is initially controlled by the transport of  $k$  into the boundary-layer from the free-stream. This is why these models are not useful in predicting transition when the free-stream is perfectly quiescent. It also explains to a large extent why the predictions are so sensitive to the initial starting location. The further upstream you begin your calculation, the larger the area over which  $k$  is diffused and convected, and thus the quicker transition is initiated. However, the simple transport of  $k$  into the boundary layer is only the necessary first step, for it is the interaction of this influx of  $k$  with the non-linear source terms in the  $k$  and  $\epsilon$  equations that provide the real driving force.

The key source term in the transition simulation is the modeled production term in the turbulent kinetic energy equation. (Note that the use of the words "production term" has been used rather loosely here to refer only to the quantity in the model, not a term in the exact form of the  $k$  equation.) Only as this term becomes larger than the dissipation can local values of  $k$  increase and exceed the free-stream value. This is the process which, in the model, simulates the amplification of free-stream disturbances and the resulting eventual transition to a turbulent state. It seems logical therefore to examine ways to modify the behavior of this term during the simulated transition process in order to improve the predictions.

#### 4.4 STABILITY CONSIDERATIONS

The actual physical process by which an initially laminar boundary layer undergoes transition to a fully turbulent state is very complex, but its onset is inseparably tied to stability considerations. Fundamental to the process is the response of the flow to the introduction of small disturbances, from whatever source. Under some conditions, a disturbance will decay, its small energy being absorbed into the mean flow. Under other conditions, a disturbance will be amplified, and energy will be extracted from the mean flow to feed this growth. It is only under these "unstable" conditions that the onset of transition can occur.

Linear stability theory gives some insight into the conditions under which a boundary layer becomes unstable. Solutions to the well known Orr-Sommerfeld equation for a Blasius velocity profile yield a critical momentum thickness Reynolds number below which infinitesimal disturbances will not be amplified (commonly quoted as 163 due to an approximate solution, more accurate solutions have shown it to be equal to 201, see [78] pg. 469).

Numerous experiments have shown that under the influence of high free-stream turbulence, transition can occur at  $Re_{\theta}$  even less than this stability limit [2]. This is presumably due to the nonlinear behavior which the high  $Tu_e$  introduces. However, after analyzing the data available to them, Abu-Ghannam and Shaw felt justified in presuming a lower limit, as their data seems to flatten out as the  $Tu_e$  level increases (Although this has been disputed by Rued and Whittig [73]).

The LRN functions chosen by various researchers have all been modeled after data taken from fully turbulent conditions. As a result, stability considerations are not directly a part of k- $\epsilon$  LRN turbulence models. The k and  $\epsilon$  equations are simple advection diffusion equations with a particular set of nonlinear source terms. However, in a sort of indirect way, when applied to boundary layer flows they can mimic some aspects of stability. This comes through the nature of the near wall effects on the source terms.

An analogy that is useful to think in terms of here is the following. Consider the well known near wall behavior of a turbulent boundary layer. Descriptions of it's structure generally refer to at least three regions; the viscous sublayer immediately adjacent to the wall, the outer turbulent "law of the wall" region, and the so called buffer region in between. Transposing in our minds the streamwise x coordinate with the cross-stream y coordinate, we see the following correspondence.

developing laminar boundary layer  $\Leftrightarrow$  viscous sublayer

transitional region  $\Leftrightarrow$  buffer layer

turbulent boundary layer  $\Leftrightarrow$  turbulent "law of the wall" region

When the boundary layer thickness is very thin, such as is the case at low-Reynolds numbers, the outer edge only extends out to a relatively small  $y^+$ . Thus the LRN functions designed to simulate the proper viscous sublayer in a turbulent boundary layer, also damp out any turbulent production which

might otherwise occur in the laminar low-Reynolds-number boundary layer (due to the influx of turbulent energy from the free-stream).

This correspondence between two different phenomenon is the basic reason why all LRN models are able to mimic the correct qualitative aspects of boundary-layer transition with free-stream turbulence as described in chapter 3. However, because of the important time dependent nature of the stability aspects of boundary-layer transition – for which there is no analogy in a steady-state turbulent boundary near a wall – it is not particularly surprising that deficiencies exist.

#### 4.5 A MODIFICATION TO THE PRODUCTION TERM

After exploring a number of different alternatives to improve the model, one method was found to be fairly successful. The method focuses on two ideas developed earlier in this thesis. The first is that some means of incorporating stability considerations into the calculational procedure must be provided. The second, related to the first, is that the process by which the model simulates transition, once started, must proceed at a finite rate and in accord with experiment. When translated to practical implementation within a LRN turbulence model, this implies the following;

- (1) Since the production term " $P_k$ " is the term in the model which simulates the amplification of perturbations, below some critical momentum thickness Reynolds number ( $Re_{\theta,c}$ ), The production term in the  $k$  equation should always be insignificant.

- (2) The rate at which  $P_k$  can change must be assumed to have some finite limit.

The purpose of this section is to describe the development of these ideas into a practical engineering model.

As a sidelight, it may be interesting for the reader to consider the harmony between the approach to be developed here and the basic idea suggested by Maslow when he writes "... a successful predictive scheme (*for transition*) would require, as a minimum, not only a critical value of the Reynolds number, but also some nonlinear dependence on an amplitude parameter..." [50, italics added].

#### 4.5.1 Applying a Stability Criteria

As a first step in developing these ideas, a number of calculations were made with the following stipulation. If the calculated momentum thickness was less than 162, the production term in the  $k$  equation is arbitrarily set equal to zero. The value of 162 was chosen as this is the lower limit which Abu-Ghannam and Shaw use in their correlation. This effectively prevents the magnitude of the turbulent kinetic energy from ever exceeding the free-stream value when  $Re_\theta < 162$ . However, it does not prevent the transport of  $k$  into the boundary layer, which by itself will influence the flow to some extent.

Figure 4.4 plots the streamwise development of  $C_f$  for four different free-stream turbulence conditions as calculated both with and without this modification. (These conditions were modeled after the experiments of Blair[11], but the experimental results will not be compared at this point.) A number of very interesting things are illustrated in this figure. First, the location of transition in each case has been shifted downstream such that the computed values of  $Re_\theta$  at the start of transition are now all fairly close to the predicted value using the correlation of Abu-Ghannam and Shaw. This is also illustrated in figure 4.5. Second, for the higher turbulence cases, it is clear that despite setting  $P_k=0$ , the effect of high free-stream turbulence does influence the boundary-layer prior to transition. Third, The length of transition is as short or even shorter than the unmodified calculations.

It may be recalled that, excluding the effect of high free-stream turbulence on the laminar boundary layer shown here, tests of the method of Rodi and Scheuerer showed very similar results. However, there is one important difference which is illustrated in figure 4.6. In contrast to the method they propose, which is limited to starting at a very specific location, this procedure has yielded results virtually independent of the initial starting location for  $Re_{x,i} < 2.3 \times 10^4$ . This also implies that the results are independent of the  $k$  and  $\epsilon$  starting profiles in this region.

#### **4.5.2 Limiting the Growth Rate of the Production Term**

The turbulent kinetic energy equation used in our numerical calculations (eq. (2.12)) is derived through various modeling assumptions from a more exact form. For fully turbulent flow where the boundary-layer

assumptions are valid, the production term in the model corresponds to the production term in the "exact" equation as follows.

$$\overline{u'v'} \left( \frac{\partial U}{\partial y} \right) \approx \mu_t \left( \frac{\partial U}{\partial y} \right)^2 = \rho C_\mu \frac{k^2}{\varepsilon} \left( \frac{\partial U}{\partial y} \right)^2 \quad (4.5)$$

The success of k-ε modeling has clearly verified that this approximation is quite good in many situations of interest. However, in a "pseudo laminar", developing transitional boundary layer - where experiments show a complex, three-dimensional development characterized by increasingly frequent "bursts" of local turbulence production - there is no justification to assume that the "exact" term above (the term on the left) together with the dissipation ε, are the only source terms that are significant. Thus from a modeling standpoint, there is no compelling reason precluding us from introducing modifications in our numerically represented production term in order to improve transition predictions, as long as the fully turbulent form is not changed. Furthermore, the process by which small disturbances are amplified in an unstable boundary layer is time dependent, where as our equations are in a steady state form.

With these things in mind, it seems reasonable to consider improving our predictions by introducing a modification to limit the growth rate of the production term. This would allow us to leave the fully turbulent form of the equations undisturbed, and yet introduce a time dependent modification to slow down the transition simulation. The time scale would simply be related to the local velocity.

Preliminary tests with a number of formulations showed that a simple but flexible representation that worked quite well was the following;

$$\left[ \frac{\partial P_k}{\partial t} \right]_{\max} = A * P_k + B \quad (4.6)$$

where  $A$  and  $B$  are empirical parameters. The dependence of the linear term on  $P_k$  itself is arbitrary, being suggested in analogy with reaction rate theory, but was found to work quite well. The need for two independent parameters however, stems directly from wanting to predict both the start and the end of transition at the correct location.

Figure 4.7 illustrates the benefits that introducing each of these ideas has had on the transition predictions. The heat transfer data being compared is from the tests of Blair[11]. Note that the unmodified prediction yields transition too far upstream, introducing the stability criteria shifts it downstream but doesn't effect the error in the transition length, but addition of the growth rate limitation provides a very excellent representation of the data. However, this calculation is only preliminary, and it still remains to be shown whether the empirical parameters can be properly correlated to yield consistently accurate predictions over a wide range of free-stream turbulence conditions.

### 4.5.3 Numerical Implementation

At this point, a brief explanation as to the numerical implementation of eq. (4.6) may be beneficial. We first define the following;

- $x$  : The streamwise location at the current point in the calculation  
 $dx$  : The step size in the streamwise direction  
 $PK(j,x)$  : The computed positive source term in the  $k$  equation for the  $j$ th control volume and at streamwise location  $x$   
 $U_j$  : The local streamwise velocity at the  $j$ th control volume

To compute the value of " $PK(j, x+dx)$ " to be used over the next step in the solution; we implement the following (written in pseudo fortran)

If  $Re_\theta < Re_{\theta,C}$  then

$$PK(j, x+dx) = 0$$

else

$$PK(j, x+dx) = PK(j, x) + \min\left[\mu_t \left(\frac{\partial U}{\partial y}\right)^2 - PK(j, x), \Delta P_{k,max}\right]$$

endif

where

$$\Delta P_{k,max} = (A * PK(j, x) + B) \frac{dx}{U_j} \quad (4.7)$$

For convenience, this modification will be referred to by the acronym "PTM" (for Production Term Modification).

#### 4.5.4 Determining the Transition Parameters $A$ and $B$

##### Method of Calibration

A series of numerical tests must be performed to determine the appropriate values of  $A$  and  $B$ . Initially it was not known if they could be held constant, or if they must become dependent on the free-stream turbulence intensity. However, preliminary tests showed that for good results, they must be made functions of  $Tu_e$ . The conditions for the tests are the same as considered in chapter 3; ie. flat plate, zero pressure gradient flow with variable free-stream turbulent intensity. For calibration purposes, the free-stream dissipation was kept low so that  $Tu_e$  remained essentially constant (free-stream length scale effects will be discussed in the next section). The start and end of transition was taken to be where  $C_f$  was at it's minimum and maximum respectively. Computations were started a very low  $Re_{x,i}$  to assure that the calculations were independent of the initially specified profiles of  $k$  and  $\epsilon$ .

Starting at one specific free-stream turbulence level, a series of computations were made. After an initial guess,  $A$  and  $B$  were appropriately adjusted after each run, so that each succeeding calculation agreed more closely with the correlation of Abu-Ghannam and Shaw. After a number of iterations it was then possible to find the "correct" values so as to achieve the start and end of transition exactly in accord with the correlation. For clarity, that correlation is repeated here;

$$Re_{\theta,S} = 163 + \exp(6.91 - 100 * Tu_e) \quad (4.8)$$

$$Re_{\theta,E} = 2.667 * Re_{\theta,S} \quad (4.9)$$

Once  $A$  and  $B$  were found at one free-stream turbulence intensity, the level was changed, and the process was repeated.

In Section 4.5.1 and 4.5.2, two distinct ideas for controlling the production term were explored, but their combined use was not discussed. For computing flows at high  $Tu_e$ , where transition should occur very near to  $Re_{\theta}=163$ , there is not sufficient time for the production term to grow if  $P_k$  is maintained at zero up until  $Re_{\theta}=162$ , as was done in 4.2.1. However, a few computational tests showed that choosing a value of about 125 would be sufficiently low. This value will hereafter be referred to as  $Re_{\theta,C}$ . Initially,  $Re_{\theta,C}=125$  was adopted as a constant for all of the calculations with the Lam-Bremhorst model. This may seem somewhat arbitrary, but it was actually constrained by the following two factors;

- (1) If  $Re_{\theta,C}$  is too high, the correct start and end of transition could not be obtained through the use of eq. (4.6) for any values of  $A$  and  $B$ .
- (2) The lower  $Re_{\theta,C}$  becomes, the smaller the region near the leading edge within which starting profiles of  $k$  and  $\epsilon$  are not significant to the calculations.

Since insensitivity to the initial profiles of  $k$  and  $\epsilon$  is a desired characteristic, there seemed no reason to consider reducing  $Re_{\theta,C}$  further, and the calibration tests for  $A$  and  $B$  were performed with this value. Afterward, tests were made to determine just how dependent or sensitive the

computations were to this value. It was found that reducing  $Re_{\theta,C}$  did somewhat shorten the acceptable starting region as explained above, although it did not require the values of  $A$  and  $B$  to be changed. At high turbulence intensities, although the  $Re_{\theta}$ -transition relationship remained unchanged, the actual location where transition occurred was slightly shifted upstream. However, for low  $Tu_e$ , there was no significant effect at all. This will be illustrated in the next section where results will be shown for both  $Re_{\theta,C}=125$ , and for  $Re_{\theta,C}=0$ .

#### Calculated Values of $A$ and $B$ for the L.B. Model

Calculations to determine the transition model parameters  $A$  and  $B$  were made for a range of turbulence intensities of from 0.5 to 10.0 %. The results of these calculations are presented in figures 4.8 and 4.9. Note that both  $A$  and  $B$  have been non-dimensionalized with respect to local free-stream conditions as follows;

$$\bar{A} = \frac{A \mu_e}{\rho_e U_e^2} \quad (4.10)$$

$$\bar{B} = \frac{B \mu_e^2}{\rho_e^3 U_e^6} \quad (4.11)$$

After these computational experiments were completed, curve fits were made to the data, which are also shown in the figures. It was found that the

variation in  $\bar{A}$  and  $\bar{B}$  could be represented very well as follows;

Let  $\phi = Tu_e$ ,  $\bar{B} = \bar{B} * 10^{12}$ , and  $\bar{A} = \bar{A} * 10^6$

---


$$\begin{aligned}
 0.0 < \phi < .07 \quad \log_e(\bar{B}) &= -5.4549 + 389.2806 * \phi - 7556.0334 * \phi^2 \\
 &\quad + (7.278 * 10^4) * \phi^3 - (2.85036 * 10^5) * \phi^4 \\
 0.0 < \phi \quad \log_e(\bar{B}) &= 1.8625 + 14.6786 * \phi
 \end{aligned}$$

(4.12)

---

---


$$\begin{aligned}
 0.0 < \phi < .02 \quad \bar{A} &= 6.8475 - 367.00 * \phi + 9200.0 * \phi^2 \\
 .02 < \phi < .081 \quad \bar{A} &= -6.4711 + 1177.586 * \phi - 45930.0 * \phi^2 \\
 &\quad + (6.152 * 10^5) * \phi^3 - (2.767 * 10^6) * \phi^4 \\
 .081 < \phi \quad \bar{A} &= -4.6011
 \end{aligned}$$

(4.13)

---

It should be noted that the calibration tests showed the predicted location of transition to be more strongly influenced by the value of  $B$ , than it was by  $A$ . The linear term within which  $A$  is found has only a secondary role, but was necessary to control the length of transition properly.

Figure 4.10 is a duplication of Figure 3.4 with the results of these new calculations added. It simply indicates that  $A$  and  $B$  were properly found so as to match the correlation.

In Figure 4.11, typical turbulent kinetic energy profiles produced during transition are plotted. When compared with Figure 4.3 we see very clearly the effect of controlling the production term. The overshoot so visible before is almost completely removed and the profiles vary smoothly from the laminar to turbulent state in a physically plausible manner. (It is interesting to consider the similarities with the data of Dyban, Epik, and Suprun [24].)

#### 4.5.6 The Effects of High Free-stream Dissipation Rate

Almost all of the calculations presented up to this point have been done on flow conditions where the free-stream turbulence intensity was assumed to be essentially constant. This was accomplished computationally by simply setting the starting value of  $\epsilon_e$  equal to a very small number. However, in real situations this is not normally encountered, especially in flows of high  $Tu_e$ , where invariably the dissipation rate is also high. Thus the question naturally arises as to how to properly account for a free-stream turbulence intensity that is changing significantly before transition occurs.

One of the advantages of using a  $k$ - $\epsilon$  approach is that the effects of this type of variation are naturally included as part of the model. As far as the transition parameters are concerned, we simply base them on the local free-stream conditions. Computationally, since the step size is usually quite small relative to the rate at which  $k$  and  $\epsilon$  decay, it is usually quite sufficient to only update  $A$  and  $B$  after every 10 or 20 steps.

Since the relationship between  $k_e$  and  $Tu_e$  involves the free-stream velocity, acceleration can also have dramatic effects on the free-stream turbulence intensity. If the flow accelerates,  $Tu_e$  goes down, even though  $k_e$  may have remained relatively constant. Deceleration has just the opposite effect, yielding an increase in  $Tu_e$ . This does not present any additional difficulty for the model, and as before, we simply continue to base our calculations on the local free-stream conditions.

#### **4.6 TRANSITION CALCULATIONS WITH THE PTM VERSION OF THE LAM-BREMHORST MODEL**

Results from a number of calculations are presented here to show the location and characteristics of transition as predicted by the modified Lam-Bremhorst model. Calculations for seven free-stream turbulence conditions covering a range of 1.0 to 8.0% were made. As before, the conditions considered were simple flat plate, zero pressure gradient flows with the free-stream turbulence being the only variable parameter. The results are represented through three different plots. In Figure 4.12, the variation in  $C_f$  with  $Re_x$  is shown. This can be compared with Figures 3.3-a, 3.3-b, and 4.1, which show the calculations made with the unmodified Lam-Bremhorst, unmodified Jones-Lauder, and method of Rodi and Scheuerer respectively. Figure 4.13 replots  $C_f$  as a function of momentum thickness Reynolds number. This will be helpful when comparing the effect that changing  $Re_{\theta,C}$  has on the predictions. Finally, Figure 4.14 shows the calculated variation in the shape-factor ( the ratio of displacement to momentum thickness) with Reynolds number.

In addition to the transition aspects that these figures show, it is interesting to note the predicted effect that high free-stream turbulence has on both the "pseudo" laminar region prior to transition, and on the fully turbulent conditions. This is manifest in an increase in  $C_f$ , and a decrease in shape factor, and can be easily observed far before  $C_f$  reaches its minimum. This carries through to the turbulent region where  $C_f$  shows a 15-20 % increase over the value for the 1% case. Both of these trends are consistent with experiment and will be discussed again later.

Figures 4.15 through 4.17 show the effect of removing the restriction that sets  $P_k=0$  for  $Re_{\theta,C}<125$ . Except for this difference the calculations were identical. The results are compared at  $Tu_e=2\%$  and  $6\%$  as representative of the effects in general. The following three items should be mentioned relative to this comparison.

- (1) The most significant differences occur at higher turbulence intensities.
- (2) When  $Re_{\theta,C}=0$ , the boundary layer is more strongly affected in the upstream "pseudo laminar" region than before. This is due to allowing  $P_k$  to begin to grow sooner. However, as can be seen in Figure 4.16, although the magnitude of  $C_f$  has changed, the location with respect to  $Re_{\theta}$  where a minimum is reached is not changed. Thus the agreement of these calculations with the correlation of Abu-Ghannam and Shaw has not been significantly altered.
- (3) When  $Re_{\theta,C}=0$ , the change in shape factor over the transition region takes a less abrupt and smoother path from its fully laminar value of 2.6 down to the turbulent conditions.

The only other difference relates to the sensitivity of the calculations to the initial starting location. This will be shown in section 4.8.

#### 4.7 APPLICATION OF THE MODIFICATION TO THE JONES-LAUDER MODEL

The previous sections of this chapter have explained the application of the PTM modifications almost entirely in terms of the Lam-Bremhorst model. However, in principle, the only difference in using another model should be with respect to the calibration of the parameters  $A$  and  $B$ . To assure that this was indeed the case, The Jones-Lauder model was modified in exact analogy to the Lam-Bremhorst model, and the parameters  $A$  and  $B$  determined. It may be recalled that the Jones-Lauder model differs from the Lam-Bremhorst model in its dissipation rate variable and in the introduction of some additional source terms. However, on applying the transition modifications only the production term in the modeled  $k$  equation ( $P_k = \mu_t (\partial U / \partial Y)^2$ ) was controlled.

The only real question that needed to be answered was whether or not to apply a critical momentum thickness criteria (as explained in section 4.5.1) in addition to limiting the growth rate (recall that the Lam-Bremhorst model was applied both with and without this modification). To answer this question  $A$  and  $B$  were first found at a relatively high turbulence intensity. Then a number of experiments were made to determine the highest value of  $Re_{\theta,C}$  that could be used and still match the correlation of Abu-Ghannam and

Shaw. It was found that in contrast to the Lam-Bremhorst model, The highest value of  $Re_{\theta,C}$  that could be used was only about 75. This can be attributed to the additional source terms in the Jones-Launder model, all of which act to suppress the turbulent kinetic energy in the developing region. Since this was so small the application of a critical momentum thickness parameter in addition to growth rate limitation was neglected (ie.  $Re_{\theta,C}=0$ ).

Figures 4.18 and 4.19 show the behavior of  $\bar{A}$  and  $\bar{B}$  as found through a series of numerical experiments. Also shown for comparison is the previously determined variation of  $\bar{A}$  and  $\bar{B}$  for the Lam-Bremhorst model. A curve fit representing the data is given as follows in eqs. (4.14) and (4.15).

Let  $\phi=100*Tu_e$ ,  $\bar{B} = \bar{B} * 10^{12}$ , and  $\bar{A} = \bar{A} * 10^6$

---


$$\begin{array}{ll}
 0.0 < \phi < 2.0 & \log_e(\bar{B}) = -5.8084 + 2.995*\phi \\
 2.0 < \phi < 6.0 & \bar{B} = 18.738 - 26.8085*\phi + 12.7536*\phi^2 \\
 & \quad - 2.1152*\phi^3 + 0.1218*\phi^4 \\
 6.0 < \phi & \log_e(\bar{B}) = 1.950 + 0.1573*\phi
 \end{array}$$

(4.14)

---

---


$$\begin{array}{ll}
 0.0 < \phi < 6.0 & \bar{A} = 12.2266 - 1.7904*\phi - 2.4229*\phi^2 \\
 & \quad + 0.57595*\phi^3 - 0.0365*\phi^4 \\
 6.0 < \phi & \bar{A} = -7.5 - 0.19*\phi
 \end{array}$$

(4.15)

---

It is interesting to note that they are qualitatively quite similar to the the Lam-Bremhorst parameters except for the small dip in the "B " parameter curve at about  $Tu_e=2\%$ . This dip is directly associated with the problem in the Lam-Bremhorst  $f_\mu$  function that was explained in section 4.2.

After  $A$  and  $B$  were found, the same seven flow conditions considered in section 4.6 were calculated and the transition predictions plotted. These are shown in figures 4.20 to 4.22. They are very similar to the results using the Lam-Bremhorst model, as can be more clearly seen in figures 4.23-4.25. In these figures, calculations at  $Tu_e=2\%$  and  $6\%$  are compared with both Lam-Bremhorst model calculations ( ie.  $Re_{\theta,C}=125$  and  $Re_{\theta,C}=0$ ). It may be noted that in each of these cases the Jones-Launder model predicts a slightly lower  $C_f$  in the fully turbulent region than the Lam-Bremhorst model. This is due to the particular choice of constants used in the LRN function equations (some variation exists in the literature) and is not a result of the transition modifications made. Of greater interest is that results of the PTM Jones-Launder model, which are for  $Re_{\theta,C}=0$ , compare very well with the results of the PTM Lam-Bremhorst models for  $Re_{\theta,C}=125$ .

One problem occurred in applying the modifications to the Jones-Launder model. When calculating transition at  $Tu_e=1\%$ , the simulation proceeded smoothly until transition was about 20% complete. At that point there was an abrupt decay of the predicted results back to a laminar-like state. If computations were allowed to continue, this process would repeat itself. Investigation revealed that the problem was related to the  $f_\mu$  function decaying to values less than one in the outer regions of the boundary layer. It

was apparently due to the production term in the fully turbulent region near the boundary layer edge naturally growing faster than the transition prediction modification would allow (At low  $Tu_e$ , the parameter  $B$  becomes quite small). Note that near the boundary layer edge we normally do not desire any near-wall LRN effects. As a result, this would cause a small decay in the ratio of  $k$  to  $\epsilon$  in that region, reducing the turbulent Reynolds number " $Re_t$ ", which then yields a smaller  $f_\mu$ . When  $f_\mu$  begins to drop, the production term is directly diminished, and the imbalance between  $k$  and  $\epsilon$  then starts to become significant. This cycle quickly grows and causes the behavior mentioned.

Although the root of the problem appears to be the undesired effect of the transition modification in the fully turbulent region, without the decrease in  $f_\mu$ , the effect would be negligible because the unstable cycle mentioned would be broken. For example, since the Lam-Bremhorst model  $f_\mu$  is also a function of  $Re_y$ , a similar problem is precluded. Thus, for practical purposes, the problem can be overcome by requiring  $f_\mu$  to behave monotonically with  $y$ . This is accomplished by simply preventing  $f_\mu$  from decreasing (with respect to the  $y$  coordinate) once it has reached its maximum value of one. This is what was done for the 1% calculation shown. Of course, this is admittedly only a symptomatic treatment of the problem. A more general solution would require that the production term growth limitation be restricted to local areas where the turbulent Reynolds number is not large, ie. the introduction of an additional LRN function. Considering that the problem occurs only for  $Tu_e < 1\%$ , this additional complexity did not seem justified at this time.

In summary, it has been shown in this section that the PTM modifications can be applied with equal success to other k- $\epsilon$  LRN turbulence models. To do so simply requires the determination of the parameters  $A$  and  $B$  as explained. However, it also may require a simple additional restraint on the behavior  $f_\mu$  to avoid a problem at low  $Tu_e$ .

#### 4.8 STARTING CONDITIONS AND THE "PTM" MODELS

To assure consistent repeatable predictions it is important that the sensitivity of the method to the initial starting location be clearly identified. As this was done for the unmodified models in Chapter 3, it is now important to determine this for the PTM form of the models. To do so, tests were made for flows with  $Tu_e=3\%$ , and at  $Tu_e=8\%$ . The initial starting location was then varied from  $Re_{x,i}=1. \times 10^2$ , to  $Re_{x,i} = 2.27 \times 10^4$ , and the results compared. Some plots of these results can be seen in Figures 4.26, 4.27, and 4.28, which correspond to using the Lam-Bremhorst model with  $Re_{\theta,C}=125$ , the Lam-Bremhorst model with  $Re_{\theta,C}=0$ , and the Jones-Launder model respectively.

The important aspects of this comparison can be listed as follows;

- (1) As compared to the 3% calculations presented in chapter 3, the Lam-Bremhorst model with  $Re_{\theta,C}=125$  shows a greatly reduced sensitivity to starting location. However, the free-stream turbulence effects in the region prior to transition are also diminished. In

contrast, the Lam-Bremhorst model with  $Re_{\theta,C}=0$ , together with the Jones Launder model show only a limited decreases in sensitivity.

- (2) For the Lam-Bremhorst model, the importance of the starting location seems to increase as  $Tu_e$  goes up. This does not appear to be the case for the Jones-Launder model.
- (3) For the Lam-Bremhorst model, the actual location in  $x$  where the minimum in  $C_f$  occurs is not very sensitive to the starting location. Instead, it tends to affect the magnitude of  $C_f$  at which this minimum occurs. For the Jones-Launder model, this is not the case.
- (4) For each of the models and for both of the conditions tested, starting the calculation at a  $Re_{x,i}$  less than  $10^3$  is sufficiently low to reduce the starting location effects to insignificance. Note that this implies that the calculations are also insensitive to the starting profiles of  $k$  and  $\epsilon$  under these conditions.

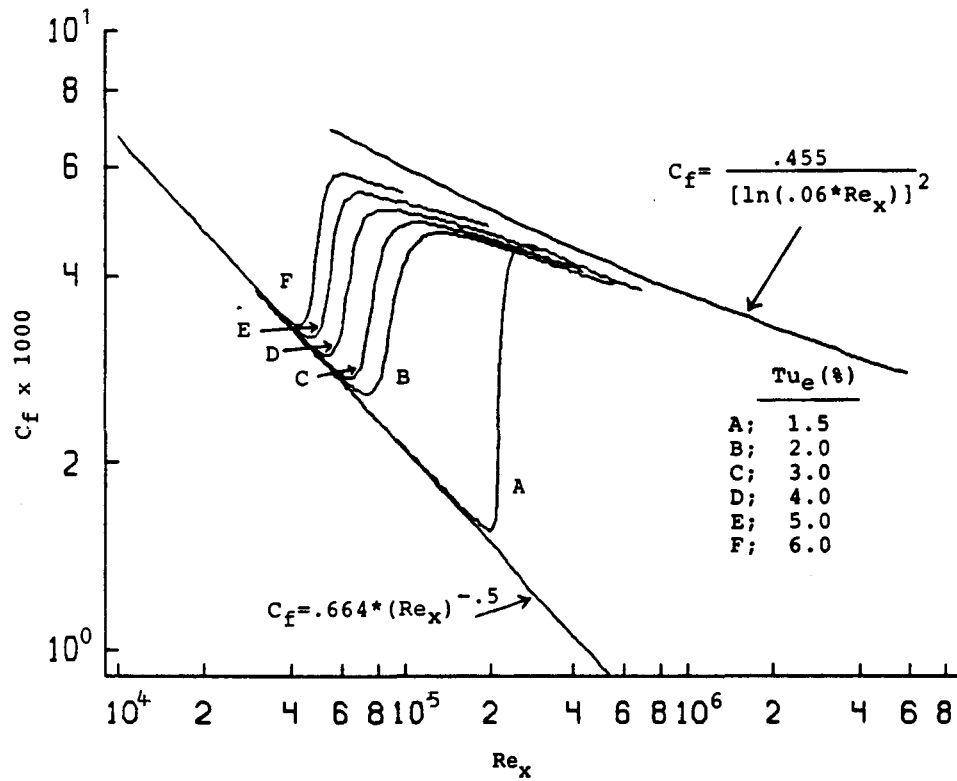


Figure 4.1 Plot of  $C_f$  vs  $Re_x$  for different levels of free-stream turbulence intensity as calculated by the method of Rodi and Scheuerer

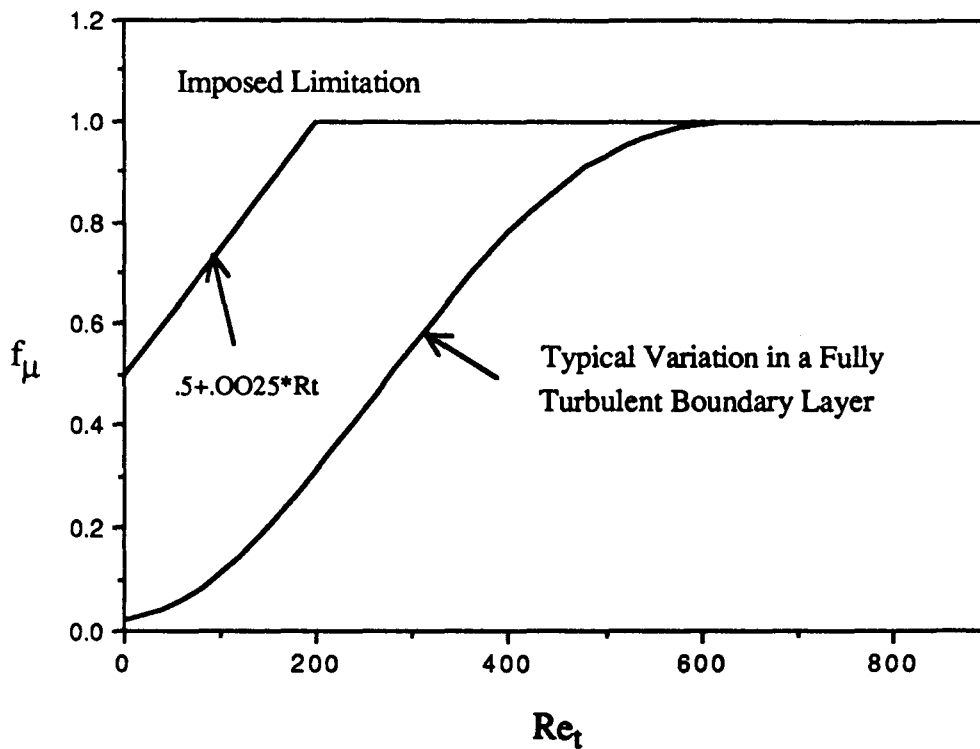


Figure 4.2 The limitation placed on the Lam-Bremhorst  $f_\mu$  function

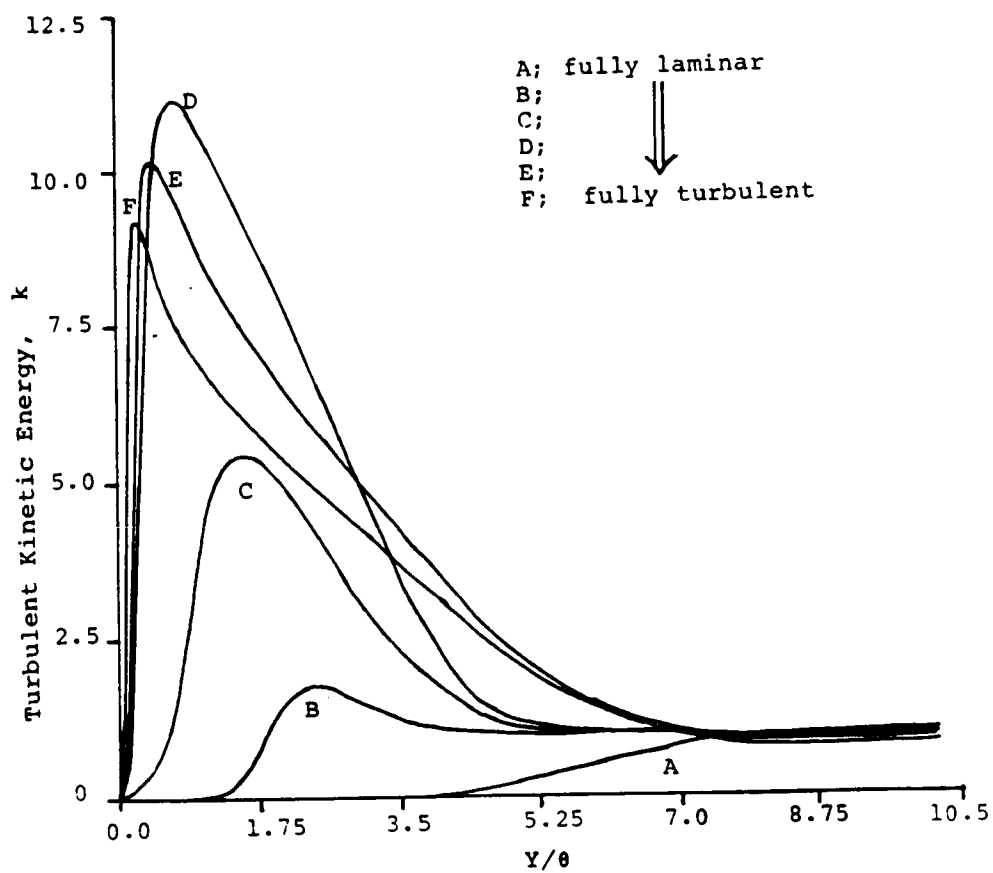


Figure 4.3 Development of the turbulent kinetic energy profiles as simulated by the unmodified Lam-Bremhorst model

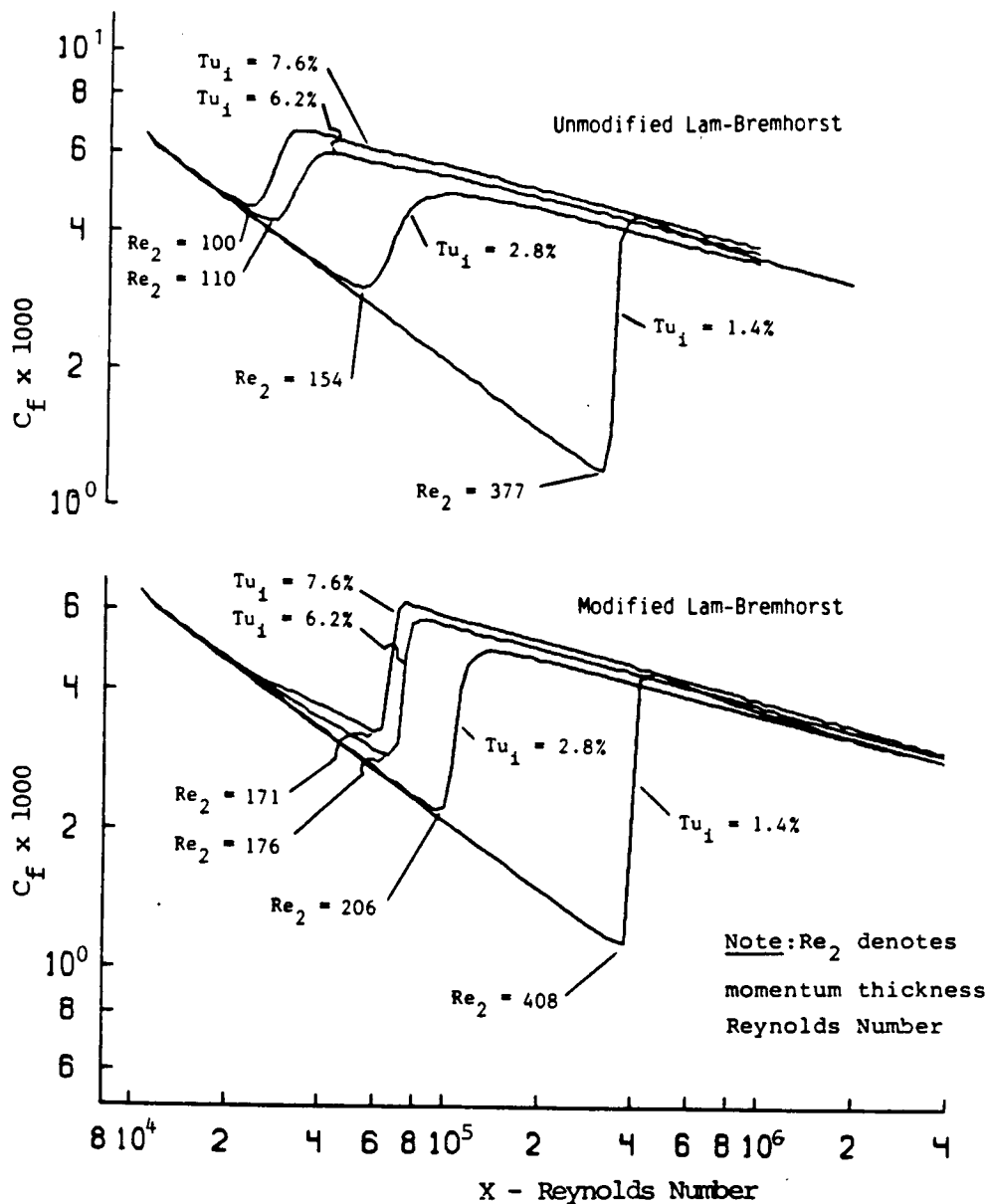


Figure 4.4 Plot of  $C_f$  vrs  $Re_x$  showing the effect of requiring the production term to be zero for  $Re_2 < 162$ .

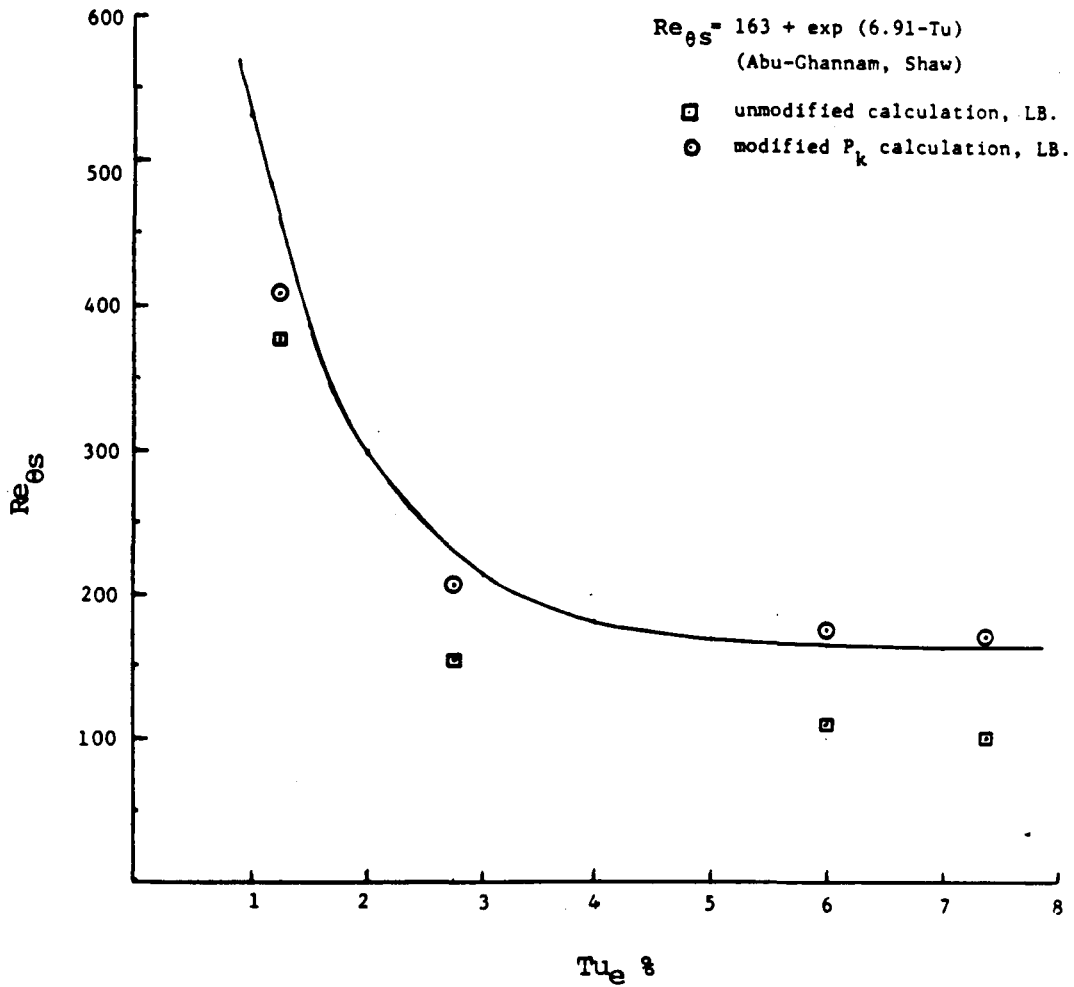


Figure 4.5 Plot of  $Re_{\theta S}$  vs  $Tu_e$  showing the effect of requiring the production term to be zero for  $Re_2 < 162$ .

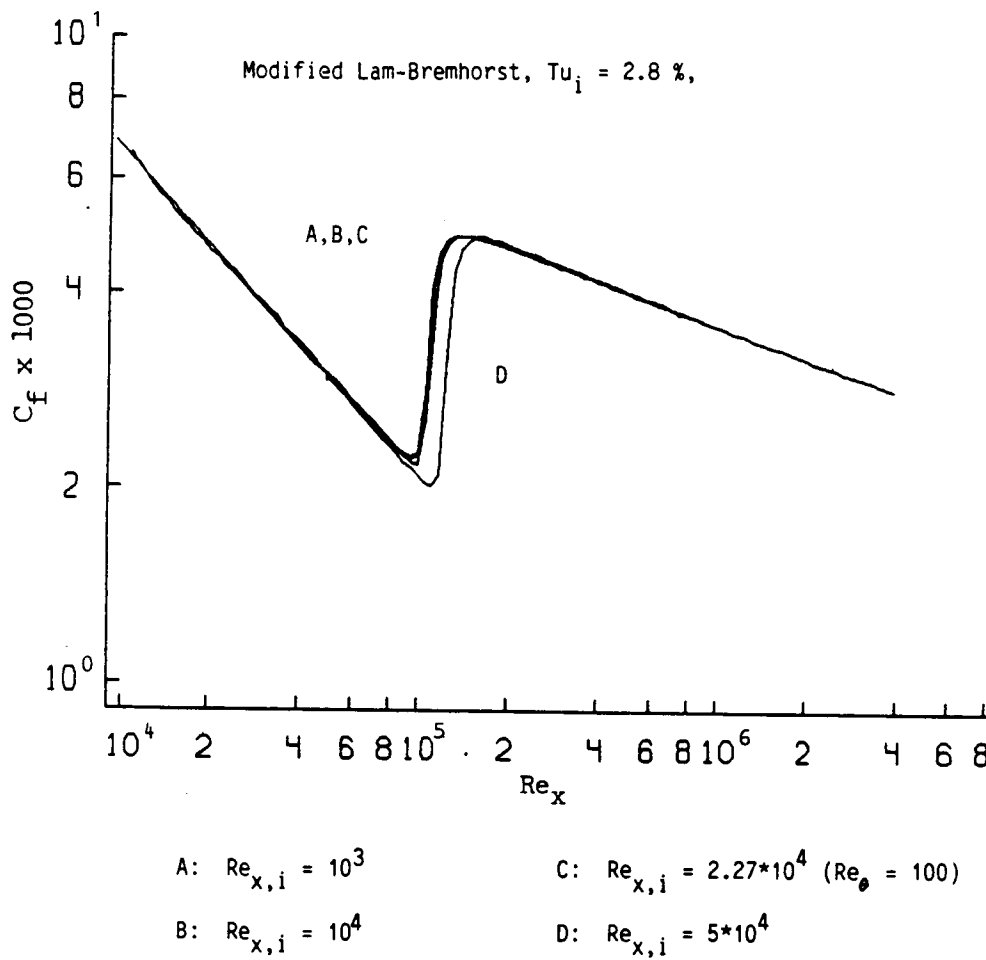


Figure 4.6 Plot of  $C_f$  vrs  $Re_x$  showing the effect that requiring the production term to be zero for  $Re_2 < 162$  has on the starting location sensitivity

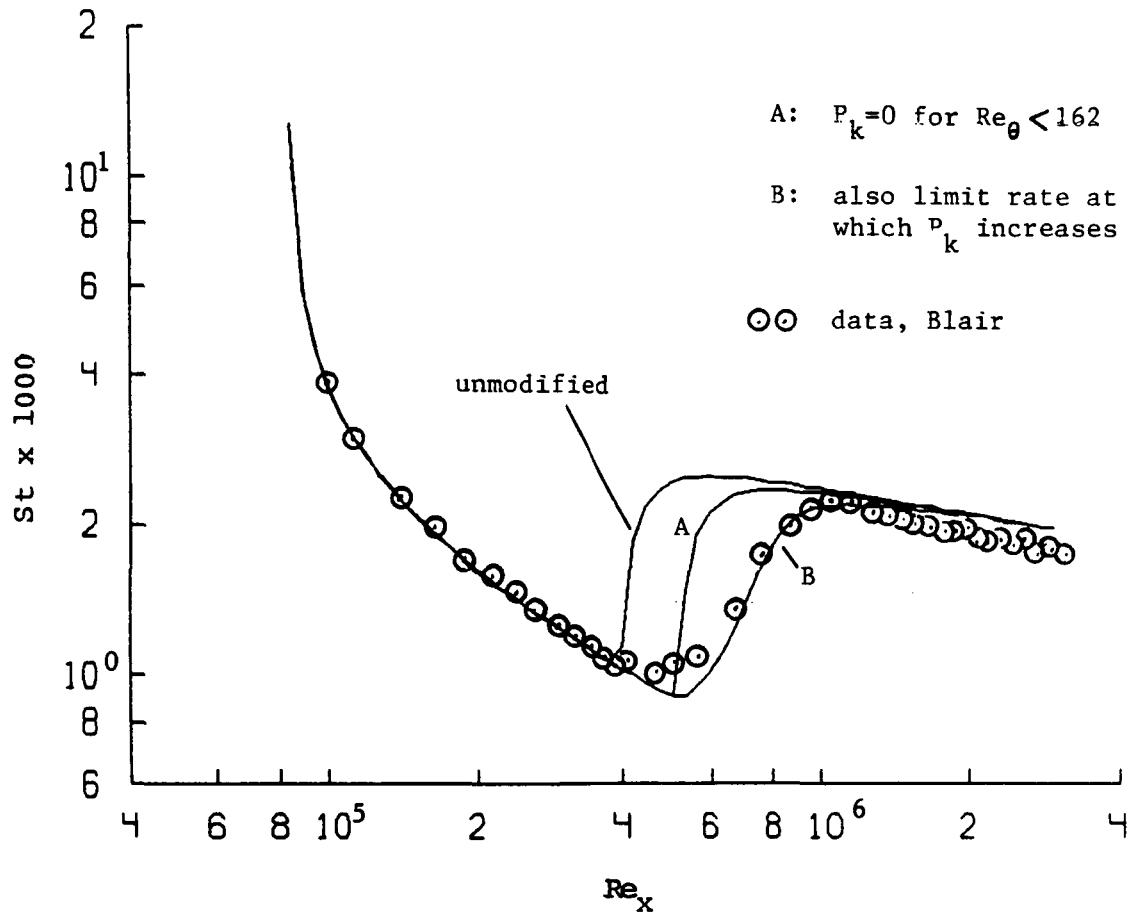
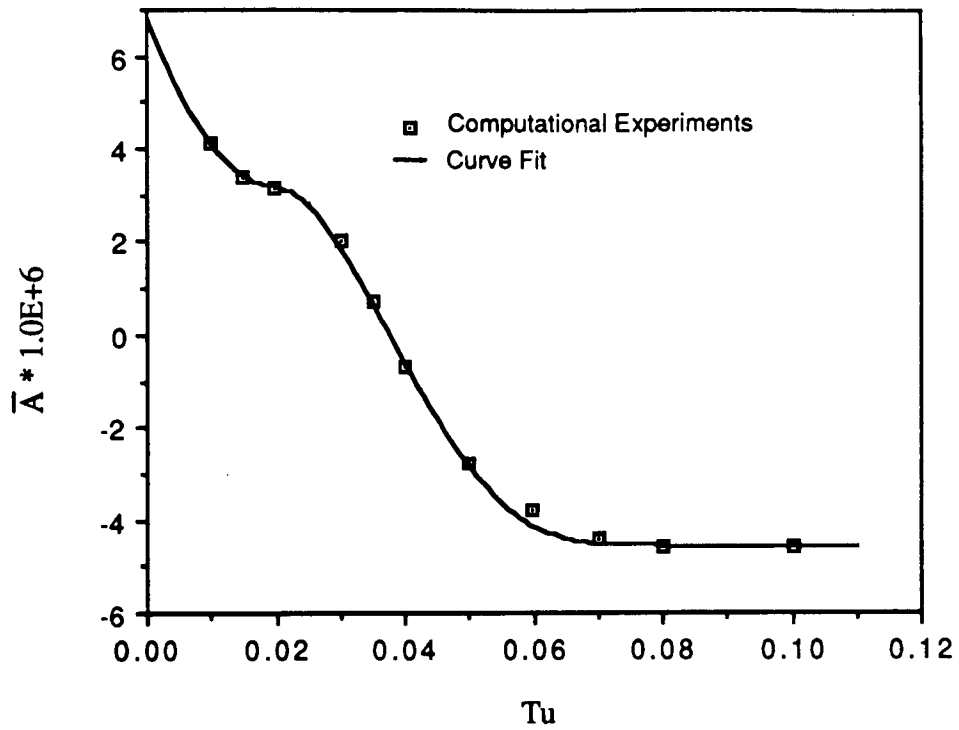
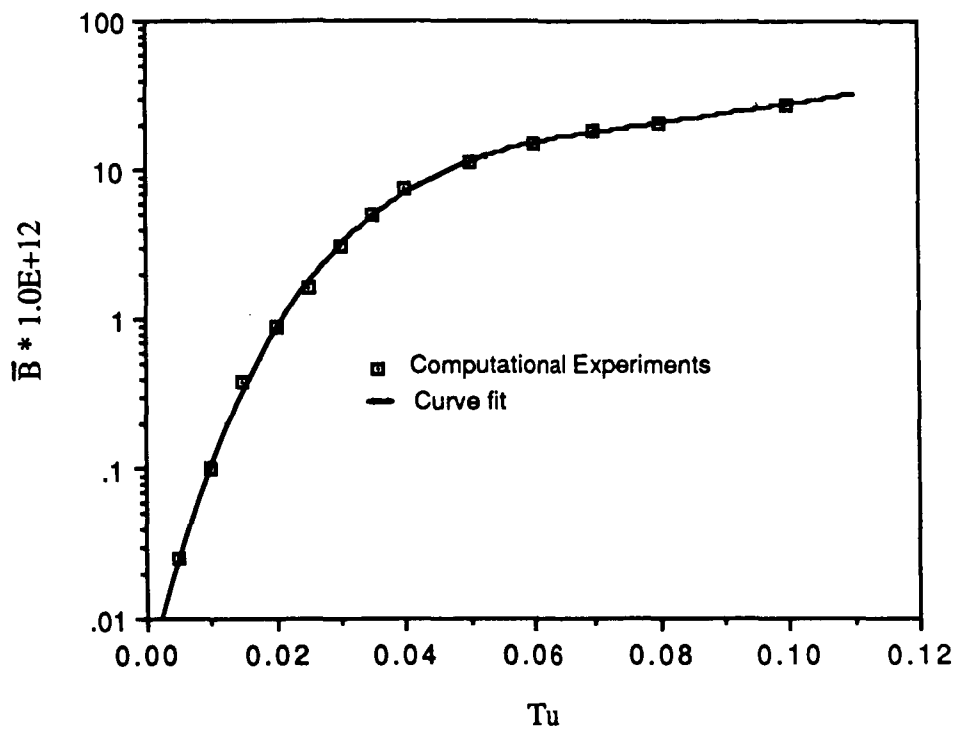


Figure 4.7 Effect of different production term modifications on the calculated Stanton number.  $Tu_{e,i} = 1.4\%$



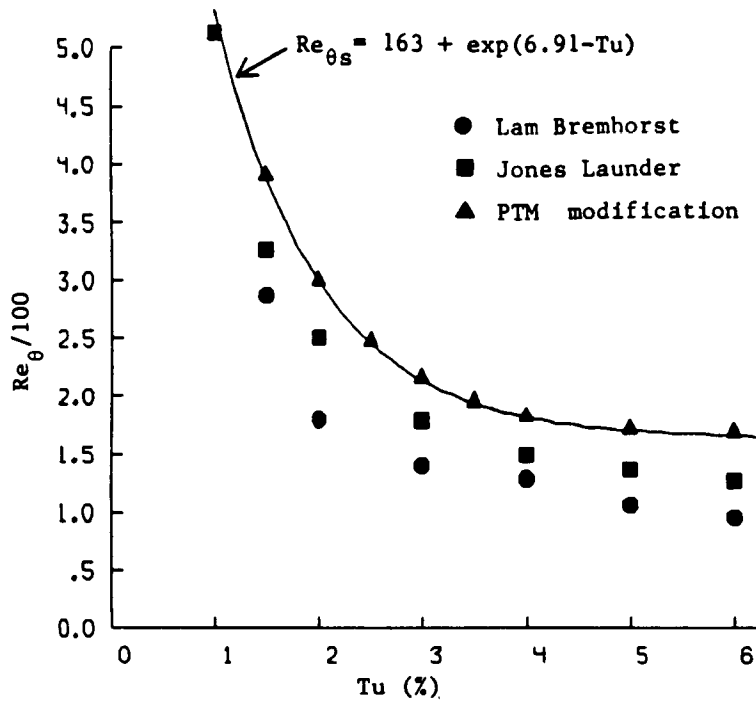
$$\bar{A} = \frac{A \mu_e}{\rho_e U_e^2}$$

Figure 4.8 Variation of "A " with free-stream turbulence intensity for the Lam-Bremhorst model

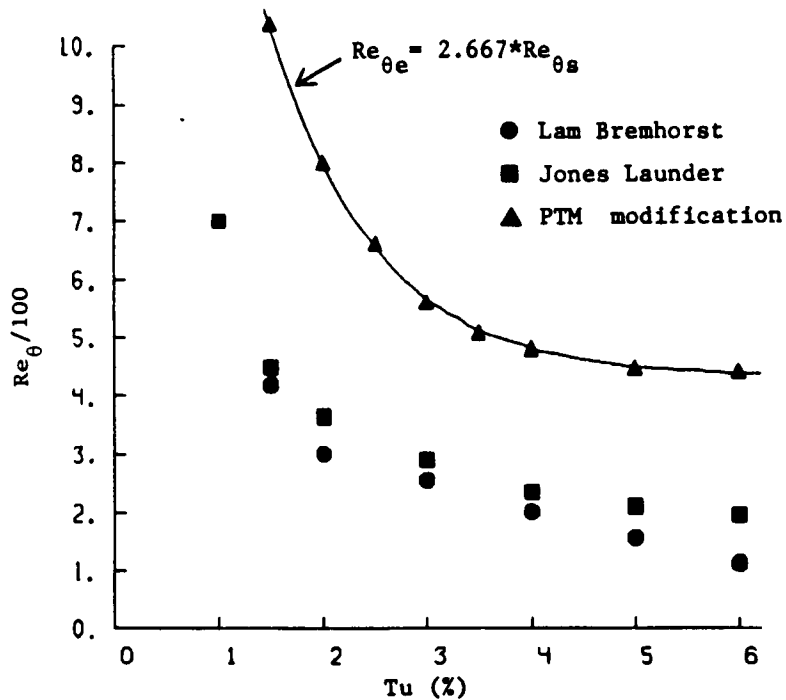


$$\bar{B} = \frac{B \mu_e^2}{\rho_e^3 U_e^6}$$

Figure 4.9 Variation of "B " with free-stream turbulence intensity for the Lam-Bremhorst model



a) Start of transition



b) End of transition

Figure 4.10 Calculated momentum thickness Reynolds numbers at the start and end of transition using the "PTM" model

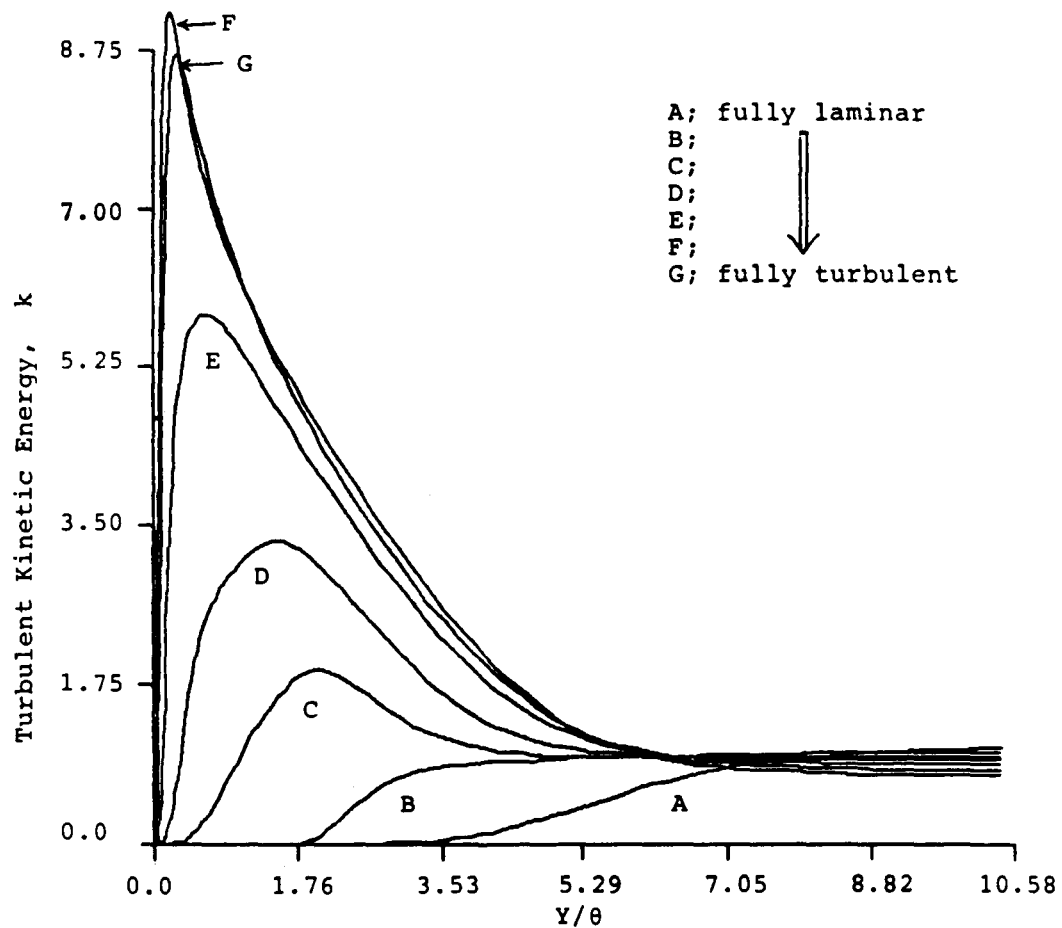


Figure 4.11 Development of the turbulent kinetic energy profiles as simulated by the "PTM" Lam-Bremhorst model

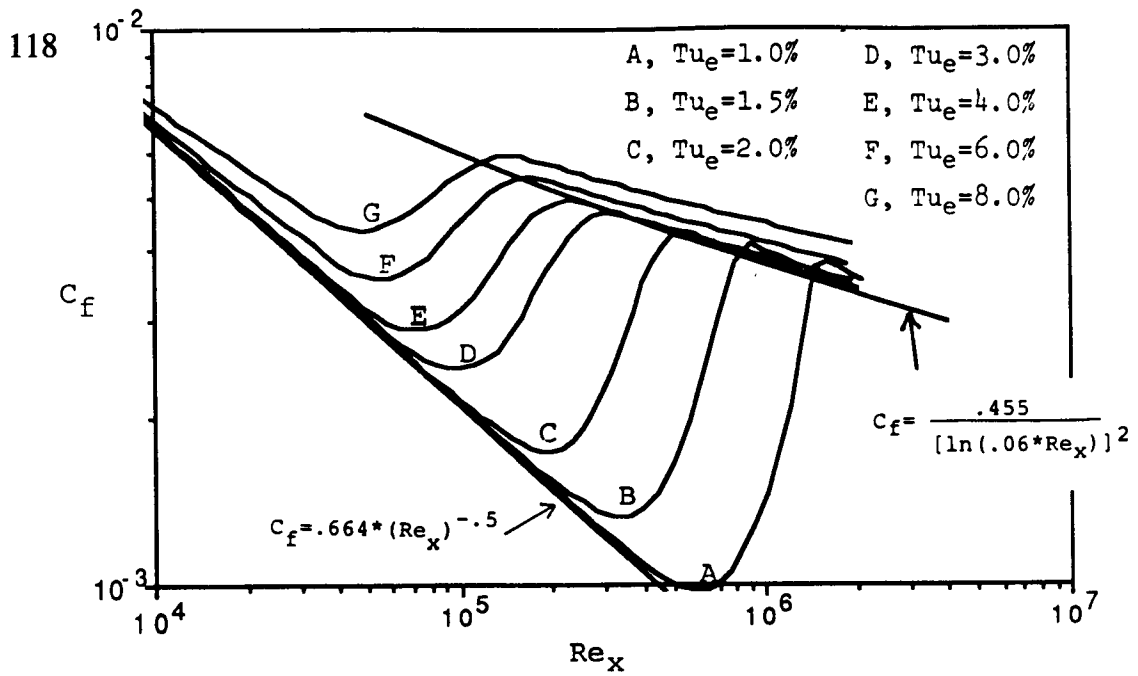


Figure 4.12 Plot of  $C_f$  vs  $Re_x$  at different levels of free-stream turbulence intensity using the "PTM" Lam-Bremhorst model  $Re_{\theta,C}=125$

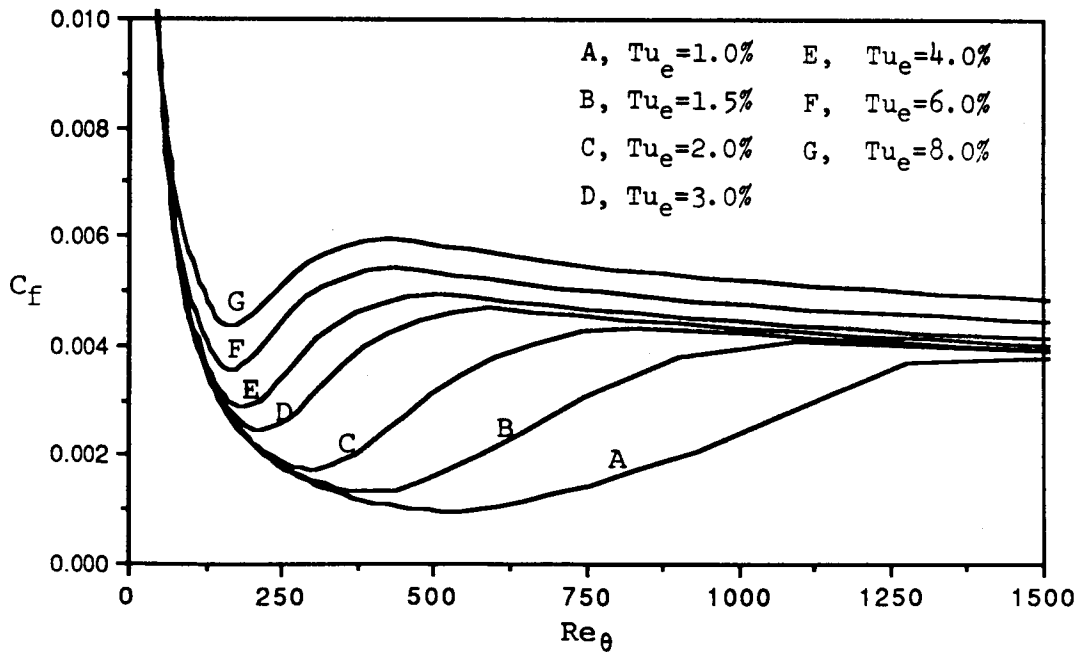


Figure 4.13 Plot of  $C_f$  vs  $Re_\theta$  at different levels of free-stream turbulence intensity using the "PTM" Lam-Bremhorst model  $Re_{\theta,C}=125$

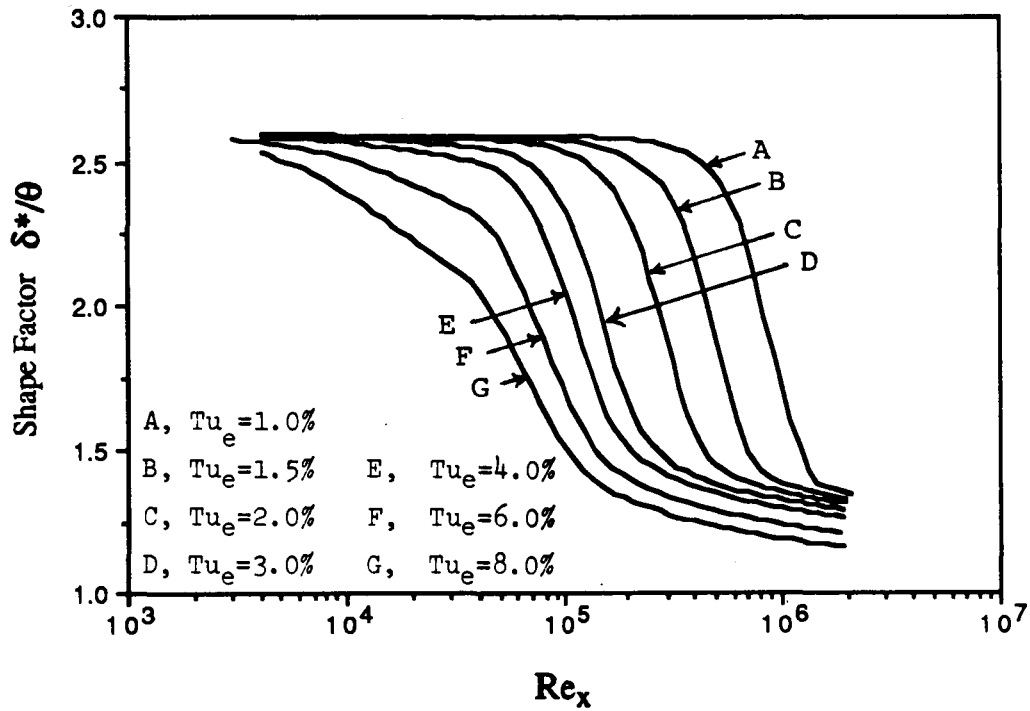


Figure 4.14 Plot of  $\delta^*/\theta$  vs  $Re_x$  at different levels of free-stream turbulence intensity using the "PTM" Lam-Bremhorst model.  $Re_{\theta,C} = 125$

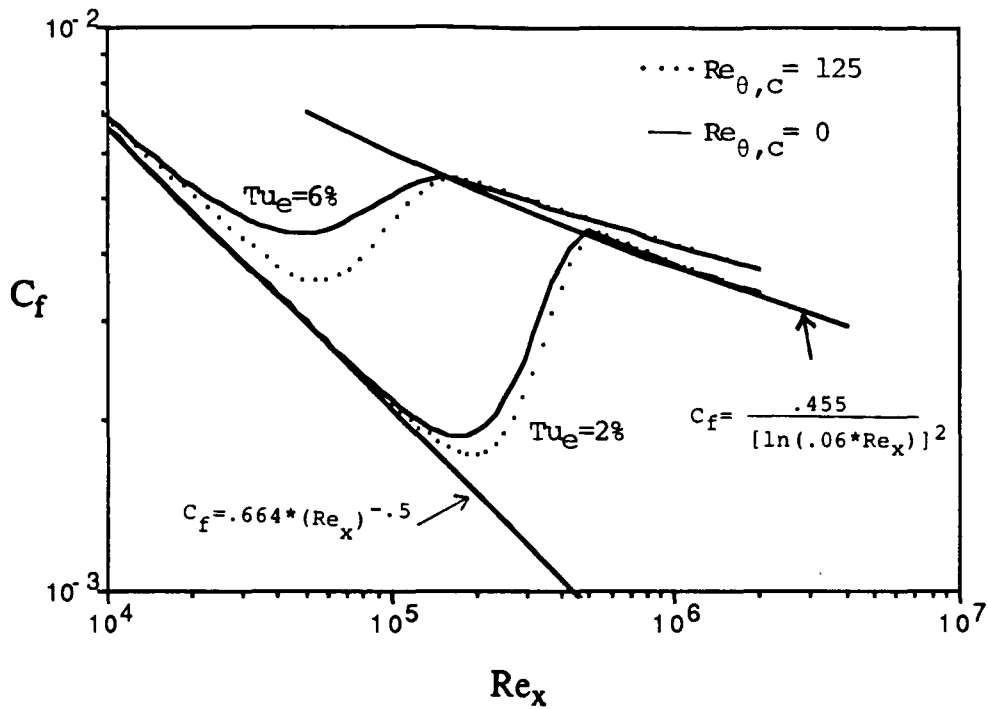


Figure 4.15 Plot of  $C_f$  vs  $Re_x$  comparing results for  $Re_{\theta,C} = 125$  with  $Re_{\theta,C} = 0$ . ("PTM" Lam-Bremhorst model)

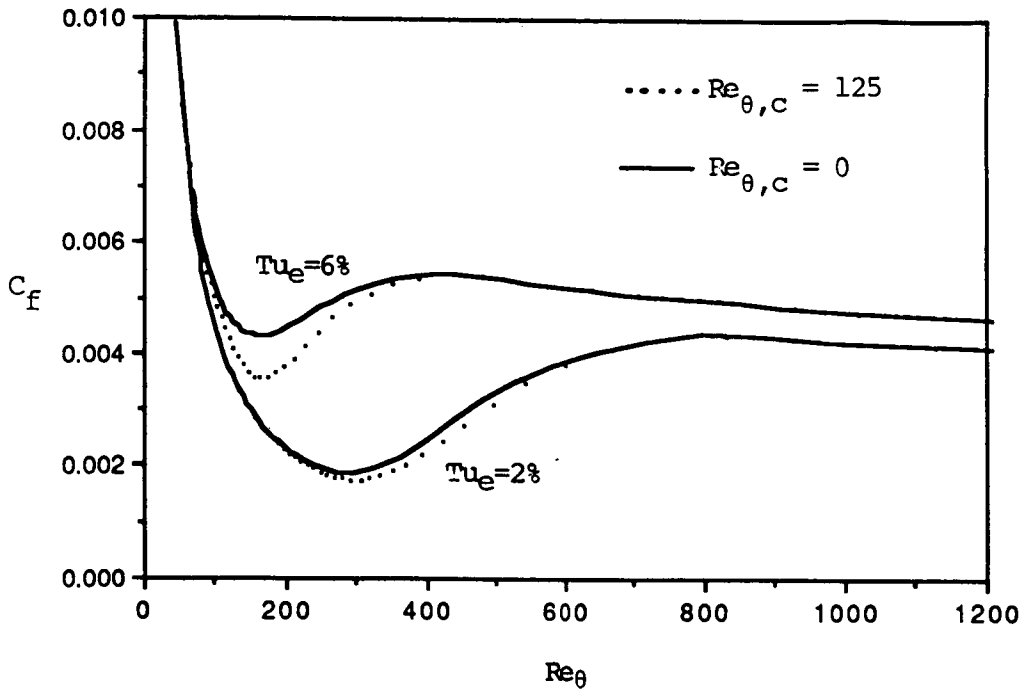


Figure 4.16 Plot of  $C_f$  vrs  $Re_\theta$  comparing results for  $Re_{\theta,C}=125$  with  $Re_{\theta,C}=0$ . ("PTM" Lam-Bremhorst model)

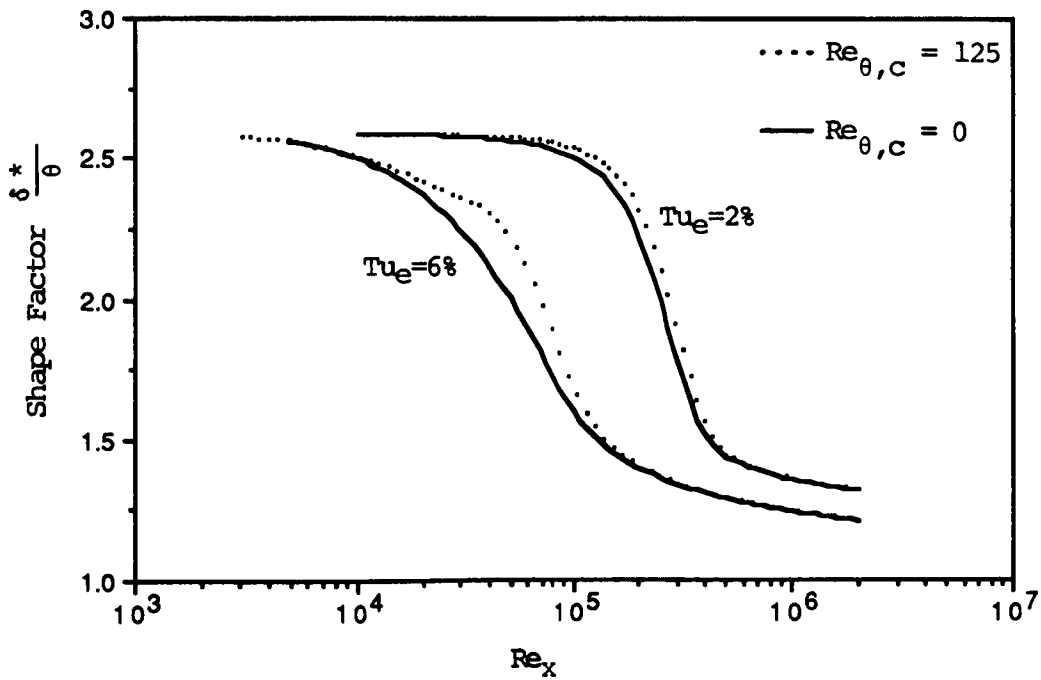
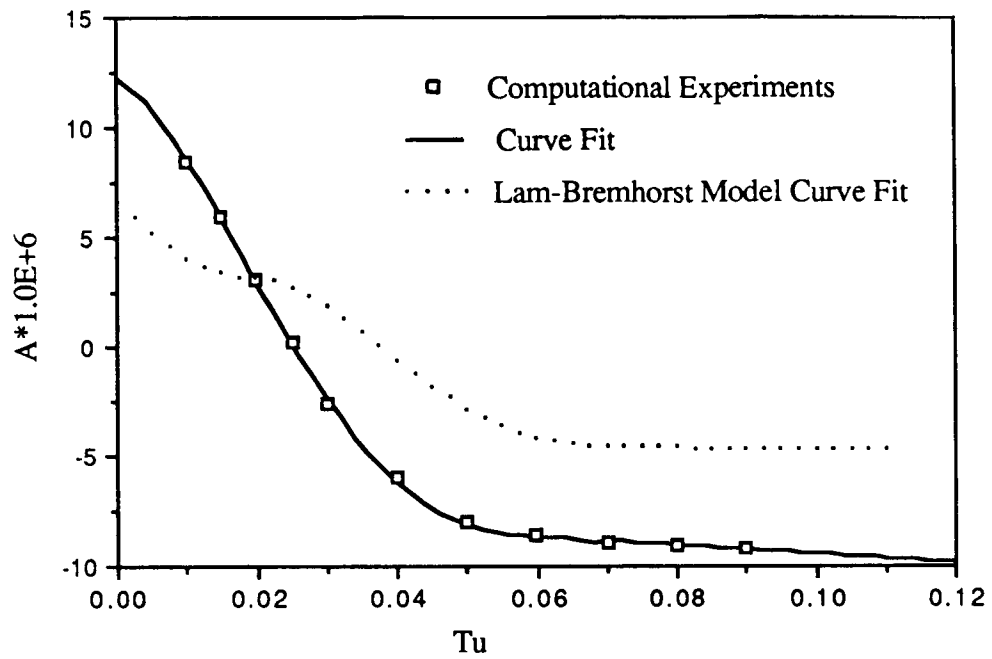
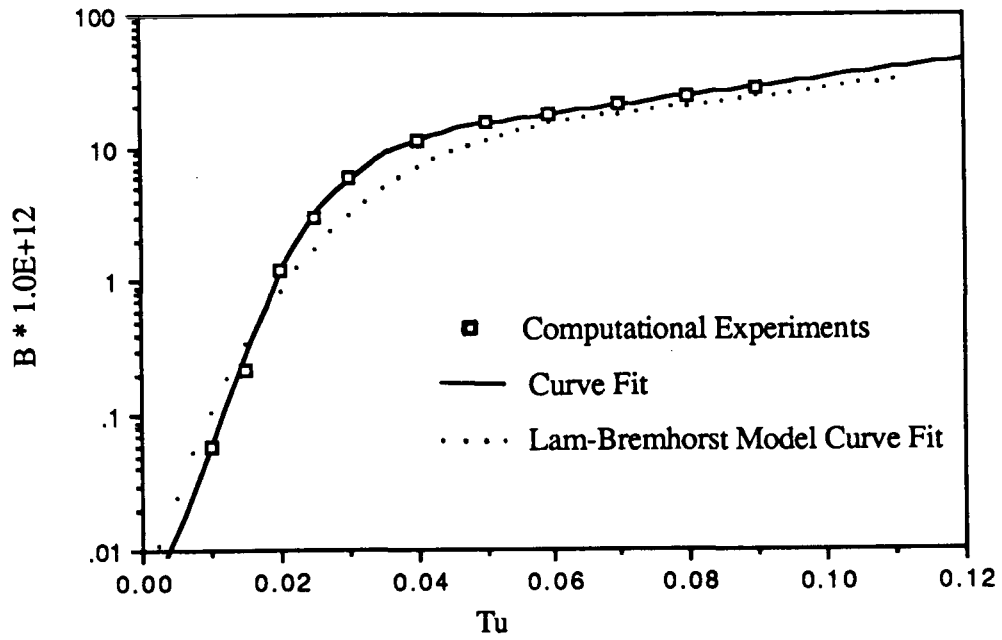


Figure 4.17 Plot of  $\delta^*/\theta$  vrs  $Re_x$  comparing results for  $Re_{\theta,C}=125$  with  $Re_{\theta,C}=0$ . ("PTM" Lam-Bremhorst model)



$$\bar{A} = \frac{A \mu_e}{\rho_e U_e^2}$$

Figure 4.18 Variation of "A " with free-stream turbulence intensity for the Jones-Launder model



$$\bar{B} = \frac{B \mu_e^2}{\rho_e^3 U_e^6}$$

Figure 4.19 Variation of "B " with free-stream turbulence intensity for the Jones-Launder model

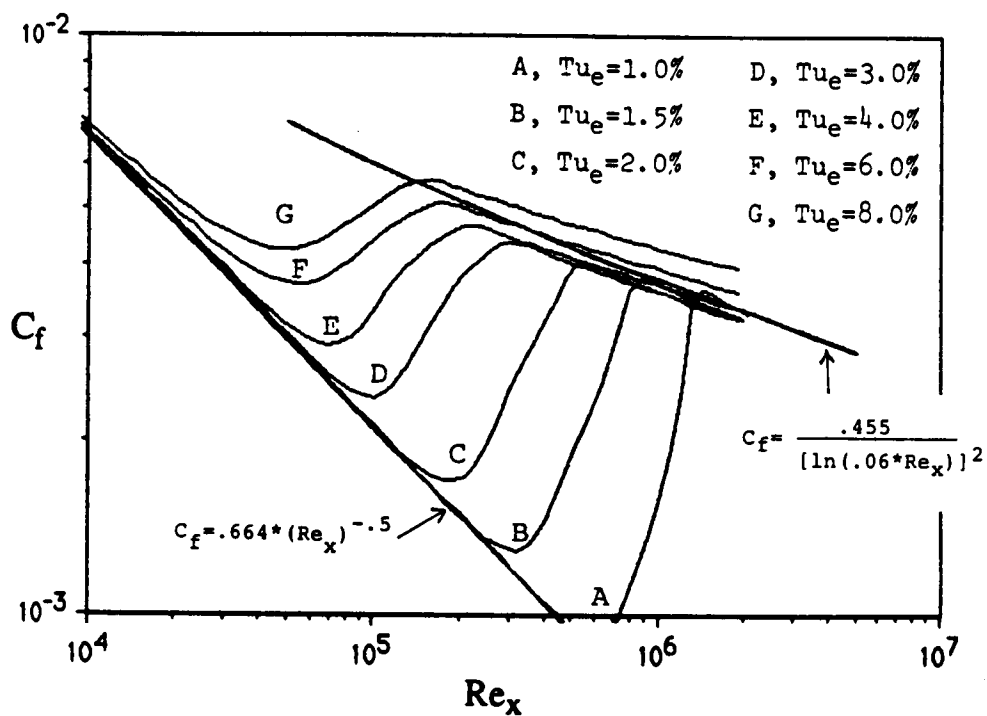


Figure 4.20 Plot of  $C_f$  vrs  $Re_x$  at different levels of free-stream turbulence intensity using the "PTM" Jones-Launder model

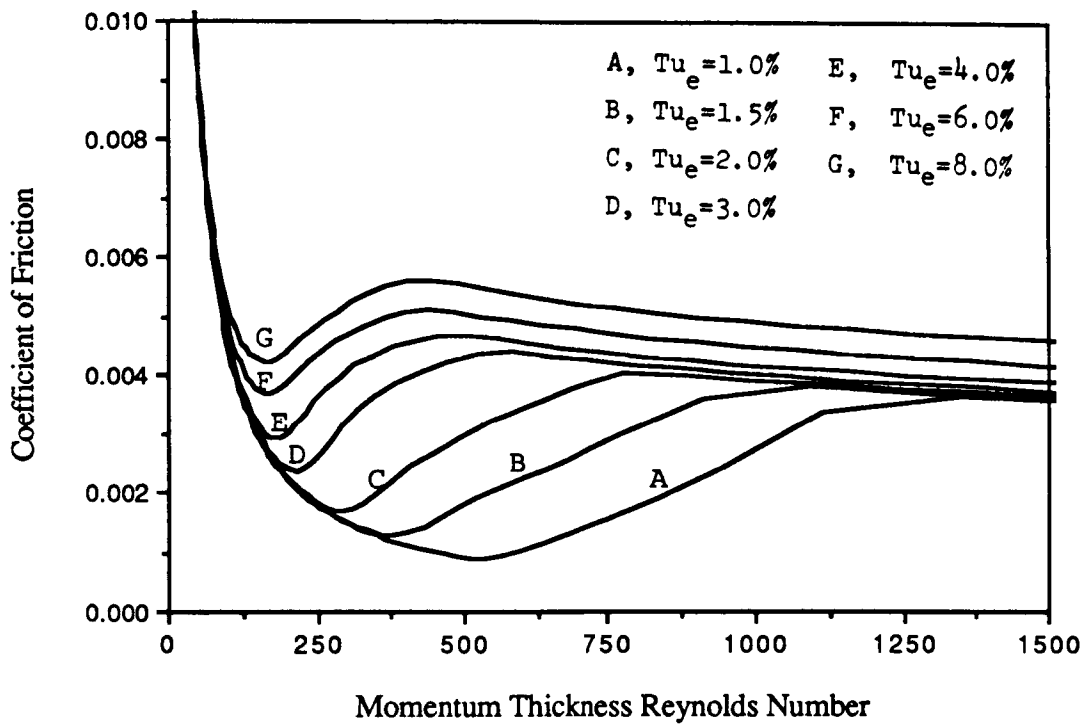


Figure 4.21 Plot of  $C_f$  vs  $Re_\theta$  at different levels of free-stream turbulence intensity using the "PTM" Jones-Launder model

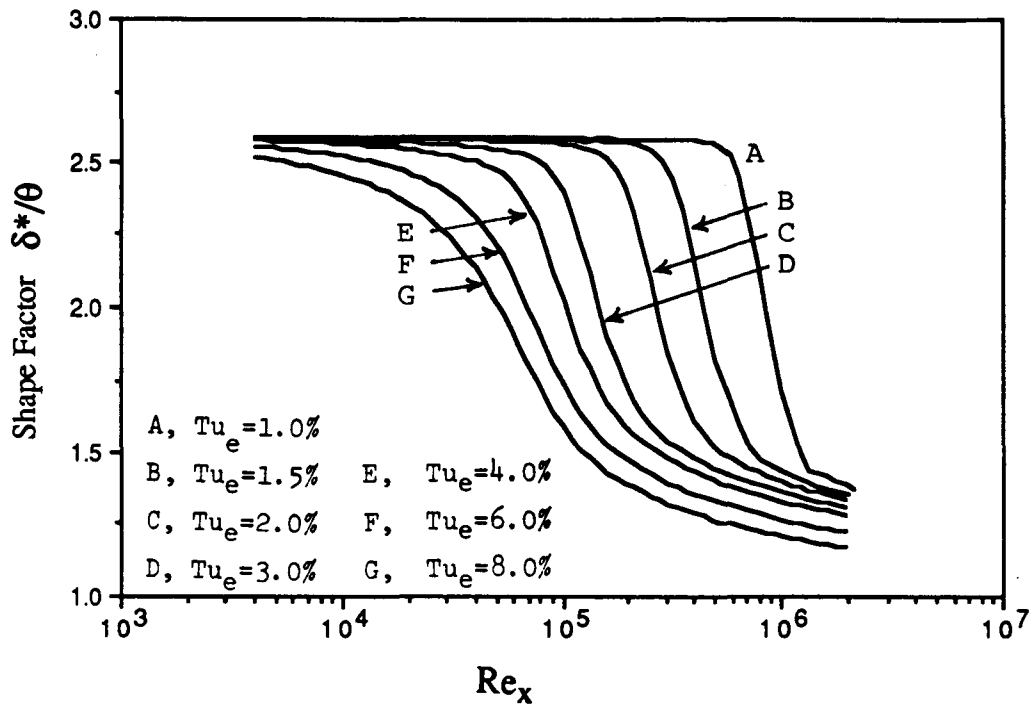


Figure 4.22 Plot of  $\delta^*/\theta$  vs  $Re_x$  at different levels of free-stream turbulence intensity using the "PTM" Jones-Launder model.

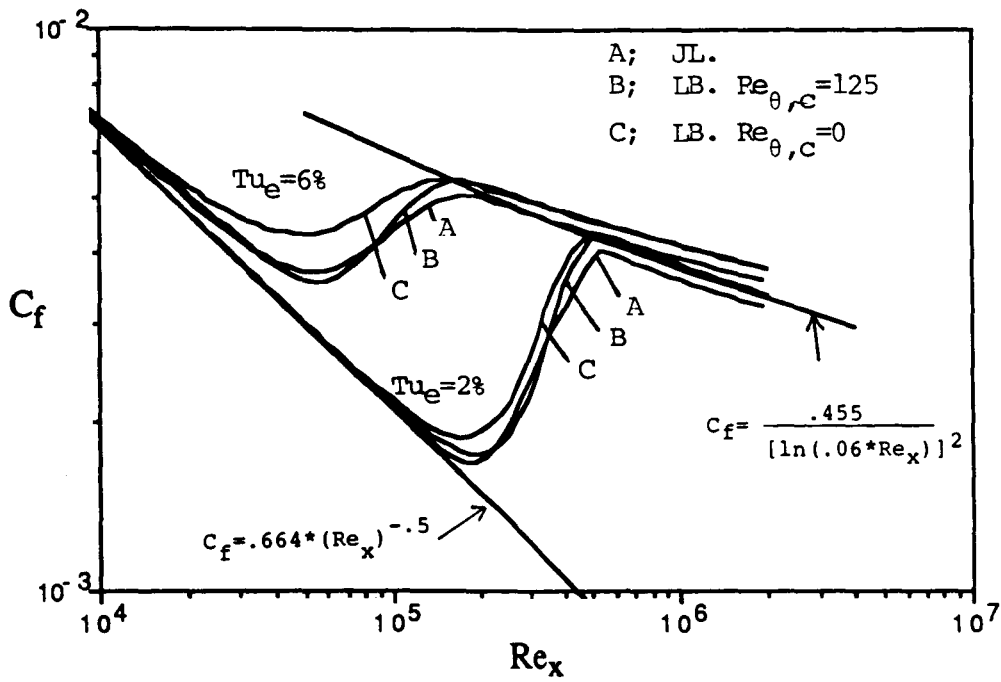


Figure 4.23 Plot of  $C_f$  vs  $Re_x$  comparing the Jones-Launder PTM version with the Lam-Bremhorst model calculations

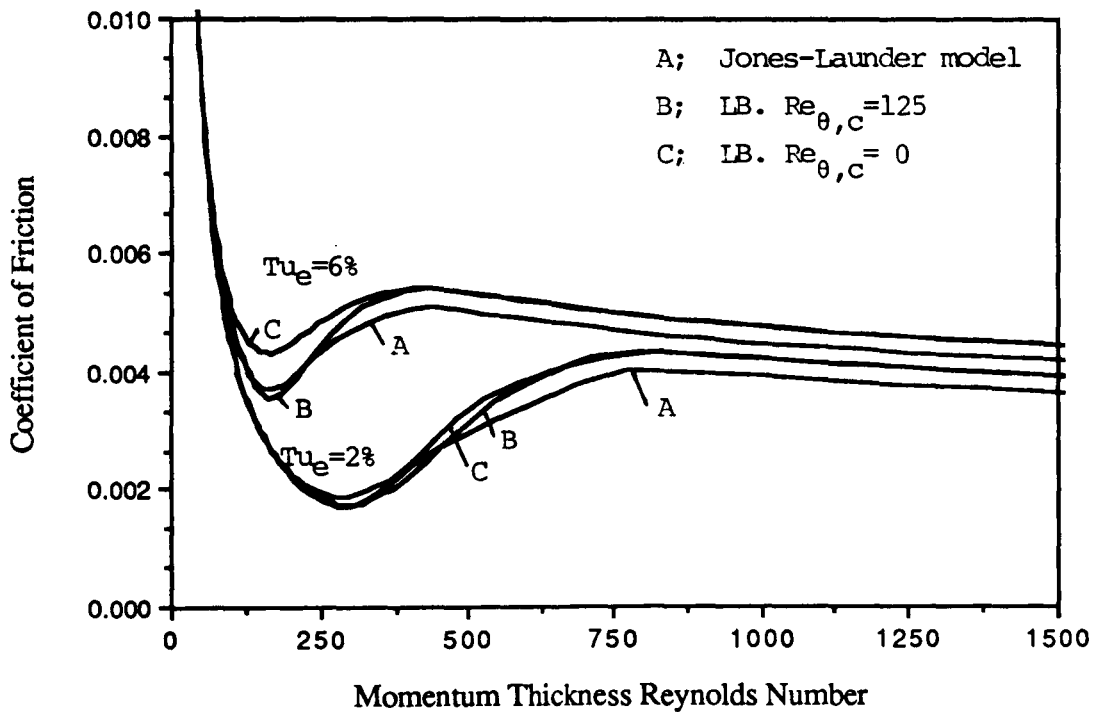


Figure 4.24 Plot of  $C_f$  vs  $Re_{\theta}$  comparing the Jones-Launder PTM version with the Lam-Bremhorst model calculations

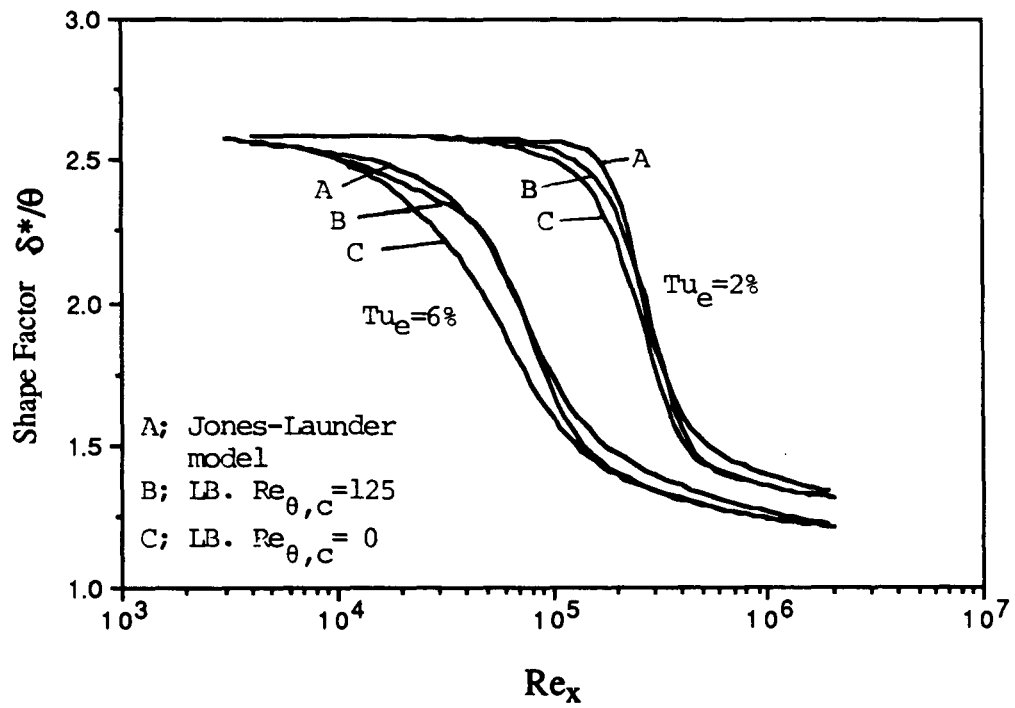


Figure 4.25 Plot of  $\delta^*/\theta$  vs  $Re_x$  comparing the Jones-Launder PTM version with the Lam-Bremhorst model calculations

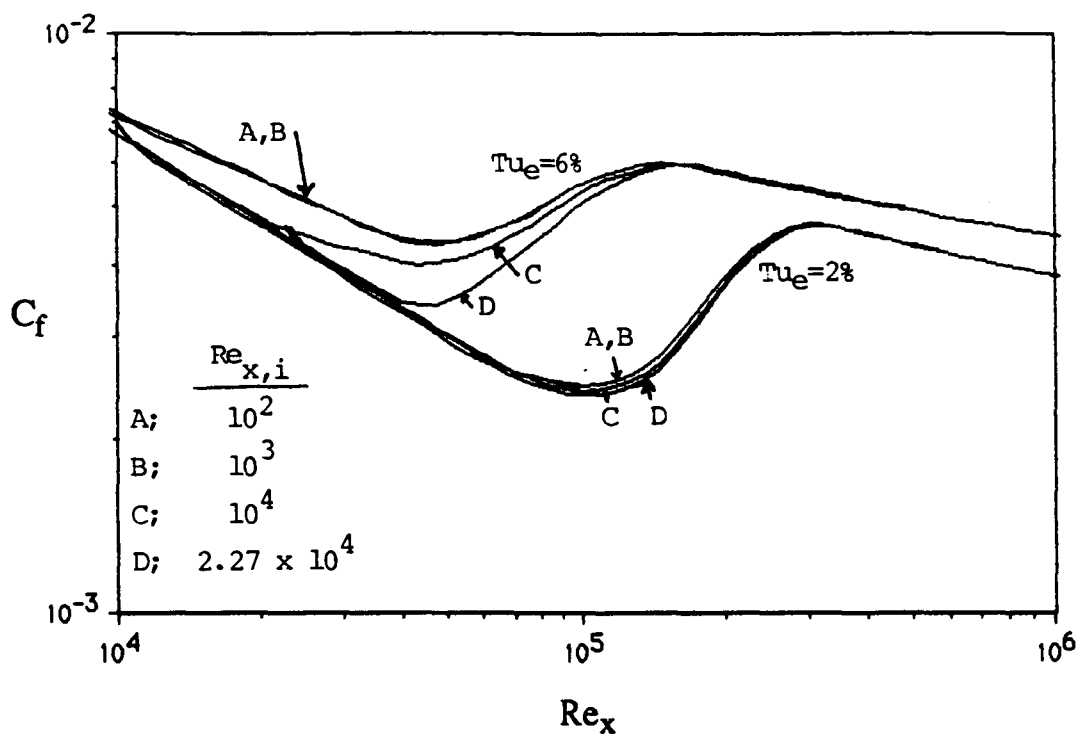


Figure 4.26 Plot of  $C_f$  vrs  $Re_x$  for different starting locations using the Lam Bremhorst model with  $Re_{\theta,C} = 125$

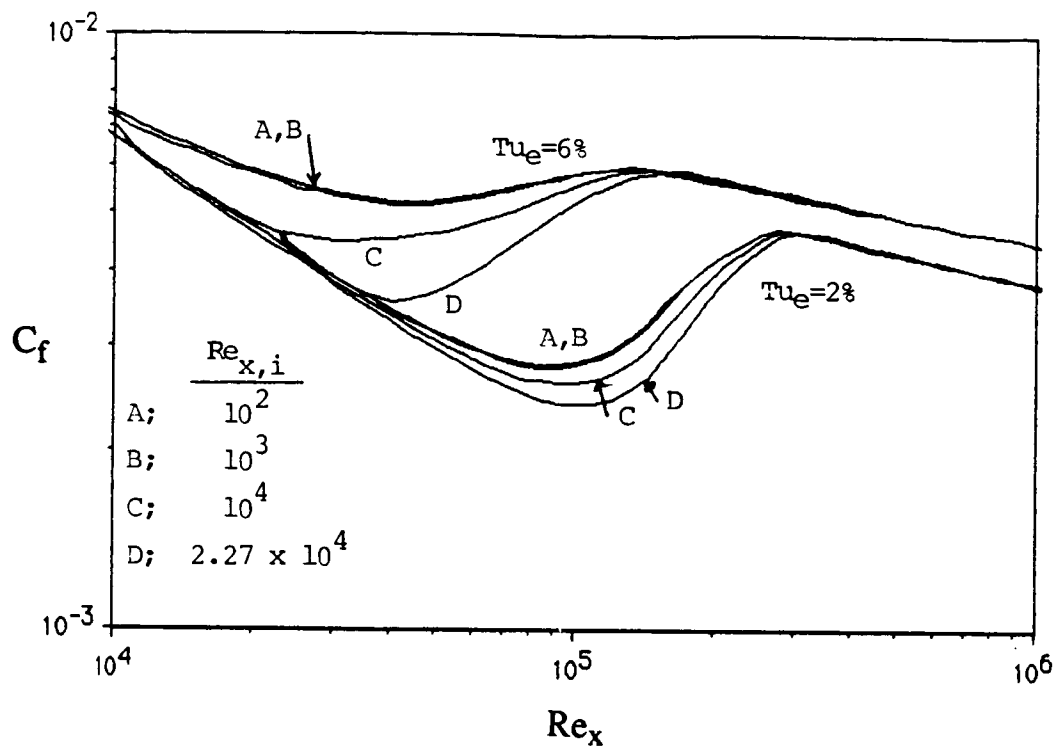


Figure 4.27 Plot of  $C_f$  vrs  $Re_x$  for different starting locations using the Lam Bremhorst model with  $Re_{\theta,C} = 0$

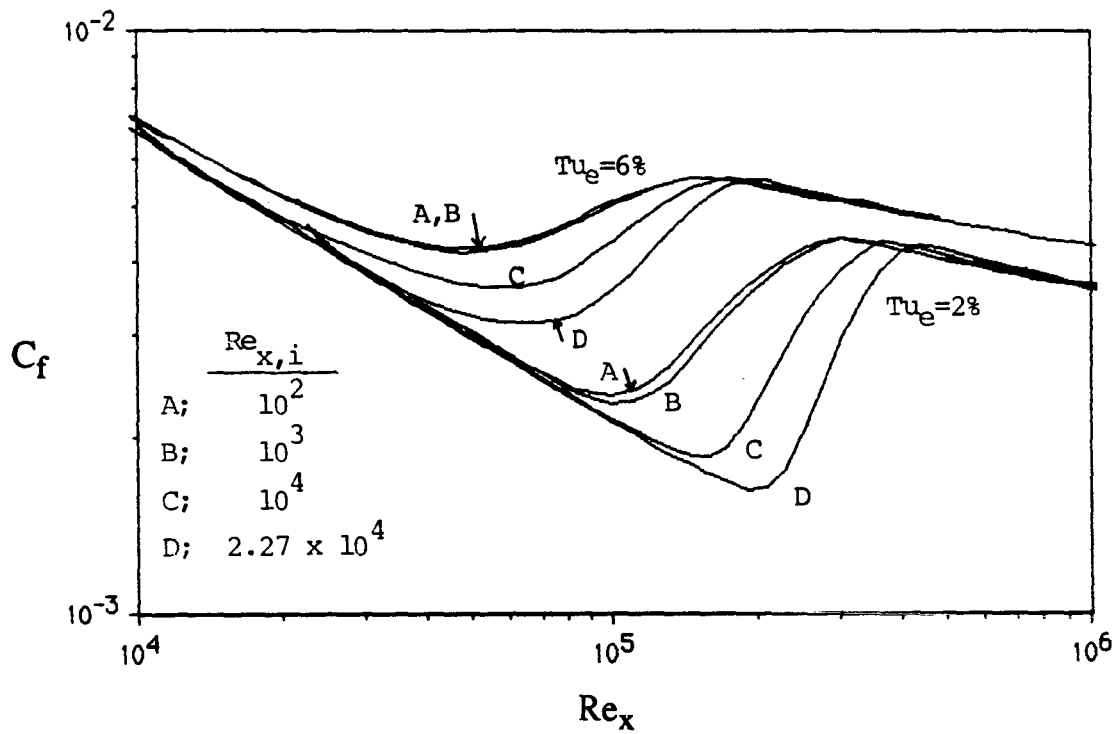


Figure 4.28 Plot of  $C_f$  vrs  $Re_x$  for different starting locations using the Jones-Launder model

## CHAPTER FIVE

### COMPARISON OF THE PROPOSED MODEL WITH EXPERIMENTAL DATA

Up to this point, direct comparison with experiment has been deferred in favor of developing the models as guided by empirical and semi-empirical correlations. This was deliberately done to avoid the potential bias that might occur if the method were "tuned" so to speak to only one or two experimental data sets. However, in order to truly evaluate the effectiveness of the model, careful comparison with a wide range of experiments is crucial.

In this chapter, the calculations will be compared with the results of 34 separate experiments taken from six different sources. Table 5.1 summarizes some of the important conditions of interest for each of these experiments. The flow conditions most thoroughly considered are flat plate flow both with and without favorable pressure gradients, but the calculations will also be compared to turbine blade cascade data. All of these experiments involve transition occurring under the influence of free-stream turbulence.

The model used in all of these calculations is the PTM form of the Lam-Bremhorst model with  $Re_{\theta,c}=125$ .

TABLE 5.1 Experimental Conditions for the Selected Data Sets

	Reference	Identifier	Tu (%) (at x=0)	Acceleration	Thermal Boundary Condition	Tw/Te (approx.)	Te (total)	Ue (at x=0)
1	Wang (and Simon)	flat plate test	2.3	Nb	Qw=160 W/(m <sup>2</sup> m)	1.03	298 K	13.5 m/s
2	Rued (and Wittig)	Nr. 2., no grid	1.6	Nb	Tw=302 K (29 C)	0.8	378 K	47 m/s
3	Rued (and Wittig)	Nr. 2., Grid 1	2.3	Nb	Tw=302 K (29 C)	0.8	378 K	47 m/s
4	Rued (and Wittig)	Nr. 2., Grid 2	3.8	Nb	Tw=302 K (29 C)	0.8	378 K	47 m/s
5	Rued (and Wittig)	Nr. 2., Grid 3	6.5	Nb	Tw=302 K (29 C)	0.8	378 K	47 m/s
6	Rued (and Wittig)	Nr. 2., Grid 4	8.6	Nb	Tw=302 K (29 C)	0.8	378 K	47 m/s
7	Blair and Werle	Grid 1	1.4	Nb	Qw=850 W/(m <sup>2</sup> m)	1.03	295 K	30.5 m/s
8	Blair and Werle	Grid 2	2.8	Nb	Qw=850 W/(m <sup>2</sup> m)	1.03	295 K	30.5 m/s
9	Blair and Werle	Grid 3	6.2	Nb	Qw=850 W/(m <sup>2</sup> m)	1.03	295 K	30.5 m/s
10	Blair and Werle	Low K, Grid 1	1.0	K=.20*10e-6	Qw=850 W/(m <sup>2</sup> m)	1.03	297 K	15.9 m/s
11	Blair and Werle	Low K, Grid 2	2.1	K=.20*10e-6	Qw=850 W/(m <sup>2</sup> m)	1.03	297 K	15.9 m/s
12	Blair and Werle	Low K, Grid 3	5.2	K=.20*10e-6	Qw=850 W/(m <sup>2</sup> m)	1.03	297 K	15.9 m/s
13	Blair and Werle	High K, Grid 2	2.2	K=.75*10e-6	Qw=850 W/(m <sup>2</sup> m)	1.03	297 K	9.93 m/s
14	Blair and Werle	High K, Grid 3	5.2	K=.75*10e-6	Qw=850 W/(m <sup>2</sup> m)	1.03	297 K	9.93 m/s
15	Rued (and Wittig)	Nr. 6., Grid 1	2.4	Kmax=1.2*10e-6	Tw=298 K (25 C)	0.64	466 K	49 m/s
16	Rued (and Wittig)	Nr. 6., Grid 2	3.9	Kmax=1.2*10e-6	Tw=298 K (25 C)	0.64	466 K	49 m/s
17	Rued (and Wittig)	Nr. 6., Grid 3	7.7	Kmax=1.2*10e-6	Tw=298 K (25 C)	0.64	466 K	49 m/s
18	Rued (and Wittig)	Nr. 6., Grid 4	11.1	Kmax=1.2*10e-6	Tw=298 K (25 C)	0.64	466 K	49 m/s
19	Rued (and Wittig)	Nr. 10, Grid 1	2.6	Kmax=3.2*10e-6	Tw=296 K (23 C)	0.64	463 K	48 m/s
20	Rued (and Wittig)	Nr. 10, Grid 2	3.6	Kmax=3.2*10e-6	Tw=296 K (23 C)	0.64	463 K	48 m/s
21	Rued (and Wittig)	Nr. 10, Grid 3	7.0	Kmax=3.2*10e-6	Tw=296 K (23 C)	0.64	463 K	48 m/s
22	Rued (and Wittig)	Nr. 10, Grid 4	10.1	Kmax=3.2*10e-6	Tw=296 K (23 C)	0.64	463 K	48 m/s
23	Rued (and Wittig)	Nr. 12, Grid 1	2.6	Kmax=5.7*10e-6	Tw=299 K (26 C)	0.64	467 K	27 m/s
24	Rued (and Wittig)	Nr. 12, Grid 2	3.6	Kmax=5.7*10e-6	Tw=299 K (26 C)	0.64	467 K	27 m/s
25	Rued (and Wittig)	Nr. 12, Grid 3	7.0	Kmax=5.7*10e-6	Tw=299 K (26 C)	0.64	467 K	27 m/s
26	Rued (and Wittig)	Nr. 12, Grid 4	10.1	Kmax=5.7*10e-6	Tw=299 K (26 C)	0.64	467 K	27 m/s
27	Daniels (and Browne)	ReD, suction	* 4.0	Turbine Blade	Tw=289 K (16 C)	0.67	432 K	Vinf=146 m/s
28	Daniels (and Browne)	ReD, pressure	* 4.0	Turbine Blade	Tw=289 K (16 C)	0.67	432 K	Vinf=146 m/s
29	Daniels (and Browne)	Re+, suction	* 4.0	Turbine Blade	Tw=289 K (16 C)	0.67	432 K	Vinf=135 m/s
30	Daniels (and Browne)	Re+, pressure	* 4.0	Turbine Blade	Tw=289 K (16 C)	0.67	432 K	Vinf=135 m/s
31	Hylton et al.	Run 145 - S	* 6.5	Turbine Blade	Tw=650 K (377 C)	0.81	792 K	Vinf=90 m/s
32	Hylton et al.	Run 145 - P	* 6.5	Turbine Blade	Tw=650 K (377 C)	0.81	792 K	Vinf=90 m/s
33	Hylton et al.	Run 149 - S	* 6.5	Turbine Blade	Tw=650 K (377 C)	0.81	795 K	Vinf=90 m/s
34	Hylton et al.	Run 149 - P	* 6.5	Turbine Blade	Tw=650 K (377 C)	0.81	795 K	Vinf=90 m/s

\* upstream value

## 5.1 SIMPLE FLAT PLATE FLOW WITH FREE-STREAM TURBULENCE

This section will consider experimental data from transitional flows occurring under the influence of free-stream turbulence, but without pressure gradients or curvature. A comparison will be made between results of calculations made with the PTM Lam-Bremhorst model and the experiments of Wang [91,92], Rued[72-74], and Blair and Werle[8]. These are listed as the first nine entries in Table 5.1. Taken together these experiments span a range of total free-stream turbulence intensity levels from less than 1% to nearly 9%. In each experiment, the effects of transition are given in terms of heat transfer, thus the evaluation will be restricted to comparing local Stanton numbers. This is defined in a standard way as

$$St = \frac{Nu}{Pr Re} = \frac{q_w}{\rho_e U_e C_p [T_w - T_e]} \quad (5.1)$$

### 5.1.1 Data of Wang

This experiment was conducted in a low speed wind tunnel ( $U_e=13.5$  m/s) under ambient atmospheric pressure with air. The test section was heated with a uniform heat flux of about  $160 \text{ W/m}^2$ . Suction was applied at the leading edge such that the growth of the boundary layer simulated a classical sharp-leading edge. A square grid was placed upstream of the test section such that the turbulence intensity was about 2% over the test section.

The streamwise component of the free-stream turbulence was measured at a number of different locations using hot wire anemometry. In Fig 5.1, these experimentally reported values are shown together with the approximated conditions applied in the computations. Since only the streamwise component of the free-stream turbulence was reported, the turbulence was assumed to be isotropic for the purpose of setting the turbulent kinetic energy boundary conditions. For a velocity of 13.5 m/s, this translates to  $k_e = .15 \text{ m}^2/\text{s}^2$  and  $\epsilon_e = .70 \text{ m}^2/\text{s}^3$  at the location  $x=0$ .

In Fig. 5.2 the heat transfer results for calculations using the PTM form of the Lam-Bremhorst model are compared with this experiment. Also shown is a calculation by Park and Simon [60] using standard mixing length type transition modeling as per Abu-Ghannam and Shaw [2] and Dhawan and Narasimha [22]. Their evaluation of a number of different models showed this combination to be the best. The agreement is excellent, and an improved simulation of the transition path is compared to mixing length type models is indicated. It is interesting to note that although the PTM model was also tuned to the correlation of Abu-Ghannam and Shaw, transition begins somewhat earlier because the momentum thickness itself is altered through the turbulent transport. Furthermore, the overshoot predicted by the mixing length type of models is avoided. Thus for this experiment the path of transition is more realistically simulated as a gradual process that actually begins far upstream of the point where the heat transfer shows a sharp increase. (It should be noted that in this case both methods used the experimentally determined turbulent Prandtl number in the turbulent heat transfer calculations. This however has no real bearing on the transition predictions.)

### 5.1.2 The Use of the Streamwise vrs. Total Turbulence Intensity

At lower turbulence intensities and at distances relatively far downstream from grids, the turbulence in wind tunnels is quite isotropic. As a result, the experiment of Wang is not unusual in reporting only the streamwise component of the turbulence intensity. However, to generate test conditions with high turbulence intensities, experimentalists are required to install relatively coarse grids at locations fairly close to the test section. Because grid generated turbulence is not isotropic (generally characterized by  $\overline{u'^2} > \overline{v'^2} > \overline{w'^2}$ ), a different turbulence intensity can be defined and measured for each of the three spatial directions. Unfortunately, transition experiments conducted in the past have usually neglected this and reported only the streamwise component. Only recently have transition experiments appeared in the literature where a more complete description of the turbulence is given. The experiments of Rued, and Blair and Werle, which will be considered next, are examples of this.

In eqs. 1.1 and 1.2, the distinction between the streamwise turbulent intensity " $Tu_e$ ", and the total turbulence intensity " $Tu_{e,T}$ " is defined. Since the turbulent kinetic energy is the sum of the fluctuating energy in each direction, this difference affects k- $\epsilon$  models through the specification of  $k_e$  as a boundary condition, ie;

$$k_e = 1.5(U_e Tu_{e,T})^2 \quad (5.2)$$

If only  $\overline{u'^2}$  is known, and  $Tu_e$  replaces  $Tu_{e,T}$  in eq. (5.2), then  $k_e$  would

obviously be in error if the turbulence is not isotropic. For a fully turbulent boundary layer this difference would probably be insignificant. However, since the effect (if any) of non-isotropic free-stream turbulence on transition is unknown, a question arises concerning the PTM model. Many of the experiments used in developing the correlation of Abu-Ghannam and Shaw are based on  $Tu_e$  only. Thus, even if  $\bar{v}'^2$  and  $\bar{w}'^2$  are known, is it better to base  $k_e$  on  $Tu_e$  in the PTM model?

As a result of questions like this, as well as the added benefit of examining how sensitive the predictions are to small changes in the boundary conditions, the results to be presented next will be calculated both ways, ie. using eq. (5.2) as is, or replacing  $Tu_{e,T}$  with  $Tu_e$ . Afterwards, the relative importance of this issue can more adequately be discussed.

### 5.1.3 Data of Rued

Rued[72-74] has conducted a large number of experiments dedicated to examining the influence of free-stream turbulence, pressure gradient, and large temperature variations on transition. In this section we will consider only those tests conducted without pressure gradients. In contrast to the experiments of Wang, Rued's test facility provided for the incoming air to be heated while the test section surface was cooled and kept at a constant temperature. Turbulence measurements were made using laser-doppler-anemometry, and turbulence grids were installed to provide total turbulence intensities of from 1.6 to 8.7 % at the leading edge. The free-stream velocity was constant and equal to 47 m/s. Two components of the turbulence,  $\bar{u}'^2$

and  $\overline{v'^2}$  were measured and reported at different locations along the test section. Since  $\overline{w'^2}$  was not measured, it was assumed to be equal to  $\overline{v'^2}$  in the definition of  $Tu_{e,T}$ . Figures 5.3 and 5.4 show the streamwise distribution of both  $Tu_{e,T}$  and  $Tu_e$  for each of the turbulence grids. Comparing these two figures one can observe the higher values of  $Tu_e$  relative to  $Tu_{e,T}$ . Also shown is the streamwise variation of the turbulence intensity as approximated in the computations. Note that the excellent agreement between the computationally specified distributions and the data from each grid verifies the accuracy of the reduced equations for  $k_e$  and  $\epsilon_e$  given in equations (2.35) and (2.36). Table 5.2 provides the exact values of  $k_e$ ,  $\epsilon_e$  and  $Tu$  at the start of the test section as used in the computations.

TABLE 5.2 Free-Stream Turbulence Conditions Specified in Computing the Zero-Pressure Gradient Flows of Rued [72]

Parameter	No grid	Grid 1	Grid 2	Grid 3	Grid 4
$Tu_{e,T}$ at $x=0$	1.6%	2.3%	3.75%	6.5%	8.6%
$k_e$ ( $m^2/s^2$ ) "	.848	1.75	4.66	14.0	24.5
$\epsilon_e$ ( $m^2/s^3$ ) "	55.0	365.0	1589	8214	14,905
$Tu_{e,T}$ at $x=.4$ m	1.28%	1.36%	1.85%	2.55%	3.32%
$Tu_e$ at $x=0$	1.71%	2.8%	4.65%	7.4%	10.8%
$k_e$ ( $m^2/s^2$ ) "	.969	2.60	7.16	18.14	38.6
$\epsilon_e$ ( $m^2/s^3$ ) "	62.3	480	1600	9530	24,000
$Tu_e$ at $x=.4$ m	1.37%	1.72%	2.68%	3.05%	4.13%

In Figure 5.5, the experimental Stanton numbers are compared with the computations which used the total turbulence intensity. In general, very good agreement is shown except with grid 2, where the calculation predicts transition somewhat downstream of the data. Although not as much as the grid 2 case, it is interesting to note that the calculations for grid 1 and the no-grid case also are slightly downstream of the data.

In Figure 5.6 the experimental Stanton numbers are compared with the computations which used the streamwise turbulence intensity. Since  $Tu_e$  is larger than  $Tu_{e,T}$ , the calculations show a general upstream shift in the predicted transition locations. This improves the agreement for the grid 2 case, leaves the overall agreement about the same for the no grid and grid 3 cases, but reduces the agreement for grids 1 and 4. This behavior will be discussed further after considering the results of calculating the experiments of Blair and Werle.

#### 5.1.4 Data of Blair and Werle

Similar to Wang, these experiments were conducted in a low speed wind tunnel ( $U_e=30.5$  m/s) under ambient atmospheric pressure with air. After a short unheated starting length, the test section was heated with a uniform heat flux of about  $800$  W/m<sup>2</sup>. Suction was applied at the leading edge such that the growth of the boundary layer simulated a classical sharp-leading edge. Three different turbulence generating grids were placed upstream of the test section to provide total free-stream turbulence levels of 1.4%, 2.8%, and 6.2% respectively at the leading edge. (Data from a fourth grid was also taken but will not be considered here because transition

occurred before the heated test section.) Hot wire anemometry was used to determine all three components of the turbulence ( $\bar{u}'^2$ ,  $\bar{v}'^2$ , and  $\bar{w}'^2$ ) at a number of different locations. As a result of a contraction in the wind tunnel upstream of the test section, the  $\bar{u}'^2$  component was reduced to a value less than  $\bar{v}'^2$  and  $\bar{w}'^2$ . However, evaluation of the data showed that the streamwise variation of  $Tu_{e,T}$  could still be accurately represented in the following theoretical form ( see Baines and Peterson [5]);

$$Tu_{e,T} = 0.78 \left( \frac{x + 132}{b} \right)^{-5/7} \quad (5.3)$$

where  $x$  is in cm. and  $b=$ .48, 1.27, and 3.81 for grids 1, 2 and 3 respectively. This is shown as the dashed lines in Figure 5.7. Also shown in Fig. 5.7 is the reported variation in  $Tu_e$  and the corresponding approximate variation used in the calculations. Table 5.3 gives the exact values of  $k_e$ ,  $\epsilon_e$  and  $Tu$  that are used in the computations at  $x=0$ .

Figure 5.8 compares the calculations using  $Tu_{e,T}$  with the experimental data. Good agreement is shown for grid one, but transition is predicted significantly upstream for the grid two case. For grid 3, transition is just ending as the flow passes the end of the unheated starting length, thus the only quantitative information that can be gained is that the model does not predict transition too late.

When the calculations are made using the  $Tu_e$  data, the result is to shift the location of transition downstream. These calculations are shown in Fig. 5.9. ( Recall that this is opposite of Rued's case because for Blair's data,  $\bar{u}'^2$  is less than  $\bar{v}'^2$  and  $\bar{w}'^2$ ) This appears to reduce the accuracy of the grid one

TABLE 5.3 Free-Stream Turbulence Conditions Specified in Computing the Zero-Pressure Gradient Flows of Blair and Werle [8]

Parameter	Grid 1	Grid 2	Grid 3
$Tu_{e,T}$ at $x=0$	1.41%	2.82%	6.20%
$k_e$ ( $m^2/s^2$ ) "	.277	1.12	5.36
$\epsilon_e$ ( $m^2/s^3$ ) "	11.8	47.5	228
$Tu_{e,T}$ at $x=1.6$ m	0.80%	1.60%	3.52%
$Tu_e$ at $x=0$	1.12%	2.33%	5.75%
$k_e$ ( $m^2/s^2$ ) "	.175	.757	4.60
$\epsilon_e$ ( $m^2/s^3$ ) "	2.75	19.5	150
$Tu_e$ at $x=1.6$ m	0.82%	1.50%	3.44%

prediction, but improves the agreement with grid 2 and grid 3. In considering this contrast it should be noted that Blair and Werle report that when doing experiments without a grid (the data is not shown here), the transition location was clearly shifted upstream due to wall effects propagating into the boundary layer. Since grid one is still at a relatively low free-stream turbulence level, it is possible that this case was slightly affected also. If so, the tendency of the  $\overline{u}^2$  based calculation to be somewhat closer to the data would be a consistent trend for all three cases.

### 5.1.5 Discussion and Summary

Since a point was made earlier in this section to make a distinction between  $Tu_{e,T}$  and  $Tu_e$ , a further discussion of this is now warranted.

When using  $Tu_{e,T}$  in the calculations, the only significant difference with experiment occurred in the mid turbulence intensity range. However, when comparing the calculations of Rued's cases with Blair and Werle's cases, the direction of the error was opposite. For Rued's data, grid 2, the predicted transition was a little late, whereas for Blair's data grid 2, the predicted location of transition comes too early.

When comparing the two experiments, the one quantifiable dissimilarity likely to be significant is the difference in anisotropy. This hypothesis is supported by the calculations where, in almost every case, the direction of the error correlates with the variance between the  $\bar{u}'^2$  component of turbulence relative to the mean. When  $\bar{u}'^2$  was high, using  $Tu_{e,T}$  tended to yield predictions somewhat downstream of the data. When  $\bar{u}'^2$  was low, using  $Tu_{e,T}$  tended to yield predictions somewhat upstream of the data. This leads to the conclusion that one or both of the following may be true; (1) the model as currently correlated is somewhat biased to the  $u'$  component of turbulence, and/or (2) the transition process itself is significantly influenced by the anisotropy.

In light of these observations, it is also interesting to recall something about the origin of the production term ( $\bar{u}'v' \partial U/\partial Y$ ) that appears in the exact form of the  $k$  equation. One way to derive this equation is to start with a transport equation for each of its components, ie.  $\bar{u}'^2$ ,  $\bar{v}'^2$  and  $\bar{w}'^2$ . The  $k$  equation is then found by appropriate addition of each of these equations.

Upon examination of these equations individually, one sees that the production term comes entirely from the  $\overline{u}^2$  equation. Since this term is clearly important in the transition process, this tends to support the possibility of a connection between the anisotropy and transition as observed here.

In summary, the predictions of the PTM form of the Lam Bremhorst model have proved excellent at reproducing both the start, the end, and the path of transition as manifest in the heat transfer. Although some differences between the data and the calculations exist, they are not large, and there appear to be rational explanations to justify most of the discrepancies. Considering the amount of scatter in the data used as a basis for the correlation of the Abu-Ghannam and Shaw [2] – which correlation is the basis for finding the parameters  $A$  and  $B$  – the results have been very encouraging.

## 5.2 TRANSITIONAL FLOWS WITH ACCELERATION

In this section the calculations will be compared against pressure gradient experiments reported by Blair and Werle [9], and by Rued [72]. Taken together, these experiments provide an excellent range of different accelerating flow conditions with which to test the calculational procedure. No additional modifications will be introduced into the model at this point. This is possible because the LRN form of the  $k$ - $\epsilon$  model is also inherently responsive (at least qualitatively) to the effects of acceleration. In fact, it was the early demonstration of the ability of the LRN  $k$ - $\epsilon$  model of Jones and

Lauder to simulate relaminarization[37] that helped attract further research into models of this type.

In characterizing acceleration, it is useful to define an acceleration parameter  $K$ . Previously defined in equation (1.4), it is repeated here;

$$K = \frac{\nu}{U_e^2} \frac{\partial U_e}{\partial x} \quad (1.4)$$

For the experiments of Blair, two sets of data are presented. Each set corresponds to a different level of constant  $K$  being maintained over the entire test section, but provides data at a number of different free-stream turbulence conditions. In contrast, the experiments of Rued are such that the value of  $K$  is changing dramatically over the length of the test section. Three representative sets of this data will be used.

### 5.2.1 Some Limitations Inherent in the 2-Equation Approach

Under strong acceleration such as is caused by a test section contraction, each of the components of the Reynolds stress tensor are affected differently. For example, if  $x$  is the stream-wise direction, a contraction in the test section along the  $y$  direction, will yield a stratification from an initially isotropic state such that  $\overline{v'^2} > \overline{w'^2} > \overline{u'^2}$ . This in fact is the effect which caused the significantly different nature of the anisotropy in Blair's experiments as compared to Rued's. However, more than a simple redistribution of energy within the different components can occur. In

addition to this, energy can be extracted from the flow to cause a net increase in the total turbulent kinetic energy. Figure 5.10 is presented as an illustration of this. Here the experimentally reported turbulence intensities for one of the data sets of Rued have been converted to turbulent kinetic energy and then normalized with respect to the conditions at  $x=0$ . Although qualitative differences occur, the data all show the same trend; ie. a rapid decrease in  $k$  followed by a period of significant increase, which finally begins to decrease again. The solid curve shown is simply a polynomial curve fit to all of the data in order to represent the trends clearly.

From a mathematical standpoint, this behavior can be explained through examination of the various nonlinear terms that appear in the set of transport equations describing each component of the Reynolds stress tensor. These form the basis of the so called Reynolds-Stress-Equation turbulence models. Together with certain closure assumptions, these equations can be solved to yield a fairly accurate prediction of these effects, at least for simple geometries. However, this behavior is beyond the capabilities of the  $k$ - $\epsilon$  model to simulate, at least in the standard form used here. This is clearly seen by recalling that in the free-stream, the reduced set of equations given by eq.( 2.35) and (2.36) are assumed valid. Examination shows that since  $\epsilon$  is an always positive variable, these equations preclude the possibility of  $k$  increasing in the streamwise direction.

Because of this limitation, under some of the conditions for which Rued carried out experiments, the calculational procedure will only allow an approximation to the correct boundary conditions for  $k$  and  $\epsilon$ . This will be

documented in the presentation of the results in order to evaluate its significance.

### 5.2.2 Data of Blair and Werle

The pressure gradient experiments of Blair and Werle[10] were conducted at the same basic facility as those reported in Blair and Werle[8] for zero pressure gradient conditions. However, the side opposite of the test section in the wind tunnel was modified so as to produce a flow of almost constant acceleration. The two values of  $K$  obtained were  $K=.20 \times 10^{-6}$  and  $K=.75 \times 10^{-6}$ . The corresponding free-stream velocity distribution for each of these cases is shown in Fig. 5.11.

Figures 5.12 and 5.13 document the approximated free-stream turbulence conditions used in the calculations as compared to the experimental data. As was done in section 5.1, calculations were made using both  $Tu_{e,T}$  and  $Tu_e$ . In Fig. 5.12 a curve for grid 3 is shown but no data is indicated. Blair reports heat transfer results for this condition but did not document the free-stream turbulence. However, since the actual grid was the same as used for the data shown in Fig. 5.13, it was possible to estimate the actual variation in  $Tu$  with a high degree of confidence. The exact values of  $k_e$ ,  $\epsilon_e$  and  $Tu$  used in the calculations are given in Table 5.4.

Figure 5.14 presents the calculated heat transfer results for the lowest acceleration cases. Excellent agreement is obtained, and once again, the small variation that does exist is shown to correlate to the anisotropy as previously explained. In the fully turbulent region, the data tends to be higher than the

TABLE 5.4 Free-Stream Turbulence Conditions Specified in Computing the Pressure Gradient Flows of Blair and Werle [9]

Parameter	$K=0.2 \times 10^{-6}$			$K=0.75 \times 10^{-6}$	
	Grid 1	Grid 2	Grid 3	Grid 2	Grid 3
$Tu_{e,T}$ at $x=0$	1.03%	2.1%	-	2.24%	5.3%
$k_e$ ( $m^2/s^2$ ) "	.0402	.1672	-	.0742	.415
$\epsilon_e$ ( $m^2/s^3$ ) "	.07	1.20	-	.14	2.70
$Tu_{e,T}$ at $x=1.6$ m	0.64%	1.10%	-	0.45%	0.91%
$Tu_e$ at $x=0$	0.94%	1.86%	4.80%	1.90%	4.77%
$k_e$ ( $m^2/s^2$ ) "	.0335	.1312	.341	.0534	.336
$\epsilon_e$ ( $m^2/s^3$ ) "	.01	1.0	20.0	.14	3.20
$Tu_e$ at $x=1.6$ m	0.62%	0.97%	1.89%	.37%	.75%

predictions. This apparently is due to the acceleration since the calculations with zero pressure gradient do not show this difference. In any case, the issue is a separate one from the transition predictions.

Figure 5.15 compares the results of the higher acceleration tests. Here both experiments show transition displaced further downstream than the calculations predict, although the effect is small for the higher turbulence case. Furthermore, this cannot be correlated with the the anisotropy. However, by comparing the calculations with those at  $K=0.2 \times 10^{-6}$ , it is clear that the calculations have responded to the acceleration in the right direction (ie. the predicted transition location has moved downstream). Also, it will be noted that once again, in the fully turbulent region the Lam-Bremhorst model under predicts the heat transfer.

Also documented in Blair and Werle's report are the displacement thickness  $\delta^*$ , the momentum thickness  $\theta$ , and the shape factor  $\delta^*/\theta$ . These was measured at various locations along the test section, allowing an alternative comparison between experiment and predictions during transition. Examples of this for grids 1 and 2 at  $K=0.2 \times 10^{-6}$  are shown in Fig. 5.16, where  $\delta^*$  and  $\theta$  are compared with experiment, and in Fig. 5.17, where the variation in shape factor is compared. For the higher turbulence case of grid 2, only small differences are apparent in both figures, the most pronounced being the quicker change in the shape factor. However, a larger difference is seen for grid 1 where the free-stream turbulence effects do not dominate. In this case, the shape factor found computationally begins to change earlier and also undergoes a more gradual change than the data. This difference is somewhat surprising considering the close agreement in the heat transfer results for this case. Unfortunately, no explanation of this result can be given at this time.

### 5.2.3 Data of Rued

This data was taken in the same basic facility as described in section 5.1.2. To introduce acceleration, the channel boundary opposite the test section was modified by installing two different and specially contoured walls. Flow conditions were then varied to achieve a variety of different acceleration conditions over the test section. As representative of these results, three of the data sets were chosen for use in this evaluation. These correspond in Rued's specification to Nr 6, Nr 10, and Nr 12. Figure 5.18 shows the experimentally measured variation in the acceleration parameter  $K$

for each of these conditions. Also shown are the smoothed continuous representations used in the calculations. Nr 6 is seen to be similar to the higher acceleration conditions of Blair since the variation in  $K$  is not very great over the test section. Conditions of this type are similar in many respects to typical behavior on the pressure side of a turbine blade. However, Nr 10 and 12 are very different, producing a very strong region of acceleration over the first two-thirds of the test section followed by a rapid relaxation to a region of very small negative acceleration. These conditions are designed to provide a closer approximation to the acceleration characteristics on the suction side of a typical blade. The maximum  $K$  produced in Nr. 12 is eight times as great as the acceleration in Blair's strongest case. The corresponding velocity distribution for each of these cases, together with the approximations used in the calculations is shown in Fig. 5.19.

Figures 5.20 and 5.21 show the experimentally measured total turbulence intensity distributions over the test section produced by the grids for these conditions. The estimated uncertainties in the measurements are also shown to illustrate how the uncertainty increased significantly for the larger the turbulence intensity conditions. Note that separate figures for the stream-wise turbulence intensity are not shown as was done before. This is because Rued did not document the individual components for experiments with acceleration. Only the net  $Tu_{e,T}$  was reported.

As was discussed in section 5.2.1, a  $k$ - $\epsilon$  model is not able to reproduce these conditions exactly. The solid curves shown indicate the decay as calculated using equations 2.35 and 2.36 and which were used in the calculations. In each case, the initial turbulent kinetic energy was chosen so

as to correspond to  $Tu_{e,T}$  at the upper bound of the uncertainty for that grid. However, the dashed line in Fig 5.20 for the grid 4 conditions illustrates that after a short region, this choice makes little difference. In all cases the major error in free-stream turbulence intensity occurs in the region centered about  $x=.1$  meter. Table 5.5 lists the actual starting conditions for  $k_e$ ,  $\epsilon_e$  and  $Tu$  which correspond to the calculations shown.

TABLE 5.5 Free-Stream Turbulence Conditions Specified in Computing the Pressure Gradient Flows of Rued [72]

Experiment	at $x=0$			at $x=.4$ m
	$Tu_{e,T}$	$k_e$ ( $m^2/s^2$ )	$\epsilon_e$ ( $m^2/s^3$ )	$Tu_{e,T}$
Nr 6, Grid 1	2.63%	2.481	320	0.75%
Nr 6, Grid 2	4.30%	6.632	2290	0.92%
Nr 6, Grid 3	8.33%	24.89	26600	1.12%
Nr 6, Grid 4	12.1%	52.51	39500	1.91%
Nr 10, Grid 1	2.88%	2.810	720	0.63%
Nr 10, Grid 2	3.95%	5.280	1200	0.89%
Nr 10, Grid 3	7.73%	20.22	5040	1.68%
Nr 10, Grid 4	11.13%	41.92	24000	1.87%
Nr 12, Grid 1	2.88%	0.874	126	0.63%
Nr 12, Grid 2	3.95%	1.644	210	0.89%
Nr 12, Grid 3	7.73%	6.294	882	1.70%
Nr 12, Grid 4	11.13%	13.05	4200	1.87%

Figure 5.22 compares the calculations with the data for each of the four grids in Nr 6. Because of the complexity of the flow, it is not as easy to clearly distinguish laminar, turbulent, and transitional regions in the data. Grid 1, shows the clearest identifiable transition region, which extends over almost the entire length of the plate. This is very accurately reproduced by the model. The only real discrepancy occurs in the region immediately subsequent to the start of the cooled section. This under-prediction over the first 15-20% of the cooled test section was characteristic of all the calculations made of Rued's acceleration data. Careful examination of the grid 2-4 data from  $x=.05$  to  $.1$  m, shows that although only small differences occur in the data, a transitional effect is manifest. However, the overall magnitude of the heat transfer in the region is more characteristic of a near turbulent boundary-layer becoming fully turbulent, than a laminar boundary-layer becoming turbulent. The calculations do not reproduce this, and show a clear transition from very laminar-like state up to the turbulent level in this region. This seems to indicate a deficiency in predicting the character of the "pseudo-laminar" boundary layer more than a deficiency in the correct location and extent of transition.

The comparison between the calculations and the data from Nr 10 is given in Fig. 5.23. Here the characteristic initial under-prediction is also indicated. However, the introduction of strong acceleration followed by a rapid relaxation (see figure 5.18) provides some very interesting additional insight into the response of the model. When  $Tu_e$  is high, as for grids 3 and 4, the model quite accurately represents the somewhat modified but still

turbulent region during the high acceleration. After the acceleration is relaxed, although there is a slight increase, the data is still reproduced quite well. However, as the turbulence intensity decreases, the model shows a higher sensitivity to the acceleration than the experiment, and a relaminarization is shown for the grid 2 cases which is not reflected in the data. Once the acceleration is removed, the calculation moves quickly back in line with the data. At the lowest turbulence intensity, the model once again correctly reproduces the acceleration effects, but when the acceleration is removed, a too rapid rise back to the turbulent state is predicted. This figure illustrates the complex interaction between the competing effects of high free-stream turbulence and rapidly changing but large negative pressure gradients that are so difficult to predict. The relative success of the model at predicting most of these trends correctly without any additional modifications is very encouraging.

In Figure 5.24, the calculations are compared to the data from Nr 12. Recall that this test has the highest acceleration of all. Interestingly, it is also the most well predicted by the model. Except for the under-prediction in the initial region (which however is not as pronounced as before), the model predicts the data for each turbulence level very accurately. Note that both the start, the path, and the length of transition is well reproduced. The faithful reproduction of this set of data is one of the most outstanding successes of the model.

#### **5.2.4 Summary of the Prediction Capabilities for Flows with Acceleration**

With respect to the overall predictive capabilities of the model, the following items can serve as a summary of what the comparisons made in this section seem to indicate.

1. Transition under the combined influence of both free-stream turbulence and low constant favorable pressure gradients ( $K \approx .2 \times 10^6$ ) is predicted very well by the model. This includes not only the location but also the extent over which it occurs.

2. For flows with moderate constant acceleration, comparison with experiments indicates that the model tends to under predict the length over which transition occurs, but not severely. The location of the start also tends to be predicted somewhat early. These are qualitative errors only, as the quantitative trends are very well reproduced.

3. A consistent under prediction of the heat transfer near the leading edge of the boundary layer was observed in all of the experiments where both high increasing acceleration and high free-stream turbulence intensity were present. However, as the ratio of acceleration to free-stream turbulence increases, this difference tends to diminish. Examination of the data seems to indicate transition beginning with the boundary layer already in a nearly turbulent state. This contrasts with the model which allows only a limited variation from the laminar state prior to transition.

4. Apart from the initial region mentioned in 3., the competing effects of both strong acceleration and free-stream turbulence on transition were

accurately predicted for all but two cases, both at moderate to low turbulence intensity. In one case the model predicted a partial relaminarization, while the data did not. In the other case, the length of the transition region was under predicted.

### 5.3 Turbine Blade Cascade Data

The major motivation for the work presented in this thesis is the need for a reliable engineering tool for predicting the effect of transition on heat transfer on gas turbine blades. Thus to complete the examination of the transition model developed here, it is appropriate that calculations be performed for a number of turbine blade cascade data sets. However, before doing so we must recognize that only two of the major factors affecting transition on a turbine blade have so far been considered in the development of the model. These two, free-stream turbulence and pressure gradients, are usually the most dominant, but significant effects with respect to other factors must be neglected at this point in order to perform a calculation. Two of the most notable of these are the effects of curvature, and the proper calculation of the flow in a stagnation region.

The data to be considered here is the data of Daniels [19], and the data of Hylton et al [34] for the blade they designated as "C3X". Two flow conditions over each blade will be considered, both on the suction side and the pressure side. This yields eight separate runs with which to compare our numerical model. Before introducing the details of these, we will first

consider some of the additional complexities and problems associated with these calculations.

### 5.3.1 Preliminary Comments about the Calculations

#### Compressibility and High Mach Number Effects:

In all of the flat plate cases discussed previously, the velocity has been sufficiently low that compressibility effects were small. However, this is not the case for typical turbine blades where inlet mach numbers may be low, but exit mach numbers frequently exceed one. To account for this, a state equation must be included in the calculations to provide for the proper description of the gas under different temperatures and pressures. For the data to be considered here, the working gas was essentially air, and the ideal gas law is used in the calculations. Also, viscous dissipation terms must be included in the energy equation to account for the conversion of mechanical energy to thermal energy which will occur in areas of high shear. The resulting form of the energy equation expressed in terms of the total enthalpy  $H$  was previously given in Chapter 2, eq. ( 2.7).

An appropriate Stanton number to be used in presenting the results for high speed flow is defined in terms of the total enthalpy as follows;

$$St = \frac{q_w}{\rho_e U_e [H_w - H_e]} \quad (5.4)$$

### Property Variations:

In addition to large pressure changes that occur in the streamwise direction, large temperature gradients will occur across the boundary layer. For the data of Daniels, the total wall to free-stream temperature ratio was 0.67. For the Hilton et al's C3X blade conditions that we will consider, it was about .8. Thus the physical properties of air must be continuously varied on a local basis to properly account for this.

For computational purposes, simple temperature dependent equations were applied to calculate various properties of interest. These are given in the appendix together with plots showing how well they compare to experiment.

### Blade Geometry and Velocity Profiles:

The geometry of each blade together with the operating conditions determine the free-stream velocity around each surface. In the work reported by Hylton et al., a two dimensional inviscid numerical method developed by Delaney [21] was used to predict the free-stream flow field. This was then compared with the experimental data to confirm the results. Since the results of this calculation for the C3X blade were made available in the appendix of their report, these free-stream velocities were used for the purposes of the calculations made here. For Daniel's blade, the experimental velocity data reported was functionally approximated by a series of

polynomials to produce a smooth continuous representation of the data. The match points were required to be continuous through the first derivative. The velocity profiles for both of these blades are shown for the suction side in Fig 5.25, and the pressure side in Fig. 5.26.

In the calculations that will be presented, curvature effects will not be introduced. This implies that although the calculations proceed over a streamwise distance which corresponds to traveling around the curved surface of the blade, they do not include additional terms or corrections to otherwise account for the curvature. When the ratio of the boundary-layer thickness to the radius of curvature is small, and the local free-stream velocity is accurately specified, this approximation is fairly good. However, this is not always the case, and it is the opinion of this author that the appropriate incorporation of these effects will need to be addressed in the future. For now, this must be reserved for later consideration.

In the figures, the streamwise coordinate around the blade will be represented with the letter  $S$ .

### 5.3.2 Comparison with the Data of Daniels

Two different flow conditions are selected from the data of Daniels[19] for evaluation here. Following Daniels and Browne [20], these are designated with respect to the design operating conditions as  $Re_D$  ( design Reynolds number) and  $Re^+$ , (ie. a higher flow rate yielding a Reynolds number greater than the design condition). The free stream turbulence intensity measured upstream of the blade was 4.2%. At the actual location of the blade, Rodi and

Scheuerer estimated this to have decayed to about 3% based on empirical decay rates given in Townsend [86]. However, Daniels and Browne appear to have applied the value of 4% in their numerical calculations presented in [20]. For comparison, calculations will be presented here assuming free-stream turbulence levels of both 3% and 3.5%.

In Figures 5.27 and 5.28, the calculations are compared to the actual experimental data. As can be seen, the location and extent of transition as represented in the heat transfer is very well predicted for these cases. Also, the only place the 3% vrs 3.5%  $Tu_c$  difference matters is for the design Reynolds number case, and here the two calculations bracket the experimental data. The only significant variation between the data and the computation occurs at the higher Reynolds number in regions downstream of transition. This occurs on both the suction and the pressure side.

### **5.3.3 Comparison with the C3X blade of Hylton et al.**

In Figures 5.29 and 5.30, comparisons with the data of Hylton et al.[34] are shown. The conditions considered correspond to runs 145 and 149 in their designation. These calculations show trends similar to those pointed out on the Daniels and Browne data, i.e., an excellent prediction of the lower Reynolds number data, but some discrepancies with the higher Reynolds number data. In particular, after transition begins on the suction surface of run 145, the calculations show a very large overshoot as compared to the data. Since this degree of error was observed in any of the previous runs, an effort was made to try and determine the source of the problem. One

explanation that initially seemed reasonable, has to do with the response of the k- $\epsilon$  model to adverse pressure gradient conditions. On the suction side starting at a point just after transition has started for run 145, the flow experiences a region of adverse pressure gradient. Previous research has documented the failure of 2-eq. LRN models such as that of Lam-Bremhorst to correctly calculate the near wall turbulence length scale in adverse pressure gradient flows, resulting in an over prediction of the skin friction and heat transfer (see[68]). Thus, for comparison, a computation is shown where the dissipation equation was modified in line with a suggestion of Launder [46] in the following manner.

$$C_1 = 1.44 * \max(1, L/L_{\max})$$

where

$$L = k^{1.5} / \epsilon, \quad L_{\max} = 2.7y \quad (5.5)$$

The effect of this modification is to prevent the model from producing a near wall length scale more than a few percent over that observed experimentally. As shown in the figure, the results of this additional modification show an improved prediction of the heat transfer on the suction side without influencing the transition predictions. Unfortunately, when more general testing of the modification was made, it also affected ( this time adversely) the fully turbulent results for calculations without pressure gradients, albeit to a lesser degree. Thus, at best, the adverse pressure gradient problem is only a partial answer.

The results of the modified calculation are presented despite their limited validity to help distinguish between the error due to the fully turbulent model, and that due to the transition predictions. In the case of run 145, even if the fully turbulent calculations were corrected as shown, there still remains a significant overshoot as compared to the data. At this point a clearly justifiable explanation of this is not known to the author. However, one plausible possibility is that these effects are due to a somewhat delayed curvature influence similar to what occurs in the so-called recovery region after the release of curvature in a fully turbulent boundary layer. This was briefly mentioned in section 1.2.5 of chapter 1. Since on the C3X blade the radius of curvature is small until about  $S/\text{arc} = .2$ , which is just as transition is beginning, it seems possible that the transition is being influenced by this effect.

### **5.3.3 Brief Summary of the Turbine Blade Data Predictions**

Although this comparison has been somewhat limited, two important comments can be made in summary.

(1) With respect to the streamwise location, of the 8 specific runs compared, in 7 of them the correct start and length of transition was predicted. For the one case where this was not true, although the length was in significant error, the starting location was only slightly different than the experiments. ( Note that we are not considering differences in the fully turbulent region here)

(2) For both blades, the accuracy of the heat transfer predictions in the fully turbulent region diminished as the blade Reynolds number was increased. This was manifest in an over prediction of the heat transfer. However, all aspects of the four lower Reynolds number cases were predicted with good accuracy.

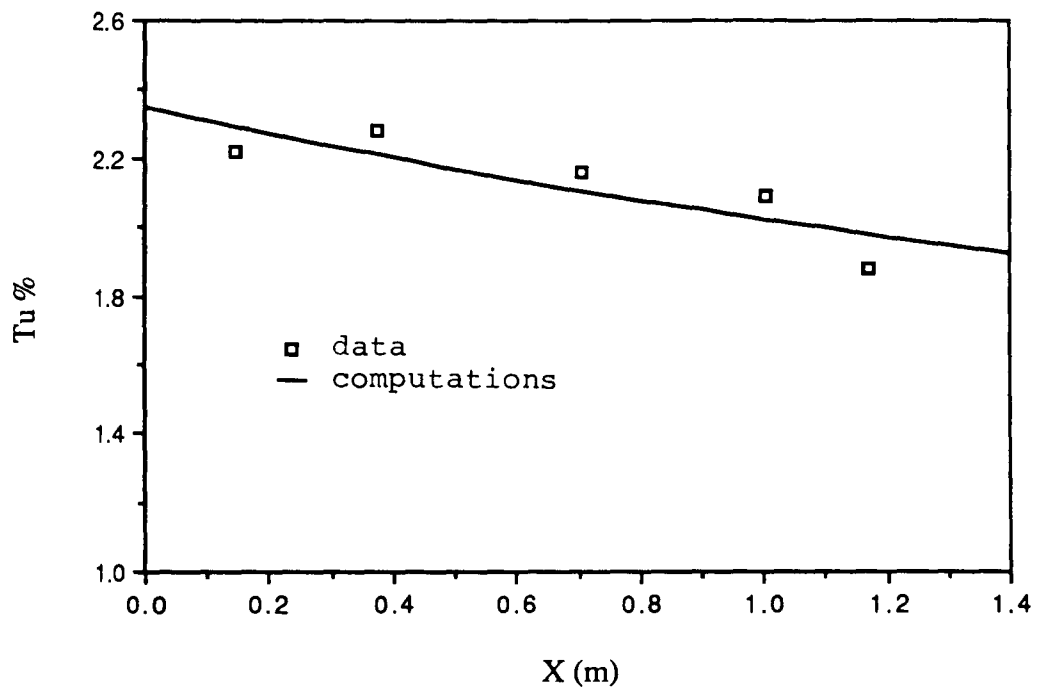


Figure 5.1 Free-stream turbulence conditions for the experiment of Wang [91]

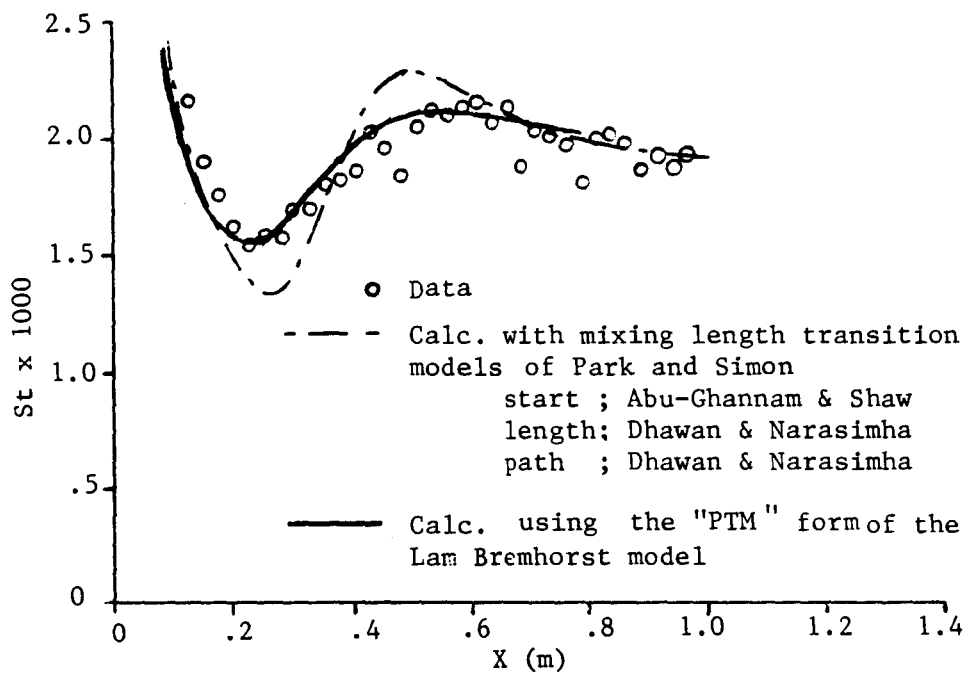


Figure 5.2 Comparison of the predicted heat transfer during transition with the data of Wang[91]

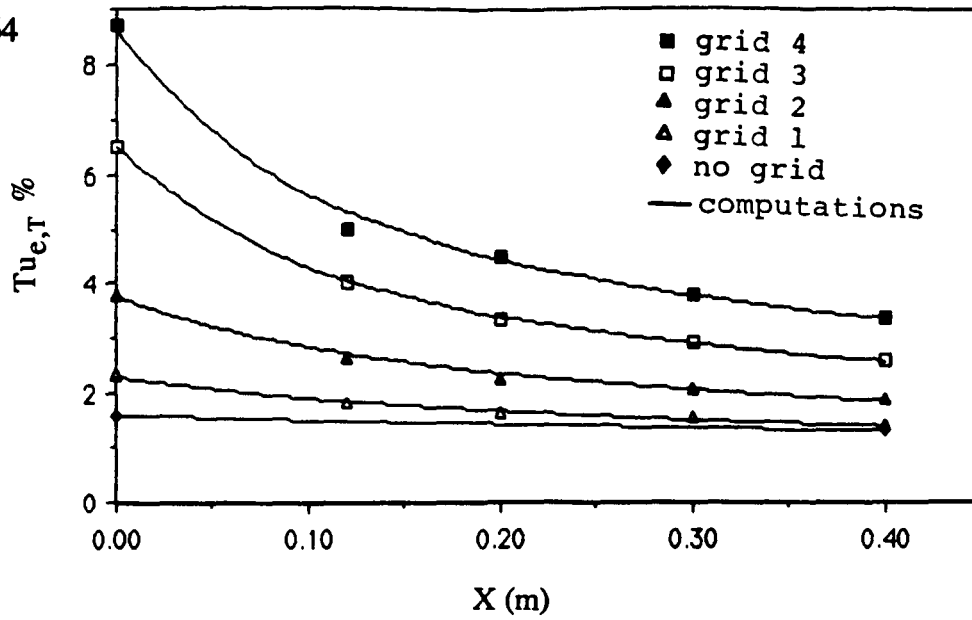


Figure 5.3 Free-stream total turbulence intensity conditions for the zero pressure gradient experiments of Rued [72]

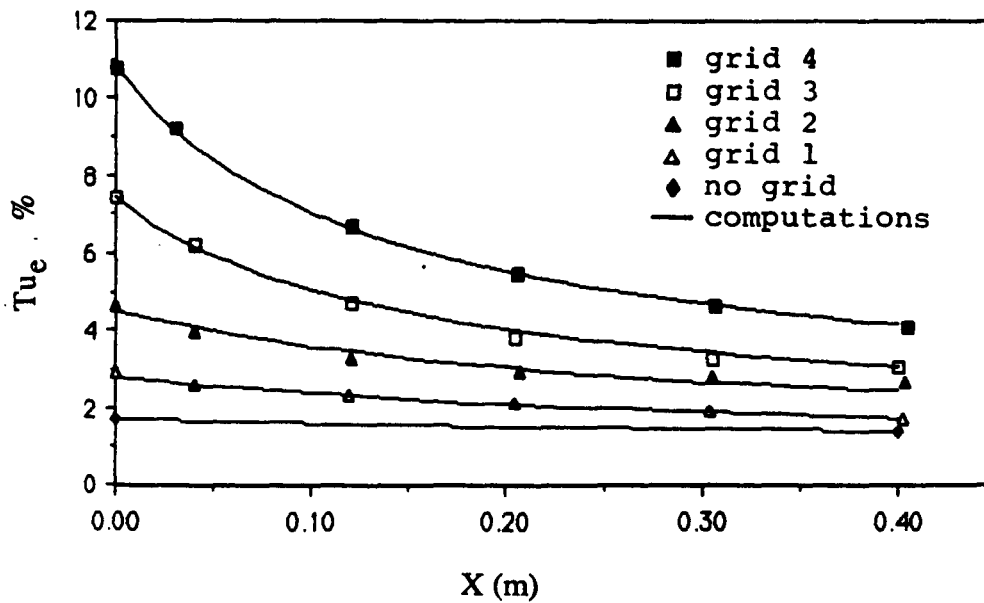


Figure 5.4 Stream-wise turbulence intensity conditions for the zero pressure gradient experiments of Rued [72]

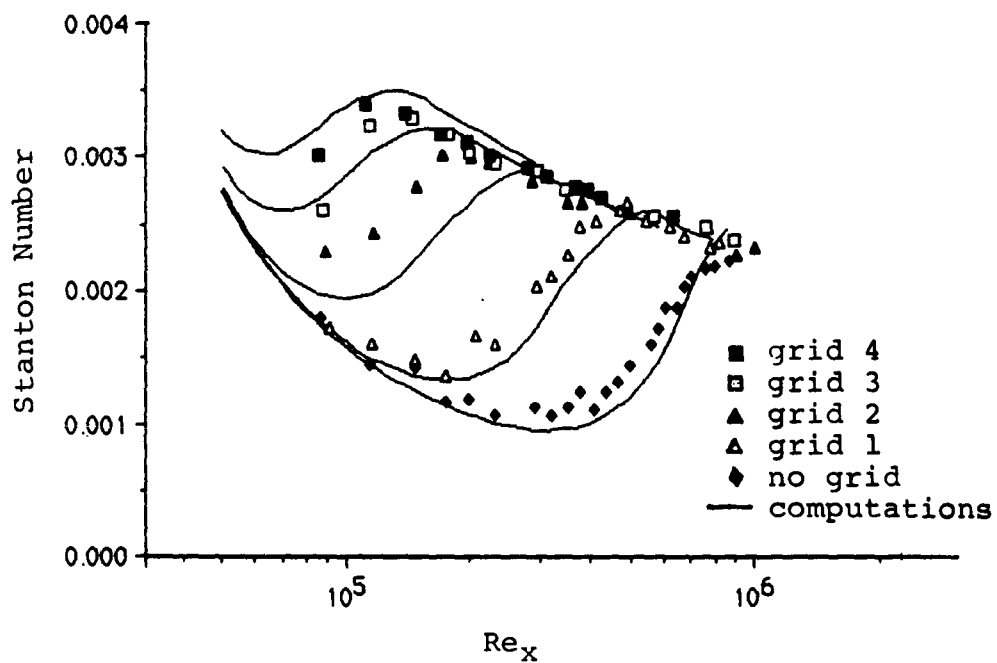


Figure 5.5 Comparison of the predicted heat transfer during transition with the zero pressure gradient data of Rued [72] for  $k_e$  based on  $Tu_{e,T}$ .

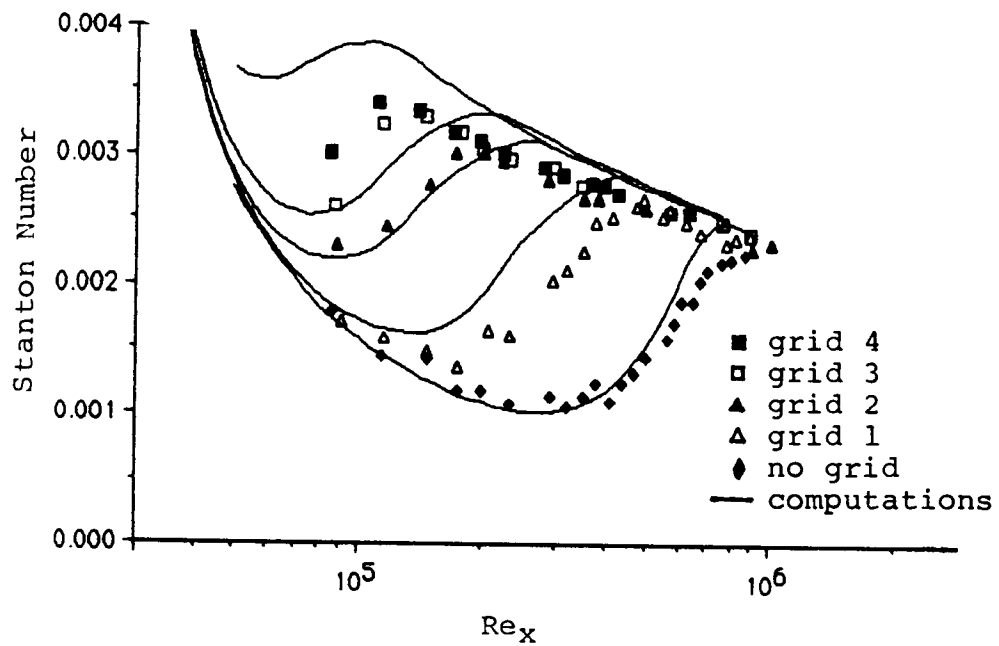


Figure 5.6 Comparison of the predicted heat transfer during transition with the zero pressure gradient data of Rued [72] for  $k_e$  based on  $Tu_e$ .

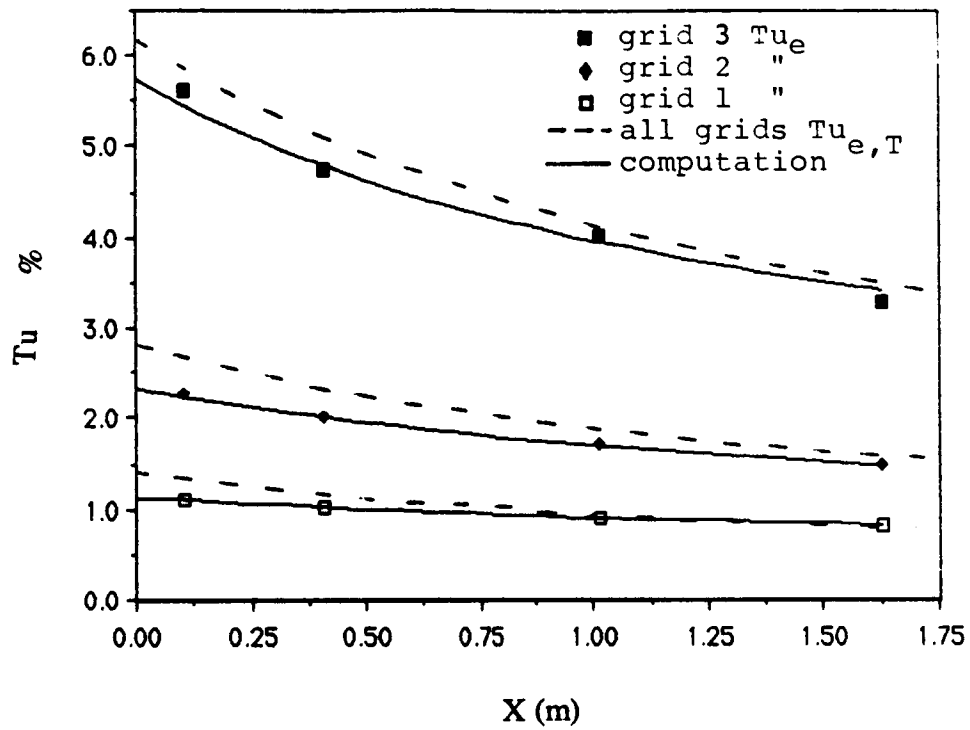


Figure 5.7 Free-stream turbulence intensity conditions for the zero pressure gradient experiments of Blair and Werle [8]

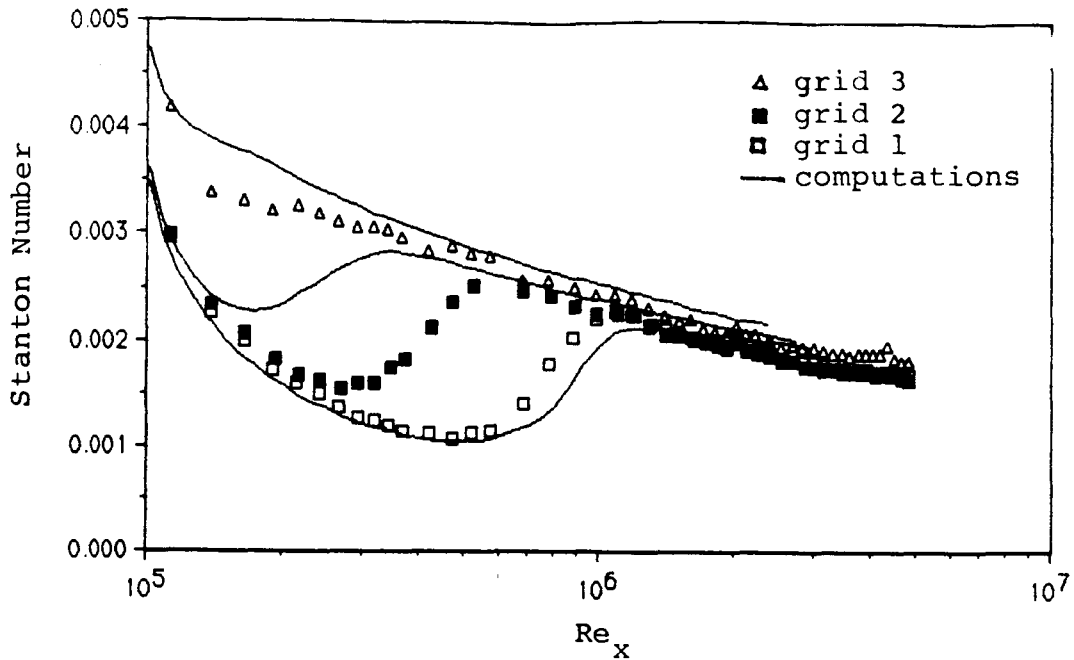


Figure 5.8 Comparison of the predicted heat transfer during transition with the zero pressure gradient data of Blair and Werle [8] for  $k_e$  based on  $Tu_{e,T}$ .

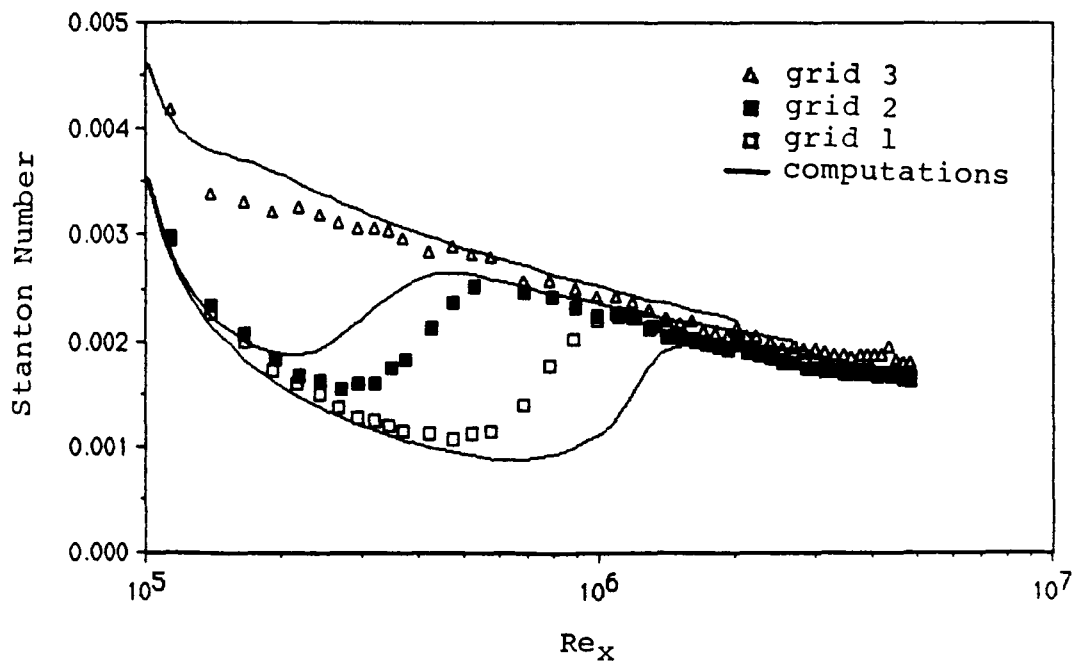


Figure 5.9 Comparison of the predicted heat transfer during transition with the zero pressure gradient data of Blair and Werle [8] for  $k_e$  based on  $Tu_e$ .

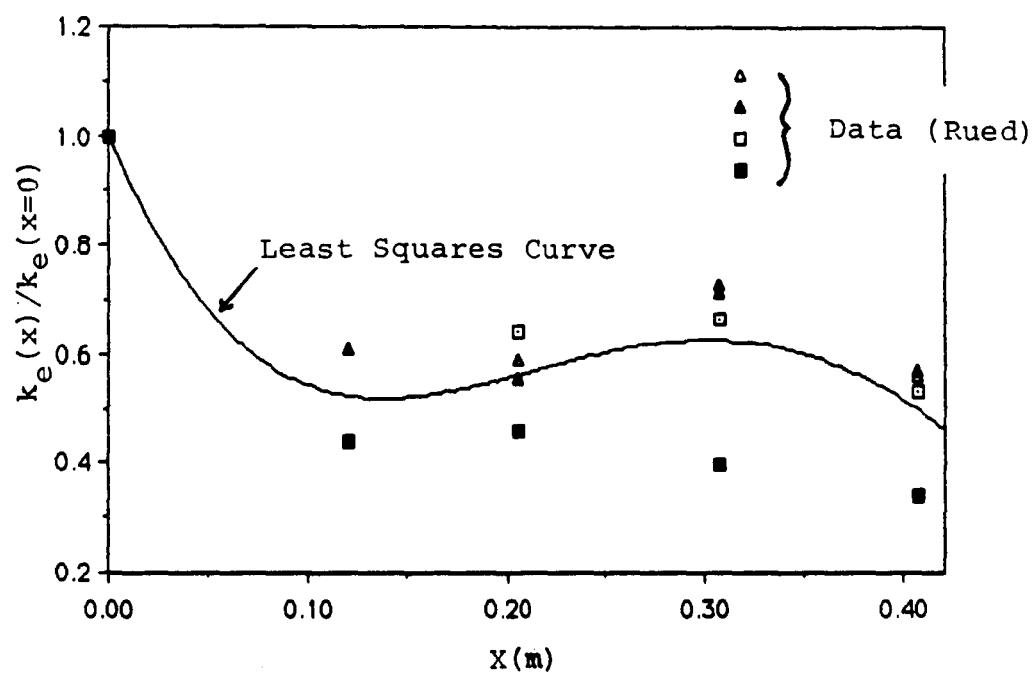


Figure 5.10 The influence of strong acceleration on the freestream turbulent kinetic energy

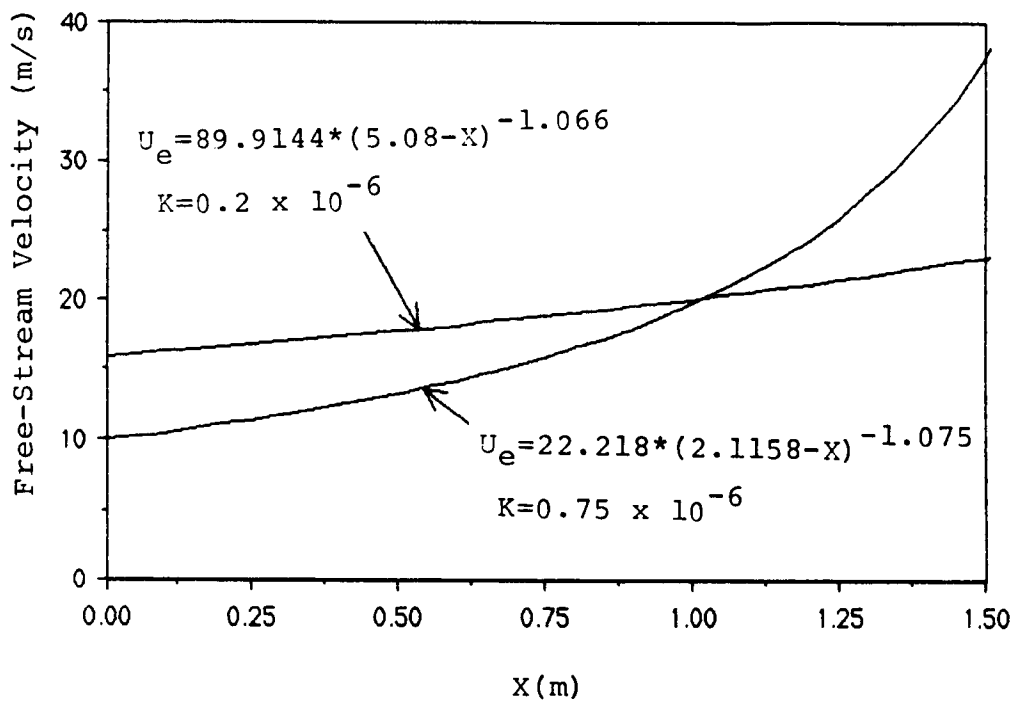


Figure 5.11 Free-stream velocity for the accelerating flow experiments of Blair and Werle [9].

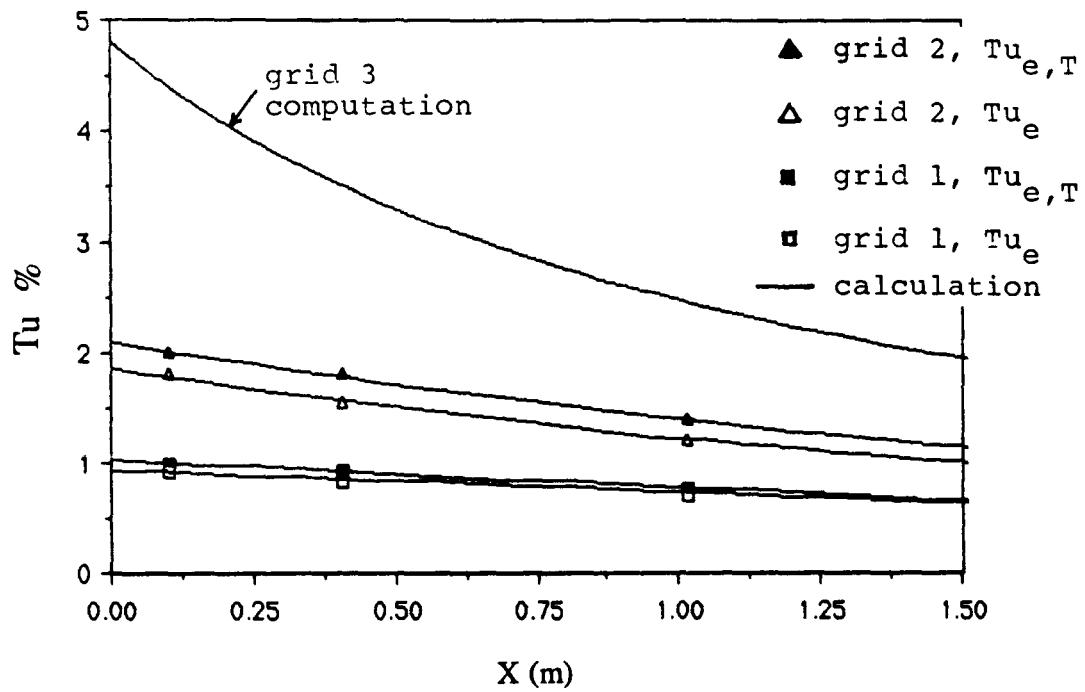


Figure 5.12 Free-stream turbulence intensity conditions for the low constant acceleration experiments of Blair and Werle [9]

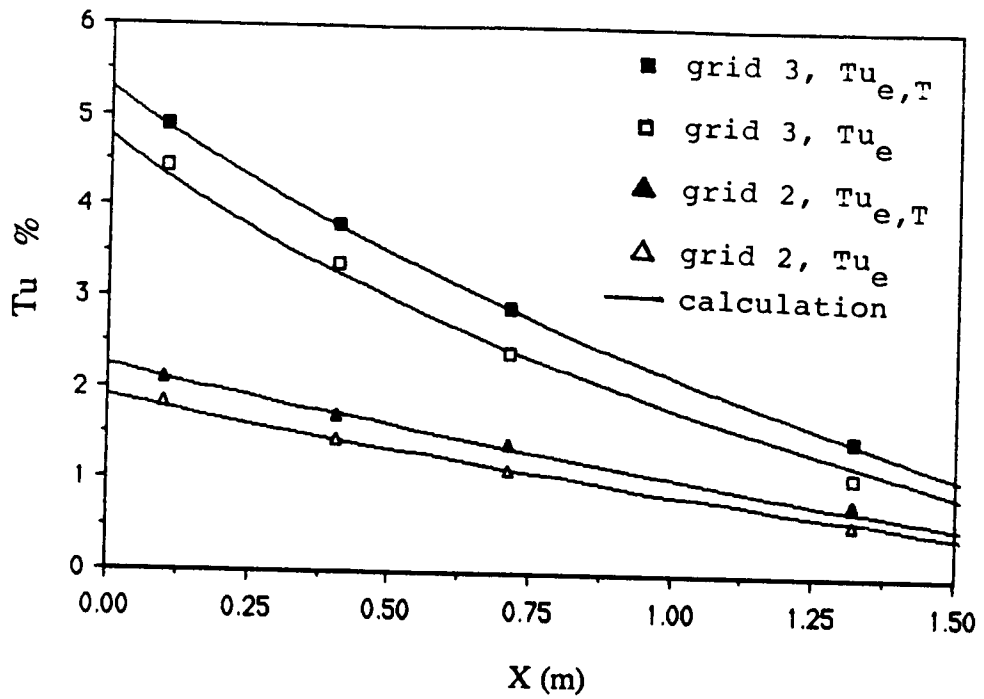


Figure 5.13 Free-stream turbulence intensity conditions for the high constant acceleration experiments of Blair and Werle [9]

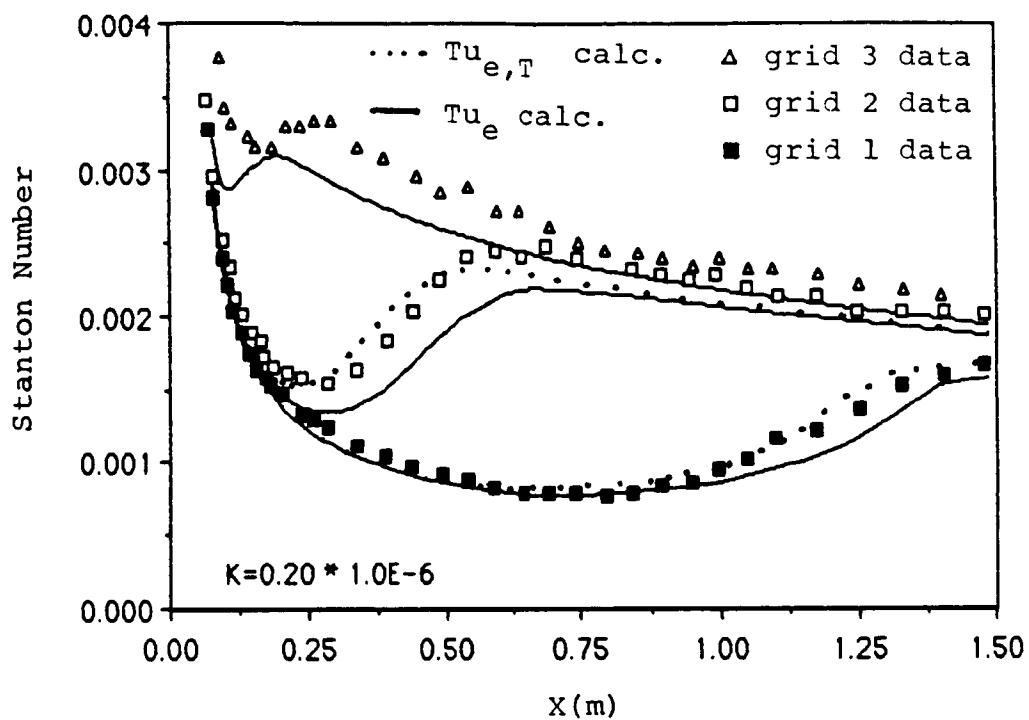


Figure 5.14 Comparison of the predicted heat transfer during transition with the low acceleration data of Blair and Werle [9]

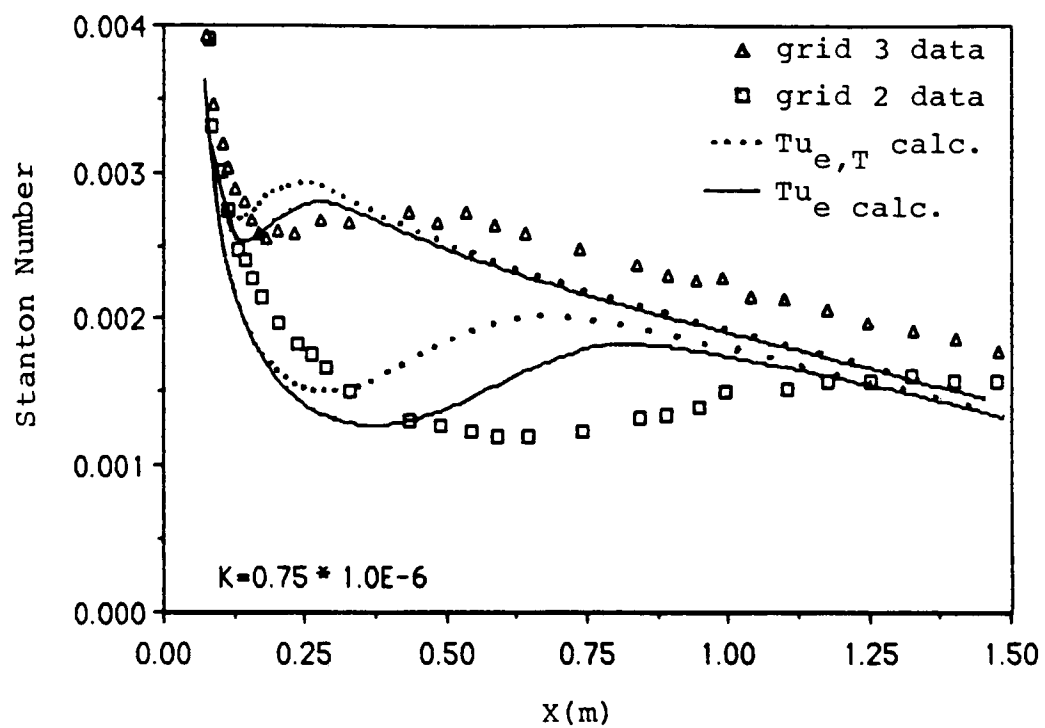


Figure 5.15 Comparison of the predicted heat transfer during transition with the high acceleration data of Blair and Werle [9]

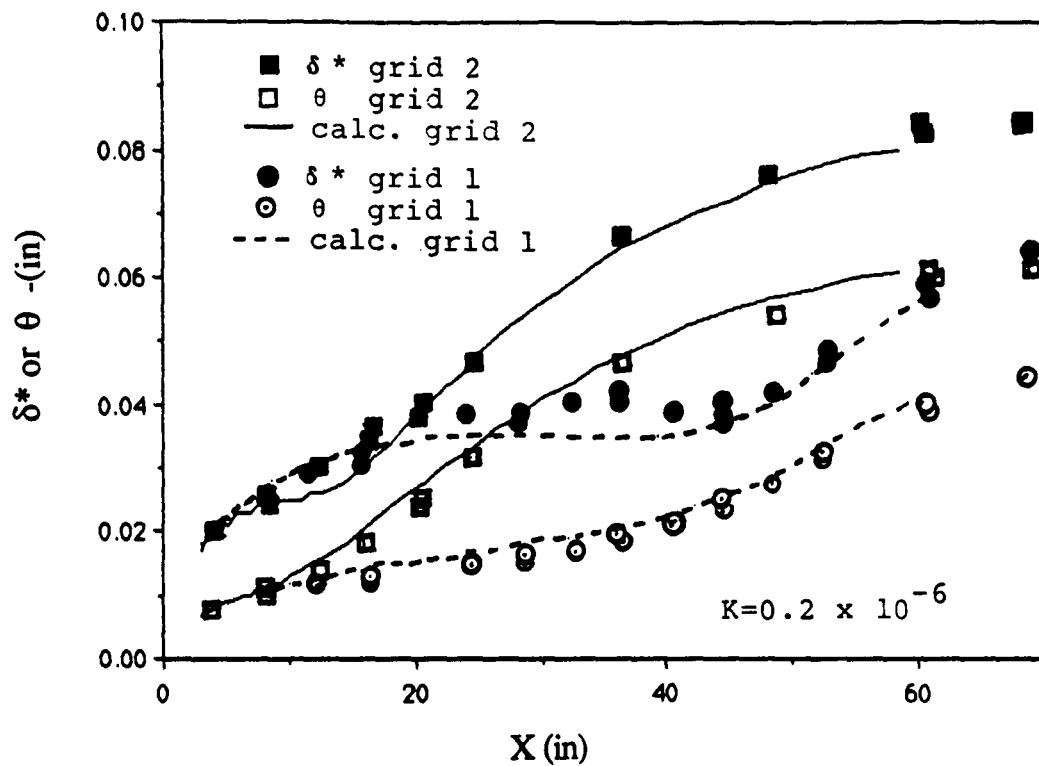


Figure 5.16 Comparison of the predicted momentum and displacement thicknesses with the low acceleration data of Blair and Werle [9]

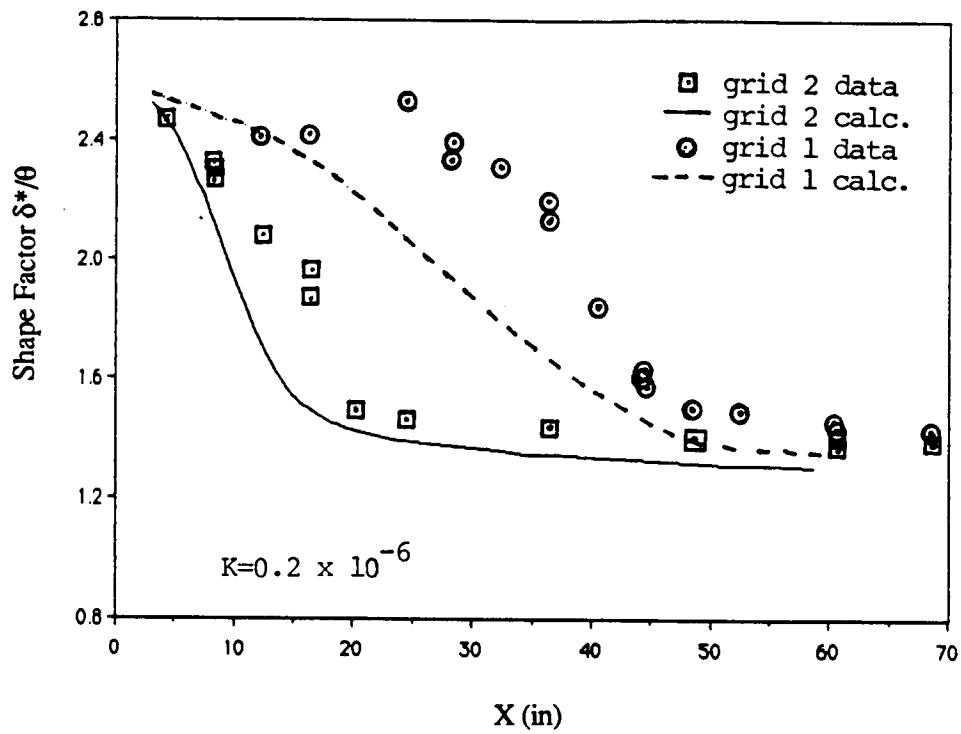


Figure 5.17 Comparison of the predicted shape factor  $\delta^*/\theta$  with the low acceleration data of Blair and Werle [9]

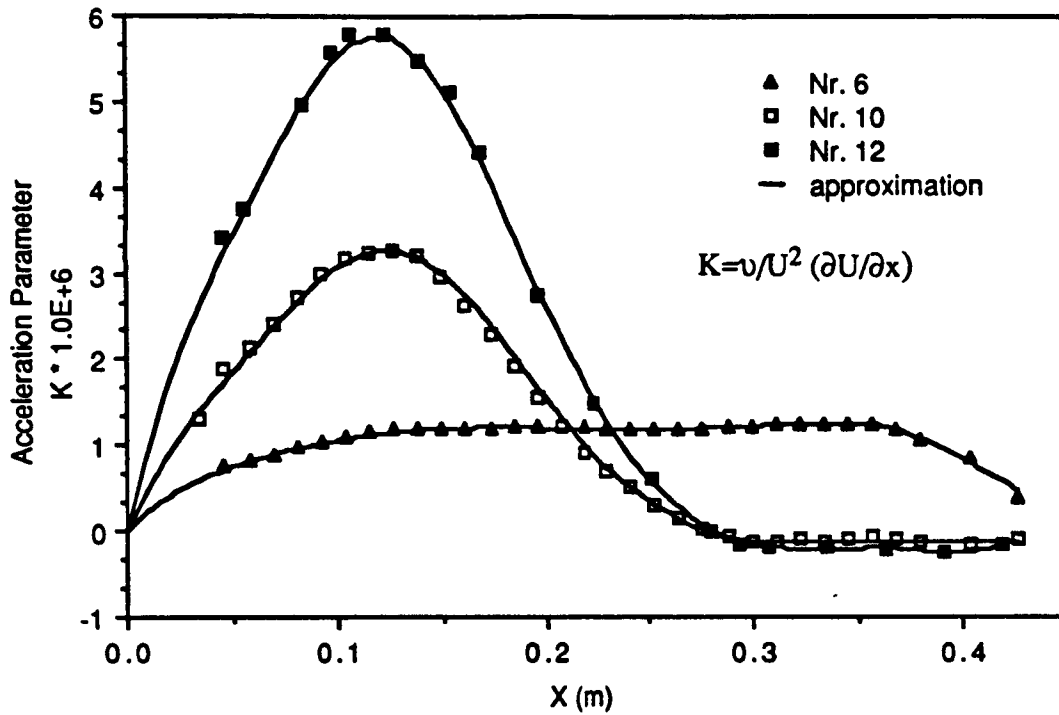


Figure 5.18 Variation of the acceleration parameter "K" for the three experimental data sets of Rued [72] .( Nr. 6,10,12)

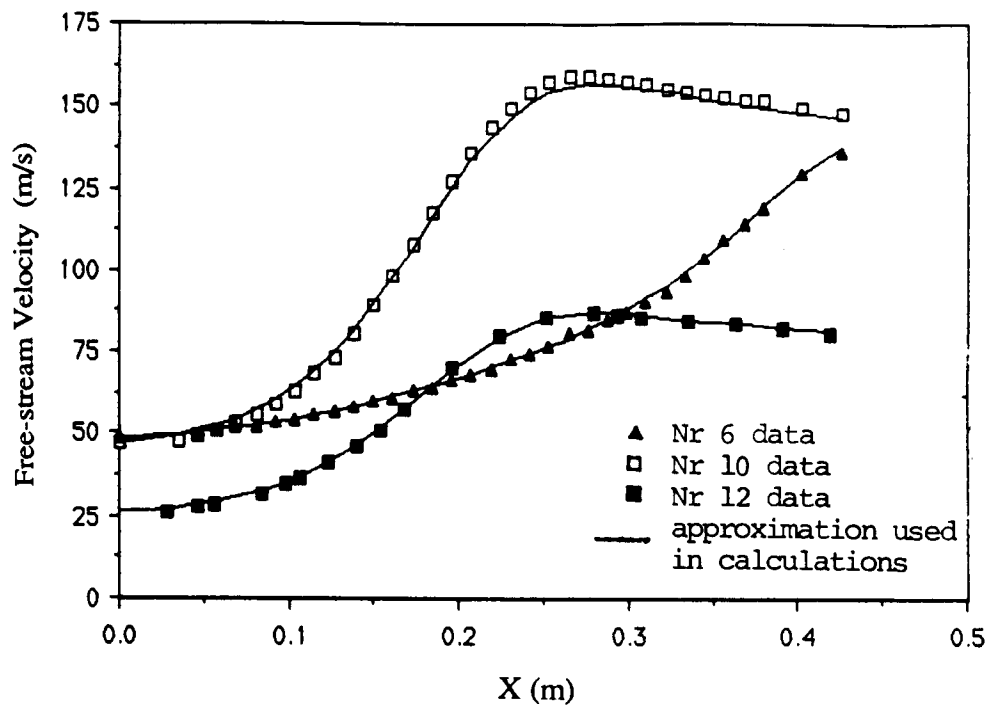


Figure 5.19 Free-stream velocity for the experimental data sets of Rued.

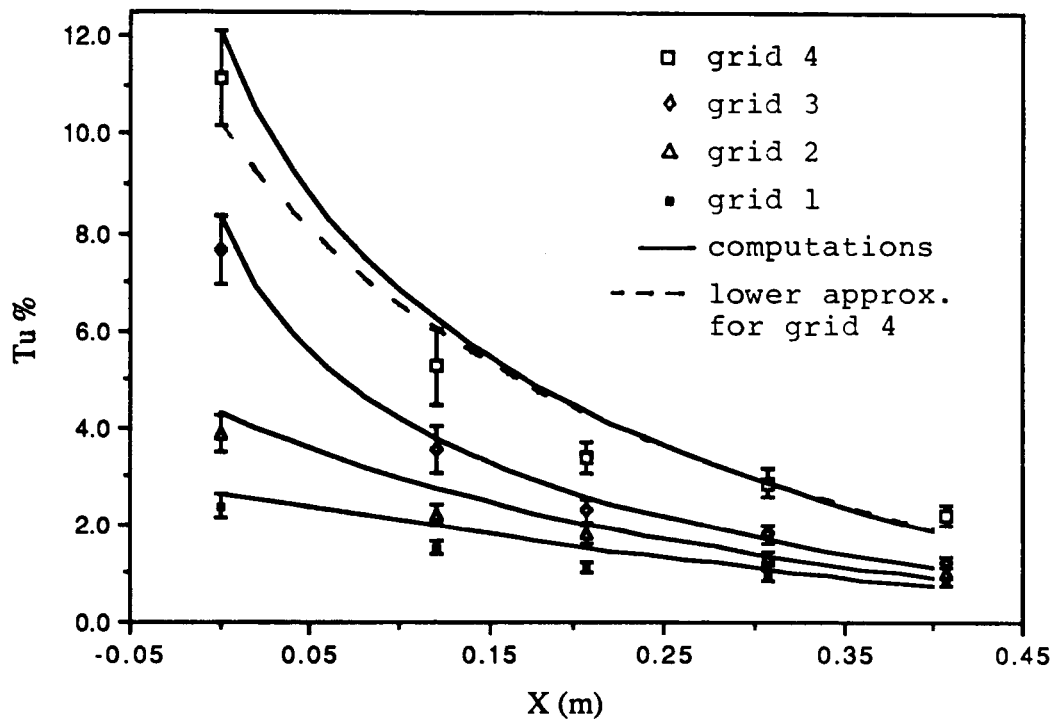


Figure 5.20 Free-stream turbulence intensity conditions for the experiments with contour 1 (Nr. 6) of Rued [72]

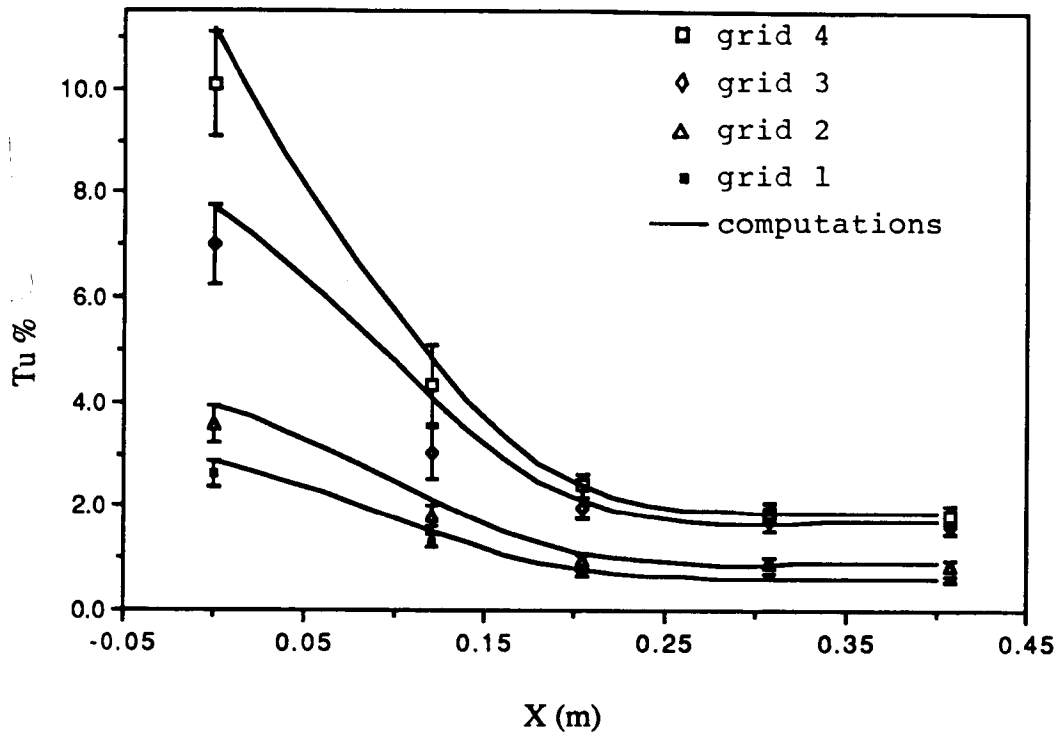


Figure 5.21 Free-stream turbulence intensity conditions for the experiments with contour 2 (Nr. 10,12) of Rued [72]

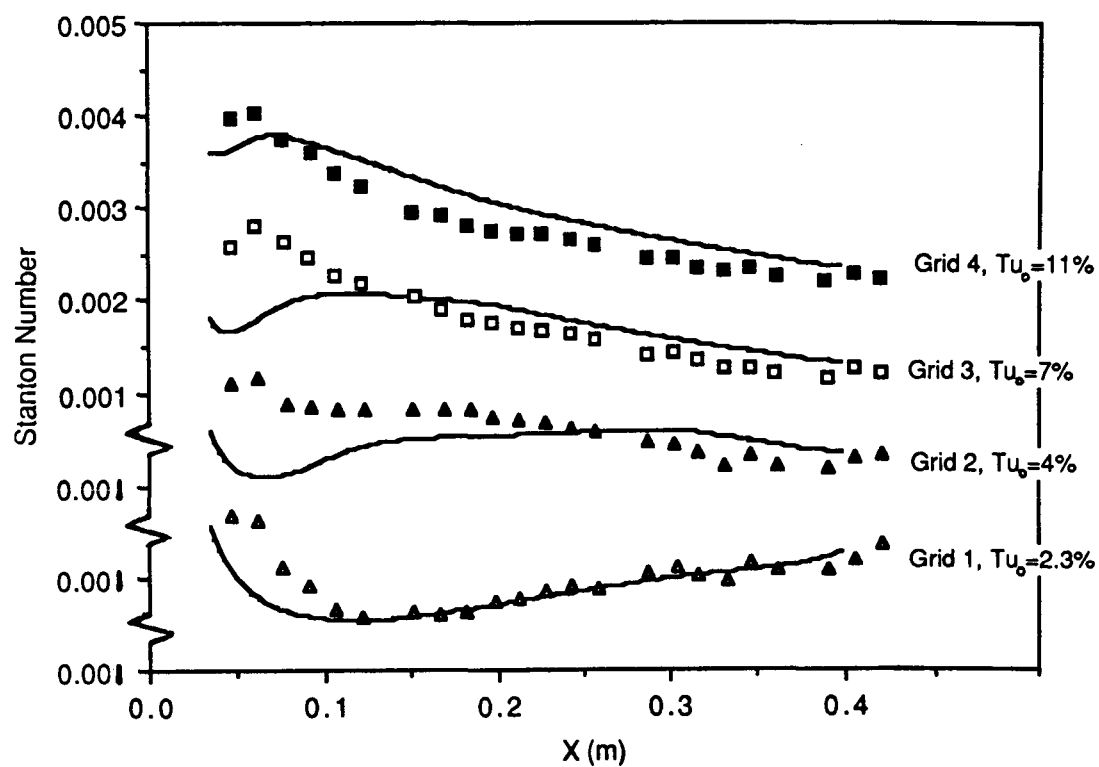


Figure 5.22 Comparison of the predicted heat transfer with the data from Nr. 6 of Rued [72]

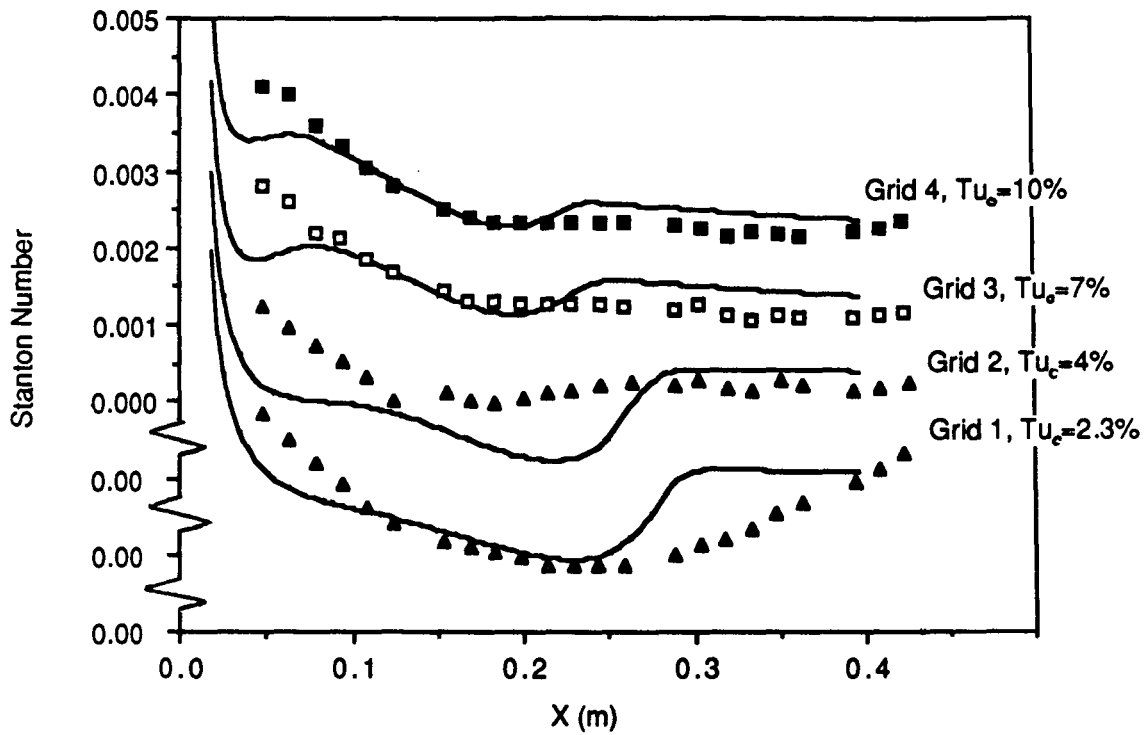


Figure 5.23 Comparison of the predicted heat transfer with the data from Nr. 10 of Rued [72]

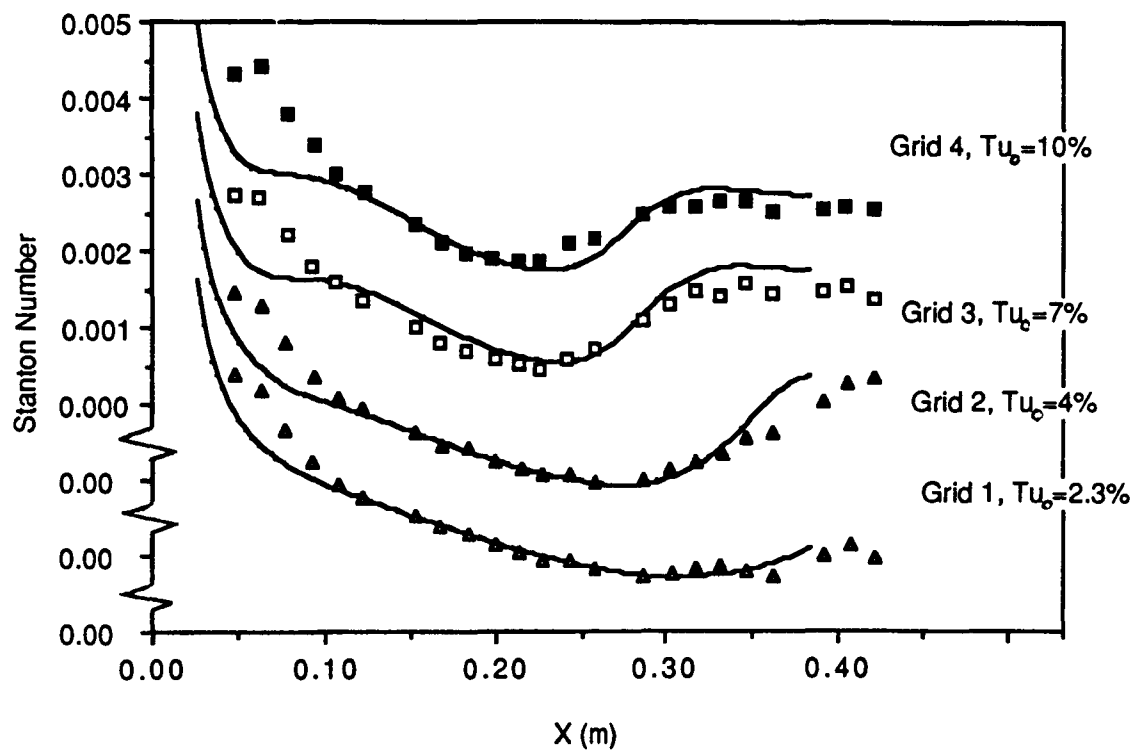


Figure 5.24 Comparison of the predicted heat transfer with the data from Nr. 12 of Rued [72]

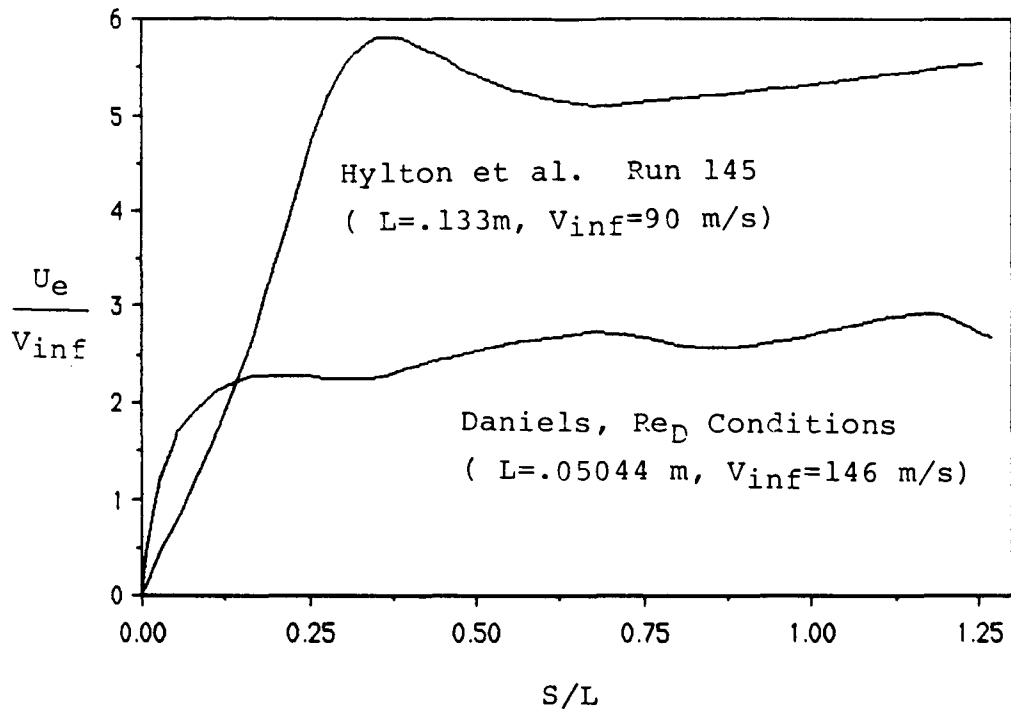


Figure 5.25 The free-stream velocity on the suction side of the blades of Daniels [19] and Hylton et al. [34]

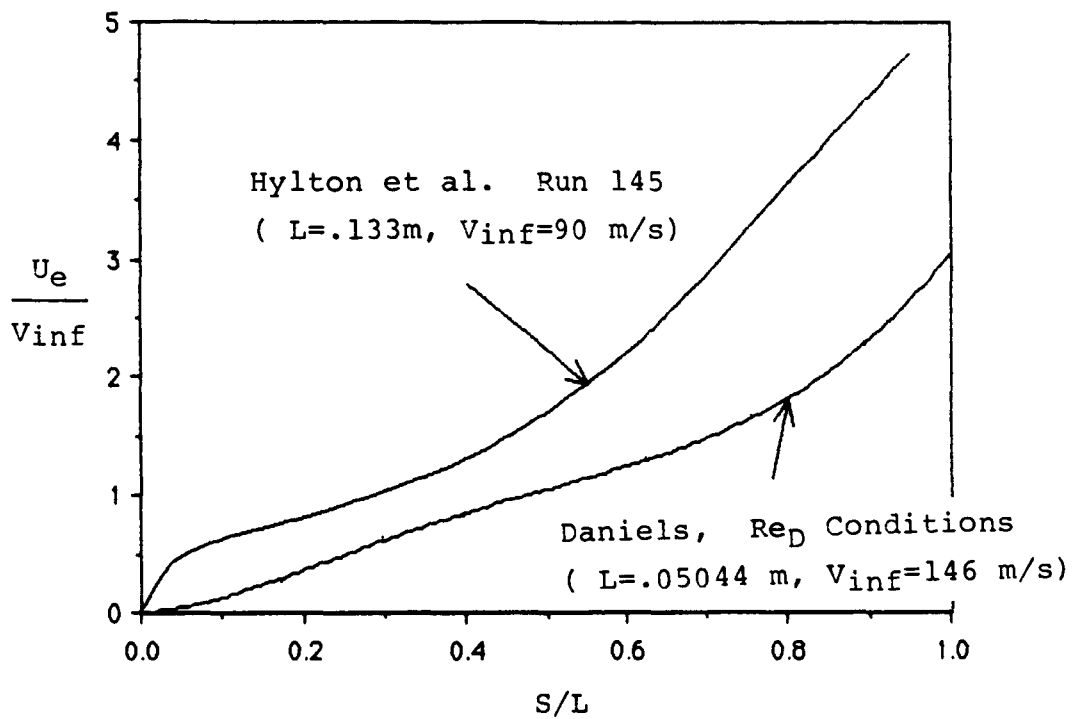


Figure 5.26 The free-stream velocity on the pressure side of the blades of Daniels [19] and Hylton et al. [34]

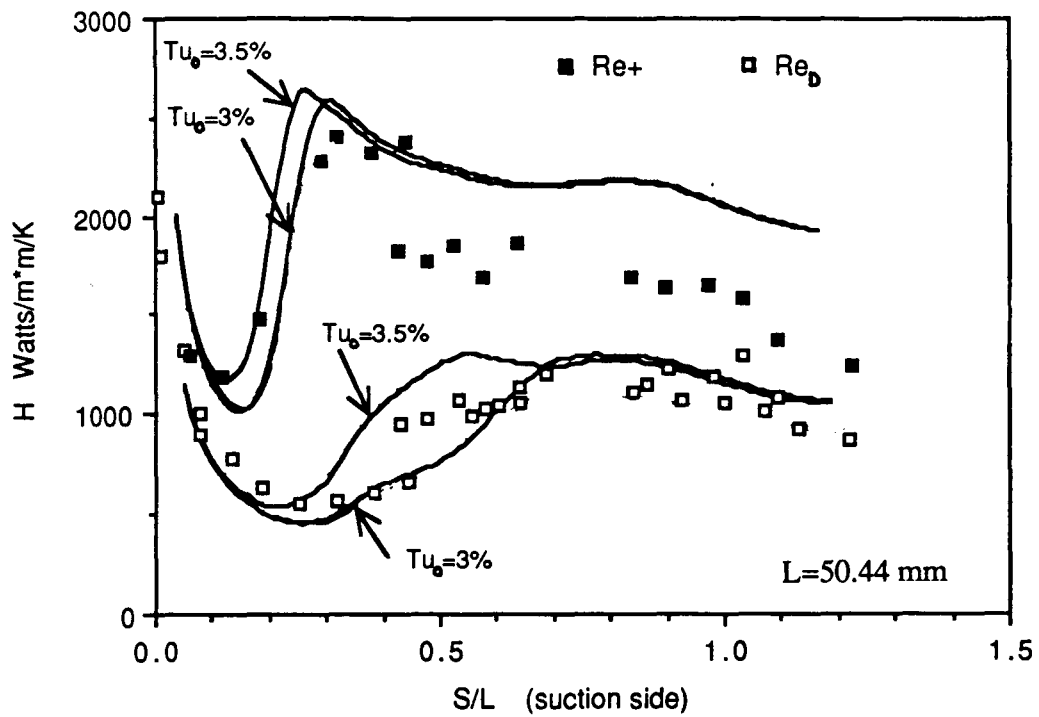


Figure 5.27 Comparison of the predicted and experimental heat transfer around the suction side of Daniels' blade

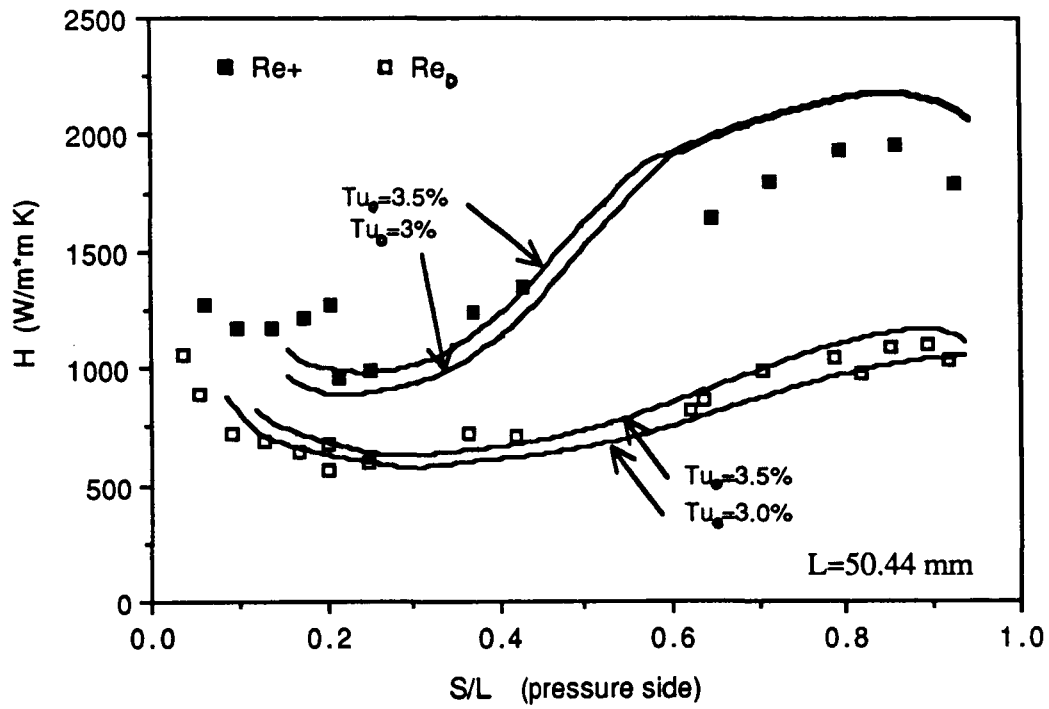


Figure 5.28 Comparison of the predicted and experimental heat transfer around the pressure side of Daniels' blade

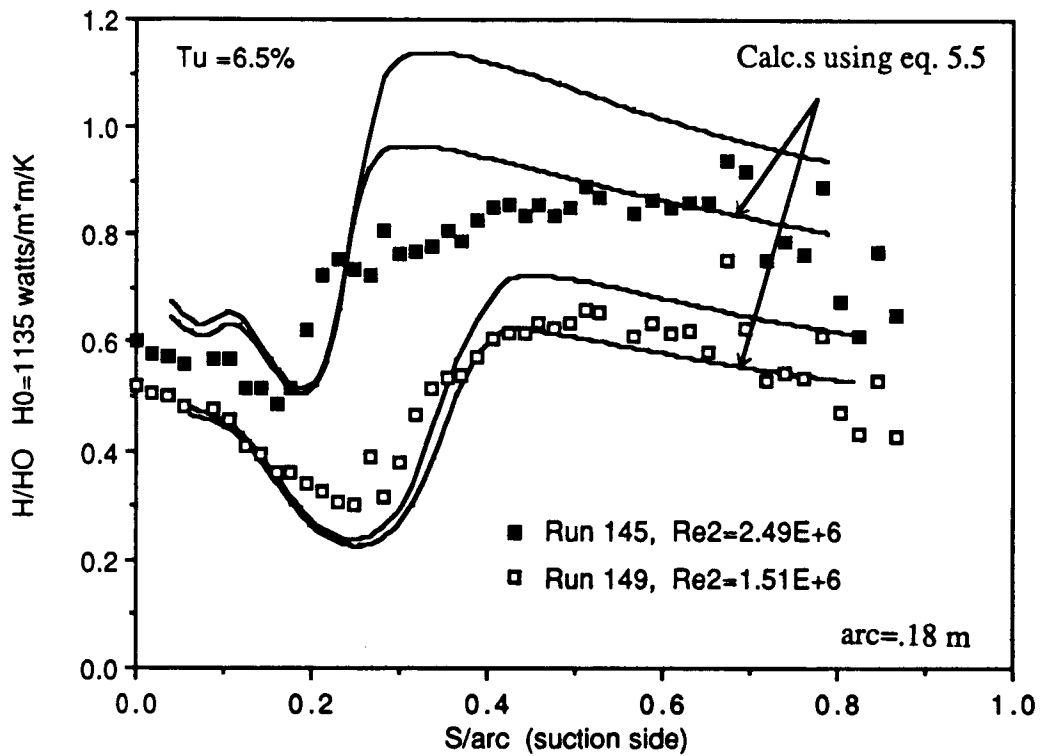


Figure 5.29 Comparison of the predicted and experimental heat transfer around the suction side of Hylton et al.'s C3X blade

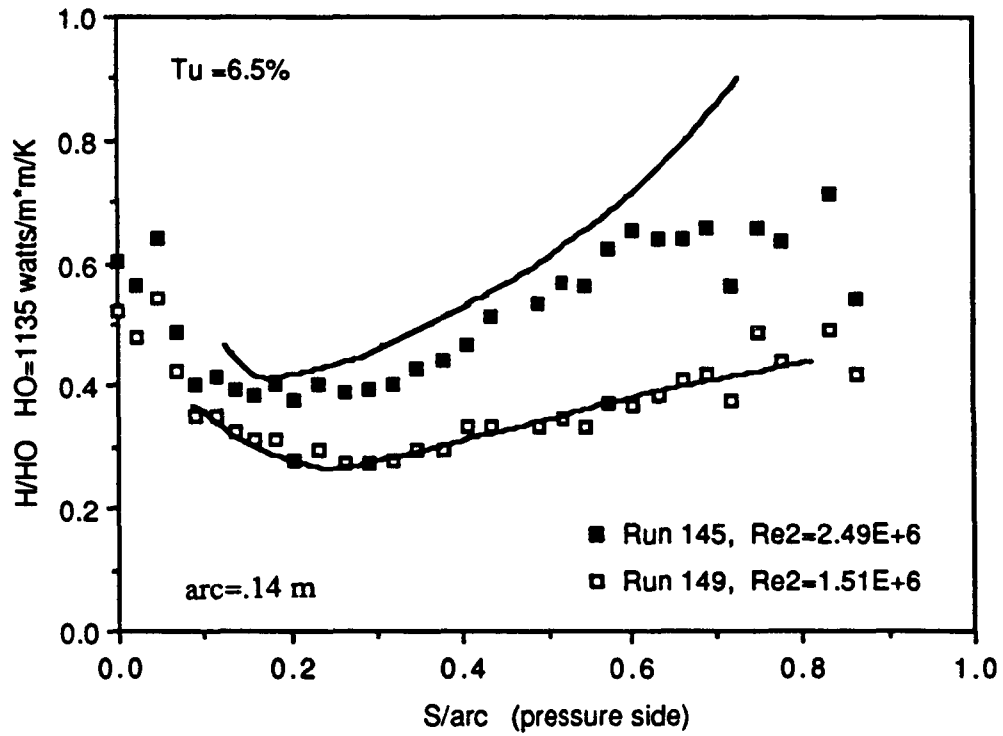


Figure 5.30 Comparison of the predicted and experimental heat transfer around the pressure side of Hylton et al.'s C3X blade

## CHAPTER SIX

### CONCLUDING REMARKS

#### 6.1 CONTRIBUTIONS OF THIS WORK

In concluding this thesis, it is important to review the work completed and summarize the important things learned and accomplished. In the estimation of the author, the following items are the most significant contributions of this work.

- (1) The first thorough evaluation of two contrasting LRN  $k-\epsilon$  turbulence models relative to predicting transition has been made and documented. In doing so, the importance of initial starting profiles and the initial starting location has been quantified. Also, the shortcomings of these models in predicting both the correct start and length of transition have been clearly pointed out and quantified for free-stream turbulence intensities of from less than 1% to 6%.
- (2) The mechanism by which transition is simulated in these models has been delineated and related to the results of the evaluation just mentioned. In doing so, some of the differences between the model's predictions have been traced to specific differences in the low-Reynolds number functions adopted.

- (3) A defect in the Lam-Bremhorst  $f_{\mu}$  formulation was shown to be responsible for the failure of the Lam-Bremhorst model to predict transition at low free-stream turbulence intensities. This has led to a simple modification to eliminate this problem which does not affect the predictions for fully turbulent flow.
- (4) A simple modification limiting the production term in the  $k$  equation has been developed and tested to improve the transition predictions. This modification was shown to be sufficiently general to be applicable to any  $k$ - $\epsilon$  LRN model. After calibration of the two empirical parameters, the "PTM" forms of the both the Lam-Bremhorst and Jones-Launder models were shown to yield transition predictions in accord with the correlation of Abu-Ghannam and Shaw for both the start and the end of transition. Also, after the addition of this modification the sensitivity of the calculations to the initial starting location was reduced. This was especially so for the Lam-Bremhorst model implementation.
- (5) The PTM form of the Lam-Bremhorst model has been thoroughly tested against a large number of test cases in order to clearly document its prediction capabilities both in terms of accuracy and reliability. These included flows both with and without pressure gradients, including a number turbine blade experiments. The results of these tests showed excellent agreement in terms of heat transfer predictions with most of these experiments. Furthermore, the wide range of the comparison is hoped to be sufficient to provide two additional benefits;

- i) Instill confidence in the ability of  $k$ - $\epsilon$  LRN modeling to reliably and consistently predict transition as well and in many cases better than the more traditionally used mixing length type of models.
- ii) Provide clear guidance for further improvements.

## 6.2 LIMITATIONS OF THE APPROACH DEVELOPED

The approach developed in this thesis should be viewed as a practical engineering tool, for it clearly is not a rigorous mathematical model of the physics of transition. However, because a greater degree of meaningful physical phenomenology is naturally accounted for by working within the  $k$ - $\epsilon$  approach, the author believes that this type of model is certainly more general than say, the mixing length approach. An example of this is the relative success of this model in predicting transition in the accelerating flow cases without any additional changes.

The following limitations that are inherent in this approach should be kept in mind.

- (1) The method has only been demonstrated for use in wall bounded shear flows.
- (2) The method can only be as accurate as the correlation upon which the parameters  $A$  and  $B$  are calibrated.
- (3) The transition model has no salutary effect on fully turbulent conditions where the  $k$ - $\epsilon$  model has previously demonstrated deficiencies.
- (4) Since the model is driven by the free-stream turbulence intensity, limitations on the ability of the  $k$ - $\epsilon$  model to accurately predict this – as

was shown to occur under high acceleration – also effect the transition predictions to some extent.

### 6.3 THOUGHTS ABOUT FURTHER RESEARCH

The comparisons made with experiment pointed out a number of areas that could be investigated and which would probably lead to improvements in the approach developed here. In particular, the transition predictions for a moderate constant acceleration showed the tendency to under predict the length of transition. This might be improved by introducing a small pressure gradient effect into the  $A$  parameter. Also, the correlation of Abu-Ghannam and Shaw could be justifiably evaluated and updated in terms of the more extensive data that is now available, especially at higher turbulence intensities. Any improvement there would of course lead to an improved calibration of the transition parameters. This may also shed light on the failure of the model to adequately reproduce the heat transfer data reported by Rued near the leading edge of his pressure gradient tests. Finally, it is important that the effects of curvature on transition be clearly determined and appropriately incorporated into the models.

In addition to what some might consider the somewhat external approach or path taken in this thesis, a more fundamental look at developing better LRN functions themselves may provide even greater improvement and a more general method than has been demonstrated here. One motivation for this lies in the close analogy that exists between the processes observed in near wall behavior, and those observed in transitional boundary layers.

Since a number of aspects of near wall behavior are still not predicted well by current two-equation models( see for example Bernard [7]), improvements in these areas may also have a salutary effect on the transition prediction capabilities of these models.

## REFERENCES

1. Abu-Ghannam, B. J., "Boundary Layer Transition in Relation to Turbomachinery Blades", Ph.D. Thesis, Univ. of Liverpool, Liverpool, 1979
2. Abu-Ghannam, B. J., and Shaw, R., "Natural Transition of Boundary Layers -The Effects of Turbulence, Pressure Gradient, and Flow History", J. of Mech. Eng. Science, Vol. 22, No. 5, pp. 213-228, 1980
3. Alving, A. E., and Smits, A. J., "The Recovery of a Turbulent Boundary Layer from Longitudinal Curvature", AIAA Paper AIAA-86-0435, 1986
4. Arad, E., Berger, M., Israeli, M., and Wolfshtein, M., "Numerical Calculation of Transitional Boundary Layers", Int. Journal for Numerical Methods in Fluids, Vol. 2, pp. 1-23, 1982
5. Baines, W.D., and Peterson, E.G., "An Investigation of Flow Through Screens", ASME Trans., Vol. 73, pp. 467-480, July 1951
6. Barlow, R.S., and Johnston, J.P., "Structure of Turbulent Boundary Layers on a Concave Surface", Thermal Sciences Division Report MD-47, Dept. of Mech. Engineering, Stanford University, Aug. 1985
7. Bernard, P. S., "Limitations of the Near-Wall  $k-\epsilon$  Turbulence Model", AIAA Journal, Vol 24, No. 4, April 1986
8. Blair, M. F., and Werle, M. J., "The Influence of Free-Stream Turbulence on the Zero Pressure Gradient Fully Turbulent Boundary Layer", UTRC Report R80-915388-12, Sept. 1980
9. Blair, M. F., and Werle, M. J., "Combined Influence of Free-Stream Turbulence and Favorable Pressure Gradients on Boundary Layer Transition", UTRC Report R81-914388-17, Mar. 1981
10. Blair, M. F., "Influence of Free-Stream Turbulence on Boundary Layer Transition in Favorable Pressure Gradients", ASME J. of Engineering for Power, Vol. 104, pp. 743-750, Oct. 1982,

11. Blair, M. F., "Influence of Free-Stream Turbulence on Turbulent Boundary Layer Heat Transfer and Mean Profile Development, Part I - Experimental Data", ASME J. of Heat Transfer, Vol. 105, pp. 33-40, Feb. 1983
12. Blair, M. F., "Influence of Free-Stream Turbulence on Turbulent Boundary Layer Heat Transfer and Mean Profile Development, Part II - Analysis of Results", ASME J. of Heat Transfer, Vol. 105, pp. 41-47, Feb. 1983
13. Brown, A., and Martin, B.W., "Flow Transition Phenomena and Heat Transfer Over the Pressure Surfaces of Gas Turbine Blades", ASME paper 81-GT-107, 1981
14. Bradshaw, P., "Effects of Streamline Curvature on Turbulent Flow", AGARograph No. 169, 1973
15. Bradshaw, P., Ferriss, D. H., and Atwell, N. P., "Calculation of Boundary-Layer Development Using the Turbulent Energy Equation", J. Fluid Mechanics, Vol. 28, p. 593, 1967
16. Bousinesq, J., "Mem. Pres. Acad. Sci., Paris, vol. 23, p. 46, 1877
17. Cebeci, T., and Smith, A.M.O., Analysis of Turbulent Boundary Layers, Academic Press, New York, 1974
18. Crawford, M.E., and Kays, W.M., Convective Heat and Mass Transfer, 2nd ed., McGraw-Hill Inc., 1980
19. Daniels L. C., "Film-Cooling of Gas Turbine Blades', Ph. D. Thesis, Dept. of Eng. Sci., U. of Oxford, England, 1978
20. Daniels, L. D., Browne, W. B., "Calculation of Heat Transfer Rates to Gas Turbine Blades", Int. J. of Heat and Mass Transfer, Vol 24, No. 5, pp. 871-879, 1981
21. Delaney, R.A., "Time-Marching Analysis of Steady Transonic Flow in Turbo-machinery Cascades Using the Hopscotch Method", ASME Paper No. 82-GT-152, 1982

22. Dhawan, S., and Narasimha, R., "Some Properties of Boundary Layer Flow During Transition for Laminar to Turbulent Motion", *J. of Fluid Mech.*, Vol. 3, pp. 418-436, 1958
23. Dutoya, D., and Michard, P., "A Program for Calculating Boundary Layers along Compressor and Turbine Blades", *Numerical Methods in Heat Transfer*, eds. R.W. Lewis, K. Morgan, and O.C. Zienkiewicz, J. Wiley & Sons Ltd., pp. 413-428, 1981
24. Dyban, Y. P., Epik, E. Y., and Suprun, T. T., "Characteristics of the Laminar Boundary Layer in the presence of Elevated Free-Stream Turbulence", *FLUID MECHANICS-Soviet Research*, Vol. 5, No. 4, July-August 1976
25. Forest, A. E., "Engineering Predictions of Transitional Boundary Layers", *AGARD Conference Proceedings*, No. 229, 21.1-22.19, 1977
26. Gillis, J.C., and Johnston, J. P., "Turbulent Boundary-Layer on a Convex Curved Surface", *NASA-CR3391*, March 1981
27. Gillis, J.C., and Johnston, J. P., "Turbulent Boundary-Layer Flow and Structure on a Convex Wall and its Redevelopment on a Flat Plate", *Journal of Fluid Mechanics*, Vol. 135, pp. 123-153, 1983
28. Graham, R.W., "Fundamental Mechanisms that Influence the Estimate of Heat Transfer to Gas Turbine Blades", *ASME Paper 79-HT-43*
29. Grundmann, R., Nehring, U., "Berechnung von zweidimensionalen, inkompressiblen, transitionellen Grenzschichten an gekrummten Oberflächen," *Z. Flugwiss. Weltraumforsch.*, Vol. 8, pp. 249-255, 1984
30. Hall, D. J., Gibbings, J. C., "Influence of Stream Turbulence and Pressure Gradient Upon boundary Layer Transition", *J. of Mech. Eng. Science*, Vol. 14, No. 2, 1972
31. Hancock, P. E., and Bradshaw, P., "The Effect of Free Stream Turbulence on Turbulent Boundary Layers", *J. of Fluids Engineering*, Vol. 105, pp. 284-289, Sept. 1983

32. Harlow, F. H., and Nakayama, P., "Transport of Turbulence Energy Decay Rate" Los Alamos Science Lab., University California Report LA-3854, 1968
33. Hassid, S., and Poreh, M., "A Turbulent Energy Model for Flows with Drag Reduction", Trans. ASME, J. Fluid Eng., vol. 97, pp. 234-241, 1975
34. Hylton, L. D., Mihelc, M. S., Turner, E. R., Nealy, D. A., and York, R. E., "Analytical and Experimental Evaluation of the Heat Transfer Distribution Over the Surfaces of Turbine Vanes", NASA CR-168015, May 1983
35. Ilegbusi, J. O. and Spalding, D. B. "An Improved Version of the k-W Model of Turbulence", ASME Paper No. 83-HT-27, 1983
36. Jones, W. P., and Launder, B. E., "The Calculation of Low Reynolds Number Phenomena With a Two-Equation Model of Turbulence", Int. J. of Heat and Mass Transfer, Vol. 16, pp. 1119-1130, 1973
37. Jones, W. P., and Launder, B. E., "The Prediction of Laminarization With a Two-Equation Model of Turbulence", Int. J. of Heat and Mass Transfer, Vol. 15, pp. 301-314, 1972
38. Junkhan, G. H., Serovy, G. K., "Effects of Free-Stream Turbulence and Pressure Gradient on Flat-Plate Boundary-Layer Velocity Profiles and on Heat Transfer", J. of Heat Transfer, pp. 169-176, May 1967
39. Kays, W. M., Crawford, M. E., "Convective Heat and Mass Transfer", 2nd ed., McGraw-Hill Book Co., 1980
40. Kays, W. M., Moffat, R. J., "A Review of Turbulent-Boundary Layer Heat Transfer Research at Stanford, 1958-1983" Advances in Heat Transfer, Vol. 16, pp. 241-365
41. Kestin, J., Maeder, P. F. and Sogin, H. H., "The Influence of Turbulence on the Transfer of Heat to Cylinders near the Stagnation Point", Zeitschrift fuer Angewandte Mathematik and Physik, Vol. 12, No. 2, pp. 115-132, 1961

42. Kestin, J., Maeder, P. F. and Wang H. E., "Influence of Turbulence on the Transfer of Heat from Plates With and Without Pressure Gradient", *Int. Journal of Heat and Mass Transfer*, Vol 3, p. 133, 1961
43. Kestin, J., and Wood, R. T., "The Mechanism Which Causes Free-Stream Turbulence to Enhance Stagnation-Line Heat and Mass Transfer", *Heat Transfer* 1970, Vol. 2, Elsevier Publishing Co., Amsterdam, 1970, Paper FC 2.7
44. Kolmogorov, A. N. , "Equations of Turbulent Motion of an Incompressible Turbulent Fluid", *Izv. Akad. Nauk SSSR Ser. Phys.* VI, No. 1-2 p. 56, 1942
45. Lam, C. K. G., and Bremhorst, K., "A Modified Form of the k-e Model for predicting Wall Turbulence", *J. of Fluids Engineering*, Vol. 103, pp. 456-460, Sept. 1981
46. Launder, B. E., "Second Moment Closure: Methodology and Practice", *Turbulence Models and Their Applications*, Vol 2, Edition Eyrolles, Saint-Germain Paris, 1984
47. Launder, B. E., Sharma, B. I., "Application of the Energy-Dissipation Model of Turbulence to the Calculation of Flow Near a Spinning Disk", *Letters in Heat and Mass Transfer*, Vol. 1, pp. 131-138, 1974
48. Launder, B.E., and Spalding, D. B. "The Numerical Computation of Turbulent Flows", *Computer Methods in Applied Mechanics and Engineering* 3, pp.269-289, 1974
49. Martin, B. W., Brown, A. "Factors Influencing Heat Transfer to the Pressure Surface of Gas Turbine Blades", *Int. Journal of Turbines and Jet Engines*, Vol. 1, pp. 247-258 ,1984
50. Maslowe, S.A., "Shear Flow Instabilities and Transition", in *Hydrodynamic Instabilities and the Transition to Turbulence*, 2nd edition, eds. H.L. Swinney and J.P. Gollub, Springer-Verlag, pp. 180-228, 1985

51. McDonald, H. and Camarata, F. J. "An Extended Mixing Length Approach for Computing the Turbulent Boundary Layer Development" in Proceedings of the AFOSR-IFP-Stanford Conference on Turbulent Boundary Layer Prediction, Stanford, California, 1968
52. McDonald, H., Fish, R. W., "Practical Calculations of Transitional Boundary Layers", Int. J. of Heat and Mass Transfer, Vol. 16, pp. 1729-1744, 1973
53. Meir, H. V., and Kreplin, H. P., "Influence of Free-Stream Turbulence on Boundary Layer Development", AIAA Journal, Vol. 18, No. 1, pp. 11-15, Jan. 1980
54. Miyazaki, H., Sparrow, E. M., "Analysis of Effects of Free-Stream Turbulence on Heat Transfer and Skin Friction", J. of Heat Transfer, Vol. 99, pp. 614-619, 1977
55. Moffat, R. J. "Turbine Blade Cooling", Heat Transfer and Fluid Flow in Rotating Machinery, ed. Yang, W. J., Hemisphere, 1985
56. Nee, V. W. and Kovaszny, L. S. G., "The Calculation of the Incompressible Turbulent Boundary Layer by a Simple Theory", Proc. of AFOSR/IFP Conference on Computation of Turbulent Boundary Layers Vol. 1, Stanford University, 1968 (see also Physics of Fluids 12 (1969) p.473.)
57. Ng, K. H., "Predictions of Turbulent Boundary Layer Developments Using a Two-Equation Model of Turbulence", Ph.D. Thesis, Imperial College, London, 1971
58. Ng, K. H., and Spalding, D. B. "Some Applications of a Model of Turbulence to Boundary Layers Near Walls", Phys. Fluids 15, p. 20, 1972
59. Ng, K. H., and Spalding, D. B. "Predictions of Two-Dimensional Boundary Layers on Smooth Walls with a 2-equation Model of Turbulence", Imperial College, Mechanical Engineering Department Report BL/TN/A/25, 1970

60. Park, W., and Simon, T., "Prediction of Convex-Curved Transitional Boundary Layer Heat Transfer Behavior using MLH Models", Presented at the 2nd ASME/JSME Thermal Engineering Conference, March 1987
61. Patankar, S. V., and Spalding, D. B., Heat and Mass Transfer in Boundary Layers, 2nd. ed., Intertext, London, 1970
62. Patel, V. C., Rodi, W., and Scheuerer, G., "A Review and Evaluation of Turbulence Models for Near Wall and Low Reynolds Number Flows", AIAA Journal, Vol. 23, p. 1308, 1985
63. Prandtl, L., "Bericht über Untersuchungen zur ausgebildeten Turbulenz" Z. Angew. Math. Mech., vol 5, pp. 136-139, 1925
64. Prandtl, L., "Über ein neues Formalsystem für die ausgebildete Turbulenz, Nachrichten von der Akad. der Wissenschaft in Göttingen" 1945
65. Pridden, C.H., The Behaviour of Turbulent Boundary Layer on Curved Porous Walls", Ph.D. Thesis, Imperial College, London, 1975
66. Rodi, W., and Scheuerer, G., "Calculation of Heat Transfer to Convection-Cooled Gas Turbine Blades", J. of Engineering for Gas Turbines and Power, Vol. 107, pp. 20-627, July 1985
67. Rodi, W., and Scheuerer, G., "Calculation of Laminar-Turbulent Boundary Layer Transition on Turbine Blades", AGARD-CP-390
68. Rodi, W., and Scheuerer, G., "Scrutinizing the k- $\epsilon$  Turbulence Model Under Adverse Pressure Gradient Conditions", ASME J. of Fluids Eng., Vol 108, pp. 174-179, June 1986
69. Rodi, W., and Spalding, D. B. "A Two Parameter Model of Turbulence and its Application to Free Jets" *Wärme und Stoffübertragung* 3, p. 85, 1970
70. Rodi, W., Turbulence Models and Their Application in Hydrolics- A State of the Art Review, Book publication of the International Association for Hydrolic Research, Delft, The Netherlands, 1980

71. Rotta, J.C., Statistische Theorie nichthomogener Turbulenz, Zeitschrift f. Physik, Bd. 192, pp. 547-572, and Bd. 131, pp. 51-77(1951) (English Translation' Imperial College, Dept. of Mech. Eng., Reports TWF/TN/38, 39, 1968)
72. Rued, K "Transitionale Grezschichten unter dem Einfluss hoher Freistromturbulenze, intensiver Wandkuehlung und starken Druckgradienten in Heissgasstroemungen", Thesis submitted at the University of Karsruhe, 1985
73. Rued, K., and Wittig, S., "Free Stream Turbulence and Pressure Gradient Effects on Heat Transfer and Boundary Layer Development on Highly Cooled Surfaces", J. of Engineering for Gas Turbines and Power, Vol. 107, No. 1, pp. 54-59, Jan. 1985
74. Rued, K., and Wittig, S., "Laminar and Transitional Boundary Layer Structures in Accelerating Flow with Heat Transfer", ASME Paper No. 86-GT-97, 1986
75. Saffman, P. G., "A Model for Inhomogeneous Turbulent Flow." Proceedings of the Royal Society, London, Vol. A317, pp. 417-433, 1970
76. Saffman, P. G., and Wilcox, D.C., "Turbulence-Model Predictions for Turbulent Boundary Layers", AIAA Journal, Vol. 12, No. 4, pp. 541-546, April 1974
77. Scheuerer, G., "Entwicklung eines Verfahrens zur Berechnung zweidimensionaler Grenzschichten an Gasturbineschaufeln", Ph.D. Thesis, Universitat Karlsruhe, 1983
78. Schlichting, H., Boundary Layer Theory, 7th ed., McGraw-Hill, 1979, p. 469
79. Schmidt, R. C., and Patankar, S. V., "Prediction of Transition on a Flat Plate under the Influence of Free-Stream Turbulence using Low-Reynolds-Number Two-Equation Turbulence Models", ASME Paper 87-HT-32, 1987

80. Simonich, J. C., and Bradshaw, P., "Effect of Free-Stream Turbulence on Heat Transfer Through a Turbulent Boundary-Layer", ASME J. of Heat Transfer, Vol. 100, No. 4, pp. 671-677, Nov. 1978
81. So, R.M.C., and Mellor, G.L., "Experiment on Convex Curvature Effects in Turbulent Boundary Layers", Journal of Fluid Mechanics, Vol. 60, pp. 43-62, 1973
82. Spalding, D. B. "The Prediction of Two-dimensional, Steady Turbulent Flows" Imperial College, Heat Transfer Section Report ER/TN/A/16, 1969
83. Spalding, D. B. "The k -W Model of Turbulence", Imperial College, Mechanical Engineering Department Report TM/TN/A/16, 1972
84. Tani, I., "Boundary-Layer Transition", Annual Review of Fluid Mechanics, Vol. 1, pp. 169-196, 1969
85. Thwaites, B., Aeronaut. Q., vol. 1, pp. 245-280, 1949
86. Townsend, A.A., "The Structure of Turbulent Shear Flow", 2nd. ed., Cambridge Univ. Press, Cambridge, 1976
87. Turner, A. B., "Local Heat Transfer Measurements on a Gas Turbine Blade", Journal of Mechanical Engineering Science, Vol. 13, No. 1, 1971
88. Van Driest, E. R. "On Turbulent Flow Near a Wall", J. Aeronautical Sciences, Vol. 23, p. 1007, 1956
89. Van Driest, E. R., Blumer, C. B., "Boundary Layer Transition; Freestream Turbulence and Pressure Gradient Effects", AIAA Journal, Vol. 1, No. 6, pp. 1303-1306, June 1963
90. Wang, J. H., Jen, H. F., and Hartel, E. O., "Airfoil Heat Transfer Using Low Reynolds Number Version of a Two Equation Turbulence Model.", J. of Engineering for Gas Turbines and Power, Vol. 107, No. 1, pp. 60-67, Jan. 1985

91. Wang, T., "An Experimental Investigation of Curvature and Free-Stream Turbulence Effects on Heat Transfer and Fluid Mechanics in Transitional Boundary Layers", Ph.D. Thesis, Dept. of Mech. Engr., University of Minnesota, December 1984
92. Wang, T., Simon, T. W., and Buddhavarapu, J., "Heat Transfer and Fluid Mechanics Measurements in Transitional Boundary Layer Flows", J. of Eng. Gas Turbines and Power, Trans. ASME, Vol. 107, No. 4, pp. 1007-1015
93. Wang, T., Simon, T. W., "Heat Transfer and Fluid Mechanics Measurements in Transitional Boundary Layers on Convex-Curved Surfaces", ASME paper No. 85-HT-60, 1985
94. White, F. M., Viscous Fluid Flow, McGraw-Hill, Inc. 1974
95. Wilcox, D.C., "Turbulence Model Transition Predictions", AIAA Journal, Vol. 13, No. 2, pp. 241-243, Feb. 1975
96. Wilcox, D. C., "A Model for Transitional Flows", AIAA Paper 77-126, 1977
97. Wilcox, D.C., "Development of an Alternative to the e<sup>9</sup>-Procedure for Predicting Boundary-Layer Transition", Office of Naval Research, Arlington, ONR-CR-298-005-ZF, 1979
98. Wolfshtein, M., "On the Length-Scale-of Turbulence Equation", Israel J. Technology, Vol. 8, pp. 87-99, 1970
99. Zerkle, R.D., and Lounsbury, R.J., "The Influence of Freestream Turbulence and Pressure Gradient on Heat Transfer to Gas Turbine Airfoils", AIAA Paper 87-1917, 1987

## Appendix A1

### The Computer Code

The computer code used to perform the calculations in this work is documented here. This will begin with a brief description of the code and of the major FORTRAN variables and arrays. Next, a complete FORTRAN listing of each of the routines which make up the code will be given. Finally, a number of representative input decks will be listed.

#### A Brief Description of the Code

The computer code used has two major divisions. The first part, called program MAIN, serves as the driver for the solution procedure. It also contains that portion of the code which is not dependent upon the specifics of the problem at hand, but rather is dictated by the general nature of the parabolic equations themselves. This part of the program was not developed by the author. It was simply adapted with minor changes from the general purpose parabolic computer code made available to students at the University of Minnesota who take Professor Suhas Patankar's course ME 8353. It is a FORTRAN implementation of the basic solution techniques explained in [61]. Since excellent documentation of this portion of the code is readily available through professor Patankar, a detailed description will not be given here. However, a listing is provided here following all of the other subroutines. Note that the utility routines UYGRID and PROFIL are located within MAIN as entry statements.

The remaining portion of the code contains problem specific coding (written of course within the framework required by part one). It is this part

of the code which was written by the author, and this is where the computational models developed in this thesis are implemented. A major portion of this is contained within an umbrella subroutine called USER. Although technically only one subroutine, numerous other subroutines are effectively contained within this one large routine by appropriate use of entry statements. This technique facilitates a shared set of common blocks and variable information without eliminating the advantages of modular code design and development.

Although the code itself is documented reasonably well, a brief description of each of the subroutines and functions written for use in this thesis will be given as follows. Note that for the purpose of this explanation, calls to entry statements contained within subroutine USER, will be treated as if they are separate subroutines themselves.

**BOUND**      Five important things are accomplished in this subroutine.

- (1) The transition model parameters  $A$  (TCI) and  $B$  (DPKDTM) are calculated for the next step.
- (2) Turbulent Reynolds numbers and the associated functions and source terms in the  $k$  and  $\epsilon$  equations are calculated for use during the next time step.
- (3) The appropriate entrainment at the boundary is calculated.
- (4) Boundary conditions for  $U, H, k$ , and  $\epsilon$  are calculated.
- (5) The pressure gradient and the step size are computed.

**DENSE**      First, the temperature field is calculated from the associated enthalpy values. Then, if constant properties are not being assumed (ie., `LCSOL=.FALSE.`), all material properties (including the density) are calculated here as functions of temperature. The functional approximations used are given in appendix A2

- ENTRAIN** This subroutine (called from BOUND) calculates an appropriate entrainment value based on either the velocity and/or the enthalpy profiles. Note that the purpose of this is to expand the computational domain in response to the growth of the boundary layers.
- GAMSOR** The diffusion coefficients and source terms for each of the transport equations are calculated here.
- OUTPUT** This subroutine provides the means of writing out to data files the important calculated quantities of interest. These include the heat transfer and skin friction coefficients, profile data, and integral parameters such as the momentum thickness.
- PROFIL** Simple utility routine to output the profiles of the calculated quantities of interest. Located as an entry statement routine within MAIN.
- RCURVE** Subroutine provided to calculate and return the local radius of curvature. This was not used in the work presented in this thesis since curvature effects were neglected.
- RUNGA** Uses a simple fourth order Runga-Kutta scheme to integrate ordinary differential equations. This FORTRAN coding was taken directly from reference [94]. It is used to find the upstream boundary conditions for  $k$  and  $\epsilon$  as the solution procedure advances ( See eqs. (2.35) and (2.36) ).
- START** Sets the initial starting profiles and boundary conditions for  $k$ ,  $\epsilon$ , and  $H$ . Also gives starting values to a number of miscellaneous parameters.
- TRANS** Calculates the nondimensional values of the transition parameters  $A$  (TCI) and  $B$  (DPK) as a function of the local free-stream turbulence intensity
- USER** Sets the values to constants, reads the input data (which will control the computation) from a data file, specifies the

computational grid, and calculates the starting velocity profile.

**UYGRID** Utility routine to set the appropriate stream function values between control volumes once the velocity profile has been set. It is located as an entry statement routine within MAIN.

**VELPROF** Calculates the appropriate values for velocity at each control volume in accordance with a Pohlhausen velocity profile. This is used to generate a starting velocity profile

**FMU (function)** Returns the value of the LRN function  $f_m$

**F1 (function)** Returns the value of the LRN function  $f_1$

**F2 (function)** Returns the value of the LRN function  $f_2$

**UM1 (function)** Returns the value of the free-stream velocity as a function of streamwise distance. This of course is completely problem dependent and must be written uniquely for each problem solved.

### Definitions of FORTRAN variables and arrays

**A1** The parameter  $a_1$  in equation (2.39) used in specifying the initial starting  $\epsilon$  profile.

**AGRID**  $\eta$  as defined in eq. (2.29)

**AH(J)** Total enthalpy at location J

**AHTC** Local Heat Transfer Coefficient  $h$

**AJTI(NF)** The calculated total flux at the wall boundary for the dependent variable  $F(J,NF)$ . Note  $NF=1$  corresponds to the momentum flux (wall shear stress), and  $NF=4$  corresponds to the wall enthalpy (heat) flux

**AK(J)** Turbulent kinetic energy at location J

**AMU(J)** The molecular viscosity at location J

AMU0	Average viscosity of the starting profile
AMUT(J)	Turbulent viscosity at location J
AP(J)	In subroutine GAMSOR, it is set equal to the negative part of the source term - of whichever variable's equation is currently being solved - divided by the current local value of that variable. (See section on source term linearization in [61]) It is further modified in MAIN.
ASN	A Small Number. Set equal to 1.e-20
BO, B1...	Constants in a polynomial approximation of the thermal conductivity
C1	The turbulence model constant $C_1$
C2	The turbulence model constant $C_2$
CC	Input parameter that is not currently used
CF	Coefficient of friction
CGRID	The grid generation quantity $\eta(b-1)(\chi_1)^b$ . See eq. (2.28)
COMMENT	General purpose character variable used mainly for input
CON(J)	The positive part of the source term of whichever equation is currently being solved
CP(J)	The specific heat at location J
CPAVG	$.5*(CP(M1) + CP(1))$
CPO,CP1,...	Constants in a polynomial approximation of the specific heat
CRVM	Input parameter that is not currently used
CU	The turbulence model constant $C_\mu$
D99	99% boundary layer thickness (based on velocity)
DEL	The boundary layer thickness specified in the input file at the starting location
DELT	The thermal boundary layer thickness specified in the input file at the starting location

DELTA T	Temperature difference across the boundary layer
DEN	Average density of the starting profile
DEN1	$DYP + R2 * DYM$ , Used in calculating $DU1(J)$
DGRID	Grid generation quantity $(b-1)(\chi_1)^b$ . See eq. (2.29)
DL1	Displacement thickness
DL2	Momentum thickness
DLS	A Dissipation Length Scale. See line 306
DPDSC	$UM10 * DUDSP$
DPK	The maximum increase in $P_k$ allowed over the next forward step. This is found through the transition model. See lines 438-439 and eqs. (4.6) and (4.7)
DPKDTM	Dimensional value of the transition model parameter B. It is calculated in line 393 from $DPKDTM0$
DPKDTM0	Nondimensional value of the transition model parameter B. It is calculated by TRANS as a function of $Tu$ and shown in Figure 4.9
$DU1(J)$	Velocity gradient $dU/dY$ at location J
DUDS	Free-stream velocity gradient in the stream-wise direction
DUDSP	$RHO(M1) * DUDS$
DX	Computational step size in the streamwise direction
DXFC	The step size in the streamwise direction is calculated as $DX = DXFC * DL2$ ( $DL2 = \text{momentum thickness}$ )
DYM	$Y(J) - Y(J-1)$
DYP	$Y(J+1) - Y(J)$
E(J)	Dissipation rate at location J
EIN	Input value of the free-stream dissipation at the starting location

EKI	The exponent "n" in equation (2.38) used in specifying the initial starting k profile.
ENEXP	An exponent used in the entrainment calculation. Called POWER in subroutine ENTRAIN, it affects how strongly the calculation responds to changes in the near free-stream profile
F(J,NF)	The general dependent variable matrix. Note that NF=1-11 have been equivalenced to other arrays
FILNAME	Input character array containing the names of input and output files used in the calculation
FKE(N)	For N=1, $dk_e/dx$ . For N=2, $d\varepsilon_e/dx$
FRAC	An entrainment parameter used in specifying the desired fractional difference between the last few nodes at the outer edge of the boundary layer. See subroutine ENTRAIN
FSCON	If $RE2 < RE2C$ , FSCON=0, else FSCON=1. Multiplying the positive source term in the k equation, it implements part of the transition model developed.
GEXP	The exponent "b" associated with the grid generation. See Chapter two, equations (2.25) through(2.29)
GGRID	The grid generation quantity $\eta [b (\chi_1)^{b-1}]$ . See eq. (2.28)
GX1	The matching point $\chi_1$ (in terms of the grid coordinate $\chi$ ) used in the grid generation. See chapter two, equations (2.25) through(2.29)
HTC	An input parameter that is not currently used
IPP	ISTEP must be greater than IPP before PROFIL can be called
ISTEP	Integer counter keeping track of the number of forward steps taken

ITBFLG	Integer flag set equal to 1 once the transition model requires information from subroutine TRANS. This occurs when RE2 exceeds RE2C.
ITM	Input parameter which if set equal to 0, prevents transition to turbulence by setting DPKDTM=0 and skipping the calls to subroutine TRANS
IWTBC	Specifies the type of Wall Thermal Boundary Condition. If IWTBC=1, a specified wall temperature is assumed. Else, a specified wall heat flux is assumed.
JUMP1	Every JUMP1 forward steps, subroutine PROFIL is called
JUMP2	Every JUMP2 forward steps, a small number of specified quantities are printed out to monitor the calculation
JUMPT	Every JUMPT forward steps, the transition parameters are updated by calling subroutine TRANS. Only implemented if ITBFLG=1
KBCI(NF)	Boundary condition index for the inner boundary required by MAIN. =1 for a given value, =2 for a given flux, =3 for the total flux expressed in the form $(a-b\phi_1)$
KCM	Input parameter which is not currently used
KCRM	Curvature flag not used in this version of the code
KENT	Integer value fixing the profile(s) used in the entrainment calculation. If KENT=1, the velocity profile is used. If KENT=4, the enthalpy profile is used. Any other value and both profiles are used.
KEX	Outer boundary condition index used by MAIN. It is set equal to 2 indicating the outer edge is a free boundary
KIN	Inner boundary condition index used by MAIN. It is set equal to 1 indicating the inner boundary is a wall
LASTEP	The largest allowable number of forward steps allowed before stopping the calculation

LCPSOL	Logical input parameter. If .TRUE., material properties are considered constant and set equal to their respective values at T=TAVG. If .FALSE., material properties are calculated as functions of temperature in subroutine DENSE
LPRINT(NF)	Logical input array. When .TRUE., the profile of F(J,NF) is printed out whenever subroutine PROFIL is called
LSOLVE(NF)	Logical input array. When .TRUE. , the differential equation for F(J,NF) is solved.
LSTOP	Logical variable which if set equal to .TRUE. will terminate the calculation in MAIN.
M1	The total number of grid points in the cross stream direction
NDPTS	Integer counter keeping track of how many times certain data has been written out to a file. See lines 309-310
NP2	Integer counter associated with RE2P. See lines 295-298
OMEGA	The acceleration parameter $\Lambda = \delta^2 U' / \nu$ used in calculating the initial starting profile for the velocity. It must be specified in the input. See Chapter Two, section 2.3.3
PR(J)	The Prandtl number at location J
PRO	Average Prandtl number of the starting profile
PRDR	PRESS / RCON
PRESS	The local pressure. Must be specified in the input file at the starting location
PRT	The turbulent Prandtl number
PRT	The turbulent Prandtl number
R2	(DYP/DYM)**2
RC	Radius of curvature. Not used in this version of the code
RCON	Gas constant in the ideal gas law
RE2	Momentum thickness Reynolds number

RE2C	The critical momentum thickness Reynolds number below which the modeled production term is set equal to zero.
RE2F	If $Re_{\theta}$ exceeds RE2F, the calculation will stop
RE2P(N)	Input array containing the specified values of the momentum thickness Reynolds numbers at which all calculated quantities and profiles are to be written out to a file
REP	When $Re_x=REP$ , computed boundary layer properties and parameters are writing out. REP is then increased to the next desired value (See REPF C)
REPF C	REP is incremented such that over every 1 cycle logarithmic increase in $Re_x$ , boundary layer properties are printed out REPF C times. See line 308 of the subroutine USER listing
REPI	The first value assigned to REP. Given in the input file
REX	Reynolds number based on x
RFILE	Character variable read in the input file which is not used in this version of the code.
RHO(J)	Density at location J
RME	Free-stream boundary entrainment rate. This is what is controlled through subroutine ENTRAIN
SCE(J)	Positive source term(s) in the $\epsilon$ equation at location J
SCEMF	Set equal to $\max(1.,L/L_{max})$ , see eq. (5.5). However, this effect is suppressed by setting AKAPI extremely small in line 178 (in eq. (5.5) it is 2.7), thus SCEMF is always equal to one in this version of the code
SCK(J)	Positive source term(s) in the k equation at location J
SCONB	Constant in the viscosity approximation
SCONS	Constant in the viscosity approximation
SCU	Local variable used in GAMSOR. If $DPDSC < 0$ , $SCU=0$ , else $SCU=DPDSC$

SE	The turbulence model constant $\sigma_\epsilon$
SI(J)	Used in calculating the source term in the enthalpy equation
SK	The turbulence model constant $\sigma_k$
SK1	Temporarily holds the local value of $\mu_t \left( \frac{\partial U}{\partial y} \right)^2$ . See line 436
SKC	FSCON * SK1
SPE(J)	Negative source term(s) in the $\epsilon$ equation at location J
SPK(J)	Negative source term(s) in the k equation at location J
SPU	Local variable used in GAMSOR. If DPDSC < 0, SPU=DUDSP, else SPU=0
STAN	Stanton Number
T(J)	The temperature at location J
TAVG	(TW+TINF)/2
TCI	Dimensional value of the transition model parameter A. It is calculated in line 394 from TCIO
TCIO	Nondimensional value of the transition model parameter A. It is calculated by TRANS as a function of Tu and shown in Figure 4.8
TCOND	Thermal conductivity
TINF	The free-stream value of the temperature
TITLE(NF)	Character input array containing the specified titles of each F(J,NF) profile. Used in PROFIL when printing
TK	Temperature in deg K
TRE(J)	The turbulent Reynolds number $Re_t$ at location J
TU	Input value of the free-stream turbulence intensity at the starting location
TUINF	Free-stream Turbulence intensity
TW	The temperature at the wall

U(J)	Streamwise velocity at location J
UFRIC	Friction velocity
UHSL	Unheated or uncooled starting length.
UINF	Free-Stream Velocity
UJ	$U(J) / U(M1)$
UJD	$UJ * RHO(J) / RHO(M1)$ . Used in calculating DL1
UM10	Free-stream velocity of the previous step
UPLS(J)	$U^+$ at location J
UU1	The coordinate $\chi$ used in generating the grid. See eq. (2.23)
VINF	An input variable which is not used in this version of the code
WTOHF	Either the specified wall temperature (IWTBC=1) or heat flux (IWTBC $\neq$ 1).
XU	Streamwise location $x$
XUF	Input final or maximum value of the streamwise location $x$
XUI	Input starting value of the streamwise location $x$
XUNEW	Streamwise location $x$ at the next step
Y(J)	The cross-stream distance $y$ at location J
YCVM(J)	Distance between the grid point J and the lower edge of the control volume J. Referred to in documentation for subroutine MAIN as $\Delta y^-$
YCVP(J)	Distance between the grid point J and the upper edge of the control volume J. Referred to in documentation for subroutine MAIN as $\Delta y^+$
YKE(N)	The free-stream value of $k$ (N=1) or dissipation rate (N=2)
YPLS(J)	$y^+$ at location J
YPLSCAL	Variable used in calculating YPLS(J). See lines 282,288
YRE(J)	The turbulent Reynolds number $Re_y$ at location J

## A Listing of the Subroutines and Functions

```

1      C*****
2      SUBROUTINE USER
3      C
4      LOGICAL LSTOP, LPR, LGPG, LTIME, LSOLVE, LPRINT, LCPSOL
5      CHARACTER TITLE (13) *7, COMMENT*60, FILNAME (4) *25, RFILE*40
6      COMMON F (99, 11), RHO (99), GAM (99), CON (99),
7      1      AP (99), AN (99), AS (99), PT (99), QT (99), RT (99),
8      2      OM (99), OMF (99), OMF1 (99), OMCV (99), Y (99),
9      3      YF (99), YCVR (99), YCVP (99), YCVM (99), R (99),
10     4      RF (99), FLO (99)
11     COMMON /INDX/ NF, NFMAX, NU, NRHO, NGAM, M1, M2, KIN, KEX, DPDX,
12     1      ISTEP, LASTEP, MODE, ITMX, LGPG, LTIME, XU, DX, XLAST,
13     2      PEI, PSII, PSIE, PSIT, YM1, POWER, CSALFA, RMI, RME, ARI, ARE
14     COMMON /VARB/ LSOLVE (11), LPRINT (13),
15     1      AJTI (11), AJTE (11), AFXI (11), BFXI (11),
16     2      AFXE (11), BFXE (11), KBCI (11), KBCE (11)
17     COMMON /CHAR/ TITLE
18     COMMON /CNTL/ LSTOP
19     COMMON /COEF/ FLOW, DIFF, ACOF
20     DIMENSION SPK (99), SCK (99), SPE (99), SCE (99), SI (99)
21     DIMENSION YPLS (99), U (99), UPLS (99), AK (99), E (99), AH (99)
22     DIMENSION AMUT (99), DU1 (99), TRE (99), YRE (99), T (99), AMU (99)
23     DIMENSION PR (99), CP (99), YKE (2), FKE (2), RE2P (10)
24     EQUIVALENCE (F (1, 1), U (1)), (F (1, 2), AK (1)), (F (1, 3), E (1))
25     EQUIVALENCE (F (1, 4), AH (1)), (F (1, 5), T (1)), (F (1, 6), TRE (1))
26     EQUIVALENCE (F (1, 7), YRE (1)), (F (1, 8), AMUT (1)), (F (1, 9), YPLS (1))
27     EQUIVALENCE (F (1, 10), UPLS (1)), (F (1, 11), DU1 (1))
28     C.....
29     C
30     C 1.00 -- SUBROUTINE "USER" OF A PROGRAM TO CALCULATE LAMINAR,
31     C TRANSITIONAL, AND TURBULENT BOUNDARY LAYER FLOWS UNDER THE
32     C INFLUENCE OF PRESSURE-GRADIENTS AND FREE-STREAM TURBULENCE. A
33     C SLIGHTLY MODIFIED FORM OF THE LAM-BREMHORST LOW-REYNOLDS-NUMBER
34     C K-e TURBULENCE MODEL IS EMPLOYED TOGETHER WITH THE ADDITIONAL
35     C MODIFICATIONS FOR TRANSITION DEVELOPED BY SCHMIDT AND PATANKAR
36     C THIS VERSION IS SET UP FOR VARIABLE PROPERTIES OF AIR.
37     C.....VERSION AS OF AUGUST, 1987.....
38     C.....WRITTEN BY RODNEY C. SCHMIDT .....
39     C.....
40     C
41     C 1.10  CONSTANTS IN POLYNOMIAL APPROXIMATIONS OF THE THERMAL
42     C CONDUCTIVITY AND SPECIFIC HEAT. ALSO "SUTHERLAND" VISCO-
43     C SITY APPROXIMATION CONSTANTS AND THE GAS CONSTANT FOR AIR
44     C
45     DATA B0, B1, B2/2.41916E-2, 7.3851E-5, -3.203E-8/
46     DATA B3, CP0, CP1/1.829E-11, 1003.6, .01155/
47     DATA CP2, CP3, SCONB/5.453E-4, -4.2422E-7, 1.465E-6/
48     DATA SCONS, RCON/110.4, 287.0/

```

```

49      C
50      C 1.20 -- ASK FOR THE INPUT FILE NAME AND THEN READ THE RUN
51      C          PARAMETERS FROM THE INPUT FILE
52      C
53          PRINT*, 'INPUT THE NAME OF THE INPUT FILE'
54          READ*, COMMENT
55          OPEN (UNIT=1, FILE=COMMENT)
56          READ (1, *) COMMENT
57          READ (1, *) (FILNAME (I), I=1, 4)
58          READ (1, *) COMMENT
59          READ (1, *) (LSOLVE (I), I=1, 4)
60          READ (1, *) COMMENT
61          READ (1, *) (LPRINT (I), I=1, 11)
62          READ (1, *) COMMENT
63          READ (1, *) (TITLE (I), I=1, 11)
64          READ (1, *) COMMENT
65          READ (1, *) (RE2P (I), I=1, 10)
66          READ (1, *) COMMENT
67          READ (1, *) LASTEP, JUMP1, JUMP2, IPP, JUMPT
68          READ (1, *) COMMENT
69          READ (1, *) KENT, HTC, ITM, LCPSOL
70          READ (1, *) COMMENT
71          READ (1, *) TU, EIN, XUI, XUF, RE2F, RE2C
72          READ (1, *) COMMENT
73          READ (1, *) PRESS, VINF
74          READ (1, *) COMMENT
75          READ (1, *) IWTBC, PRT, TINF, TW, UHSL, WTOHF
76          READ (1, *) COMMENT
77          READ (1, *) M1, DEL, DELT, GEXP, GX1, EKI, A1, DXFC, REPI, REFFC
78          READ (1, *) COMMENT
79          READ (1, *) CU, C1, C2, SK, SE, CC, CRVM
80          READ (1, *) COMMENT
81          READ (1, *) OMEGA, FRAC, ENEXP, RC, KCRC, KCM, RFILE
82          CLOSE (UNIT=1)
83      C
84          PRINT*, 'LOW REYNOLDS NUMBER FUNCTIONS OF LAM AND BREMHORST'
85      C
86      C 1.30 -- CALCULATE INITIAL DENSITY AND VISCOSITY
87      C
88          PRDR=PRESS/RCON
89          TAVG=(TW+TINF)/2.
90          TK=TAVG+273.15
91          DEN=PRDR/TK
92          AMU0=SCONB*TK**1.5 / (SCONS+TK)
93          TCOND=B0+B1*TAVG+B2*TAVG*TAVG+B3*TAVG*TAVG*TAVG
94          CP (M1)=CP0+CP1*TAVG+CP2*TAVG*TAVG+CP3*TAVG**3
95          PRO=AMU0*CP (M1) / TCOND
96          DO 100 J=1, M1
97              RHO (J)=DEN
98              AMU (J)=AMU0
99              PR (J)=PRO
100             CP (J)=CP (M1)
101      100 CONTINUE
102      C
103      C 1.40 -- SPECIFY THE GRID AND THE INITIAL VELOCITY PROFILE

```

```

104 C
105 XU=XUI
106 UINF=UM1 (XU)
107 REX=XU*RHO (M1) *UINF/AMU (M1)
108 Y (M1) =DELT
109 Y (1) =0.
110 DGRID= (GEXP-1.) *GX1**GEXP
111 AGRID=1. / (1.+DGRID)
112 GGRID=AGRID*GEXP*GX1** (GEXP-1)
113 CGRID=AGRID*DGRID
114 DO 110 J=2,M1-1
115     UU1= (FLOAT (J-1) -.5) / (FLOAT (M1-2))
116     Y (J) =UU1*GGRID*Y (M1)
117     IF (UU1.GT.GX1) Y (J) = (AGRID*UU1**GEXP+CGRID) *Y (M1)
118 110 CONTINUE
119 C
120 U (1) =0.
121 CALL VELPROF (DEL, OMEGA, UINF, M1, U, Y)
122 CALL UYGRID
123 RETURN
124 C*****
125 C 2.00 ENTRY POINT FOR SUBROUTINE 'START'.
126 C*****
127     ENTRY START
128     OPEN (UNIT=3, FILE=FILENAME (3))
129     OPEN (UNIT=4, FILE=FILENAME (4))
130 C
131 C 2.10 -- CALCULATE INITIAL BOUNDARY CONDITIONS FOR K AND E
132 C
133     AK (M1) =1.5* (U (M1) *TU) **2
134     E (M1) =EIN
135     TRE (M1) =AK (M1) **2*RHO (M1) / (AMU (M1) *E (M1))
136 C
137 C 2.20 --SPECIFY INITIAL PROFILES FOR K, E, & RELATED QUANTITIES
138 C
139     DO 210 J=2,M1-1
140         DYP=Y (J+1) -Y (J)
141         DYM=Y (J) -Y (J-1)
142         R2= (DYP/DYM) **2
143         DEN1=DYP+R2*DYM
144         DU1 (J) = (U (J+1) - (1-R2) *U (J) -R2*U (J-1)) /DEN1
145         AK (J) =AK (M1) * (U (J) /UINF) **EKI
146         E (J) =A1*AK (J) *DU1 (J)
147         IF (E (J) .LT. E (M1)) E (J) =E (M1)
148         TRE (J) =AK (J) **2*RHO (J) / (AMU (J) *E (J))
149         YRE (J) =SQRT (AK (J) ) *Y (J) *RHO (J) /AMU (J)
150         AMUT (J) =AMU (J) *CU*FMU (TRE (J) , YRE (J) ) *TRE (J)
151 210 CONTINUE
152     AK (1) =0.
153     E (1) =E (2)
154     AMUT (1) =0.
155     YPLS (1) =0.
156     UPLS (1) =0.
157     TRE (1) =0.
158     DU1 (M1) =0.

```

```

159 C
160 C 2.30 -- SET INITIAL TEMPERATURE AND ENTHALPY PROFILES
161 C
162 T(1)=TW
163 IF (.NOT.LCPSOL) CP(1)=CP0+CP1*TW+CP2*TW*TW+CP3*TW**3
164 AH(1)=CP(1)*TW
165 DO 215 J=2,M1
166 YY=Y(J)/DELT
167 T(J)=TW+(TINF-TW)*(2.*YY-2.*YY**3+YY**4+OMEGA/6.*YY
168 1 * (1.-YY)**3)
169 SAH=CP(J)*T(J)
170 IF (.NOT.LCPSOL) THEN
171 CP(J)=CP0+CP1*T(J)+CP2*T(J)**2+CP3*T(J)**3
172 SAH=AH(1)+.5*(CP(J)+CP(1))*(T(J)-T(1))
173 ENDIF
174 215 AH(J)=SAH+.5*U(J)*U(J)
175 C
176 C 2.40 -- SET OTHER MSC. PARAMETERS AND VALUES
177 C
178 AKAPI=1.E10
179 C PRINT*, 'INPUT CHOICE FOR AKAPI'
180 C READ*, AKAPI
181 KIN=1
182 KEX=2
183 ASN=1.E-20
184 REP=REPI
185 RME=-.05*PEI
186 TUINF=SQRT(AK(M1)/1.5)/U(M1)
187 DPKDTM=0.
188 IF (ITM.EQ.0) DPKDTM=1.E20
189 TCI=1.
190 FSCON=0.
191 ITBFLG=0
192 DX=Y(M1)/20.
193 STAN=0.
194 YCVP(1)=0.
195 YCVM(M1)=0.
196 NDPTS=0
197 NP2=1
198 C
199 C
200 C
201 C
202 C
203 RETURN
204 C*****
205 C 3.00 -- ENTRY POINT TO SUBROUTINE 'DENSE'.
206 C*****
207 ENTRY DENSE
208 C
209 C 3.10 -- CALCULATE TEMPERATURE FROM THE ENTHALPY
210 C
211 IF(LCPSOL) THEN
212 T(1)=TW
213 DO 280 J=2,M1

```

```

214      280  T(J)=(AH(J)-.5*U(J)**2)/CP(J)
215      RETURN
216      ENDIF
217      T(1)=TW
218      CP(1)=CP0+CP1*TW+CP2*TW*TW+CP3*TW**3
219      DO 285 J=2,M1
220          T(J)=T(1)+2.*(AH(J)-.5*U(J)**2-AH(1))/(CP(1)+CP(J-1))
221          CP(J)=CP0+CP1*T(J)+CP2*T(J)**2+CP3*T(J)**3
222      285  T(J)=T(1)+2.*(AH(J)-.5*U(J)**2-AH(1))/(CP(1)+CP(J))
223  C
224  C 3.20 -- CALCULATE DENSITY FROM IDEAL GAS LAW, THERMAL CONDUCTI
225  C      VITY FROM A POLYNOMIAL APPROXIMATION, VISCOSITY FROM
226  C      THE SUTHERLAND VISCOSITY LAW, AND PRANDTL NUMBER.
227  C
228      DO 290 J=1,M1
229          TK=T(J)+273.15
230          RHO(J)=PRDR/TK
231          TCOND=B0+B1*T(J)+B2*T(J)*T(J)+B3*T(J)*T(J)*T(J)
232          AMU(J)=SCONB*TK**1.5 / (SCONS+TK)
233          PR(J)=AMU(J)*CP(J)/TCOND
234      290 CONTINUE
235      RETURN
236  C*****
237  C 4.00 -- ENTRY POINT FOR SUBROUTINE 'OUTPUT'. BEGIN BY CHECKING
238  C      IF TIME TO STOP COMPUTATION (IE. IS X > XFINAL).
239  C*****
240      ENTRY OUTPUT
241      IF(XU.GT.XUF) LSTOP=.T.
242  C
243  C 4.10 --CALCULATE THE MOMENTUM THICKNESS AND MOMENTUM THICKNESS
244  C      REYNOLDS NUMBER. STOP IF RE2 IS GREATER THAN RE2-FINAL.
245  C
246      DL2=0.
247      DO 300 J=2,M2
248          UJ=U(J)/U(M1)
249      300  DL2=DL2 + RHO(J)*UJ*(1.-UJ)*YCVR(J)
250          DL2=DL2/RHO(M1)
251          RE2=RHO(M1)*U(M1)*DL2/AMU(M1)
252          IF(RE2.GT.RE2F) LSTOP=.T.
253  C
254  C 4.20 -- CHECK IF TIME FOR OUTPUT OF ANY KIND. IF NOT, RETURN
255  C
256          IF(RE2.GT.RE2P(NP2)) GO TO 310
257          IF(REX.GT.REP) GO TO 310
258          IF(MOD(ISTEP,JUMP1).EQ.0) GO TO 310
259          IF(MOD(ISTEP,JUMP2).EQ.0) GO TO 310
260          IF(.NOT.LSTOP) RETURN
261      310 CONTINUE
262  C
263  C 4.30 -- CALCULATE COEFICIENTS OF FRICTION AND HEAT TRANSFER
264  C      NOTE THAT ALL PROPERTIES USED IN THE NONDIMENSIONAL-
265  C      IZATION ARE EVALUATED AT THE FREE-STREAM CONDITIONS.
266  C
267          CF=-AJTI(1)*2./ (RHO(M1)*U(M1)**2)
268          CPAVG=.5*(CP(1)+CP(M1))

```

```

269      DELTAT=(AH(1)-AH(M1))/CPAVG
270      IF(XU.GT.UHSL) STAN=AJTI(4)/(RHO(M1)*U(M1)
271      1      *CPAVG*DELTAT+ASN)
272      AHTC=AJTI(4)/(DELTAT+ASN)
273      C
274      C
275      C 4.40 -- CALCULATE THE DISPLACEMENT THICKNESS AND THE 99% BOUND
276      C      ARY LAYER THICKNESS. ALSO COMPUTE Y+ AND U+ USING FREE-
277      C      STREAM FLUID PROPERTIES TO NONDIMENSIONALIZE.
278      C
279      D99=0.
280      DL1=0.
281      UFRIC=SQRT(-AJTI(1)/RHO(M1))
282      YPLSCAL=SQRT(-RHO(M1)*AJTI(1))/AMU(M1)
283      DO 320 J=2,M2
284          UJ=U(J)/U(M1)
285          UJD=UJ*RHO(J)/RHO(M1)
286          IF(U(J+1)/U(M1).GT..99.AND.UJ.LT..99) D99=
287      1      (.99-UJ)/(U(J+1)/U(M1)-UJ)*(Y(J+1)-Y(J))+Y(J)
288          YPLS(J)=Y(J)*YPLSCAL
289          UPLS(J)=U(J)/(UFRIC+ASN)
290      320      DL1=DL1+(1.-UJD)*YCVR(J)
291      C
292      C 4.50 -- IF AT DESIRED MOMENTUM THICKNESS REYNOLDS NUMBER,
293      C      WRITE OUT COMPLETE PROFILE INFORMATION TO A FILE.
294      C
295          IF(RE2.GT.RE2P(NP2)) THEN
296              WRITE(4,305) M1,XU,REX,RE2,D99,DL1,DL2
297              WRITE(4,306) (Y(J),(F(J,I),I=1,11),J=1,M1)
298              NP2=NP2+1
299          ENDIF
300      C
301      C 4.60 IF AT DESIRED REX, WRITE OUT COMPUTED BOUNDARY LAYER
302      C      PROPERTIES AND PARAMETERS.
303      C
304      C
305          TUINF=SQRT(AK(M1)/1.5)/U(M1)
306          DLS=AK(M1)*U(M1)*U(M1)*RHO(M1)/(AMU(M1)*E(M1))
307          IF(REX.GT.REP) THEN
308              REP=10.** (ALOG(REP)/ALOG(10.))+1./REPFC)
309              NDPTS=NDPTS+1
310              WRITE(3,303) NDPTS,XU,REX,D99,DL1,DL2,RE2,CF,STAN,AHTC,
311      1      U(M1),DUDS,PRESS,DLS,TUINF
312          ENDIF
313      C
314      C 4.70 -- AT INTERVALS OF 'JUMP1', WRITEOUT DESIRED QUANTITIES
315      C      BY CALLING SUBROUTINE 'PROFIL'
316      C
317          IF(LSTOP.OR.MOD(ISTEP,JUMP1).EQ.0) THEN
318              E(1)=E(2)
319              IF(ISTEP.GT.IPP) CALL PROFIL
320              WRITE(6,301)
321          ENDIF
322      C
323      C 4.80 -- AT INTERVALS OF 'JUMP2', WRITEOUT SPECIFIED PARAMETERS

```

```

324 C          TO MONITOR THE COMPUTATIONS.
325 C
326 C          IF (LSTOP.OR.MOD(ISTEP,JUMP2).EQ.0) THEN
327 C              WRITE(6,302) XU,RE2,CF,STAN,AHTC,TUINF,DLS,U(M1)
328 C          ENDIF
329 C
330 C 4.90 -- IF AT END OF COMPUTATION, CLOSE FILES AND DUMP OUTPUT
331 C          FOR FUTURE RESTART. IF NOT DONE, RETURN.
332 C
333 C          IF (.NOT.LSTOP) RETURN
334 C          CLOSE (UNIT=3)
335 C          CLOSE (UNIT=4)
336 C          RETURN
337 C
338 C 4.99 -- FORMATS USED IN SUBROUTINE OUTPUT
339 C          301 FORMAT(4X,'XU',7X,'RE2',7X,' CF',7X,'STN',7X,
340 C              1      'HTC',6X,'TUINF',5X,'DLS',7X,'UM1')
341 C          302 FORMAT(1P3E10.3,1P1E9.2,1P4E10.3)
342 C          303 FORMAT(' ',I3,1P12E10.3,1P2E9.2)
343 C          304 FORMAT (' REX=',1P1E10.3,/, ' RE1=',1P1E10.3,/,
344 C              1      ' RE2=',1P1E10.3)
345 C          305 FORMAT(I4,1P6E10.3)
346 C          306 FORMAT(1P12E10.3)
347 C*****
348 C 5.00 -- ENTRY POINT FOR SUBROUTINE 'BOUND'
349 C*****
350 C          ENTRY BOUND
351 C
352 C 5.10 -- CALCULATE ENTRAINMENT. THIS CAN BE BASED ON EITHER
353 C          THE VELOCITY OR THE ENTHALPY PROFILES.
354 C
355 C          IF (KENT.EQ.4) THEN
356 C              CALL ENTRAIN(RME,AH(1),AH(M2-1),AH(M1),FRAC,ENEXP)
357 C          ELSEIF (KENT.EQ.1) THEN
358 C              CALL ENTRAIN(RME,0.,U(M2-1),U(M1),FRAC,ENEXP)
359 C          ELSE
360 C              RMEH=RME
361 C              RMEM=RME
362 C              CALL ENTRAIN(RMEH,AH(1),AH(M2-1),AH(1),FRAC,ENEXP)
363 C              CALL ENTRAIN(RMEM,0.,U(M2-1),U(M1),FRAC,ENEXP)
364 C              RME=-AMAX1(-RMEH,-RMEM)
365 C          ENDIF
366 C          RME=AMIN1(RME,-.05*PEI)
367 C
368 C 5.20 -- AT SPECIFIED MOMENTUM THICKNESS, IMPLEMENT TRANSITION
369 C          MODEL AND COMPUTE DPKDTM AND TCI.
370 C
371 C          IF (RE2.GT.RE2C) THEN
372 C              FSCON=1.
373 C              PRINT*, 'CRITICAL MOMENTUM THICKNESS RE2 REACHED AT'
374 C              PRINT*, 'REX=',REX
375 C              PRINT*, 'RE2=',RE2
376 C              PRINT*, ' TU=',TUINF
377 C              DLS=AK(M1)*U(M1)*U(M1)*RHO(M1)/(AMU(M1)*E(M1))
378 C              PRINT*, 'DLS=',DLS

```

```

379             IF (ITM.EQ.0) GO TO 390
380             TUINF=SQRT(AK(M1)/1.5)/U(M1)
381             CALL TRANS(TUINF,DPKDTM0,TCI0)
382             PRINT*, 'SUB TRANS GIVES '
383             PRINT*, 'DPKDTM=', DPKDTM0
384             PRINT*, 'TCI=', TCI0
385             ITBFLG=1
386   390     RE2C=1.E20
387             ENDIF
388             IF (ITBFLG.EQ.1) THEN
389               IF (MOD(ISTEP, JUMPT).EQ.0) THEN
390                 TUINF=SQRT(AK(M1)/1.5)/U(M1)
391                 CALL TRANS(TUINF,DPKDTM0,TCI0)
392                 ENDIF
393                 DPKDTM=DPKDTM0*(RHO(M1)*U(M1)/AMU(M1))**2 *RHO(M1)*U(M1)**4
394                 TCI=TCI0*RHO(M1)*U(M1)*U(M1)/AMU(M1)
395             ENDIF
396   C
397   C 5.30 -- COMPUTE THE NEXT STEP SIZE, FREE STREAM VELOCITY,
398   C           REYNOLDS NUMBER BASED ON X, AND THE MEAN VELOCITY
399   C           AND PRESSURE GRADIENTS OVER THE NEXT STEP.
400   C
401             DX=DL2*DXFC
402             UM10=U(M1)
403             XUNEW=XU+DX
404             U(M1)=UM1(XUNEW)
405             UINF=.5*(U(M1)+UM10)
406             DUDS=(U(M1)-UM10)/DX
407             DUDSP=RHO(M1)*DUDS
408             DPDSC=RHO(M1)*UM10*DUDS
409             PRESS=PRESS-DPDSC*DX
410             PRDR=PRESS/RCON
411             REX=REX+RHO(M1)*UINF*DX/AMU(M1)
412   C
413   C 5.40 -- CALC THE TURBULENT REYNOLDS NUMBERS AND OTHER RELATED
414   C           PARAMETERS, SUCH AS THE SOURCE TERMS IN THE K AND E EQS.
415   C
416   C           CALL RCURV(XU,RC,KCRC,RFILE)
417   C           RCI=1./RC
418   C
419   C
420   C
421   C
422   C
423   C
424   C
425             TRE(2)=AK(2)*AK(2)*RHO(2)/(AMU(2)*E(2))
426             DO 400 J=2,M2
427               TRE(J+1)=AK(J+1)*AK(J+1)*RHO(J+1)/(AMU(J+1)*E(J+1))
428               YRE(J)=SQRT(AK(J))*Y(J)*RHO(J)/AMU(J)
429               DYP=Y(J+1)-Y(J)
430               DYM=Y(J)-Y(J-1)
431               R2=(DYP/DYM)**2
432               DEN1=DYP+R2*DYM
433               DU1(J)=(U(J+1)-(1-R2)*U(J)-R2*U(J-1))/DEN1

```

```

434      IF (J.EQ.M2) DU1 (J)=DU1 (J-1) /2.
435      AMUT (J)=AMU (J)*CU*FMU (TRE (J), YRE (J)) *TRE (J)
436      SK1=AMUT (J)*DU1 (J)*DU1 (J)
437      SKC=FSCON*SK1
438      DPK=(DPKDTM+TCI*SCK (J)) *DX/U (J)
439      SCK (J)=SCK (J)+AMIN1 (DPK, SKC-SCK (J))
440      SPK (J)=RHO (J)*E (J)
441      C
442      C-- C1 MODIFICATION WAS INSERTED HERE AS PER EQ. (5.5) IN THESIS.
443      C-- SUPPRESSED BECAUSE AKAPI=1.E10 INSTEAD OF 2.7 (SEE LINE 178)
444      C
445      SCMEF=AMAX1 (1., AK (J)**1.5/ (E (J)*AKAPI*Y (J)))
446      C
447      SCE (J)=SK1*SCMEF*C1*F1 (FMU (TRE (J), YRE (J)))
448      1      *E (J) / (AK (J)+ASN)
449      SPE (J)=C2*F2 (TRE (J))*RHO (J)*E (J)*E (J) / (AK (J)+ASN)
450      400 CONTINUE
451      YRE (M1)=SQRT (AK (M1))*Y (M1)*RHO (J)/AMU (J)
452      AMUT (M1)=AMU (J)*CU*FMU (TRE (M1), YRE (M1))*TRE (M1)
453      C
454      C 5.50 -- CALCULATE THE BOUNDARY VALUES FOR K AND E
455      C
456      C
457      YKE (1)=AK (M1)
458      YKE (2)=E (M1)
459      M=0
460      XUB=XU
461      6 CALL RUNGA (2, YKE, FKE, XUB, DX, M, K)
462      GO TO (10, 20), K
463      10 FKE (1)=-YKE (2)/UINF
464      FKE (2)=-C2*YKE (2)*YKE (2)/YKE (1)/UINF
465      GO TO 6
466      20 AK (M1)=YKE (1)
467      E (M1)=YKE (2)
468      C
469      C 5.60 CALCULATE THE BOUNDARY VALUES FOR THE TOTAL ENTHALPY
470      C
471      IF (XU.LT.UHSL) RETURN
472      KBCI (4)=IWTBC
473      IF (KBCI (4).EQ.1) THEN
474          TW=WTOHF
475          AH (1)=CP (1)*TW
476      ELSE
477          AFXI (4)=WTOHF
478      ENDIF
479      RETURN
480      C*****
481      C 6.00 ENTRY POINT FOR SUBROUTINE 'GAMSOR'.
482      C*****
483      ENTRY GAMSOR
484      C
485      C
486      C 6.10 -- CALCULATE THE MOM. EQUATION GAMMA AND SOURCE TERMS
487      C
488      IF (NF.EQ.1) THEN

```

```

489         IF (DPDSC.LT.0.) THEN
490             SPU=DUDSP
491             SCU=0.
492         ELSE
493             SPU=0.
494             SCU=DPDSC
495         ENDIF
496         DO 520 J=2,M2
497             GAM(J)=AMU(J)+AMUT(J)
498             AP(J)=SPU
499     520     CON(J)=SCU
500             GAM(1)=AMU(1)
501             GAM(M1)=AMU(M1)+AMUT(M1)
502         ENDIF
503     C
504     C 6.20 -- CALCULATE KINETIC ENERGY EQ. GAMMA AND SOURCE TERMS
505     C
506         IF (NF.EQ.2) THEN
507             DO 500 J=2,M2
508                 CON(J)=SCK(J)*FSCON
509                 AP(J)=-SPK(J)/(AK(J)+ASN)
510     500     GAM(J)=AMU(J)+AMUT(J)/SK
511             GAM(1)=AMU(1)
512             GAM(M1)=AMU(M1)+AMUT(M1)/SK
513         ENDIF
514     C
515     C 6.30 -- CALCULATE THE E EQUATION GAMMA AND SOURCE TERMS
516     C
517         IF (NF.EQ.3) THEN
518             DO 510 J=2,M2
519                 CON(J)=SCE(J)
520                 AP(J)=-SPE(J)/(E(J)+ASN)
521     510     GAM(J)=AMU(J)+AMUT(J)/SE
522             GAM(1)=0.
523             GAM(M1)=AMU(M1)+AMUT(M1)/SE
524         ENDIF
525     C
526     C 6.40 --CALCULATE TOTAL ENTHALPY EQUATION GAMMA AND SOURCE TERMS
527     C
528         IF (NF.EQ.4) THEN
529             DO 515 J=2,M1
530                 GAM(J)=AMU(J)/PR(J)+AMUT(J)/PRT
531     515     SI(J)=(AMU(J)+AMUT(J)-GAM(J))*U(J)*DU1(J)
532             SI(1)=0.
533             GAM(1)=AMU(1)/PR(1)
534             DO 516 J=2,M2
535                 DYP=Y(J+1)-Y(J)
536                 DYM=Y(J)-Y(J-1)
537                 R2=(DYP/DYM)**2
538                 DEN1=DYP+R2*DYM
539                 SC=(SI(J+1)-(1-R2)*SI(J)-R2*SI(J-1))/DEN1
540     516     CON(J)=CON(J)+SC
541             ENDIF
542             RETURN
543         END

```

```

1          SUBROUTINE VELPROF (DELTA, OMEGA, UINF, M1, U, Y)
2          DIMENSION U(99), Y(99)
3
4          C
5          C THIS SUBROUTINE GENERATES A VELOCITY PROFILE USING A
6          C POHLHOUSEN POLYNOMIAL TO FIT THE GIVEN GRID VALUES OF Y(J)
7          C
8          YOLD=0.
9          DO 10 J=2, M1
10         IF (J.LT.M1) YNEW=.5*(Y(J)+Y(J+1))
11         IF (J.EQ.M1) YNEW=Y(M1)
12         YY=.5*(YNEW+YOLD)/DELTA
13         U(J)=UINF*YY*(2.-2.*YY**2+YY**3 + OMEGA/6.*(1.-YY)**3)
14         IF (YY.GT.1) U(J)=UINF
15         YOLD=YNEW
16     10 CONTINUE
17     RETURN
18     END

```

```

19          SUBROUTINE RUNGA (N, Y, F, X, H, M, K)
20          C
21          C THIS ROUTINE PERFORMS A RUNGE-KUTTA INTEGRATION PROCEDURE
22          C BY GILLS METHOD
23          C
24          DIMENSION Y(2), F(2), Q(2)
25          M=M+1
26          GO TO (1, 4, 5, 3, 7), M
27          1 DO 2 I=1, N
28          2 Q(I)=0.
29          A=.5
30          GO TO 9
31          3 A=1.70710678118655
32          4 X=X+.5*H
33          5 DO 6 I=1, N
34          Y(I)=Y(I)+A*(F(I)*H-Q(I))
35          6 Q(I)=2.*A*H*F(I)+(1.-3.*A)*Q(I)
36          A=.292832188134525
37          GO TO 9
38          7 DO 8 I=1, N
39          8 Y(I)=Y(I)+H*F(I)/6.-Q(I)/3.
40          M=0
41          K=2
42          GO TO 10
43          9 K=1
44          10 RETURN
45          END

```

```

47          SUBROUTINE TRANS (TU,DPK,TCI)
48          C
49          DATA A1,A2,A3/-5.4549,389.2806,-7556.0334/
50          DATA A4,A5,B1,B2/7.278E4,-2.85036E5,1.8625,14.6786/
51          DATA C1,C2,C3,D1/6.8475,-367.,9200.,-6.4711/
52          DATA D2,D3,D4,D5/1177.586,-45930.,615200.,-2767000./
53          C
54          IF (TU.LT..07) THEN
55             Y=A1+A2*TU+A3*TU*TU+A4*TU**3+A5*TU**4
56          ELSE
57             Y=B1+B2*TU
58          ENDIF
59          DPK=EXP (Y) *1.E-12
60          C
61          IF (TU.LT..02) THEN
62             Y=C1+C2*TU+C3*TU*TU
63          ELSEIF (TU.GT..081) THEN
64             Y=-4.6011
65          ELSE
66             Y=D1+D2*TU+D3*TU*TU+D4*TU**3+D5*TU**4
67          ENDIF
68          TCI=Y*1.E-6
69          RETURN
70          END

98          SUBROUTINE RCURV (XU,RC,KCRC,RFILE)
99          C
100         C THIS SUBROUTINE RETURNS THE LOCAL RADIUS OF CURVATURE UNLESS
101         C KCRC IS EQUAL TO 1 (INDICATING A SPECIFIED CONSTANT RADIUS OF
102         C CURVATURE) IT MUST READ IN DATA STORED IN A FILE WHICH LISTS
103         C RADIUS OF CURVATURE VRS. ARC LENGTH COORDINATE X. IT THEN
104         C INTERPOLATES TO RETURN THE DESIRED VALUE.
105         C
106         DIMENSION X(50),R(50)
107         CHARACTER RFILE*40
108         LOGICAL LWARN
109         DATA KREAD,KRCB/1,2/
110         C
111         IF (KCRC.EQ.1) RETURN
112         IF (KREAD.EQ.1) THEN
113             OPEN (UNIT=2,FILE=RFILE)
114             READ (2,*) ND
115             DO 10 I=1,ND
116         10  READ (2,*) X(I),R(I)
117             CLOSE (UNIT=2)
118             KREAD=0
119             LWARN=.TRUE.
120         ENDIF
121         C
122         DO 20 I=KRCB,ND

```

```

123         IF (XU.LT.X(I)) THEN
124             ETA=(XU-X(I-1))/(X(I)-X(I-1))
125             RC=R(I-1)+ETA*(R(I)-R(I-1))
126             KRCB=I
127             RETURN
128         ENDIF
129     20 CONTINUE
130     IF (LWARN) THEN
131         PRINT*, 'WARNING! RADIUS OF CURVATURE NOT FOUND FOR'
132         PRINT*, 'GIVEN XU.  SETTING RC=1.E20'
133         PRINT*, 'XU=', XU
134         LWARN=.FALSE.
135     ENDIF
136     RC=1.E20
137     RETURN
138     END

```

```

140     SUBROUTINE ENTRAIN(RME, F1, FM3, FM1, FRAC, POWER)
141     C
142     IF (FM1.EQ.F1) RETURN
143     ADIF=ABS((FM1-FM3)/(FM1-F1))
144     FE=((ADIF+1.E-30)/FRAC)**POWER
145     FE=AMIN1(FE, 1.5)
146     FE=AMAX1(FE, .25)
147     RME=FE*RME
148     RETURN
149     END

```

```

1     FUNCTION FMU(X, Y)
2         A=(1.-EXP(-.0163*y-1.E-10))**2
3         FMULB=A*(1.+20./(X+1.E-10))
4         FM=.5+.0025*X
5         FMU=AMIN1(1.0, FM, FMULB)
6     RETURN
7     END

```

```

9     FUNCTION F2(X)
10        F2=1.-EXP(-X*X-1.E-10)
11    RETURN
12    END

```

```

14    FUNCTION F1(X)
15        F1=1.+(.055/(X+1.E-10))**3
16    RETURN
17    END

```

The UM1 functions used

Because the function UM1 (which returns the local free-stream velocity) is problem dependent, a number of different representations had to be written. These are listed here.

```

1      FUNCTION UM1 (X)
2      C
3      C - FREE-STREAM VELOCITY DISTRIBUTION FOR WANG'S ZERO PRESSURE
4      C   GRADIENT WIND TUNNEL TESTS ( K=0.0, UNITS IN M/S)
5      C
6      UM1=13.50
7      RETURN
8      END

1      FUNCTION UM1 (X)
2      C
3      C -FREE-STREAM VELOCITY DISTRIBUTION FOR RUED,WITTIG'S DATA RN-2
4      C   (UINF=CONSTANT=47 M/S)
5      C
6      UM1=47.
7      RETURN
8      END

1      FUNCTION UM1 (X)
2      C
3      C - FREE-STREAM VELOCITY DISTRIBUTION FOR BLAIR'S ZERO PRESSURE
4      C   GRADIENT WIND TUNNEL TESTS (NO WEDGE, K=0.0, UNITS IN M/S)
5      C
6      IF (X.GT.-100.) UM1=30.48
7      UM1=30.48
8      RETURN
9      END

1      FUNCTION UM1 (X)
2      C
3      C - FREE-STREAM VELOCITY DISTRIBUTION FOR BLAIR'S LOWER
4      C   ACCELERATION TESTS (WEDGE 1, K=.20E-6)
5      C
6      DATA A1,A2,A3/89.914435,5.08,1.066/
7      C
8      UM1=A1/ (A2-X)**A3
9      RETURN
10     END

```

```

1      FUNCTION UM1 (X)
2      C
3      C - FREE-STREAM VELOCITY DISTRIBUTION FOR BLAIR'S HIGHER
4      C ACCELERATION TESTS (WEDGE 2, K=.75E-6)
5      C
6      DATA A1,A2,A3/22.2178,2.11582,1.075/
7      C
8      UM1=A1/(A2-X)**A3
9      RETURN
10     END

```

```

1      FUNCTION UM1 (X)
2      C
3      C -FREE-STREAM VELOCITY DISTRIBUTION FOR RUED'S DATA NR-6
4      C
5      DATA X1,X2/.20,.35/
6      DATA A1,A2,A3,A4,A5/48.4,.50,-50.,25.,343.4/
7      DATA B1,B2/5200.,3.5/
8      DATA C1,C2,C3,C4/106.0136,423.9787,1665.05,-23333./
9      C
10     IF (X.LE.X2) THEN
11         UM1=A1+A2*EXP(A3*X)+A4*X+A5*X*X
12         IF (X.GT.X1) UM1=UM1+B1*(X-X1)**B2
13         RETURN
14     ELSE
15         Y=X-X2
16         UM1=C1+C2*Y+C3*Y*Y+C4*Y*Y*Y
17     ENDIF
18     RETURN
19     END

```

```

1      FUNCTION UM1 (X)
2      C
3      C -FREE-STREAM VELOCITY DISTRIBUTION FOR RUED'S DATA NR-10
4      C
5      DATA X1,X2/.179,.30/
6      DATA A1,A2,A3,A4,A5/47.5,10.81,1483.37,-5563.333,31826.75/
7      DATA A6,A7/387450.,-1742667/
8      DATA B1,B2,B3,B4/111.606856,804.61431,-60173.417,
9      DATA C1,C2/155.66475,-76.384701/
10     C
11     IF (X.LE.X1) THEN
12         UM1=A1+A2*X+A3*X*X+A4*X*X*X+A5*X**4+A6*X**5+A7*X**6
13         RETURN
14     ELSEIF (X.GT.X2) THEN

```

```

15         Y=X-X2
16         UM1=C1+C2*Y
17         RETURN
18     ELSE
19         Y=X-X1
20         UM1=B1+B2*Y+B3*Y*Y+B4*Y*Y*Y
21     ENDIF
22     RETURN
23     END

```

```

1         FUNCTION UM1 (X)
2     C
3     C -FREE-STREAM VELOCITY DISTRIBUTION FOR RUED'S DATA NR-12
4     C
5         DATA X1/.20/
6         DATA A1,A2,A3,A4/26.5, 2319., -28680, 347100./
7         DATA A5,A6/-647300., -2100000./
8         DATA B1,B2,B3,B4/71.4128, 385.72, -1654.85, -149700./
9         DATA B5,B6,B7/2.095E6, -1.026E7, 1.731E7/
10    C
11    C
12    IF (X.LE.X1) THEN
13        UM1=A1 + A2/2.*X*X + A3/3.*X*X*X + A4/4.*X**4
14        1 + A5/5*X**5 + A6/6.*X**6
15    C
16    ELSE
17        Y=X-X1
18        UM1=B1 + B2*Y + B3/2.*Y*Y + B4/3.*Y*Y*Y
19        1 + B5/4.*Y**4 + B6/5.*Y**5 + B7/6.*Y**6
20    ENDIF
21    RETURN
22    END

```

```

1         FUNCTION UM1 (XU)
2     C
3     C -FREE-STREAM VELOCITY DISTRIBUTION FOR THE DANIALS AND BROWN
4     C -BLADE (RED CONDITIONS) FOR THE PRESSURE SIDE OF THE BLADE
5     C DIMENSIONS ARE IN METERS, AND METERS/SEC RESPECTIVELY.
6     C
7         DATA S,U1/.05044,146./
8         DATA A1,A2,A3,A4/.9561,6.2799,-12.0039,7.7947/
9     C
10        X=XU/S
11        U=A1*X + A2*X**2 + A3*X**3 + A4*X**4
12        UM1=U*U1
13        RETURN
14        END

```

```

1      FUNCTION UMI (XU)
2      C
3      C -FREE-STREAM VELOCITY DISTRIBUTION FOR THE DANIALS AND BROWN
4      C -DATA DESIGNATED AS RED CONDITIONS FOR THE SUCTION SIDE OF THE
5      C BLADE. DIMENSIONS ARE IN METERS, AND METERS/SEC RESPECTIVELY.
6      C
7      DIMENSION X(55),V(55)
8      DATA JREAD,JX/0,2/
9      C
10     IF (JREAD.EQ.0) THEN
11     C      OPEN (UNIT=1,FILE='DBRDSVD')
12     C      OPEN (UNIT=1,FILE='RWVEL/DBRDSVD')
13     C      READ (1,*) ND
14     C      DO 5 J=1,ND
15     5    READ (1,*) X(J),V(J)
16     C      CLOSE (UNIT=1)
17     C      JREAD=1
18     C      ENDIF
19     C
20     DO 10 J=JX,ND
21     C      IF (XU.LT.X(J)) THEN
22     C          F=(XU-X(J-1))/(X(J)-X(J-1))
23     C          UMI=V(J-1)+F*(V(J)-V(J-1))
24     C          JX=J
25     C          RETURN
26     C      ENDIF
27     10  CONTINUE
28     C      UMI=V(ND)
29     C      RETURN
30     C      END

```

Data file "DBRDsvd". (See line 12 above)

```

1      54
2      0.00000E+00  0.00000E+00
3      4.42430E-04  6.57394E+01
4      9.05600E-04  1.23798E+02
5      1.48717E-03  1.77565E+02
6      2.09038E-03  2.17336E+02
7      2.75392E-03  2.47149E+02
8      3.73226E-03  2.72699E+02
9      4.39781E-03  2.88058E+02
10     5.57312E-03  3.09082E+02
11     6.63185E-03  3.21288E+02
12     8.14303E-03  3.31245E+02
13     9.43884E-03  3.33303E+02
14     1.04406E-02  3.33084E+02

```

15	1.15795E-02	3.32194E+02
16	1.26599E-02	3.30398E+02
17	1.36814E-02	3.28150E+02
18	1.48601E-02	3.26368E+02
19	1.60974E-02	3.26383E+02
20	1.71768E-02	3.29621E+02
21	1.83153E-02	3.33911E+02
22	1.94340E-02	3.39551E+02
23	2.08075E-02	3.47517E+02
24	2.19853E-02	3.54113E+02
25	2.32216E-02	3.60789E+02
26	2.47913E-02	3.68480E+02
27	2.64205E-02	3.75975E+02
28	2.79513E-02	3.82251E+02
29	2.96396E-02	3.88666E+02
30	3.13475E-02	3.93619E+02
31	3.29575E-02	3.97161E+02
32	3.41358E-02	3.98081E+02
33	3.51567E-02	3.97862E+02
34	3.63355E-02	3.95614E+02
35	3.74749E-02	3.91570E+02
36	3.88312E-02	3.86144E+02
37	4.04423E-02	3.79861E+02
38	4.20927E-02	3.76890E+02
39	4.34087E-02	3.75782E+02
40	4.46258E-02	3.76587E+02
41	4.61576E-02	3.79574E+02
42	4.71387E-02	3.82714E+02
43	4.85914E-02	3.88524E+02
44	4.98670E-02	3.93818E+02
45	5.12622E-02	3.99838E+02
46	5.26140E-02	4.05921E+02
47	5.40666E-02	4.12312E+02
48	5.56202E-02	4.18527E+02
49	5.72091E-02	4.24088E+02
50	5.84650E-02	4.26411E+02
51	5.95041E-02	4.26931E+02
52	6.07449E-02	4.22092E+02
53	6.19252E-02	4.13288E+02
54	6.34182E-02	3.97505E+02
55	6.41446E-02	3.90964E+02

## A Listing of program MAIN

A listing of the main driver program "MAIN", together with it's associated subroutines is given here.

```

1      PROGRAM MAIN (OUTPUT,TAPE6=OUTPUT)
2      C
3      LOGICAL LSTOP
4      COMMON/CNTL/LSTOP
5      CALL USER
6      CALL SETUP
7      CALL START
8      10 CALL DENSE
9      CALL SETUP2
10     CALL OUTPUT
11     IF (LSTOP) STOP
12     CALL BOUND
13     CALL SETUP3
14     GO TO 10
15     END
16     C*****
17     SUBROUTINE DIFLOW
18     C
19     COMMON/COEF/FLOW,DIFF,ACOF
20     ACOF=DIFF+1.E-30
21     IF (FLOW.EQ.0.) RETURN
22     TEMP=DIFF-ABS (FLOW)*0.1
23     ACOF=1.E-30
24     IF (TEMP.LE.0.) RETURN
25     TEMP=TEMP/DIFF
26     ACOF=DIFF*TEMP**5
27     RETURN
28     END
29     C*****
30     SUBROUTINE SETUP
31     C
32     LOGICAL LSTOP,LPR,LGPG,LTIME,LSOLVE,LPRINT
33     character title(13)*7
34     COMMON F(99,11),RHO(99),GAM(99),CON(99),
35     1      AP(99),AN(99),AS(99),PT(99),QT(99),RT(99),
36     2      OM(99),OMF(99),OMF1(99),OMCV(99),Y(99),
37     3      YF(99),YCVR(99),YCVF(99),YCVF1(99),R(99),
38     4      RF(99),FLO(99)
39     COMMON /INDX/ NF,NFMAX,NU,NRHO,NGAM,M1,M2,KIN,KEX,DPDX,
40     1      ISTEP,LASTEP,MODE,ITMX,LGPG,LTIME,XU,DX,XLAST,
41     2      PEI,PSII,PSIE,PSIT,YM1,POWER,CSALFA,RMI,RME,ARI,ARE
42     COMMON /VARB/ LSOLVE(11),LPRINT(13),
43     1      AJTI(11),AJTE(11),AFXI(11),BFXI(11),
44     2      AFXE(11),BFXE(11),KBCI(11),KBCE(11)
45     common /char/ title
46     COMMON /CNTL/ LSTOP
47     COMMON /COEF/ FLOW,DIFF,ACOF

```

```

48     DIMENSION U(99)
49     EQUIVALENCE (F(1,1),U(1))
50     C*****
51     DATA NEMAX,NU,NRHO,NGAM,nsolv/11,1,11,11,4/
52     DATA LSTOP,LGPG,LTIME,LSOLVE,LPRINT/.F.,.T.,25*.F./
53     DATA ISTEP,LASTEP,XU,XLAST/0,1000,0.,1.E10/
54     DATA CSALFA,PSII,MODE,ITMX,POWER,RMI,RME/1.,0.,1,10,1.,0.,0./
55     DATA AFXI,BFXI,AFXE,BFXE,KBCI,KBCE/44*0.,22*1/
56     DATA AJTI,AJTE/22*0./
57     C.....
58     C
59         M2=M1-1
60         OMF(2)=0.
61         OMF(M1)=1.
62         OM(1)=0.
63         DO 1 J=2,M2
64             AP(J)=0.
65             CON(J)=0.
66             OM(J)=0.5*(OMF(J)+OMF(J+1))
67             OMCV(J)=OMF(J+1)-OMF(J)
68             1 OMF1(J)=1.-OMF(J)
69             OM(M1)=1.
70             OMF1(M1)=0.
71             Y(1)=0.
72             YF(2)=0.
73             DO 3 J=1,M1
74                 R(J)=1.
75             3 RF(J)=1.
76             GAM(1)=0.
77             GAM(M1)=0.
78     C
79         WRITE(6,9)
80         IF(MODE.EQ.1) WRITE(6,2)
81         IF(MODE.NE.1) WRITE(6,4)
82         IF(.NOT.LGPG) WRITE(6,4)
83         IF(MODE.NE.1) STOP
84         IF(.NOT.LGPG) STOP
85         WRITE(6,9)
86         2 FORMAT(5X,*PLANE GEOMETRY*)
87         4 FORMAT(2X,*MAIN PROGRAM NOT SET UP FOR MODE>1 OR LGPG=F*)
88         9 FORMAT(1X)
89         RETURN
90     C.....
91     ENTRY SETUP2
92     C
93     PSIE=PSII+PEI
94     C
95     CALCULATION OF Y AND R VALUES
96     DO 21 J=2,M2
97         IF(U(J).LT.0.) GO TO 51
98         YCVR(J)=PEI*OMCV(J)/(RHO(J)*U(J))
99         YF(J+1)=YF(J)+YCVR(J)
100     21 Y(J)=YF(J)+0.5*YCVR(J)
101         Y(M1)=YF(M1)
102         DO 40 J=2,M2

```

```

103         YCVP(J)=YF(J+1)-Y(J)
104     40 YCVM(J)=Y(J)-YF(J)
105         GO TO 55
106     51 WRITE(6,52)
107     52 FORMAT(5(1H*),*AT LEAST ONE VELOCITY HAS BECOME NEGATIVE*,
108         1          5(1H*))
109         LSTOP=.T.
110     55 CONTINUE
111         RETURN
112 C.....
113     ENTRY SETUP3
114 C
115     IF(KIN.EQ.3) RMI=0.
116     IF(KEK.EQ.3) RME=0.
117     ARI=RF(2)*DX
118     ARE=RF(M1)*DX
119     DO 60 J=2,M1
120     60 FLO(J)=(RMI*OMF1(J)+RME*OMF(J))*DX
121 C
122     DO 100 NF1=1,nsolv
123     NF=NF1
124 C     IF(.NOT.LSOLVE(NF)) GO TO 100
125     LPR=.FALSE.
126 C
127     CALL GAMSOR
128 C
129 COEFFICIENT CALCULATION.....
130     DIFF=ARI*GAM(1)/YCVM(2)
131     IF(KIN.NE.1) DIFF=0.
132     FLOW=FLO(2)
133     CALL DIFLOW
134     AS(2)=ACOF+AMAX1(0.,FLOW)
135     AN(1)=AS(2)-FLOW
136     DO 101 J=2,M2
137     IF(J.EQ.M2) GO TO 102
138     DIFF=RF(J+1)*DX/(YCVP(J)/(GAM(J)+1.E-30)+
139     1          YCVM(J+1)/(GAM(J+1)+1.E-30))
140     GO TO 103
141     102 DIFF=ARE*GAM(M1)/YCVP(M2)
142     IF(KEK.NE.1) DIFF=0.
143     103 FLOW=FLO(J+1)
144     CALL DIFLOW
145     AS(J+1)=ACOF+AMAX1(0.,FLOW)
146     AN(J)=AS(J+1)-FLOW
147     FLUP=PEI*OMCV(J)
148     VOL=YCVR(J)*DX
149     AP(J)=AS(J)+AN(J)+FLUP-AP(J)*VOL
150     101 CON(J)=FLUP*F(J,NF)+CON(J)*VOL
151 C
152 COEFFICIENTS MODIFIED FOR THE I BOUNDARY
153     AP(1)=AS(2)
154     IF(KIN.NE.1.OR.KBCI(NF).EQ.1) GO TO 105
155     FACI=1.
156     IF(KBCI(NF).EQ.3) FACI=1.+BFXI(NF)*ARI/AP(1)
157     CON(1)=AFXI(NF)*ARI

```

```

158         AP(2)=AP(2)-AN(1)/FACI
159         CON(2)=CON(2)+CON(1)/FACI
160         AS(2)=0.
161     C
162     COEFFICIENTS MODIFIED FOR THE E BOUNDARY
163     105 AP(M1)=AN(M2)
164         IF(KEX.NE.1.OR.KBCE(NF).EQ.1) GO TO 110
165         FACE=1.
166         IF(KBCE(NF).EQ.3) FACE=1.+BFXE(NF)*ARE/AP(M1)
167         CON(M1)=AFXE(NF)*ARE
168         AP(M2)=AP(M2)-AS(M1)/FACE
169         CON(M2)=CON(M2)+CON(M1)/FACE
170         AN(M2)=0.
171     110 CONTINUE
172     C
173     C
174     CALCULATION OF THE NEW VALUES OF F(J,NF) BY TDMA
175         PT(1)=0.
176         QT(1)=F(1,NF)
177         DO 120 J=2,M2
178             DENOM=AP(J)-PT(J-1)*AS(J)
179             PT(J)=AN(J)/DENOM
180             QT(J)=(CON(J)+AS(J)*QT(J-1))/DENOM
181     120 IF(LPR) RT(J)=(RT(J)+AS(J)*RT(J-1))/DENOM
182         DO 121 JJ=2,M2
183             J=M1-JJ+1
184     121 F(J,NF)=F(J+1,NF)*PT(J)+QT(J)
185     C
186     CALCULATION THE UNKNOWN BOUNDARY VALUES OR FLUXES
187     C..... FOR THE I BOUNDARY
188         IF(KIN.EQ.2) GO TO 140
189         IF(KIN.EQ.1) GO TO 131
190         F(1,NF)=F(2,NF)
191         GO TO 140
192     131 IF(KBCI(NF).EQ.1) GO TO 132
193         F(1,NF)=(AN(1)*F(2,NF)+CON(1))/(AP(1)*FACI)
194         AJTI(NF)=AFXI(NF)
195         IF(KBCI(NF).EQ.3) AJTI(NF)=AJTI(NF)-BFXI(NF)*F(1,NF)
196         GO TO 140
197     132 AJTI(NF)=(AP(1)*F(1,NF)-AN(1)*F(2,NF))/ARI
198     C.....FOR THE E BOUNDARY
199     140 IF(KEX.EQ.2) GO TO 150
200         IF(KEX.EQ.1) GO TO 141
201         F(M1,NF)=F(M2,NF)
202         GO TO 150
203     141 IF(KBCE(NF).EQ.1) GO TO 142
204         F(M1,NF)=(AS(M1)*F(M2,NF)+CON(M1))/(AP(M1)*FACE)
205         AJTE(NF)=AFXE(NF)
206         IF(KBCE(NF).EQ.3) AJTE(NF)=AJTE(NF)-BFXE(NF)*F(M1,NF)
207         GO TO 150
208     142 AJTE(NF)=(AP(M1)*F(M1,NF)-AS(M1)*F(M2,NF))/ARE
209     150 CONTINUE
210     C
211     CON AND AP ARE RESET TO ZERO
212         DO 180 J=2,M2

```

```

213         AP(J)=0.
214     180 CON(J)=0.
215     C
216     100 CONTINUE
217     C
218         ISTEP=ISTEP+1
219         XU=XU+DX
220         PEI=PEI+(RMI-RME)*DX
221         PSII=PSII-RMI*DX
222         IF(ISTEP.GE.LASTEP) LSTOP=.TRUE.
223         IF(XU.GE.XLAST) LSTOP=.TRUE.
224         RETURN
225     C.....
226         ENTRY PROFIL
227     C
228     201 FORMAT(1X)
229     202 FORMAT(2X,*J*,4X,8(2X,I4,3X))
230     203 FORMAT(2X,*Y*,4X,1P8E9.2)
231     204 FORMAT(A6,1X,1P8E9.2)
232     C
233         JEND=0
234     210 JBEG=JEND+1
235         JROD=JEND+8
236         JEND=MIN0(JROD,M1)
237         WRITE(6,201)
238         WRITE(6,202) (J,J=JBEG,JEND)
239         WRITE(6,203) (Y(J),J=JBEG,JEND)
240         DO 225 NF1=1,NFMAX
241         IF(.NOT.LPRINT(NF1)) GO TO 225
242         WRITE(6,204) TITLE(NF1),(F(J,NF1),J=JBEG,JEND)
243     225 CONTINUE
244         IF(JEND.LT.M1) GO TO 210
245         WRITE(6,201)
246         RETURN
247     C.....
248         ENTRY UYGRID
249     C
250         M2=M1-1
251         YF(2)=0.
252         DO 251 J=3,M2
253     251 YF(J)=0.5*(Y(J)+Y(J-1))
254         YF(M1)=Y(M1)
255         OMF(2)=0.
256         DO 252 J=2,M2
257         RDY=YF(J+1)-YF(J)
258     252 OMF(J+1)=OMF(J)+RHO(J)*U(J)*RDY
259         PEI=OMF(M1)
260         DO 253 J=2,M1
261     253 OMF(J)=OMF(J)/PEI
262         RETURN
263         END

```

Sample Input Files

Listing of file "wangin". This is the input data file for calculating Wang's flat plate experiment.

```

1      '---- FILNAME(1) - FILNAME(4) ----'
2      'BLDATIN', 'BLDATO1', 'BLDATO2', 'BLDATO3'
3      '---- LSOLVE(1) - LSOLVE(4) ----'
4      .T. .T. .T. .T.
5      '---- LPRINT(1) - LPRINT(11) ----'
6      .T. .T. .T. .T. .T. .T. .T. .T. .T. .T.
7      '---- TITLE(1) - TITLE(11) ----'
8      'U' 'K' 'E' 'H' 'T' 'TRE' 'YRE' 'AMUT' 'YPLS' 'UPLS' 'DU1'
9      '---- RE2P(1) - RE2P(10) ----'
10     200.0, 300.0, 400.0, 500.0, 750.0, 1000., 1200., 1500., 2000., 1.E9
11     '---LASTEP, JUMP1, JUMP2, IPP, JUMPT ---'
12     5000, 5000, 100, 5001, 10
13     '--- KENT, HTC, ITM, LCPSOL ---'
14     1 1 1 .T.
15     '--- TU, EIN, XUI, XUF, RE2F, RE2C ---'
16     .0235, 0.70, .0001, 1.01, 5000., 125.
17     '--- PRESS, VINP ---'
18     1.019E+5, 13.50
19     '--- IWIBC, PRT, TINF, TW, UHSL, WTOHF ---'
20     2, .90, 22., 22., .01000, 850.
21     '--- M1, DEL, DELT, GEXP, GX1, EKI, A1, DXFC, REPI, REPFC ---'
22     88, 5.39E-4, 5.39E-4, 2.30, .1, 2.0, 1.0, 1.00, 8.0E4, 30.
23     '---CU, C1, C2, SK, SE, CC, CVRM ---'
24     .09, 1.44, 1.92, 1., 1.3, 0.00, 0.
25     '---OMEGA, FRAC, ENEXP, RC, KCRC, KCM, RFILE ---'
26     0.0, .0007, 1.00, 1.E20, 1, 1, 'NOFILE'

```

Listing of file "rw22in". This is the input data file for calculating Rued's flat plate experiment using grid 2.

```

1      '---- FILNAME(1) - FILNAME(4) ----'
2      'BLDATIN', 'BLDATO1', 'BLDATO2', 'BLDATO3'
3      '---- LSOLVE(1) - LSOLVE(4) ----'
4      .T. .T. .T. .T.
5      '---- LPRINT(1) - LPRINT(11) ----'
6      .T. .T. .T. .T. .T. .T. .T. .T. .T. .T.
7      '---- TITLE(1) - TITLE(11) ----'
8      'U' 'K' 'E' 'H' 'T' 'TRE' 'YRE' 'AMUT' 'YPLS' 'UPLS' 'DU1'
9      '---- RE2P(1) - RE2P(10) ----'
10     200.0, 300.0, 400.0, 500.0, 750.0, 1000., 1200., 1500., 2000., 1.E9

```

```

11 '----LASTEP,JUMP1,JUMP2,IPP,JUMPT ----'
12 5000, 5000, 100, 5001, 20
13 '---- KENT, HTC, ITM, LCPSOL ----'
14 1 1 1 .T.
15 '---- TU, EIN, XUI, XUF, RE2F, RE2C ----'
16 .0465, 1600., .0005, .30, 5000., 125.
17 '---- PRESS, VINP ----'
18 1.01325E+5, 47.0
19 '---- IWTBC, PRT, TINF, TW, UHSL, WTOHF ----'
20 1, .90, 105., 105., .0150, 29.2
21 '---- M1, DEL,DELT, GEXP, GX1, EKI, A1, DXFC, REPI, REPFC ----'
22 88, 1.00E-4, 1.00E-4, 2.30, .1, 2.0, 1.0, 0.75, 5.0E4, 30.
23 '----CU, C1, C2, SK, SE, CC, CVRM ----'
24 .09, 1.44, 1.92, 1., 1.3, 0.00, 0.
25 '----OMEGA, FRAC, ENEXP, RC, KCRC, KCM, RFILE ----'
26 0.0, .0007, 1.00, 1.E20, 1, 1, 'NOFILE'

```

Listing of file "bl02in". This is the input data file for calculating Blair and Werle's flat plate experiment using grid 2.

```

1 '----- FILNAME(1) - FILNAME(4) -----'
2 'BLDATIN','BLDATO1','BLDATO2','BLDATO3'
3 '----- LSOLVE(1) - LSOLVE(4) -----'
4 .T. .T. .T. .T.
5 '----- LPRINT(1) - LPRINT(11) -----'
6 .T. .T. .T. .T. .T. .T. .T. .T. .T. .T.
7 '----- TITLE(1) - TITLE(11) -----'
8 'U' 'K' 'E' 'H' 'T' 'TRE' 'YRE' 'AMUT' 'YPLS' 'UPLS' 'DU1'
9 '----- RE2P(1) - RE2P(10) -----'
10 200.0,300.0,400.0,500.0,750.0,1000.,1200.,1500.,2000.,1.E9
11 '----LASTEP,JUMP1,JUMP2,IPP,JUMPT ----'
12 5000, 5000, 100, 5001, 10
13 '---- KENT, HTC, ITM, LCPSOL ----'
14 1 1 1 .T.
15 '---- TU, EIN, XUI, XUF, RE2F, RE2C ----'
16 .0233, 19.5, .0005, 1.50, 5000., 125.
17 '---- PRESS, VINP ----'
18 1.019E+5, 30.48
19 '---- IWTBC, PRT, TINF, TW, UHSL, WTOHF ----'
20 2, .90, 22., 22., .0425, 850.
21 '---- M1, DEL,DELT, GEXP, GX1, EKI, A1, DXFC, REPI, REPFC ----'
22 88, 0.94E-4, 0.94E-4, 2.30, .1, 2.0, 1.0, 8.0E4, 30.
23 '----CU, C1, C2, SK, SE, CC, CVRM ----'
24 .09, 1.44, 1.92, 1., 1.3, 0.00, 0.
25 '----OMEGA, FRAC, ENEXP, RC, KCRC, KCM, RFILE ----'
26 0.0, .0007, 1.00, 1.E20, 1, 1, 'NOFILE'

```

Listing of file "bl12in". This is the input data file for Blair and Werle's lower acceleration case with  $Tu_{e,T}$  equal to 2.1%.

```

1      '---- FILNAME(1) - FILNAME(4) ----'
2      'BLDATIN', 'BLDATO1', 'BLDATO2', 'BLDATO3'
3      '---- LSOLVE(1) - LSOLVE(4) ----'
4      .T. .T. .T. .T.
5      '---- LPRINT(1) - LPRINT(11) ----'
6      .T. .T. .T. .T. .T. .T. .T. .T. .T.
7      '---- TITLE(1) - TITLE(11) ----'
8      'U' 'K' 'E' 'H' 'T' 'TRE' 'YRE' 'AMUT' 'YPLS' 'UPLS' 'DU1'
9      '---- RE2P(1) - RE2P(10) ----'
10     200.0, 300.0, 400.0, 500.0, 750.0, 1000., 1200., 1500., 2000., 1.E9
11     '---LASTEP, JUMP1, JUMP2, IPP, JUMPT ---'
12     5000, 5000, 100, 5001, 10
13     '--- KENT, HTC, ITM, LCPSOL ---'
14     1 1 1 .T.
15     '--- TU, EIN, XUI, XUF, RE2F, RE2C ---'
16     .0210, 1.20, .0010, 1.50, 5000., 125.
17     '--- PRESS, VINP ---'
18     1.019E+5, 30.48
19     '--- IWTBC, PRT, TINF, TW, UHSL, WTOHF ---'
20     2, .90, 22., 22., .0430, 850.
21     '--- M1, DEL, DELT, GEXP, GX1, EKI, A1, DXFC, REPI, REPFC ---'
22     88, 1.80E-4, 1.80E-4, 2.30, .1, 2.0, 1.0, 1.00, 8.0E4, 30.
23     '---CU, C1, C2, SK, SE, CC, CVRM ----'
24     .09, 1.44, 1.92, 1., 1.3, 0.00, 0.
25     '---OMEGA, FRAC, ENEXP, RC, KCRC, KCM, RFILE ---'
26     0.0, .0007, 1.00, 1.E20, 1, 1, 'NOFILE'

```

Listing of file "rw123in". This is the input data file for calculating Rued's pressure gradient experiment set 12 using grid 3.

```

1      '---- FILNAME(1) - FILNAME(4) ----'
2      'BLDATIN', 'BLDATO1', 'BLDATO2', 'BLDATO3'
3      '---- LSOLVE(1) - LSOLVE(4) ----'
4      .T. .T. .T. .T.
5      '---- LPRINT(1) - LPRINT(11) ----'
6      .T. .T. .T. .T. .T. .T. .T. .T. .T.
7      '---- TITLE(1) - TITLE(11) ----'
8      'U' 'K' 'E' 'H' 'T' 'TRE' 'YRE' 'AMUT' 'YPLS' 'UPLS' 'DU1'
9      '---- RE2P(1) - RE2P(10) ----'
10     200.0, 300.0, 400.0, 500.0, 750.0, 1000., 1200., 1500., 2000., 1.E9
11     '---LASTEP, JUMP1, JUMP2, IPP, JUMPT ---'
12     5000, 5000, 100, 5001, 20
13     '--- KENT, HTC, ITM, LCPSOL ---'
14     1 1 1 .F.
15     '--- TU, EIN, XUI, XUF, RE2F, RE2C ---'
16     .0773, 882., .0010, .40, 5000., 125.
17     '--- PRESS, VINP ---'

```



```

8      'U' 'K' 'E' 'H' 'T' 'TRE' 'YRE' 'AMUT' 'YPLS' 'UPLS' 'DU1'
9      '---- RE2P(1) - RE2P(10) ----'
10     200.0,300.0,400.0,500.0,750.0,1000.,1200.,1500.,2000.,1.E9
11     '---LASTEP,JUMP1,JUMP2,IPP,JUMPT ---'
12     8000, 8000, 200, 9001, 20
13     '--- KENT, HTC, ITM, LCPSOL ----'
14     1 1 1 .F.
15     '--- TU, EIN, XUI, XUF, RE2F, RE2C ----'
16     .3913, 10., .0030, .048, 50000., 125.
17     '--- PRESS, VINP ----'
18     2.920E5, 146
19     '--- IWIBC, PRT, TINF, TW, UHSL, WTOHF ----'
20     1, .90, 150., 16., .00001, 16.
21     '--- M1, DEL,DELTA, GEXP, GX1, EKI, A1, DXFC, REPI, REPFC ----'
22     88, 1.111E-4, 1.111E-4, 2.3, .1, 2., 1.0, 1.00, 5.E3, 20.
23     '---CU, C1, C2, SK, SE, CC, CVRM ----'
24     .09, 1.44, 1.92, 1., 1.3, 0.20, 0.0
25     '---OMEGA, FRAC, ENEXP, RC, KCRC, KCM, RFILE ----'
26     7.65, .0008, 1.00, 1.E20, 1, 1, 'RCDBP'

```

Listing of file "d145sin". This is the input data file for Hilton et al.'s C3X blade on the suction side.

```

1      '---- FILNAME(1) - FILNAME(4) ----'
2      'BLDATIN', 'BLDATO1', 'BLDATO2', 'BLDATO3'
3      '---- LSOLVE(1) - LSOLVE(4) ----'
4      .T. .T. .T. .T.
5      '---- LPRINT(1) - LPRINT(11) ----'
6      .T. .T. .T. .T. .T. .T. .T. .T. .T. .T.
7      '---- TITLE(1) - TITLE(11) ----'
8      'U' 'K' 'E' 'H' 'T' 'TRE' 'YRE' 'AMUT' 'YPLS' 'UPLS' 'DU1'
9      '---- RE2P(1) - RE2P(10) ----'
10     200.0,300.0,400.0,500.0,750.0,1000.,1200.,1500.,2000.,1.E9
11     '---LASTEP,JUMP1,JUMP2,IPP,JUMPT ---'
12     8000, 8000, 100, 9001, 10
13     '--- KENT, HTC, ITM, LCPSOL ----'
14     4 1 1 .F.
15     '--- TU, EIN, XUI, XUF, RE2F, RE2C ----'
16     .147, 20., .0040, .160, 50000., 125.
17     '--- PRESS, VINP ----'
18     4.00E5, 90.
19     '--- IWIBC, PRT, TINF, TW, UHSL, WTOHF ----'
20     1, .90, 515., 375., .00001, 375.
21     '--- M1, DEL,DELTA, GEXP, GX1, EKI, A1, DXFC, REPI, REPFC ----'
22     99, 1.12E-4, 2.20E-4, 2.8, .1, 2., 1.0, 1.03, 4.E4, 25.
23     '---CU, C1, C2, SK, SE, CC, CVRM, ----'
24     .09, 1.44, 1.92, 1., 1.3, 0.00, 0.00
25     '---OMEGA, FRAC, ENEXP, RC, KCRC, KCM, RFILE ----'
26     7.16, .0007, 1.00, 1.E20, 1, 0, 'RC3X145S'

```

Listing of file "d145pin". This is the input data file for Hilton et al.'s C3X blade on the pressure side.

```

1      '---- FILNAME(1) - FILNAME(4) ----'
2      'BLDATIN', 'BLDATO1', 'BLDATO2', 'BLDATO3'
3      '---- LSOLVE(1) - LSOLVE(4) ----'
4      .T. .T. .T. .T.
5      '---- LPRINT(1) - LPRINT(11) ----'
6      .T. .T. .T. .T. .T. .T. .T. .T. .T. .T.
7      '---- TITLE(1) - TITLE(11) ----'
8      'U' 'K' 'E' 'H' 'T' 'TRE' 'YRE' 'AMUT' 'YPLS' 'UPLS' 'DU1'
9      '---- RE2P(1) - RE2P(10) ----'
10     200.0, 300.0, 400.0, 500.0, 750.0, 1000., 1200., 1500., 2000., 1.E9
11     '---LASTEP, JUMP1, JUMP2, IPP, JUMPT ---'
12     8000, 8000, 100, 9001, 10
13     '--- KENT, HTC, ITM, LCPSOL ---'
14     1 1 1 .F.
15     '--- TU, EIN, XUI, XUF, RE2F, RE2C ---'
16     .1846, 10., .004, .100, 50000., 125.
17     '--- PRESS, VINP ---'
18     4.00E5, 90.
19     '--- IWTBC, PRT, TINF, TW, UHSL, WTOHF ---'
20     1, .90, 515., 375., .00001, 375.
21     '--- M1, DEL, DELT, GEXP, GX1, EKI, A1, DXFC, REPI, REPFC ---'
22     88, 1.37E-4, 1.8E-4, 2.3, .1, 2., 1.0, .50, 3.E4, 25.
23     '---CU, C1, C2, SK, SE, CC, CVRM ---'
24     .09, 1.44, 1.92, 1., 1.3, 0.00, 0.
25     '---OMEGA, FRAC, ENEXP, RC, KCRC, KCM, RFILE ---'
26     6.03, .00075, 1.00, 1.E20, 1, 1, 'RC3X145P'

```

## Appendix A2

### Variable property equations

The equations used to functionally approximate the material properties of air are given below in eqs. (A2.1) through (A2.3). Figures A2-1 through A2-3 compare the approximations with the data given in Crawford and Kays [18].

Thermal Conductivity ( W/(m K) ):

$$K \approx .0241926 + (7.3851 \times 10^{-5}) T - (3.203 \times 10^{-8}) T^2 + (1.829 \times 10^{-11}) T^3 \quad (\text{A2.1})$$

where T is in degrees C.

Dynamic Viscosity ( Pa Sec):

$$\mu \approx 1.465 T^{1.5} / (110.4 + T) \quad (\text{A2.2})$$

where T is expressed in K

Specific Heat ( J/(kg K) ):

$$C_p \approx 1003.6 + .01155 T + (5.453 \times 10^{-4}) T^2 - (4.2422 \times 10^{-7}) T^3 \quad (\text{A2.3})$$

where T is expressed in C.

-----

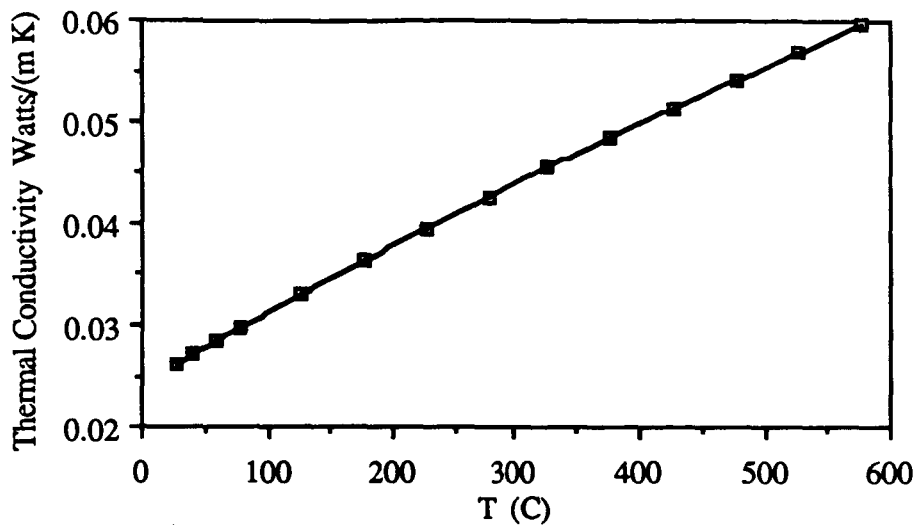


Figure A2-1. A comparison of the approximated thermal conductivity with experimental data [18].

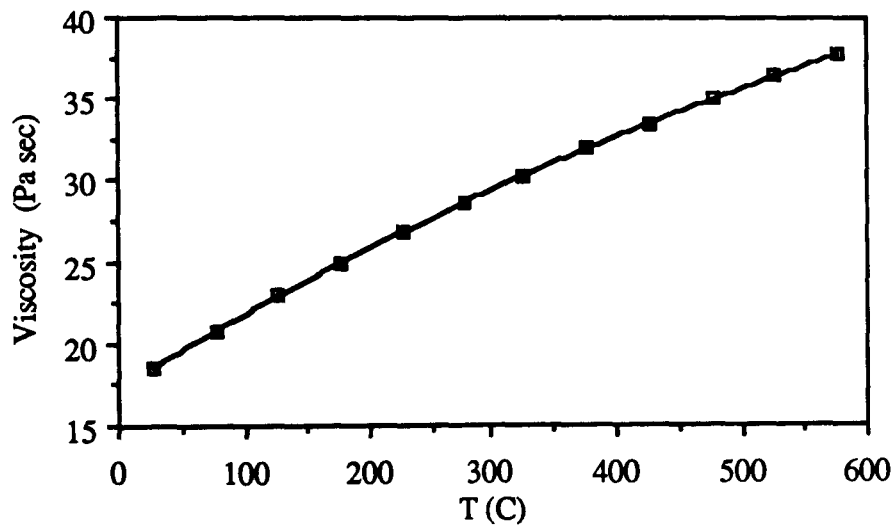


Figure A2-2. A comparison of the approximated dynamic viscosity with experimental data [18].

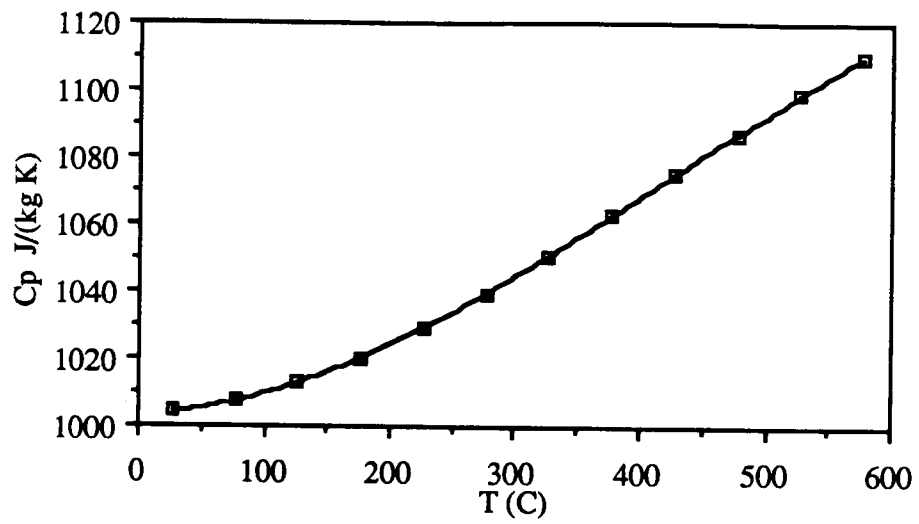


Figure A2-3. A comparison of the approximated  $C_p$  with experimental data [18].



Tabulation of the experimental data shown in Figures 5.8 and 5.9 as extracted from reference [8]. (Blair and Werle)

Rex Grid 1	Stanton No Grid 1	Rex Grid 2	Stanton No Grid 2	Rex Grid 3	Stanton No Grid 3
1.123E+05	2.965E-03	1.132E+05	2.982E-03	1.124E+05	4.179E-03
1.379E+05	2.272E-03	1.390E+05	2.337E-03	1.381E+05	3.374E-03
1.635E+05	1.986E-03	1.649E+05	2.073E-03	1.638E+05	3.307E-03
1.891E+05	1.716E-03	1.907E+05	1.823E-03	1.894E+05	3.208E-03
2.148E+05	1.600E-03	2.165E+05	1.660E-03	2.151E+05	3.259E-03
2.404E+05	1.489E-03	2.424E+05	1.605E-03	2.408E+05	3.180E-03
2.660E+05	1.380E-03	2.682E+05	1.541E-03	2.664E+05	3.101E-03
2.917E+05	1.281E-03	2.940E+05	1.592E-03	2.921E+05	3.052E-03
3.173E+05	1.240E-03	3.199E+05	1.591E-03	3.178E+05	3.051E-03
3.429E+05	1.185E-03	3.457E+05	1.732E-03	3.434E+05	3.027E-03
3.685E+05	1.142E-03	3.716E+05	1.812E-03	3.691E+05	2.958E-03
4.198E+05	1.120E-03	4.232E+05	2.106E-03	4.204E+05	2.827E-03
4.711E+05	1.072E-03	4.749E+05	2.359E-03	4.718E+05	2.883E-03
5.223E+05	1.114E-03	5.266E+05	2.511E-03	5.231E+05	2.822E-03
5.736E+05	1.146E-03	5.783E+05		5.744E+05	2.780E-03
6.761E+05	1.397E-03	6.816E+05	2.451E-03	6.771E+05	2.572E-03
7.786E+05	1.758E-03	7.850E+05	2.421E-03	7.798E+05	2.564E-03
8.811E+05	2.008E-03	8.883E+05	2.325E-03	8.824E+05	2.500E-03
9.836E+05	2.187E-03	9.917E+05	2.243E-03	9.851E+05	2.402E-03
1.086E+06	2.262E-03	1.095E+06	2.240E-03	1.088E+06	2.401E-03
1.189E+06	2.218E-03	1.198E+06	2.205E-03	1.190E+06	2.357E-03
1.291E+06	2.113E-03	1.302E+06	2.134E-03	1.293E+06	2.282E-03
1.394E+06	2.079E-03	1.405E+06	2.036E-03	1.396E+06	2.218E-03
1.496E+06	2.038E-03	1.508E+06	2.045E-03	1.498E+06	2.176E-03
1.599E+06	2.009E-03	1.612E+06	1.994E-03	1.601E+06	2.181E-03
1.701E+06	1.981E-03	1.715E+06	1.959E-03	1.704E+06	2.088E-03
1.804E+06	1.954E-03	1.819E+06	1.945E-03	1.806E+06	2.068E-03
1.906E+06	1.940E-03	1.922E+06	1.910E-03	1.909E+06	2.045E-03
2.009E+06	1.978E-03	2.025E+06	1.955E-03	2.012E+06	2.126E-03
2.111E+06	1.898E-03	2.129E+06	1.892E-03	2.114E+06	2.036E-03
2.214E+06	1.887E-03	2.232E+06	1.858E-03	2.217E+06	2.028E-03
2.368E+06	1.873E-03	2.387E+06	1.849E-03	2.371E+06	1.978E-03
2.521E+06	1.843E-03	2.542E+06	1.796E-03	2.525E+06	1.924E-03
2.675E+06	1.831E-03	2.697E+06	1.794E-03	2.679E+06	1.940E-03
2.829E+06	1.784E-03	2.852E+06	1.749E-03	2.833E+06	1.917E-03
2.983E+06	1.788E-03	3.007E+06	1.738E-03	2.987E+06	1.904E-03
3.136E+06	1.766E-03	3.162E+06	1.714E-03	3.141E+06	1.897E-03
3.290E+06	1.754E-03	3.317E+06	1.715E-03	3.295E+06	1.872E-03
3.444E+06	1.721E-03	3.472E+06	1.685E-03	3.449E+06	1.856E-03
3.598E+06	1.696E-03	3.627E+06	1.681E-03	3.603E+06	1.837E-03
3.752E+06	1.719E-03	3.782E+06	1.692E-03	3.757E+06	1.857E-03
3.905E+06	1.723E-03	3.937E+06	1.684E-03	3.911E+06	1.864E-03
4.059E+06	1.701E-03	4.092E+06	1.678E-03	4.065E+06	1.866E-03
4.213E+06	1.703E-03	4.247E+06	1.686E-03	4.219E+06	1.875E-03
4.367E+06	1.689E-03	4.402E+06	1.660E-03	4.373E+06	1.930E-03
4.520E+06	1.697E-03	4.557E+06	1.665E-03	4.527E+06	1.825E-03
4.674E+06	1.639E-03	4.712E+06	1.632E-03	4.681E+06	1.794E-03
4.828E+06	1.657E-03	4.867E+06	1.607E-03	4.835E+06	1.795E-03

Tabulation of the experimental data shown in Figure 5.14 as extracted from reference [9]. (Blair and Werle, lower K)

X (m) Grid 1	Stanton No Grid 1	X (m) Grid 2	Stanton No Grid 2	X (m) Grid 3	Stanton No Grid 3
0.0528	0.004648	0.0547	0.004833	0.0619	0.005462
0.0680	0.003283	0.0646	0.003473	0.0785	0.004157
0.0775	0.002813	0.0776	0.002962	0.0897	0.003768
0.0941	0.002399	0.0951	0.002519	0.0996	0.003415
0.1019	0.002223	0.1083	0.002340	0.1124	0.003311
0.1116	0.002030	0.1162	0.002127	0.1410	0.003220
0.1293	0.001891	0.1304	0.002020	0.1554	0.003161
0.1425	0.001748	0.1481	0.001886	0.1869	0.003149
0.1567	0.001640	0.1624	0.001831	0.2100	0.003297
0.1700	0.001580	0.1694	0.001739	0.2372	0.003295
0.1816	0.001534	0.1854	0.001655	0.2617	0.003325
0.2039	0.001471	0.2086	0.001618	0.2904	0.003333
0.2350	0.001333	0.2363	0.001579	0.3405	0.003152
0.2591	0.001304	0.2856	0.001547	0.3878	0.003083
0.2841	0.001247	0.3350	0.001639	0.4451	0.002960
0.3340	0.001113	0.3891	0.001837	0.4909	0.002851
0.3858	0.001051	0.4377	0.002039	0.5411	0.002876
0.4340	0.000974	0.4872	0.002252	0.5927	0.002719
0.4894	0.000926	0.5376	0.002421	0.6372	0.002726
0.5386	0.000886	0.5878	0.002449	0.6973	0.002617
0.5859	0.000832	0.6397	0.002411	0.7475	0.002506
0.6431	0.000796	0.6864	0.002481	0.7948	0.002451
0.6933	0.000785	0.7418	0.002401	0.8536	0.002434
0.7399	0.000785	0.8403	0.002333	0.8966	0.002402
0.7945	0.000782	0.8931	0.002297	0.9554	0.002342
0.8429	0.000797	0.9468	0.002245	0.9999	0.002392
0.8950	0.000844	0.9944	0.002282	1.0544	0.002325
0.9498	0.000867	1.0480	0.002192	1.0974	0.002316
0.9975	0.000953	1.1035	0.002148	1.1792	0.002285
1.0478	0.001019	1.1752	0.002145	1.2495	0.002221
1.0984	0.001174	1.2467	0.002040	1.3341	0.002178
1.1728	0.001222	1.3274	0.002032	1.4029	0.002143
1.2502	0.001369	1.4062	0.002029		
1.3266	0.001526	1.4805	0.002022		
1.4056	0.001605				
1.4783	0.001671				

Tabulation of the experimental data shown in Figure 5.15 as extracted from reference [9]. (Blair and Werle, higher K)

X (m) Grid 2	Stanton No Grid 2	X (m) Grid 3	Stanton No Grid 3
0.05013	0.006165	0.05098	0.006061
0.06645	0.004539	0.06463	0.004506
0.08134	0.003904	0.07598	0.003932
0.08276	0.003325	0.08914	0.003465
0.10226	0.003010	0.10510	0.003198
0.11461	0.002751	0.11575	0.003039
0.12872	0.002472	0.12640	0.002887
0.14212	0.002412	0.14157	0.002790
0.15724	0.002281	0.15493	0.002677
0.17235	0.002146	0.16921	0.002581
0.20357	0.001975	0.18084	0.002544
0.23658	0.001823	0.20243	0.002599
0.26073	0.001757	0.23293	0.002580
0.28484	0.001661	0.27610	0.002668
0.33038	0.001511	0.32903	0.002654
0.43505	0.001317	0.43231	0.002730
0.48880	0.001267	0.48519	0.002650
0.54442	0.001245	0.53553	0.002728
0.59012	0.001208	0.58478	0.002629
0.64486	0.001199	0.63950	0.002583
0.74097	0.001246	0.73901	0.002477
0.84343	0.001329	0.83945	0.002374
0.89014	0.001341	0.89141	0.002300
0.94945	0.001394	0.94524	0.002254
0.99540	0.001498	0.99012	0.002276
1.10315	0.001530	1.04206	0.002156
1.17506	0.001586	1.09858	0.002129
1.25133	0.001577	1.17569	0.002067
1.32497	0.001619	1.24737	0.001972
1.39939	0.001571	1.32540	0.001928
1.47658	0.001574	1.40249	0.001858
		1.47958	0.001782

Tabulation of the experimental data shown in Figure 5.18 as extracted from reference [72] (Rued)

X (m) Nr. 6	K x 10 <sup>6</sup> Nr. 6	X (m) Nr. 10	K x 10 <sup>6</sup> Nr. 10	X (m) Nr. 12	K x 10 <sup>6</sup> Nr. 12
		0.0345	1.32		
0.0460	0.751	0.0460	1.894	0.0461	3.427
0.0575	0.822	0.0575	2.132	0.0559	3.749
0.0690	0.893	0.0690	2.395	0.0838	4.977
0.0806	0.965	0.0806	2.704	0.0978	5.561
0.0921	1.036	0.0921	2.99	0.1061	5.795
0.1036	1.108	0.1036	3.157	0.1229	5.795
0.1151	1.156	0.1151	3.24	0.1397	5.474
0.1266	1.179	0.1266	3.252	0.1536	5.123
0.1381	1.179	0.1381	3.205	0.1676	4.421
0.1496	1.179	0.1496	2.943	0.1955	2.754
0.1611	1.179	0.1611	2.609	0.2235	1.497
0.1726	1.191	0.1726	2.275	0.2514	0.620
0.1841	1.222	0.1841	1.93	0.2793	0.006
0.1956	1.227	0.1956	1.561	0.2933	-0.140
0.2071	1.227	0.2071	1.227	0.3073	-0.184
0.2186	1.215	0.2186	0.929	0.3352	-0.184
0.2301	1.203	0.2301	0.703	0.3631	-0.199
0.2417	1.203	0.2417	0.512	0.3911	-0.228
0.2532	1.203	0.2532	0.322	0.4190	-0.140
0.2647	1.203	0.2647	0.155		
0.2762	1.203	0.2762	0.036		
0.2877	1.215	0.2877	-0.06		
0.2992	1.227	0.2992	-0.107		
0.3107	1.239	0.3107	-0.107		
0.3222	1.251	0.3222	-0.095		
0.3337	1.251	0.3337	-0.107		
0.3452	1.263	0.3452	-0.095		
0.3567	1.251	0.3567	-0.06		
0.3682	1.203	0.3682	-0.083		
0.3797	1.084	0.3797	-0.119		
0.4028	0.846	0.4028	-0.143		
0.4258	0.393	0.4258	-0.083		

Tabulation of the experimental data shown in Figure 5.19 as extracted from reference [72]. (Rued)

X (m) Nr. 6	U (m/s) Nr. 6	X (m) Nr. 10	U (m/s) Nr. 10	X (m) Nr. 12	U (m/s) Nr. 12
0.0000	48.96	0.0000	47.50		
0.0345	49.91	0.0345	48.30	0.0279	26.47
0.0460	49.91	0.0460	49.32	0.0461	27.94
0.0575	51.10	0.0575	51.10	0.0559	28.68
0.0690	51.58	0.0690	53.48	0.0838	32.35
0.0806	52.29	0.0806	55.85	0.0978	35.00
0.0921	53.48	0.0921	59.42	0.1061	36.77
0.1036	54.66	0.1036	62.98	0.1229	41.18
0.1151	55.85	0.1151	68.33	0.1397	46.32
0.1266	57.04	0.1266	73.68	0.1536	51.47
0.1381	58.23	0.1381	80.81	0.1676	57.35
0.1496	59.66	0.1496	89.13	0.1955	70.59
0.1611	61.08	0.1611	98.04	0.2235	80.15
0.1726	62.75	0.1726	108.14	0.2514	85.88
0.1841	64.17	0.1841	117.65	0.2793	86.77
0.1956	65.95	0.1956	127.15	0.2933	86.62
0.2071	67.74	0.2071	135.47	0.3073	85.59
0.2186	69.76	0.2186	143.79	0.3352	84.56
0.2301	72.49	0.2301	149.73	0.3631	83.82
0.2417	74.39	0.2417	154.49	0.3911	82.35
0.2532	76.65	0.2532	157.46	0.4190	80.88
0.2647	80.45	0.2647	158.65		
0.2762	81.64	0.2762	159.24		
0.2877	84.37	0.2877	158.29		
0.2992	87.34	0.2992	157.10		
0.3107	90.43	0.3107	156.27		
0.3222	93.88	0.3222	155.20		
0.3337	98.63	0.3337	154.25		
0.3452	103.62	0.3452	153.30		
0.3567	109.33	0.3567	152.35		
0.3682	114.44	0.3682	152.11		
0.3797	119.43	0.3797	151.52		
0.4028	129.17	0.4028	149.73		
0.4258	136.07	0.4258	147.95		

Tabulation of the experimental data shown in Figure 5.22 as extracted from reference [72]. (Rued, Nr. 6)

X (m) Grid 1	Stanton No Grid 1	X (m) Grid 2	Stanton No Grid 2	X (m) Grid 3	Stanton No Grid 3	X (m) Grid 4	Stanton No Grid 4
4.6703E-02	2.6780E-03	4.7385E-02	3.0880E-03	4.6773E-02	3.5883E-03	4.6547E-02	3.9678E-03
6.2027E-02	2.6098E-03	6.1888E-02	3.1483E-03	6.1667E-02	3.8216E-03	6.1593E-02	4.0212E-03
7.6423E-02	2.0976E-03	7.8558E-02	2.8805E-03	7.7127E-02	3.6279E-03	7.6926E-02	3.7427E-03
9.1347E-02	1.9073E-03	9.2260E-02	2.8526E-03	9.1913E-02	3.4578E-03	9.2251E-02	3.6064E-03
1.0654E-01	1.6595E-03	1.0744E-01	2.8080E-03	1.0657E-01	3.2572E-03	1.0664E-01	3.3921E-03
1.2120E-01	1.5776E-03	1.2289E-01	2.8109E-03	1.2175E-01	3.1685E-03	1.2143E-01	3.2388E-03
1.5103E-01	1.6204E-03	1.5150E-01	2.8231E-03	1.5171E-01	3.0284E-03	1.5127E-01	2.9593E-03
1.6663E-01	1.5861E-03	1.6856E-01	2.8127E-03	1.6784E-01	2.9094E-03	1.6807E-01	2.9182E-03
1.8114E-01	1.6261E-03	1.8387E-01	2.8088E-03	1.8209E-01	2.7935E-03	1.8272E-01	2.8123E-03
1.9754E-01	1.7342E-03	1.9663E-01	2.7265E-03	1.9646E-01	2.7691E-03	1.9643E-01	2.7604E-03
2.1218E-01	1.7810E-03	2.1248E-01	2.7024E-03	2.1245E-01	2.7009E-03	2.1228E-01	2.7326E-03
2.2751E-01	1.8448E-03	2.2632E-01	2.6711E-03	2.2615E-01	2.6628E-03	2.2599E-01	2.7180E-03
2.4269E-01	1.9052E-03	2.4190E-01	2.6266E-03	2.4254E-01	2.6320E-03	2.4185E-01	2.6530E-03
2.5842E-01	1.8946E-03	2.5789E-01	2.5755E-03	2.5812E-01	2.5875E-03	2.5811E-01	2.6117E-03
2.8812E-01	2.0391E-03	2.8812E-01	2.4660E-03	2.8809E-01	2.4270E-03	2.8795E-01	2.4712E-03
3.0398E-01	2.1064E-03	3.0343E-01	2.4553E-03	3.0380E-01	2.4300E-03	3.0353E-01	2.4671E-03
3.1661E-01	2.0174E-03	3.1660E-01	2.3561E-03	3.1643E-01	2.3679E-03	3.1657E-01	2.3575E-03
3.3382E-01	1.9698E-03	3.3205E-01	2.2303E-03	3.3242E-01	2.2794E-03	3.3270E-01	2.3332E-03
3.4739E-01	2.1654E-03	3.4790E-01	2.3282E-03	3.4760E-01	2.2585E-03	3.4788E-01	2.3561E-03
3.6272E-01	2.0802E-03	3.6214E-01	2.2326E-03	3.6184E-01	2.2036E-03	3.6186E-01	2.2568E-03
3.9081E-01	2.0821E-03	3.9102E-01	2.2042E-03	3.9099E-01	2.1718E-03	3.9075E-01	2.2008E-03
4.0653E-01	2.1901E-03	4.0687E-01	2.3054E-03	4.0657E-01	2.2629E-03	4.0633E-01	2.2882E-03
4.2198E-01	2.3793E-03	4.2191E-01	2.3285E-03	4.2135E-01	2.2284E-03	4.2192E-01	2.2536E-03

Tabulation of the experimental data shown in Figure 5.23 as extracted from reference [72]. (Rued, Nr. 10)

X (m) Grid 1	Stanton No Grid 1	X (m) Grid 2	Stanton No Grid 2	X (m) Grid 3	Stanton No Grid 3	X (m) Grid 4	Stanton No Grid 4
4.7412E-02	2.8430E-03	4.7418E-02	3.2482E-03	4.8016E-02	3.8119E-03	4.8788E-02	4.1055E-03
6.3253E-02	2.4796E-03	6.3419E-02	2.9590E-03	6.3112E-02	3.6208E-03	6.2844E-02	4.0091E-03
7.8311E-02	2.1805E-03	7.8634E-02	2.7240E-03	7.8667E-02	3.2068E-03	7.8531E-02	3.5883E-03
9.4048E-02	1.9015E-03	9.3862E-02	2.5261E-03	9.3126E-02	3.1137E-03	9.3865E-02	3.3094E-03
1.0790E-01	1.6126E-03	1.0922E-01	2.3080E-03	1.0793E-01	2.8652E-03	1.0840E-01	3.0407E-03
1.2366E-01	1.4079E-03	1.2347E-01	2.0157E-03	1.2343E-01	2.6673E-03	1.2442E-01	2.8089E-03
1.5377E-01	1.1608E-03	1.5463E-01	2.1026E-03	1.5341E-01	2.4437E-03	1.5302E-01	2.4944E-03
1.6904E-01	1.0945E-03	1.6829E-01	2.0062E-03	1.6799E-01	2.3236E-03	1.6829E-01	2.4181E-03
1.8351E-01	1.0149E-03	1.8276E-01	1.9705E-03	1.8247E-01	2.2946E-03	1.8316E-01	2.3317E-03
1.9838E-01	9.6900E-04	1.9916E-01	2.0459E-03	1.9830E-01	2.2790E-03	1.9899E-01	2.3261E-03
2.1364E-01	8.5889E-04	2.1327E-01	2.1182E-03	2.1333E-01	2.2769E-03	2.1348E-01	2.3343E-03
2.2893E-01	8.3993E-04	2.2832E-01	2.1601E-03	2.2835E-01	2.2681E-03	2.2811E-01	2.3256E-03
2.4369E-01	8.4468E-04	2.4498E-01	2.2186E-03	2.4460E-01	2.2896E-03	2.4515E-01	2.3469E-03
2.5873E-01	8.5952E-04	2.6297E-01	2.2567E-03	2.5853E-01	2.2336E-03	2.5883E-01	2.3180E-03
2.8763E-01	1.0041E-03	2.8831E-01	2.1992E-03	2.8831E-01	2.2093E-03	2.8821E-01	2.2938E-03
3.0323E-01	1.1168E-03	3.0230E-01	2.2952E-03	3.0282E-01	2.2614E-03	3.0296E-01	2.2749E-03
3.1775E-01	1.2060E-03	3.1850E-01	2.1951E-03	3.1901E-01	2.1208E-03	3.1849E-01	2.1681E-03
3.3336E-01	1.3220E-03	3.3364E-01	2.1525E-03	3.3349E-01	2.0817E-03	3.3353E-01	2.2201E-03
3.4725E-01	1.5430E-03	3.4965E-01	2.2719E-03	3.4893E-01	2.1201E-03	3.4856E-01	2.2113E-03
3.6179E-01	1.6828E-03	3.6184E-01	2.2027E-03	3.6100E-01	2.0914E-03	3.6088E-01	2.1556E-03
3.9315E-01	1.9588E-03	3.9188E-01	2.1615E-03	3.9199E-01	2.0872E-03	3.9164E-01	2.2392E-03
4.0717E-01	2.1257E-03	4.0679E-01	2.1899E-03	4.0691E-01	2.1493E-03	4.0721E-01	2.2506E-03
4.2066E-01	2.3331E-03	4.2424E-01	2.2347E-03	4.2167E-01	2.1710E-03	4.2027E-01	2.3838E-03

Tabulation of the experimental data shown in Figure 5.24 as extracted from reference [72]. (Rued, Nr. 12)

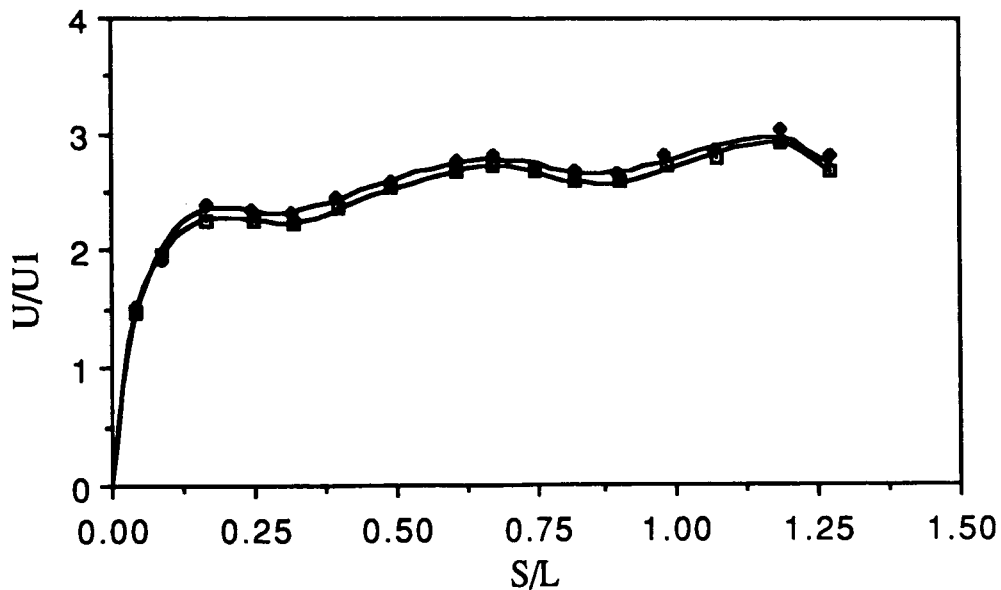
X (m) Grid 1	Stanton No Grid 1	X (m) Grid 2	Stanton No Grid 2	X (m) Grid 3	Stanton No Grid 3	X (m) Grid 4	Stanton No Grid 4
4.7877E-02	3.3694E-03	4.8072E-02	3.4574E-03	4.7725E-02	3.7321E-03	4.7730E-02	4.3220E-03
6.3058E-02	3.1751E-03	6.2591E-02	3.2769E-03	6.2067E-02	3.6839E-03	6.2842E-02	4.4159E-03
7.7484E-02	2.6658E-03	7.7038E-02	2.7981E-03	7.8658E-02	3.1977E-03	7.8937E-02	3.7943E-03
9.3312E-02	2.2408E-03	9.3514E-02	2.3391E-03	9.3294E-02	2.7968E-03	9.3563E-02	3.3798E-03
1.0748E-01	1.9418E-03	1.0771E-01	2.0807E-03	1.0699E-01	2.5894E-03	1.0714E-01	3.0097E-03
1.2160E-01	1.7648E-03	1.2225E-01	1.9307E-03	1.2227E-01	2.3409E-03	1.2296E-01	2.7610E-03
1.5353E-01	1.5080E-03	1.5321E-01	1.6301E-03	1.5253E-01	2.0066E-03	1.5289E-01	2.3320E-03
1.6755E-01	1.3887E-03	1.6774E-01	1.4632E-03	1.6731E-01	1.8057E-03	1.6818E-01	2.1004E-03
1.8320E-01	1.2858E-03	1.8355E-01	1.4010E-03	1.8282E-01	1.6995E-03	1.8261E-01	1.9809E-03
1.9869E-01	1.1457E-03	1.9943E-01	1.2438E-03	1.9860E-01	1.5966E-03	1.9841E-01	1.9119E-03
2.1326E-01	1.0330E-03	2.1413E-01	1.1378E-03	2.1292E-01	1.5111E-03	2.1263E-01	1.8773E-03
2.2690E-01	9.4086E-04	2.2711E-01	1.0628E-03	2.2603E-01	1.4428E-03	2.2552E-01	1.8600E-03
2.4235E-01	9.4315E-04	2.4283E-01	1.0617E-03	2.4078E-01	1.5877E-03	2.4275E-01	2.1024E-03
2.5853E-01	8.2996E-04	2.5849E-01	9.7913E-04	2.5833E-01	1.7080E-03	2.5810E-01	2.1590E-03
2.8788E-01	7.3328E-04	2.8727E-01	1.0148E-03	2.8790E-01	2.1164E-03	2.8761E-01	2.4725E-03
3.0375E-01	7.5918E-04	3.0347E-01	1.1254E-03	3.0282E-01	2.3189E-03	3.0312E-01	2.5697E-03
3.1816E-01	8.1262E-04	3.1819E-01	1.2364E-03	3.1891E-01	2.4668E-03	3.1831E-01	2.5788E-03
3.3271E-01	8.6602E-04	3.3344E-01	1.3336E-03	3.3258E-01	2.4187E-03	3.3221E-01	2.6697E-03
3.4716E-01	7.8045E-04	3.4797E-01	1.5633E-03	3.4814E-01	2.5837E-03	3.4751E-01	2.6449E-03
3.6245E-01	7.3872E-04	3.6293E-01	1.6234E-03	3.6336E-01	2.4437E-03	3.6369E-01	2.5283E-03
3.9285E-01	9.9091E-04	3.9224E-01	2.0454E-03	3.9254E-01	2.4860E-03	3.9231E-01	2.5369E-03
4.0787E-01	1.1391E-03	4.0663E-01	2.2650E-03	4.0670E-01	2.5531E-03	4.0525E-01	2.6010E-03
4.2184E-01	9.4858E-04	4.2240E-01	2.3350E-03	4.2243E-01	2.3756E-03	4.2228E-01	2.5486E-03

Tabulation of the experimental data shown in Figure 5.27 and 5.28 as extracted from references [20] and [77]

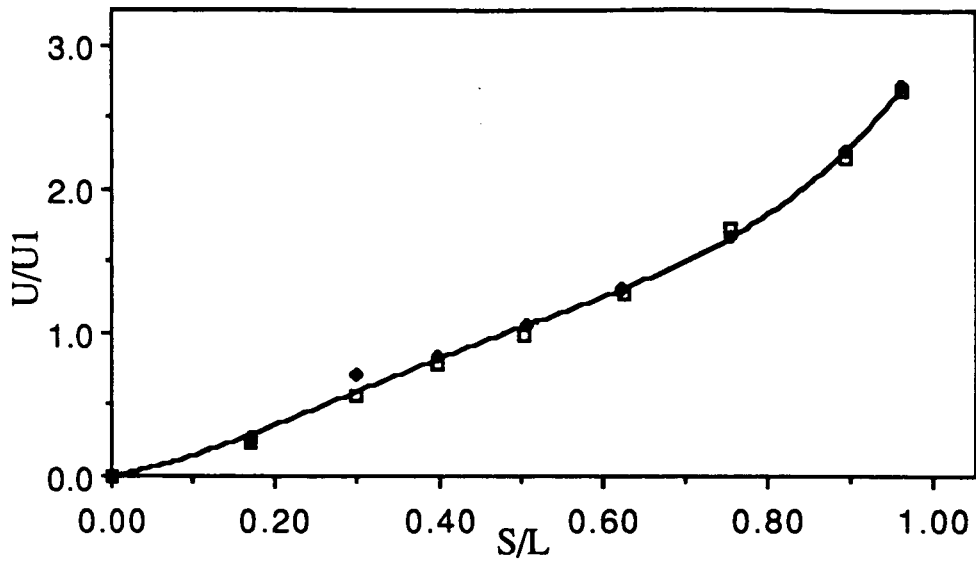
Pressure Side				Suction Side			
S/L ReD	H W/(m*m K)	S/L Re+	H W/(m*m K)	S/L ReD	H W/(m*m K)	S/L Re+	H W/(m*m K)
3.590E-02	1.056E+03	6.012E-02	1.272E+03	3.710E-03	2.096E+03	5.868E-02	1.296E+03
5.525E-02	8.929E+02	9.896E-02	1.176E+03	1.071E-02	1.795E+03	1.191E-01	1.189E+03
9.058E-02	7.220E+02	1.365E-01	1.169E+03	5.126E-02	1.321E+03	1.819E-01	1.479E+03
1.280E-01	6.838E+02	1.730E-01	1.212E+03	8.050E-02	1.005E+03	2.886E-01	2.285E+03
1.687E-01	6.454E+02	2.045E-01	1.275E+03	7.887E-02	8.999E+02	3.165E-01	2.410E+03
2.015E-01	6.752E+02	2.123E-01	9.598E+02	1.377E-01	7.845E+02	3.784E-01	2.321E+03
2.018E-01	5.604E+02	2.507E-01	9.949E+02	1.847E-01	6.399E+02	4.268E-01	1.824E+03
2.465E-01	5.923E+02	3.686E-01	1.238E+03	2.525E-01	5.522E+02	4.374E-01	2.377E+03
3.634E-01	7.249E+02	4.267E-01	1.351E+03	3.194E-01	5.741E+02	4.766E-01	1.776E+03
4.180E-01	7.105E+02	6.463E-01	1.644E+03	3.822E-01	6.077E+02	5.255E-01	1.848E+03
6.230E-01	8.171E+02	7.146E-01	1.798E+03	4.302E-01	9.569E+02	5.743E-01	1.687E+03
6.374E-01	8.646E+02	7.914E-01	1.940E+03	4.420E-01	6.633E+02	6.339E-01	1.860E+03
7.057E-01	9.891E+02	8.579E-01	1.962E+03	4.781E-01	9.817E+02	8.364E-01	1.691E+03
7.856E-01	1.049E+03	9.235E-01	1.787E+03	5.313E-01	1.068E+03	8.973E-01	1.643E+03
8.156E-01	9.769E+02			5.550E-01	9.876E+02	9.729E-01	1.658E+03
8.497E-01	1.091E+03			5.780E-01	1.030E+03	1.031E+00	1.583E+03
8.932E-01	1.098E+03			6.015E-01	1.049E+03	1.094E+00	1.370E+03
9.167E-01	1.036E+03			6.405E-01	1.059E+03	1.222E+00	1.243E+03
				6.417E-01	1.131E+03		
				6.889E-01	1.199E+03		
				8.388E-01	1.115E+03		
				8.637E-01	1.156E+03		
				9.013E-01	1.223E+03		
				9.249E-01	1.077E+03		
				9.796E-01	1.195E+03		
				9.984E-01	1.059E+03		
				1.035E+00	1.294E+03		
				1.072E+00	1.015E+03		
				1.096E+00	1.085E+03		
				1.131E+00	9.248E+02		
				1.220E+00	8.722E+02		

Tabulation of the experimental velocity data around the blade of Daniels as extracted from references [20] and [77]. This data is compared with the functional approximations used in the calculations in the two figures that follow.

S/L (Suct) ReD data	U/U1 ReD data	S/L (suct) Re+ data	U/U1 Re+ data	S/L (press) data	U/U1 data
0.040	1.474	0.040	1.518	0.0	0.0
0.086	1.970	0.086	1.927	0.172	0.279
0.165	2.259	0.168	2.386	0.298	0.706
0.250	2.262	0.248	2.337	0.397	0.828
0.319	2.227	0.318	2.334	0.507	1.051
0.397	2.379	0.397	2.469	0.624	1.307
0.494	2.552	0.493	2.601	0.755	1.670
0.608	2.675	0.609	2.768	0.894	2.271
0.675	2.734	0.674	2.815	0.959	2.719
0.747	2.672	0.746	2.712	0.0	0.0
0.821	2.591	0.820	2.687	0.172	0.231
0.899	2.590	0.898	2.657	0.298	0.560
0.982	2.727	0.981	2.808	0.397	0.775
1.071	2.802	1.068	2.852	0.505	0.985
1.184	2.930	1.183	3.049	0.625	1.270
1.272	2.680	1.270	2.809	0.755	1.723
				0.893	2.223
				0.960	2.686



a. Comparison with data on the suction side



a. Comparison with data on the pressure side

### Appendix A4

Code used to calculate starting location velocity profile parameters

This is a FORTRAN listing of the simple code written to calculate the boundary layer thickness and acceleration factor for use at the initial starting location. This is the implementation of the method explained in section 2.3.3, equations (2.30) - (2.34)

```

1      PROGRAM DELIN
2      XO=0.
3      SUM=0.
4      PRINT*, 'INPUT THE KINEMATIC VISCOSITY IN M*M/S'
5      READ*, ANU
6      PRINT*, 'INPUT DX, AND THE NUMBER OF STEPS TO TAKE, ISTEPS'
7      READ*, DX, ISTEPS
8      PRINT*, ' '
9      PRINT*, 'X (M)      U (M/S)      DU/DX (1/S)      DEL2      RE2'
10     UO=UML (XO)
11     DO 10 I=1, ISTEPS
12         X=XO+DX
13         U1=UML (X)
14         DU=(U1-UO)/DX
15         ETA=UO/U1
16         B=(XO-ETA*X)/(1.-ETA)
17         PHI0=XO-B
18         PHI1=X-B
19         A=(U1/PHI1)**5
20         SUM=SUM+A/6.*(PHI1**6-PHI0**6)
21         DEL2=SQRT(.45*ANU*SUM)/(U1**3)
22         RE2=U1*DEL2/ANU
23         WRITE (6, 99) X, U1, DU, DEL2, RE2
24         XO=X
25         UO=U1
26     10 CONTINUE
27     ALAM=DEL2*DEL2*DU/ANU
28     PRINT*, 'LAMDA=', ALAM
29     PRINT*, 'INPUT THE SHAPE FACTOR S FROM TABLE 4.8 IN WHITE'
30     READ*, SF
31     DEL99=0.
32     DO 20 J=1, 20
33         DEL99=DEL2/SF*(2.+DEL99**2*DU/(6.*ANU))
34         PRINT*, J, DEL99
35     20 CONTINUE
36     OMEGA=DEL99*DEL99*DU/ANU
37     PRINT*, 'OMEGA=', OMEGA
38     99 FORMAT (' ', F7.5, 3X, F8.3, 5X, F10.3, 3X, 1P2E12.3)
39     STOP
40     END

```



## Report Documentation Page

1. Report No. NASA CR-4145	2. Government Accession No.	3. Recipient's Catalog No.	
4. Title and Subtitle Two-Equation Low-Reynolds-Number Turbulence Modeling of Transitional Boundary Layer Flows Characteristic of Gas Turbine Blades		5. Report Date May 1988	6. Performing Organization Code
		8. Performing Organization Report No. None (E-3960)	
7. Author(s) Rodney C. Schmidt and Suhas V. Patankar		10. Work Unit No. 505-62-21	11. Contract or Grant No. NAG3-579
		13. Type of Report and Period Covered Contractor Report Final	
9. Performing Organization Name and Address University of Minnesota Mechanical Engineering Department Minneapolis, Minnesota 55455		14. Sponsoring Agency Code	
		12. Sponsoring Agency Name and Address National Aeronautics and Space Administration Lewis Research Center Cleveland, Ohio 44135-3191	
15. Supplementary Notes Project Manager, Frederick F. Simon, Internal Fluid Mechanics Division, NASA Lewis Research Center. This report was a thesis submitted by Rodney C. Schmidt in partial fulfillment of the requirements for the degree of Doctor of Philosophy to the University of Minnesota in December 1987.			
16. Abstract In this thesis the use of low-Reynolds-number (LRN) forms of the $k-\epsilon$ turbulence model in predicting transitional boundary layer flow characteristic of gas turbine blades is developed. The research presented consists of: (1) an evaluation of two existing models, (2) the development of a modification to current LRN models, and (3) the extensive testing of the proposed model against experimental data. In the first part of this thesis, the prediction characteristics and capabilities of the Jones-Lauder (1972) and Lam-Bremhorst (1981) LRN $k-\epsilon$ turbulence models are evaluated with respect to the prediction of transition on flat plates. The sensitivity of these model's predictions to free-stream turbulence intensity, initial starting location, and assumed initial starting profiles of $k$ and $\epsilon$ is determined and presented. Although both models predict the correct qualitative characteristics, they are also shown to exhibit significant quantitative deficiencies with respect to the predicted location and length of transition. Next, the mechanism by which the models simulate transition is considered and the need for additional constraints discussed. A modification to the production term in the modeled turbulent kinetic energy equation is proposed which can be correlated to the free-stream turbulence level. The modification does not affect the fully turbulent calculations but is shown to greatly improve the nature of the transition predictions. Calibration of the empirical parameters introduced is accomplished by comparison with the correlation of Abu-Ghannam and Shaw (1980). The application of the model is developed and compared for use with both the Jones-Lauder and the Lam-Bremhorst LRN $k-\epsilon$ turbulence models. In the last section, the transition predictions of the new model are compared with a wide range of different experiments. These include experiments in transitional flows with free-stream turbulence under the following conditions: (1) flat plate constant velocity, (2) flat plate, constant acceleration, (3) flat plate but strongly variable acceleration, and (4) flow around turbine blade test cascades. In general, the calculational procedure is shown to yield good agreement with most of the experiments. Some deficiencies are however exhibited, and these are discussed in the spirit of providing guidance for future improvement.			
17. Key Words (Suggested by Author(s)) By-pass transition; Turbine blades; Heat transfer; Turbulence models; Prediction		18. Distribution Statement Unclassified - Unlimited Subject Category 34	
19. Security Classif. (of this report) Unclassified	20. Security Classif. (of this page) Unclassified	21. No of pages 271	22. Price* A12